DEVELOPMENTS IN VOLCANOLOGY 5

MELT INCLUSIONS IN VOLCANIC SYSTEMS

METHODS, APPLICATIONS AND PROBLEMS

Edited by
B. DE VIVO AND R.J. BODNAR

ELSEVIER

MELT INCLUSIONS IN VOLCANIC SYSTEMS

Methods, Applications and Problems

Photographs on cover

(lower left) The melt inclusion contained in the plagioclase crystal (An45) contains numerous bubbles. Photograph made available by Dr Jay Thomas, Department of Geological Sciences, Virginia Tech, Blacksburg, Virginia, USA.

(center) Vesuvius eruption of 1794. In: P. Gasparini and S. Musella, 1991. Un Viaggio al Vesuvio. Liguori Editore, Napoli.

(upper right) Several MI contained in an allanite. Photograph made available by Dr Jay Thomas, Department of Geological Sciences, Virginia Tech, Blacksburg, Virginia, USA.

MELT INCLUSIONS IN VOLCANIC SYSTEMS

Methods, Applications and Problems

Edited by

Benedetto De Vivo
Università di Napoli Federico II, Napoli, Italy

and

Robert J. Bodnar
Virginia Polytechnic Institute & State University,
Blacksburg, VA, U.S.A.

ELSEVIER
Amsterdam – Boston – Heidelberg – London – New York – Oxford
Paris – San Diego – San Francisco – Singapore – Sydney – Tokyo

ELSEVIER SCIENCE B.V.
Sara Burgerhartstraat 25
P.O. Box 211, 1000 AE Amsterdam, The Netherlands

© 2003 Elsevier Science B.V. All rights reserved.

This work is protected under copyright by Elsevier Science, and the following terms and conditions apply to its use:

Photocopying
Single photocopies of single chapters may be made for personal use as allowed by national copyright laws. Permission of the Publisher and payment of a fee is required for all other photocopying, including multiple or systematic copying, copying for advertising or promotional purposes, resale, and all forms of document delivery. Special rates are available for educational institutions that wish to make photocopies for non-profit educational classroom use.

Permissions may be sought directly from Elsevier's Science & Technology Rights Department in Oxford, UK: phone: (+44) 1865 843830, fax: (+44) 1865 853333, e-mail: permissions@elsevier.com. You may also complete your request on-line via the Elsevier Science homepage (http://www.elsevier.com), by selecting 'Customer Support' and then 'Obtaining Permissions'.

In the USA, users may clear permissions and make payments through the Copyright Clearance Center, Inc., 222 Rosewood Drive, Danvers, MA 01923, USA; phone: (+1) (978) 7508400, fax: (+1) (978) 7504744, and in the UK through the Copyright Licensing Agency Rapid Clearance Service (CLARCS), 90 Tottenham Court Road, London W1P 0LP, UK; phone: (+44) 207 631 5555; fax: (+44) 207 631 5500. Other countries may have a local reprographic rights agency for payments.

Derivative Works
Tables of contents may be reproduced for internal circulation, but permission of Elsevier Science is required for external resale or distribution of such material.
Permission of the Publisher is required for all other derivative works, including compilations and translations.

Electronic Storage or Usage
Permission of the Publisher is required to store or use electronically any material contained in this work, including any chapter or part of a chapter.

Except as outlined above, no part of this work may be reproduced, stored in a retrieval system or transmitted in any form or by any means, electronic, mechanical, photocopying, recording or otherwise, without prior written permission of the Publisher.
Address permissions requests to: Elsevier's Science & Technology Rights Department, at the phone, fax and e-mail addresses noted above.

Notice
No responsibility is assumed by the Publisher for any injury and/or damage to persons or property as a matter of products liability, negligence or otherwise, or from any use or operation of any methods, products, instructions or ideas contained in the material herein. Because of rapid advances in the medical sciences, in particular, independent verification of diagnoses and drug dosages should be made.

First edition 2003

Library of Congress Cataloging in Publication Data
A catalog record from the Library of Congress has been applied for.

British Library Cataloguing in Publication Data
A catalogue record from the British Library has been applied for.

ISBN: 0-444-51151-2

♾ The paper used in this publication meets the requirements of ANSI/NISO Z39.48-1992 (Permanence of Paper).
Printed in The Netherlands.

Workshop-Short Course on Volcanic Systems - Melt Inclusions: Methods Applications and Problems - Seiano di Vico Equense - September 27-30, 2002

This Page Intentionally Left Blank

Contents

INTRODUCTION

Robert Bodnar[1] and Benedetto De Vivo[2]

1 – Department of Geological Sciences, Virginia Tech, Blacksburg, VA, U.S.A.
2 - Dipartimento di Geofisica e Vulcanologia, Università di Napoli Federico II, Napoli, Italy

From September 26th to 30th, 2002, a group of researchers met at Seiano di Vico Equense, on the Sorrento Peninsula, Italy, to participate in the "Workshop-Short Course on Volcanic Systems. Geochemical and Geophysical Monitoring. Melt Inclusions: Methods, Applications and Problems", sponsored by the Istituto Nazionale di Geofisica e Vulcanologia (INGV), the University of Napoli Fedrico II and by the Campania Regional Government. Approximately 90 researchers from 15 countries attended the Workshop-Short Course, which included 33 oral presentations and 16 posters. The group visited the world-famous Mt. Vesuvio volcano as part of the Workshop, to see first-hand the awesome beauty and power that volcanoes offer.

The aim of the Workshop was to discuss current state-of-the-art techniques and models for using silicate melt inclusions in crystals of volcanic rocks to determine pre-eruptive volatile concentrations in magmas, and to describe applications of melt inclusions analyses to fundamental problems of petrology in general, and volcanology, in particular. Because magmas degas as they ascend and erupt, or crystallize at depth, direct knowledge of the pre-eruptive volatile content of magmas, mainly H_2O, CO_2, S species and Cl, can be obtained from studies of melt inclusions. This information is fundamental to understand dynamics of magmas, mechanisms of explosive volcanic eruptions, gas emissions from active volcanoes, volcanic addition to the atmosphere and the magmatic contribution to hydrothermal ore deposits. Melt inclusions thus represent our best source of information on the compositions of magmatic fluids during their transport from depth to the earth's surface, and the study of dissolved volatile concentrations (H_2O, S, Cl, CO_2, F) in magmas provides a history of the complex evolution in magmatic systems.

The lecturers who kindly accepted the invitation to give presentations at the Workshop and to this volume represent top researchers at the international level. We are grateful to those who, with their participation at the Workshop first and contributions to this volume, have made possible the organization of a very successful Workshop and this publication, which we hope will be well received.

The history of melt inclusion research parallels that of fluid inclusions in general. They were already known in the eighteenth century, although the really important developments in this type of research started after 1970. In recent years, hundreds of research papers have been published on subjects related to melt inclusions compared with the few papers published only 10 years ago (see figure. Data compiled by Alex Sobolev). The impact of melt inclusion studies on understanding magmatic systems has been profound and will certainly become more so in the coming years, as analytical techniques evolve. Future advances in the development of sophisticated analytical tools, such as EPMA, LA-ICP-MS, ion microprobe, FTIR Spectroscopy, Raman and synchrotron-based XRF, combined with data available from high temperature heating/quenching stages, such as the Vernadsky Stage, developed by Sobolev group in the former Soviet Union, will further enhance our ability to use data from melt inclusions to better understand magmatic systems.

The papers in this volume include the contributions of: Lowenstern (*Melt inclusions come of age: volatiles, volcanoes, and Sorby's legacy*); Hawkesworth et al. (*Estimating the time scales of magmatic processes*); Dingwell (*Liquid to glass: quantifying properties and structure of melts across the glass transition*); Kamenetsky et al. (*Magmatic inclusions in the search for natural silicate-salt melt immiscibility: methodology and examples*); Hervig et al. (*Analyzing hydrogen (H_2O) in silicate glass by secondary ion mass spectrometry and reflectance Fourier transform infrared spectroscopy)*; Wallace (*From mantle to atmosphere: magma degassing, explosive eruptions, and volcanic volatile budgets*); Saito et al. (*Volatile evolution of Satsuma-Iwojima volcano: degassing process and mafic-felsic magma interaction*); Shinoara et al. (*Degassing process of Miyakejima volcano: implications of gas emission rate and melt inclusions data*); Tracy (*Chemistry and origin of zoned haüyne in tahitian phonolite, with implications for magmatic fractionation*); Frezzotti et al. (*Magma ascent rates and depths of crustal magma reservoirs beneath the Aeolian volcanic arc (Italy): inferences from fluid and melt inclusions in xenoliths)*; Webster et al. (*Volatiles, magmatic degassing and eruption of Mt. Somma-Vesuvius: constraints from silicate melt inclusions, Cl and H_2O solubility experiments and modeling*); Lima et al. (*Evolution of Mt. Somma-Vesuvius magmatic system based on fluid and melt inclusions investigations*).

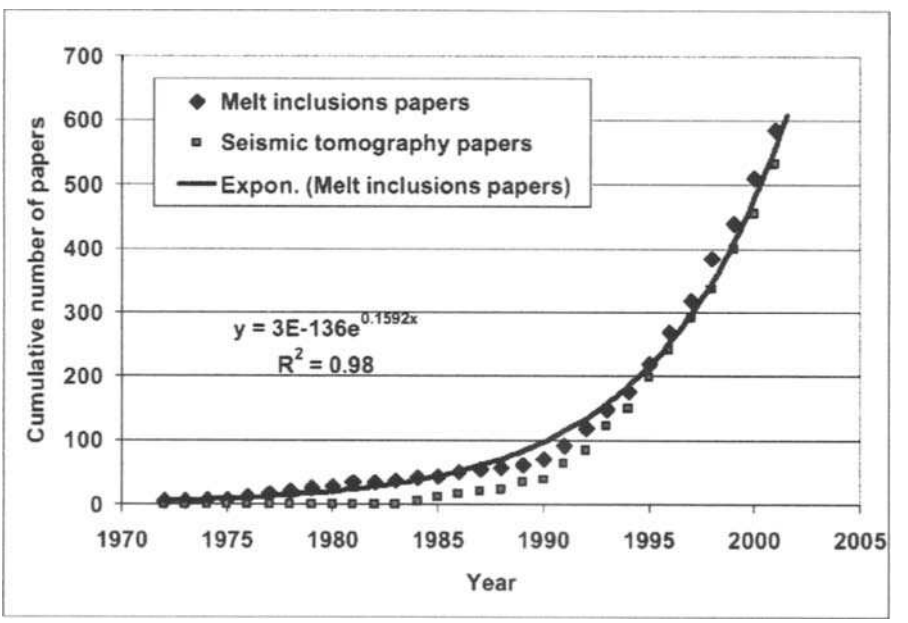

ACKNOWLEDGEMENTS

We wish to thank Prof. Enzo Boschi, President of the Istituto Nazionale di Geofisica e Vulcanologia (INGV) for the support given for the organization of the Workshop; Stefano Albanese and Alessandra Sava for their help for the activities pre- and during the Workshop, and, in particular, Dr Luca Fedele, for his invaluable help for the final editorial work necessary to format the camera-ready articles as required by Elsevier.

Presentation of the Inaugural Roedder Medal to Edwin Roedder

When we think about the first person to recognize that the planets revolve around the sun, the person that immediately comes to mind is the great Italian scientist Galileo. When we think of circumnavigation of the earth, the name Magellan comes to mind, and we all associate the theory of relativity with Einstein. Similarly, the name that everyone immediately thinks of when fluid inclusions are mentioned is Ed Roedder.

Ed Roedder took fluid inclusions from being a novelty and curiosity to being one of the most powerful tools available to determine the thermal and chemical evolution of geologic systems. For nearly half a century Roedder has been the leading researcher in fluid inclusions. He has been a teacher of countless young people, and helped to introduce many young scientists to the fascinating field of fluid inclusion research. Ed Roedder provided a valuable service to the fluid inclusion community, and to the geosciences in general, by single-handedly starting the COFFI volumes (Commission on Ore-Forming Fluids in Inclusions), which later became the well-known FIR (Fluid Inclusion Research) volumes. Ed remained as the driving force behind the publication of FIR for 30 years, until its recent demise at the hands of the worldwide web and electronic databases. Ed's well known book, simply titled "Fluid Inclusions" and published by the Mineralogical Society of America, has sold more than 6,500 copies! For many years this book has been considered the "Bible of fluid inclusions".

For his research on fluid inclusions, Ed Roedder has received numerous awards during his illustrious career. He has been honored with the highest awards of the Mineralogical Society of America (Roebling Medal) and the Society of Economic Geologists (Penrose Medal). Roedder also received the Sorby Medal, the Exceptional Scientific Achievement Medal from NASA, the Werner Medal from the German Mineralogical Association, and was awarded an honorary Doctorate of Science from Lehigh University. Ed is a member of the prestigious U.S. National Academy of Science, perhaps the highest honor that can be bestowed on any scientist, short of a Nobel Prize. Finally, Ed has served as the President of the Mineralogical Society of America and the Geochemical Society, reflecting the great respect that the scientific community has for Ed's leadership abilities.

For Ed's many past and continuing contributions to the study of fluid inclusions, we are tonight honoring Ed with the first Roedder Medal, awarded for a lifetime of contributions to the study of fluid inclusions. In the future, the Roedder Medal will serve as the ultimate recognition for those scientists who have adhered to the high standards established by Ed, and who have similarly made life-long contributions to the study of fluid inclusions.

Ladies and gentlemen, it is a great honor to present to you Dr. Edwin Roedder, the first recipient of the Roedder Medal.

Respectfully submitted,

R. J. Bodnar

This Page Intentionally Left Blank

Roedder acceptance speech

The Roedder medal

This Page Intentionally Left Blank

SIGNIFICANCE OF MELT INCLUSIONS

Edwin Roedder

Harvard University

It is a pleasure to be asked to write an introduction to the volume "Melt inclusions in Volcanic systems: methods and problems" stemming from the Short Course on Volcanic Systems - Melt Inclusions, Methods, Applications, and Problems, held in Seiano (Sorrento Peninsula), from 26th to 30th September 2002. How best to introduce the papers stemming from such a conference? In briefest form, one could say that the study of melt inclusions is a good thing, has progressed far, has a great future, and we should do more. Let me elaborate a little on that inadequate summary. Silicate melt inclusions have been actively studied for nearly 150 years, although most of the early studies were simply descriptive, with little or no interpretation of their significance in terms of geological processes. During this same period, a parallel but much more intensive study was under way of aqueous inclusions. In contrast with the study of silicate melt inclusions, the aqueous inclusion studies almost immediately began to be interpreted, yielding data on many geological and economically important processes, first on the temperatures of hydrothermal ore-formation, and then on the compositions of the long-gone fluids that were actively involved in many environments.

Similar studies of melt inclusions can, in theory, yield a similar wealth of information on the origin, nature, and evolution of the fluid (melt) that was trapped, and the processes that took place in the past. Unfortunately, many of the techniques that have been applied so effectively on aqueous inclusions are difficult or inappropriate for use on melt, but as seen in these papers, many of the disadvantages are being overcome, and some of the newly developed techniques for melt inclusions are even proving helpful in the study of aqueous inclusions.

The two such areas of research that have been most fruitful are stable isotopes (especially O, C, S, B, Cl, and the noble gases), and, most important, the volatiles. What volatiles are present, in what amounts, in solution in the seemingly simple glass of "normal" melt inclusions? The most important role of these dissolved volatiles lies in their major control of the rheological properties of the magma such as viscosity and hence the very essence of magma movement. They also affect the temperatures of crystallization and the phases formed.

However, the real significance of the volatile component of the magma becomes apparent when fluid immiscibility occurs. Once a separate volatile-rich fluid phase forms (or even several different volatile-rich phases), it results in a major geochemical fractionation - all chemical species present, the elements (and their isotopes), and their various compounds, become distributed between these two phases. The partitioning is thus similar to that taking place during the crystal-melt fractionation of normal magmatic differentiation, but the compositional divergence between the two phases is much more extreme, and even though the physical amounts of the new volatile-rich phase may be small, its separation and transport can be important. Even greater importance lies, however, in the physical properties of the new volatile phase. Its much lower density provides the major control of the bulk density of the now two-fluid-phase magma, and its expansion during eruption provides the motive energy for almost all volcanism. The trapping of portions of this volatile-rich phase as fluid inclusions at various stages in the evolution of volcanic rocks provides us with a few small but very informative samples of these fluids.

Thus the study of "ordinary" melt inclusions provides insight into the evolution of magmas by crystal/liquid equilibrium, and the study of the volatiles in magmas, as evidenced by both those dissolved in melt inclusions, and those simultaneously trapped as actual liquid inclusions, provide a history of the more complex magmatic evolution stemming from immiscibility. Both types of studies are needed to understand volcanic processes, and both are represented in the papers contained in this volume.

Melt Inclusions Come of Age: Volatiles, Volcanoes, and Sorby's Legacy

Jacob B. Lowenstern

U.S. Geological Survey
Volcano Hazards Team, Mail Stop 910
345 Middlefield Road
Menlo Park, CA 94025 USA

ABSTRACT

Despite nearly forty years of modern research on silicate melt inclusions (MI), only within the past 10-15 years have volcanologists and petrologists come to regularly accept their utility for characterizing magmatic systems. Their relatively slow acceptance was likely due to a number of factors including: 1) Lack of reliable analytical techniques, 2) Concern that MI represent anomalous boundary-layer melts or are altered by leakage or post-entrapment crystallization, 3) Data sets indicative of heterogeneous melts and, 4) Homogenization temperatures greater than those calculated by other techniques. With improvements in analytical methods and careful studies of MI systematics, workers are increasingly convinced of the utility of these features to unravel the complexities of volcanic systems: melt inclusions have "come of age." Recent studies provide compelling evidence for the compositions of dissolved and exsolved volatiles in magma reservoirs. Evidence for immiscibility of gases, hydrosaline brines and pegmatitic fluids demonstrate that magmatic phase relations are often more complicated than can be inferred by inspection of crystalline phases alone.

INTRODUCTION

Volatile gases are the fundamental cause of magma ascent, effervescence, expansion, and fragmentation. Either in dissolved or exsolved form, these gases strongly control the density and viscosity of magmatic liquids. Yet because they are released during eruption, the gases leave little trace of their former presence. Studies of bulk tephra and groundmass glass reveal little about the initial abundance of volatiles in the pre-eruptive magma. Consequently, magmatic inclusions such as silicate-melt inclusions (MI) in phenocrysts represent a vital source of information about the compositions of magmatic fluids during eruptive ascent.

The MI are typically small blebs of silicate melt that are trapped within phenocrysts at magmatic temperatures and pressures. The relatively incompressible phenocryst hosts act as pressure vessels during eruption, keeping any trapped MI from degassing. Through microbeam analysis of the quenched MI, we can quantify the pre-eruptive

concentrations of dissolved volatile gases (i.e., H_2O, CO_2, S, and Cl). We can then estimate the pressures of melt-vapor equilibration at the time of inclusion formation (Anderson et al., 1989). Through studies of MI we also recognize that elements such as B, P, and F can act just as stealthily as some of their better-known volatile brethren, having higher concentrations in MI than degassed matrix glass. Studies of ore metals such as Cu, Zn and Sn show that they also can be transported as volatiles in magmatic systems. Perhaps the most important insight from MI studies has been the revelation that magmatic fluids can be far more diverse than solely silicate melt and gas (Roedder, 1979a; Cathelineau et al., 1988; Roedder, 1992). Recent studies document chloride-, sulfate–, and carbonate-dominated melts, and silicate-silicate immiscibility at relatively low temperatures (<500°C); importantly, they have also begun to provide detailed compositional data on these immiscible phases.

Our reliance on MI has come only after several decades of concerted effort to improve analytical techniques, to assess the reliability of MI due to host-inclusion equilibration (pre-, syn- or post-trapping), and to recognize the effects of trapping multiple fluid phases. Additional effort has been placed on characterization of bubbles within MI, which can be present for a variety of very different reasons. In this article, I review some of the history of melt-inclusion studies, with special attention to the changing perceptions of MI and their utility for understanding magmatic volatiles. I also address evidence for trapped magmatic fluids within igneous phenocrysts, including those trapped along with silicate melt in mixed inclusions.

The review is necessarily subjective; it represents the accumulated perspective of a single researcher, and given its brevity, cannot begin to cite all of the many articles and abstracts relevant to the subject. My aim is to provide a starting point for workers interested in MI and the history of their role in the study of volatiles in volcanic systems.

IMPACT OF MELT INCLUSION RESEARCH PRIOR TO THE 1990s

In their pioneering 19th Century studies, Sorby (1858) and Zirkel (1873) gave detailed descriptions and drawings of MI and accompanying fluid inclusions (FI) in a wide variety of intrusive and extrusive rocks (see Table 1 for definitions). They speculated on the origins of bubbles within the inclusions and recognized that MI had marked promise for interpretation of the origin of igneous rocks. Indeed, Sorby (1858, p. 497) in a comment to skeptical colleagues stated: "There is no necessary connexion between the size of an object and the value of a fact, and ... though the objects I have described are minute, the conclusions to be derived from the facts are great."

For a variety of reasons, decades would pass before workers would follow Sorby and further scrutinize these tiny droplets of silicate melt in igneous phenocrysts. The first modern studies of MI were undertaken not by volcanologists but by workers interested primarily in the systematics of FI. Studies of FI blossomed in the 1960s, 70s and 80s, particularly in the field of economic geology (Hollister and Crawford; 1982; Roedder, 1984). At this time, the international fluid inclusion community championed the use of MI for studies of lunar samples (Roedder and Weiblen, 1970, 1971), pegmatites, granitoids and volcanic rocks (Sobolev and Kostyuk, 1975; Roedder, 1979b). These papers demonstrated abundant evidence for immiscibility among silicate

melt and diverse volatile phases from a variety of igneous rocks (Roedder, 1965; Roedder and Coombs, 1967; Roedder 1979b). Myriad references in the Russian literature refer to "salt melts", "solution-melts" or "melt-brines" (see Sobolev and Kostyuk, 1975), but the implications of this research was not fully assimilated by igneous petrologists in many other countries.

Table 1. Definitions of magmatic inclusions in phenocrysts

Melt Inclusion (MI)	Contains glass or crystallized glass
Fluid Inclusion (FI)	Contains one or more fluids at room temp. and no glass or crystallized glass.
Vapor-rich Fluid Inclusion	FI with > 50 vol.% bubble at room temp.; i.e., low density (potential gassy) fluid.
Mixed Inclusion	More than one magmatic phase trapped.
Hydrosaline Melt	Molten solution of salts and H_2O

Reservations about the utility of MI:

Perusing reviews on volatiles as well as textbooks on igneous petrology written during the 1970s and 1980s, there is little if any mention of MI (e.g., Carmichael et al., 1974; Best, 1982; Burnham, 1979a, 1979b; Holloway, 1979; McBirney, 1984; Maaløe, 1985). The 1987 issue of Reviews of Geophysics contains 5 review articles on igneous petrology and volcanology (Carlson, 1987; McCallum, 1987; Marsh, 1987; Ghiorso, 1987; Self and Francis, 1987). Of some 3000+ references cited in these articles, fewer than 5 relate to MI. The apparent low impact of MI studies on the volcanological and petrological communities can be traced to a number of factors. Some workers were unclear as to whether MI accurately represented the compositions of their host magmas. As stated by Eichelberger (1995): "Interpretation of melt inclusions is not without difficulties: 10^{-14}-g samples are taken to represent a 10^{10}-g system..." Workers cited a variety of processes that could potentially cause an MI to yield spurious data: 1) non-representative "boundary-layers" accumulated near growing crystals, 2) post-entrapment growth of the host crystal from trapped melt, 3) leakage and decrepitation, and 4) diffusion of species through the host crystals (or exchange between host and melt). These problems are real and require caution on the part of the analyst. Because of these potential pitfalls, petrologists in the 1960s to 1980s often seemed leery of MI research findings, and pointed to problems evident in published studies, some of which are discussed below.

MI temperatures appeared to be too high: Much of the work on MI by the international fluid-inclusion community focused on traditional homogenization experiments, primarily to assess magmatic temperatures. The petrological community, however, had developed a variety of experimentally based geothermometers. These

procedures relied on microprobe analyses of co-precipitating minerals or mineral-glass pairs (e.g., Kudo and Weill, 1970; Buddington and Lindsley, 1964; Stormer, 1975; Wood and Banno, 1973), and they were adapted and used successfully in numerous petrological studies (e.g., Ewart et al., 1971; Hildreth, 1979, 1981). In general, the temperatures found from MI homogenization studies were greater than those inferred by analysis of coexisting Fe-Ti oxides and other geothermometers (Sommer, 1977; Beddoe-Stephens et al., 1983). Roedder (1979b) discussed several reasons for high-homogenization temperatures (slow diffusion of melt components, thermal gradients in the stage, diffusive loss of H_2 or H_2O) and cautioned against literal interpretation of temperatures acquired through homogenization experiments. Recent studies have verified that homogenization studies can provide spurious data because of diffusion of volatiles through the host and stretching of the phenocryst container during laboratory experiments at atmospheric pressure (e.g. Massare et al., 2002).

MI volatile contents appeared too high (or too low): In the early 1970s, several workers began to use the electron microprobe to analyze MI and to estimate dissolved volatile concentrations (Anderson, 1974a, 1974b, 1975; Takenouchi and Imai, 1975; Clocchiatti, 1975). Anderson (1974a) found high Cl and S in MI from andesitic glasses of Mt. Shasta (CA, USA). He inferred high H_2O concentrations in MI, 1 to 7 wt.%, by observing that the electron microprobe analytical totals for the oxides were significantly less than 100% (aka, "volatiles by difference"). In a related paper Anderson (1975) concluded that volcanic outgassing rates far exceed the amounts that can be supplied by erupted magmas and that the subsurface reservoirs of Pacaya (Nicaragua) and Kilauea (Hawai'i, USA) were vapor-saturated prior to eruption. Sommer (1977) documented similar evidence for the pre-eruptive Bandelier Tuff magma chamber, and showed there was significant CO_2 dissolved in the magma. Such arguments were novel, and some workers were skeptical. Roedder (1979b) commented: "some workers express little faith in any results based on low electron microprobe totals, particularly when the amounts of water (and other volatile materials) estimated from them are much higher than previously thought." Reviews by Holloway (1979) and Gill (1981, p. 293) were representative of this viewpoint and expressed some doubt as to the accuracy of concentrations reported by Anderson (1974a,b, 1975). Both reviews discussed the possibility that MI may not have compositions representative of the melt from which they grew. This viewpoint was widespread among petrologists: Watson (1976) had pointed out that post-entrapment crystallization of the inclusion host could alter the MI composition. He proposed a useful method for accounting for this process by analysis of inclusions in multiple phases. In a later paper, Watson et al. (1982) predicted that MI might have dissolved H_2O and CO_2 concentrations many times in excess of their actual melt abundance due to buildup of slow-diffusing elements near the borders of rapidly growing crystals. They also estimated that bubbles may nucleate in normally volatile-undersaturated magmas as a result of this process and could mislead interpretation of magmatic conditions. Though such hypotheses are readily testable, no studies actually verified anything more than slight gradients in slow-diffusing elements (e.g., Beddoe-Stephens et al., 1983). Until workers focused directly on assessing the fidelity of MI

compositions (Lu et al., 1995; Manley, 1996), there remained the perception that MI could be unreliable.

MI studies displayed unexpected compositional variability: Another possible hindrance to wide acceptance of MI studies was the large variation in apparent volatile concentrations in MI from some eruptive units (e.g., Muenow et al., 1979; Melson, 1983; Sommer and Schram, 1983; Harris and Anderson, 1983; Palais and Sigurdsson; 1989). There are a number of geological reasons that can result in a spread of H_2O concentrations in MI from volcanic phenocrysts from a single unit. Magma mixing (Hervig and Dunbar, 1992), crystal settling (Anderson et al., 2000), degassing-induced crystallization (Sisson and Layne, 1993) and lava drainback and recycling (Wallace and Anderson, 1998) are all potential reasons to expect variations in volatiles within melt inclusions from a single pumice lump, or crystal. Moreover, MI can decrepitate and leak during or after eruptive ascent (Tait, 1992), and workers must make rigorous efforts to insure that leaked/degassed inclusions are avoided. Those workers familiar with experimental data or bulk whole-rock data on natural samples may have been somewhat leery of early data sets that showed wide and unexpected variations in the chemistry of included melts.

Lack of familiarity with MI: The problems outlined above caused some justifiable skepticism about the utility of MI for petrological and volcanological studies. To overcome the skepticism, it would be necessary to undertake numerous careful analytical studies. However, few of the critics of MI research were active in performing such analytical studies. In part, this stemmed from their general lack of familiarity with MI and their systematics. Studies of volatiles in MI often require grain-by-grain assessment of phenocrysts to observe cracks and capillaries. The most common petrographic mounts such as thin-sections or multi-grain mounts in epoxy are inadequate for inspection of MI populations (Lowenstern, 1995). As a result, to test the utility of MI requires familiarity with the principles of MI preparation and petrography. Those most likely to undertake rigorous studies of MI were those "inclusionists", already familiar with the principles of MI petrology.

Petrological priorities

Another important barrier to widespread use of melt inclusions was the lack of micro-analytical techniques, and the exploding development of high-precision bulk techniques. In the 1970s and 1980s, techniques such as x-ray fluorescence (XRF) and instrumental neutron-activation analysis (INAA) spurred a revolution in trace-element geochemistry of whole rocks. Improvements in mass spectrometers allowed researchers to focus on isotopic studies of terrestrial and planetary samples. The new data were interpreted in light of recently developed plate-tectonic theory and recognition that different magma types and environments had their unique trace-element and isotopic characteristics (Bottinga and Allègre, 1976; Basaltic Volcanism Study Project, 1981; White and Hoffmann, 1982). At the same time, funding for planetary research increased with creation of NASA and the lunar missions.

Until the 1970s, petrologists lacked analytical tools to routinely characterize the contents of materials only tens of micrometers across. Even today, electron microprobe microanalysis of hydrous glasses remains difficult, and some MI contain high concentrations of light elements such as B and Li which require alternative spectroscopic techniques (e.g., Thomas, 2002) that only recently have become available. Until the 1990s, melt inclusions could not be analyzed reliably for trace elements, and analysis of volatile elements was qualitative. As a result, the broad petrologic and volcanological communities chose not to pursue MI as a means for understanding petrogenesis and volcanic phenomena.

Experimental versus analytical studies of volatiles: Even for studies of magmatic volatiles, other research approaches were preferred. It had long been recognized that magmatic volatiles had a crucial role in the generation, ascent and crystallization of magmas (Bowen, 1928). In the 1960s, 70s and 80s a variety of noteworthy and high-profile experimental studies were undertaken to determine the thermodynamic controls on volatile solubilities (Burnham and Jahns, 1962; Burnham and Davis, 1971; Eggler and Burnham, 1973; Wyllie, 1979; Whitney, 1984). Many workers justifiably reasoned that data on natural samples could not be properly understood without an experimental and thermodynamic basis for interpretation. Money and priorities were directed towards theoretical and experimental studies of magmatic volatiles. In natural samples, volatile concentrations were estimated by bulk analytical techniques on lavas quenched at the surface (e.g., Friedman et al., 1963) or underwater (Moore and Schilling, 1973). H_2O fugacities were later estimated by thermodynamic models based on the partitioning of K and Fe between biotite and feldspar (Wones, 1972), the Na/Ca ratios of the silicate melt (Merzbacher and Eggler, 1984) and other techniques. In general, P_{H_2O} was believed to be far below P_{total} in most igneous systems (Carmichael et al., 1974, p. 326). Given the lack of strong evidence for high abundances of other volatiles (e.g., CO_2, SO_2, H_2, N_2, Cl-bearing species), many workers concluded that most crustal magmas were both H_2O and vapor-undersaturated.

EMERGING IMPORTANCE OF MI IN VOLCANOLOGICAL STUDIES

With time, and with the development of infrared spectroscopy (Newman et al., 1986), the ion microprobe (Karsten et al., 1982) and improved electron microprobe methods for analysis of hydrous glasses (Nielsen and Sigurdsson, 1981), new data on MI compositions became increasingly abundant. The number of articles on "melt inclusion" or "glass inclusion" in the bibliographic database GeoRef® expanded from ~ 8 per year in 1985 to ~60 per year in the late 1990s. As data became widespread, workers became increasingly convinced that MI provided useful and reproducible data to constrain magmatic systems. Concern about boundary-layer phenomena was decreased as workers found little evidence for heterogeneity within individual inclusions (Lu et al., 1995). Post-entrapment changes were also small (Manley, 1996) or could be modeled effectively (Sobolev and Danushevsky, 1994). Other studies found that variations in melt-inclusion compositions could be attributed primarily to magmatic processes (Dunbar and Hervig, 1992; Sisson and Layne, 1993).

Anderson et al. (1989) published the first large dataset to use infrared spectroscopic techniques to analyze a series of MI from a single eruption, the 760 ka Bishop Tuff. They found high and variable CO_2 concentrations that correlated with H_2O in a manner consistent with isobaric, gas-saturated fractionation of different magma batches. Later work by Anderson and colleagues (Skirius et al., 1990; Lu et al., 1992) and others (Dunbar and Hervig, 1992; Hervig and Dunbar, 1992) spurred the emergence of the Bishop tuff as a "proving ground" for MI-related research. The wealth of carefully collected data, and intriguing geochemical trends demonstrated that MI faithfully record a variety of magmatic processes that cannot be detected by most other avenues of petrologic research. Using the Bishop Tuff alone, recent studies have used MI to assess magma residence times (Van den Bogaard and Schirnick, 1995; Christensen and Halliday, 1996), excess Ar and geochronology (Winick et al., 2001), volatile phase accumulation (Wallace et al., 1995, 1999) and crystal settling (Anderson et al., 2000).

MI are now increasingly used as a volcanological tool to unravel the complexities of very recent eruptions. Dunbar et al. (1989) undertook one of the first studies to use the ion microprobe to quantify H_2O in MI. They analyzed dissolved volatiles in homogeneous glassy MI from the Taupo volcanic center (New Zealand). They found no significant difference between the dissolved volatile contents in phenocrysts from plinian and phreatomagmatic deposits. This non-correlation between pre-eruptive volatiles and eruptive style has been noted by many subsequent workers and is likely due to the influence of pre-eruptive (post-entrapment) degassing and ascent rate on eruptive style (Lowenstern and Mahood, 1991; Bacon et al. 1992; Lowenstern, 1993; see also Mangan and Sisson, 2000). Roggensack et al. (1997) studied the degassing history of eruptions from Cerro Negro (Nicaragua). They found that magmas erupted explosively in 1992 had equilibrated at greater depths than lavas erupted three years later as effusive lavas. Shallow subsurface degassing, plausibly during the three-year period between eruption, led to the decrease in explosivity. In a subsequent paper Roggensack (2001a) looked at the products of an 1867 eruption at Cerro Negro and found that MI glass composition and gas saturation pressures correlated with crystal size, implying that large crystals grew at greater depth (up to >15 km). All crystals apparently formed less than two years prior to eruption. A similar study at Fuego (Guatemala) showed that MI hosted by small, recently formed olivine crystals showed tremendous variability in volatiles and major-element composition, revealing hybridization of a heterogeneous magma column shortly prior to eruption (Roggensack, 2001b).

Similar studies on Italian volcanoes demonstrate the importance of degassing and crystallization in determining eruptive style. Métrich et al. (2001) looked at crystal-rich scoria at Stromboli, which are erupted during persistent and mild strombolian activity, and found that the MI are degassed and contain more evolved glass than MI from compositionally equivalent whole-rocks erupted as crystal-poor pumices during more energetic explosive activity. Evidently, volatile-rich magma batches can either ascend rapidly to produce the explosive eruptions, or they can intrude to shallow depths and degas quietly to spur the typical strombolian eruptions. Marianelli et al. (1999) were able to differentiate different depths for magma reservoirs feeding the 1944 eruption of Vesuvius including K-tephritic melts saturated with CO_2-rich gas at pressures over 300

MPa. These sorts of studies provide new opportunities for evaluating the relationship between crystal growth, ascent rate, degassing and eruptibility of magma.

Besides these volcanological studies, petrologists have increasingly used MI to understand magma generation and the diversity of melt sources available to volcanic systems (Sobolev, 1996; Frezzotti, 2001). A recent compilation (Hauri et al., 2002) provides an excellent assembly of papers on MI systematics and analysis, primarily focussed on the petrology of mafic magma systems. Clearly, the petrological and volcanological communities have become familiar with the pitfalls of melt-inclusion analysis, and have accepted that valuable data can be collected through careful studies.

NEW OBSERVATIONS OF BUBBLES, FLUIDS AND EXOTIC MELTS

With acknowledgement that glass compositions, including dissolved volatiles, can be determined successfully, we can look critically at MI with more complex petrography. Anyone who has undertaken a study of MI has likely seen at least a few challenging inclusions that defied simple interpretation. Some MI contain large bubbles or bubbles associated with little to no glass at all. Some inclusions contain crystals not normally found as phenocrysts, or melts very unlike those of the whole-rock (Davidson and Kamenetsky, 2001; Thomas et al., 2000). In some cases, inclusions seem to imply magmatic temperatures, pressures and compositions beyond the norm. Roedder (1979b) wrote: "Theoretical igneous petrology has evolved considerably in recent years, but observational petrography is still capable of providing some surprises and may even inspire some new theories."

Origins of bubbles in MI:

Many studies have avoided bubbles, or inclusions containing bubbles, in an effort to simplify interpretation of MI compositions. However, the size, distribution and composition of bubbles reveal the history of fluid immiscibility, degassing and ascent rate of the host magma. There are at least three reasons why a bubble is found within an MI: 1) it formed during near-constant-volume cooling of homogenous silicate melt, 2) it formed during decrepitation/leakage of the MI and, 3) it represents magmatic vapor that was co-trapped with melt in a mixed inclusion.

"Shrinkage Bubbles": As with all FI, a bubble can nucleate due to isochoric (constant volume) cooling of a trapped homogeneous liquid, causing depressurization and resultant saturation with a low-density phase (Fig. 1a). The bubble that forms is often called a "shrinkage bubble". As discussed by Roedder (1984, p. 50), it should be considered a separate phase formed by immiscibility of the melt and vapor. Homogenization experiments in the laboratory typically show that during heating the bubbles disappear at temperatures greater than when they re-appear during cooling (Roedder, 1979b). Apparently, significant underpressures are necessary to induce bubble nucleation, especially when cooling rates are high. Mangan and Sisson (2000) also have shown this to be the case for macroscopic rhyolitic systems depressurized rapidly in the laboratory.

When equilibrium is maintained, the internal pressure of the bubble should equal that of the melt. Melt-vapor equilibration should cease at temperatures below T_g, the

glass transition temperature, after which the bubble contents may cool isochorically. This should result in high pressures (and thus densities) for fluids within the "shrinkage" bubble. Typically, though, such bubbles appear empty, or at least without a liquid phase, allowing H_2O pressures no greater than that for liquid saturation at 25°C ($2.6x10^{-3}$ MPa). Some workers interpret the empty bubbles to reflect extreme hydration of the glass adjacent to the bubble rim during cooling of the MI (Lowenstern, 1995). It should be noted though, that high-density fluids are sometimes found within MI-hosted bubbles [Naumov et al., 1993 (Fig 2c); this article (Fig 1B)].

The volume of bubbles can range widely, (0.1 – 5 vol.%) and is known to depend on the cooling history of the MI. Small MI often fail to nucleate bubbles because of surface-tension effects (Roedder, 1979b). Many workers have shown that MI from rapidly quenched Plinian pumice often lack bubbles entirely (Clocchiatti, 1972; Sommer, 1977; Beddoe-Stephens et al., 1983). Both theoretical (Tait, 1992) and experimental (Lowenstern, 1994) studies confirm that rapid cooling is likely to permit MI quenching without bubble formation. The latter study found that quartz-hosted MI of peralkaline rhyolites (pantellerites) failed to nucleate bubbles if cooled faster than ~ 300°C/minute from their homogenization/entrapment temperatures. As cooling rates decrease, bubbles have more time to form, to equilibrate with their host melts and thus to grow and to partially crystallize (Skirius et al., 1990). In intrusions, crystallization of the melt at near-magmatic temperatures will allow the MI-hosted bubbles to reach as much as 15-20 % of the total inclusion volume (Student and Bodnar, 1996).

Decrepitation or leakage through capillaries: When the host crystal cools more slowly, within a lava or dense pyroclastic flow, the bubble has time to form, causing the internal pressure of the MI to rise (Tait, 1992). Often these slowly cooled rocks have cracked crystals with MI that contain numerous large bubbles (Lowenstern, 1995; Best and Christiansen, 1997). Best and Christiansen (1997) surveyed scores of Tertiary pyroclastic flow rocks in Nevada and Utah (USA) and noted that broken crystals in ash flow tuffs can often be attributed to the decrepitation of MI during eruption. MI that partially or fully decrepitate are likely to have numerous large bubbles and degassed glass (Skirius et al., 1990). Feldspar hosts are more likely to break than quartz owing to their good cleavage and they can show strain birefringence adjacent to the inclusion (Skirius et al., 1990). Occasionally, degassed/leaked inclusions can be recognized by their glassy nature, when compared to pristine inclusions that cool slowly from H_2O-rich melt and become partially or entirely crystalline. Lowenstern and Mahood (1991) found that leaked peralkaline rhyolite inclusions were glassy and green whereas unleaked inclusions were microcrystalline and blue, presumably from crystallites of alkali amphibole (also see Anderson, 1991).

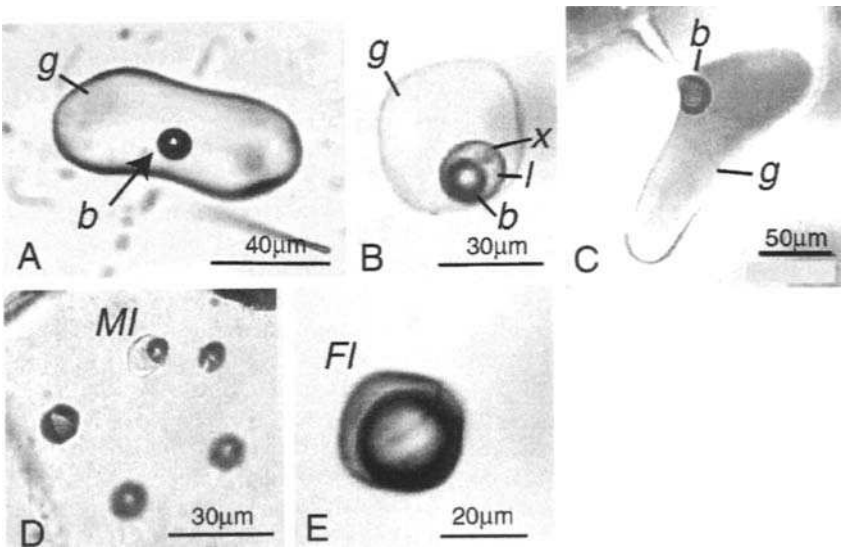

Fig. 1. MI and FI in volcanic quartz. A) MI with glass (g) and associated shrinkage bubble (b) from ignimbrite unit of the 1912 eruption at the Valley of Ten Thousand Smokes, Alaska (VTTS). B) Multiphase shrinkage(?) bubble from the "pink unit" of the "tuff of Pine Grove", (Utah) contains a vapor (b), a crystal (x) and a liquid (l). C) Hourglass inclusion from the 1912 eruption at the VTTS. D) Co-planar MI and FI in a lava from the Miocene Chocaya volcanic center, Bolivia. E) Moderate-density, vapor-rich FI from the "air fall" unit of the "tuff of Pine Grove". All photos by J.B. Lowenstern (unpublished data) except C, from Lowenstern (1993).

Another category of leaked MI has been called "hourglass" inclusions (Anderson, 1991), which consist of glass or crystallized melt connected to the outside of the host crystal by a canal or capillary (Fig. 1C). At magmatic temperatures, melt can be expelled from such inclusions, especially during magma ascent, causing nucleation and expansion of bubbles. The capillary can be sufficiently narrow that it forms a throttle that prevents complete equilibration with the external atmosphere. Anderson (1991) provided a theoretical framework and numerical method for understanding the devolatilization of such inclusions, with the aim of calculating the rate of magma ascent of hourglass-inclusion-bearing quartz. The article contains myriad observations and photos that have proven useful to a scientific community striving to understand the formation of MI and their behavior during magma ascent and eruption.

Presence of a separate vapor phase in mixed inclusions: The simplest evidence for the presence of vapors or other non-silicate fluids is their entrapment either as FI or within mixed inclusions in igneous phenocrysts. Vapor-rich FI that are trapped contemporaneously with (and separately from) silicate melt are common in intrusive rocks (Roedder, 1984, 1992; Frezzotti, 1992; Touret and Frezzoti, 1993; Lowenstern et al., 1997; Audétat et al., 2000; Dietrich et al., 2000; Frezzotti, 2001). Tuttle (1952) noted that whereas intrusive rocks often contained such inclusions, they were rare in volcanic rocks, which instead contained silicate MI. Anderson (1991) discussed a variety of possible reasons that vapor-rich FI are rarely present in the crystals within volcanic rocks. He concluded that any MI with a trapped vapor bubble would create a pressure gradient during magma ascent, preventing the inclusion from sealing. Tait (1992) postulated that MI with co-trapped vapor would be more likely to rupture during eruption. Also possible is that small bubbles are rare in long-lived magma chambers, and bubbles are unlikely to be trapped within sub-cm-sized crystals. As the magma becomes crystal-rich and the liquid is closer to saturation with a pure-H_2O vapor, small bubbles may nucleate and would be trapped more commonly, explaining the ubiquity of vapor-rich inclusions and contemporaneous entrapment of silicate liquid in intrusive rocks.

Nevertheless, some workers have discussed evidence for vapor-rich inclusions in volcanic rocks. Gutmann (1974) showed tubular voids in labradorite phenocrysts that were postulated to result from trapping of a vapor phase. Naumov and colleagues wrote a series of papers (summarized in Naumov et al., 1996) that discussed high-density H_2O-rich fluids in quartz from rhyolites of the Western Carpathians (Slovakia) and other locations. Vaggelli et al. (1993) discussed rare CO_2-rich FI in olivines and other minerals from mafic calc-alkaline eruptions at Stromboli. Métrich et al. (1993) performed 26 homogenization experiments on CO_2-rich FI in olivine phenocrysts found in tephras from the 1989-90 eruption at Etna. The thermometric data indicated entrapment at pressures of at least 100 to 140 MPa at 1100°C. Lowenstern (1995) showed photos of large (~100 μm) inclusions in quartz that had negative crystal shapes but were completely empty. As they were found in the same growth zones as glassy MI, he concluded that they were leaked FI (also see Fig. 1D, 1E). Pasteris et al. (1996) showed photos of much smaller vapor-rich and liquid-rich FI within volcanic phenocrysts from Pinatubo and concluded they were trapped during magma ascent.

Other evidence for entrapped vapors comes from anomalous bubbles within MI that cannot be explained either by shrinkage or leakage. Lowenstern et al. (1991) discovered that bubbles within some quartz-hosted MI in peralkaline rhyolites had anomalous Cu concentrations, and the Cu was located in Cu sulfides associated with salts precipitated on the bubble walls. The heterogeneous nature of the enrichment and association with large bubbles was consistent with occasional trapping of Cu-rich magmatic vapors (see also Lowenstern, 1993). Later studies from other volcanic systems have noted similar behavior for Cu and other ore metals. Yang and Scott (1996) found metal-rich bubbles in MI from submarine basalts of the Manus back-arc basin offshore in the western Pacific. Mineralization in MI-hosted bubbles included sulfides and chlorides of Cu, Zn and Fe. Kamenetsky et al. (2002) analyzed small crystals in FI, bubbles in MI and bubbles in matrix glass from a variety of young

submarine rocks. They document high volatility of a variety of metals and anions in low-pressure vapors exsolved from mafic magmas. Many of the bubbles in MI were interpreted as magmatic vapor trapped along with melt in mixed inclusions.

"Hydrosaline melts" in mixed inclusions: Perhaps hundreds of articles, primarily from the economic geology literature, have outlined evidence for highly saline fluid inclusions in shallow intrusive rocks. Typically, these hydrosaline melts coexist with CO_2-H_2O-dominated vapors at sub-magmatic temperatures (Roedder, 1984). Roedder and Coombs (1967) carefully documented immiscibility between highly saline fluids and silicate melts from the granite xenoliths of Ascension Island. More recent work on xenoliths and granitic rocks have found abundant evidence for hydrosaline phases, often in equilibrium with a CO_2-bearing vapor phase as well as silicate melt (Frezzotti, 1992; De Vivo et al. 1992, 1993; Yang and Bodnar, 1994; Belkin et al., 1996; Kamenetsky et al., 1999; Gilg et al., 2001; Fulignati et al., 2001; Campos et al., 2002). Webster and Rebbert (2001) studied Cl concentrations in silicate MI from the same xenoliths studied by Roedder and Coombs (1967). They noted a drop in Cl/H_2O with differentiation, consistent with fluid-saturated magmatic crystallization.

Though many of these saline fluids appear to form late during crystallization, hydrosaline melts have also been noted in crystal-poor volcanic rocks. Typically, they are found coexisting with silicate melt in mixed inclusions. For example, Solovova et al. (1991) and Lowenstern (1994) found hydrosaline melt droplets (~60-80% NaCl equivalent) within quartz-hosted silicate melt inclusions from peralkaline rhyolites. The hydrosaline fluids apparently were not trapped alone as discrete inclusions within the phenocryst phases, though similar crystallized salt droplets were found in the outgassed glassy matrix. The presence of the hydrosaline melt, together with a CO_2-H_2O-vapor and silicate melt at low pressure (< 100 MPa) caused buffering of the Cl concentration of the melt at a near-fixed value (Shinohara, 1994; Signorelli et al., 1999).

The hydrosaline melt need not consist solely of alkali chlorides and H_2O. Veksler et al. (2002) describe hydrothermal experiments at 100-200 MPa and 450-900°C where they formed silicate melt, vapor and a hydrosaline brine rich in P, B and F. The skarn-hosted hydrosaline melts from Vesuvius discussed both by Gilg et al. (2001) and Fulignati et al. (2001) crystallized to form carbonates, sulfates and fluorocarbonates as well as chlorides.

"Fluxed melts" and fluid-melt miscibility

Perhaps the most striking new development in melt-inclusion research is the work on pegmatitic melts, including homogenization of crystallized inclusions and quantification of their bulk compositions. Russian workers have studied this field for decades, but only recently have analytical techniques allowed quantification of some of the volatile and light elements that appear to be important in generation of these rock types. Many of these MI come from intrusive rocks, including pegmatites, but as discussed below, some are found in volcanic rocks as well. Kovalenko et al. (1996) studied MI from the pegmatites of Volhynia (Ukraine) and found them to be poor in SiO_2 (~60 wt.%), but rich in Al, F, H_2O, Li, Rb and a number of other trace elements. Thomas et al. (2000) recently showed that pegmatitic quartz from the Variscan

Ehrenfriedersdorf complex (Germany) trapped two immiscible silicate liquids, one higher in silica and lower in H_2O than the other. The fluids were trapped over a range of temperatures, beginning with a single supercritical fluid and separating along a solvus into two fluids that grew more distinct from each other as temperature declined. At 650°C, the more hydrous fluid contained ~38 wt.% SiO_2, 4% B_2O_3 2.6% F, 6% Cl and over 30% H_2O. At the same temperature, the silica-rich melt contained ~65% SiO_2, over 3% P_2O_5, 4.5% F and ~10% H_2O. Both phases contained more than 0.3% Rb_2O. A related study found enrichment of ore-related trace elements, particularly Sn (Thomas and Webster, 2000). Davidson and Kamenetsky (2001) found similar inclusions in subvolcanic rocks from the Rio Blanco porphyry system in Chile and hypothesized that these pegmatitic fluids may have an important role in some ore-forming systems. Sirbescu and Nabelek (2000) found evidence for equilibration between a pegmatitic melt containing Li, Cs, Rb, P and B with a H_2O-rich- and a CO_2-rich fluid. The three fluids coexisted at temperatures of 340°C and 270 MPa, some of the lowest known temperatures for silicate melts in the crust.

Such critical behavior is expected for melt-volatile systems, but at higher pressures and temperatures than demonstrated by Thomas et al. (2000). For example, Bureau and Keppler (1999) used an externally heated diamond-anvil cell to explore miscibility between silicate melts and hydrous fluids. Haplogranite-H_2O showed critical behavior above 900°C at 1.5 GPa. Sowerby and Keppler (2002) performed similar experiments on a synthetic pegmatite and were able to depress the critical pressure to 400 MPa at ~600°C. In comparison, the fluxed melts discussed by Thomas et al. (2000) exhibited supercritical behavior at temperatures > 700°C at only 100 MPa pressure. Such highly fluxed melts probably cannot ascend to the surface without crystallizing, and may never erupt as volcanic rocks. But erupted precursors of such rocks, including melts with very high halogen concentrations are well-documented (Congdon and Nash, 1991; Webster and Duffield, 1994). Moreover, these melts clearly have an important role in the formation of pegmatites and Sn-W, magma-hosted ore deposits.

LOOKING TO THE FUTURE

Improvements in techniques for analysis of MI have advanced our understanding of mantle melting and metasomatism, ore formation, pegmatite differentiation, volcanism, and planetary science. MI reveal that igneous melts can be diverse, can interact with unexpected materials and usually leave behind clues to their history. Sometimes igneous fluids are miscible when we expect them to unmix; other times numerous fluids are present when we expect only one. It is surprising and humbling to learn that micrometer-sized features yield so much information about km-sized magma bodies. Occasionally, analysis of MI may lead us astray. Boundary layers, re-equilibration and crystallization can somewhat alter the composition of these small parcels of igneous fluid. But through careful observation and analysis, we can identify these secondary processes and reconstruct the history of degassing, crystallization, mixing and unmixing recorded by melt inclusions in igneous rocks.

ACKNOWLEDGEMENTS

This work was supported by the U.S. Geological Survey's Volcano Hazard Program. I thank H. Belkin, P. Muffler and E. Roedder for helpful reviews.

REFERENCES

Anderson, A.T., Jr., 1974a, Evidence for a picritic, volatile-rich magma beneath Mt. Shasta, California, J. Petrol. 15, 243-267.

— 1974b, Chlorine, sulfur and water in magmas and oceans, Geol. Soc. Am. Bull. 85, 1485-1492.

— 1975, Some basaltic and andesitic gases, Rev. Geophys. Space Phys. 13, 37-55.

— 1991, Hourglass inclusions: Theory and application to the Bishop rhyolitic tuff, Am. Mineral. 76, 530-547.

Anderson, A.T., Jr., S. Newman, S.N. Williams, T.H. Druitt, C. Skirius and E. Stolper, 1989, H_2O, CO_2, Cl and gas in Plinian and ash-flow Bishop rhyolite, Geology, 17, 221-225.

Anderson, A.T., A.M. Davis and F. Lu, 2000, Evolution of Bishop Tuff rhyolitic magma based on melt and magnetite inclusions and zoned phenocrysts, J. Petrol. 41, 449-473.

Audétat, A., D. Günther and C.A. Heinrich, 2000, Magmatic-hydrothermal evolution in a fractionating granite: A microchemical study of the Sn-W-F mineralized Mole Granite (Australia), Geochim. Cosmochim. Acta 64, 3373-3393.

Bacon, C.R., S. Newman and E. Stolper, 1992, Water, CO_2, Cl, and F in melt inclusions in phenocrysts from three Holocene explosive eruptions, Crater Lake, Oregon, Am. Mineral. 77, 1021-1030.

Basaltic Volcanism Study Project, 1981, Basaltic volcanism on the terrestrial planets, Pergamon Press, New York, 1286 p.

Beddoe-Stephens, B., J.A. Aspden and T.J. Shepherd, 1983, Glass inclusions and melt compositions of the Toba tuffs, northern Sumatra, Contrib. Mineral. Petrol. 83, 278-287.

Belkin, H.E., B. De Vivo, A. Lima and K. Torok, 1996, Magmatic (silicates/saline/sulfur-rich/CO_2) immiscibility and zirconium and rare-earth element enrichment from alkaline magma chamber margins: evidence from Ponza Island, Pontine Archipelago, Italy, Eur. J. Mineral. 8, 1401-1420.

Best, M.G. , 1982, Igneous and Metamorphic Petrology, W.H. Freeman and Company, New York, 630 p.

Best, M.G. and E.H. Christiansen, 1997, Origin of broken phenocrysts in ash-flow tuffs, Geol. Soc. Am. Bull. 109, 63-73.

Bottinga, Y. and C. Allègre, 1976, Geophysical, petrological and geochemical models of the oceanic lithosphere, Tectonophys. 32, 9-59.

Bowen, N.L., 1928, The Evolution of the Igneous Rocks, Princeton University Press, Princeton, N.J., 332 p.

Buddington, A.F. and D.H. Lindsley, 1964, Iron-titanium oxide minerals and synthetic equivalents, J. Petrol. 5, 310-357.

Bureau, H. and H. Keppler, 1999, Complete miscibility between silicate melts and hydrous fluids in the upper mantle: experimental evidence and geochemical implications, Earth Planet. Sci. Lett. 165, 187-196.

Burnham, 1979a, Magmas and Hydrothermal Fluids, in Geochemistry of Hydrothermal Ore Deposits, Ed. H.L. Barnes, John Wiley and Sons, New York, pp. 71-136.

— 1979b, The importance of volatile constituents, in The Evolution of the Igneous Rocks: Fiftieth Anniversary Perspectives, Ed. H.S. Yoder , Princeton University Press, Princeton, NJ, pp. 439-482.

Burnham, C.W. and N.F. Davis, 1971, The role of H_2O in silicate melts: I. P–V–T relations in the system $NaAlSi_3O_8$–H_2O to 10 kilobars and 1000°C, Am. J. Sci. 270, 54-79.

Burnham, C.W. and R.H. Jahns, 1962, A method for determining the solubility of water in silicate melts, Am. J. Sci. 260, 721-745.

Campos, E., J.L.R. Touret, I. Nikogosian and J. Delgado, 2002, Overheated, Cu-bearing magmas in the Zaldívar porphyry-Cu deposit, Northern Chile. Geodynamic consequences, Tectonophys. 345, 229-251.

Carlson, R.W., 1987, Geochemical evolution of the crust and mantle, Rev. Geophys. 25, 1011-1020.

Carmichael, I.S.E., F.J. Turner and J. Verhoogen, 1974, Igneous Petrology (McGraw Hill Book Company), 739 p.

Cathelineau, M., C. Marignac, J. Dubessy, B. Poty, A. Weisbrod, C. Ramboz and J. Leroy, 1988, Fluids in granitic environment, Rend. Soc. Ital. Mineral. Petrol. 43, 263-274.

Christensen, J.N. and A.N. Halliday, 1996, Rb-Sr ages and Nd isotopic composition of melt inclusions from the Bishop Tuff and the generation of silicic magma, Earth Planet. Sci. Lett. 144, 547-561.

Clocchiatti, R., 1972, Les cristaux de quartz des ponces de la vallée des Dix Milles Fumées (Katmai, Alaska). CR Acad Sci Paris 274, 3037-3040.

— 1975, Les inclusions vitreuses des cristaux de quartz. Étude optique, thermo-optique et chimique. Applications géologiques, Mémoire Soc. Géol. France 122, 1-96.

Congdon, R.D. and W.P. Nash, 1991, Eruptive pegmatite magma: Rhyolite of the Honeycomb Hills, Utah, Am. Mineral. 76, 1261-1278.

Davidson, P. and V.S. Kamenetsky, 2001, Immiscibility and continuous felsic melt-fluid evolution within the Rio Blanco porphyry system, Chile: Evidence from inclusions in magmatic quartz, Econ. Geol. 96, 1921-1929.

De Vivo, B., M.–L. Frezzotti and G. Mahood, 1992, Fluid inclusions in xenoliths yield evidence for fluid evolution in peralkaline granitic bodies at Pantelleria (Italy), J. Volc. Geotherm. Res. 52, 295-301.

De Vivo, B., M.L. Frezzotti and A. Lima, 1993, Immiscibility in magmatic differentiation and fluid evolution in granitoid xenoliths at Pantelleria: Fluid inclusions evidence, Acta Vulcanol. 3, 195-202.

Dietrich, A., B. Lehmann and A. Wallianos, 2000, Bulk rock and melt inclusion geochemistry of Bolivian tin porphyry systems, Econ. Geol. 95, 313-326.

Dunbar, N.W. and R.L. Hervig, 1992, Petrogenesis and volatile stratigraphy of the Bishop Tuff: evidence from melt inclusion analysis, J. Geophys. Res. 97, 15129-15150.

Dunbar, N.W., R.L. Hervig and P.R. Kyle, 1989, Determination of pre-eruptive H_2O, F, and Cl contents of silicic magmas using melt inclusions: examples from Taupo volcanic center, New Zealand, Bull. Volc. 51, 177-184.

Eggler, D.H. and C.W. Burnham, 1973, Crystallization and fractionation trends in the system andesite–H_2O–CO_2–O_2 at pressures to 10 kb, Geol. Soc. Am. Bull., 84, 2517-2532.

Eichelberger, J.C., 1995, Silicic volcanism: Ascent of viscous magmas from crustal reservoirs, Annual. Rev. Earth Planet. Sci. 23, 41-63.

Ewart, A., D.C. Green, I.S.E. Carmichael and F.H. Brown, 1971, Voluminous low temperature rhyolitic magmas in New Zealand. Contrib. Mineral. Petrol, 33, 128-144.

Frezzotti, M.-L., 1992, Magmatic immiscibility and fluid phase evolution in the Mount Genis granite (southeastern Sardinia, Italy), Geochim. Cosmochim. Acta 56, 21-33.

Frezzotti, M.–L., 2001, Silicate-melt inclusions in magmatic rocks: applications to petrology, Lithos 55, 273-299.

Friedman, I., W. Long and R.L. Smith, 1963, Viscosity and water content of rhyolite glass, J. Geophys. Res. 68 (24), 6523-6535.

Fulignati, P., V.S. Kamenetsky, P. Marianelli, A. Sbrana and T.P. Mernagh, 2001, Melt inclusion record of immiscibility between silicate, hydrosaline and carbonate melts: Applications to skarn genesis at Mount Vesuvius, Geology 29, 1043-1046.

Ghiorso, M.S., 1987, Thermodynamics of minerals and melts, Rev. Geophys. 25, 1054-1064.

Gilg, H.A., A. Lima, R. Somma, H.E. Belkin, B. De Vivo and R.A. Ayuso, 2001, Isotope geochemistry and fluid inclusion study of skarns from Vesuvius, Mineral. Petrol. 73, 145-176.

Gill, J.,1981, Orogenic Andesites and Plate Tectonics, Springer-Verlag, Berlin, 390 p.

Gutmann, J.T., 1974, Tubular voids within labradorite phenocrysts from Sonora, Mexico, Am. Mineral. 59, 666-672.

Harris, D.M. and A.T. Anderson, Jr., 1983, Concentration, sources, and losses of H_2O, CO_2 and S in Kilauean basalt, Geochim. Cosmochim. Acta 47, 1139-1150.

Hauri, E.H., A.J.R. Kent and N. Arndt, Eds., 2002, Melt Inclusions at the Millennium: Toward a Deeper Understanding of Magmatic Processes, Spec. Vol. Chem. Geol. 103, 378 p.

Hervig, R.L. and N.W. Dunbar, 1992, Causes of chemical zoning in the Bishop (California) and Bandelier (New Mexico) magma chambers, Earth Planet. Sci. Lett. 111, 97-108.

Hildreth, W., 1979, The Bishop Tuff: evidence for the origin of compositional zonation in silicic magma chambers. Geol. Soc. Am. Spec. Paper 180, 43-75.

— 1981, Gradients in silicic magma chambers: Implications for lithospheric magmatism, J. Geophys. Res. 86, 10153-10192.

Hollister, L.S. and M.L. Crawford (eds.), 1982, Fluid Inclusions: Applications to Petrology, Mineral. Assoc. Canada Short Course Vol. 6, 304 pp.

Holloway, J.R., 1979, Volatile interactions in magmas, in Thermodynamics of Minerals and Melts, Eds. R.C. Newton, A. Navrotsky and B.J. Wood, Springer Verlag, Berlin, pp. 273-293.

Kamenetsky, V.S., R.C. Wolfe, S.M. Eggins, T.P. Mernagh and E. Bastrakov, 1999, Volatile exsolution at the Dinkidi Cu-Au porphyry deposit, Philippines: A melt-inclusion record of the initial ore-forming process, Geology 27, 691-694.

Kamenetsky, V.S., P. Davidson, T.P. Mernagh, A.J. Crawford, J.B. Gemmell, M.V. Portnyagin and R. Shinjo, 2002, Fluid bubbles in melt inclusions and pillow-rim glasses: high-temperature precursors to hydrothermal fluids? Chem. Geol. 183, 349-364.

Karsten, J.L., J.R. Holloway and J.R. Delaney, 1982, Ion microprobe studies of water in silicate melts; temperature-dependent water diffusion in obsidian, Earth Planet. Sci. Lett. 59, 420-428.

Kovalenko, V.I., G.M. Tsaryeva, V.B. Naumov, R.L. Hervig and S. Newman, 1996, Magma of pegmatites from Volhynia: Composition and crystallization parameters determined by magmatic inclusion studies. Petrology 4, 277-290.

Kudo, A.M. and D.F. Weill, 1970, An igneous plagioclase thermometer, Contrib. Mineral. Petrol. 25, 52-65.

Lowenstern, J.B., 1993, Evidence for a copper-bearing fluid in magma erupted at the Valley of Ten Thousand Smokes, Alaska, Contrib. Mineral. Petrol. 114, 409-421.

— 1994, Chlorine, fluid immiscibility, and degassing in peralkaline magmas from Pantelleria, Italy, Am. Mineral. 79, 353-369.

— 1995, Applications of silicate-melt inclusions to the study of magmatic volatiles, in Magmas, Fluids and Ore Deposits, Ed. J.F.H. Thompson, Min. Assoc. Canada Short Course vol. 23, 71-99.

Lowenstern, J.B. and G.A. Mahood, 1991, New data on magmatic H_2O contents of pantellerites, with implications for petrogenesis and eruptive dynamics at Pantelleria, Bull. Volcanol. 54, 78-83.

Lowenstern, J.B., G.A. Mahood, M.L. Rivers and S.R. Sutton, 1991, Evidence for extreme partitioning of copper into a magmatic vapor phase,. Science 252, 1405-1409.

Lowenstern, J.B., M.A. Clynne and T.D. Bullen, 1997, Comagmatic A-type granophyre and rhyolite from the Alid volcanic center, Eritrea, Northeast Africa, J. Petrol. 38, 1707-1721.

Lu, F., A.T. Anderson and A.M. Davis, 1992, Melt inclusions and crystal-liquid separation in rhyolitic magma of the Bishop Tuff, Contrib. Mineral. Petrol. 110, 113-120.

— 1995, Diffusional gradients at the crystal/melt interface and their effect on the composition of melt inclusions, J. Geol. 103, 591-597.

Maaløe, S.,1985, Principles of Igneous Petrology, Springer Verlag, Berlin, 374 p.

Mangan, M. and T.W. Sisson, 2000, Delayed, disequilibrium degassing in rhyolite magma; decompression experiments and implications for explosive volcanism, Earth Planet. Sci. Lett. 183, 441-455.

Manley, C.R., 1996, Morphology and maturation of melt inclusions in quartz phenocrysts from the Badlands rhyolite lava flow, southwestern Idaho, Am. Mineral. 81, 158-168.

Marianelli, P., N. Métrich and A. Sbrana, 1999, Shallow and deep reservoir involved in magma supply of the 1944 eruption of Vesuvius, Bull. Volc. 61, 48-63.

Marsh, B., 1987, Magmatic processes, Rev. Geophys. 25, 1043-1053.

Massare, D., N. Métrich, and R. Clocchiatti, 2002, High-temperature experiments on silicate melt inclusions in olivine at 1 atm: inference on temperatures of homogenization and H_2O concentrations, Chem. Geol. 183, 87-98.

McBirney, A.R., 1984, Igneous Petrology, Freeman, Cooper and Company, San Francisco, 504 p.

McCallum, I.S., 1987, Petrology of the igneous rocks, Rev. Geophys. 25, 1021-1042.

Melson, W.G., 1983, Monitoring the 1980-1982 eruptions of Mount St. Helens: Compositions and abundances of glass, Science 221, 1387-1391.

Merzbacher, C., and D.H. Eggler, 1984, A magmatic geohydrometer: Application to Mount St. Helens and other dacitic magmas, Geology 12, 587-590.

Métrich, N., R. Clocchiatti, M. Mosbah and M. Chaussidon, 1993, The 1989-1990 activity of Etna magma mingling and ascent of H_2O-Cl-S-rich basaltic magma. Evidence from melt inclusions, J. Volc. Geotherm. Res. 59, 131-144.

Métrich, N., A. Bertagnini, P. Landi and M. Rosi, 2001, Crystallization driven by decompression and water loss at Stromboli volcano (Aeolian Islands, Italy), J. Petrol. 42, 1471-1490.

Moore, J.G. and J.-G. Schilling, 1973, Vesicles, water and sulfur in Reykjanes Ridge Basalts, Contrib. Mineral. Petrol. 41, 105-118.

Muenow, D.W., D.G. Graham, N.W. Liu and J.R. Delaney, 1979, The abundance of volatiles in Hawaiian tholeiitic submarine basalts, Earth Planet. Sci. Lett. 42, 71-76.

Naumov, V.B., A.D. Babanskiy, A.M. Yerokhin and V.V. Shapenko, 1993, New possibilities in the methodology of studying melt and fluid inclusions in granite minerals, Geochem. Int. 30, 124-129.

Naumov, V.B., M.L. Tolstykh, V.A. Kovalenker, and N.N. Kononkova, 1996, Fluid overpressure in andesite melts from central Slovakia: Evidence from inclusions in minerals, Petrology 4, 265-276.

Newman, S., S. Epstein and E. Stolper, 1986, Measurement of water in rhyolitic glasses: calibration of an infrared spectroscopic technique, Am. Mineral. 71, 1527-1541.

Nielsen, C.H. and H. Sigurdsson, 1981, Quantitative methods for electron microprobe analysis of sodium in natural and synthetic glasses, Am. Mineral. 66, 547-552.

Palais, J.M. and H. Sigurdsson, 1989, Petrologic evidence of volatile emissions from major historic and pre-historic volcanic eruptions. In Understanding Climate Change, Eds. A. Berger, R. Dickenson and J.W. Kidson, Am. Geophys. Union Geophys. Mongr. 52, 31-53.

Pasteris, J.D., B. Wopenka, A. Wang and T.N. Harris, 1996, Relative timing of fluid and anhydrite saturation: Another consideration in the sulfur budget of the Mount Pinatubo eruption, in Fire and Mud: Eruptions and Lahars of Mount Pinatubo,

Philippines, Eds. C. G. Newhall and R.S. Punongbayan, University of Washington Press, Seattle, p. 875-891.

Roedder, E., 1965, Liquid CO_2 inclusions in olivine-bearing nodules and phenocrysts from basalts. Am. Mineral. 50, 1746-1782.

— 1979a, Fluid inclusions as samples of ore fluids, in Geochemistry of Hydrothermal Ore Deposits, Ed. H.L. Barnes, John Wiley and Sons, New York, pp. 684-737.

— 1979b, Origin and significance of magmatic inclusions. Bull. Mineral. 102, 487-510.

— 1984, Fluid Inclusions, Reviews Mineral. 12, Mineral. Soc. Am, Washington, D.C., 644 p.

— 1992, Fluid inclusion evidence for immiscibility in magmatic differentiation, Geochim. Cosmochim. Acta 56, 5-20.

Roedder, E. and D.S. Coombs, 1967, Immiscibility in granitic melts, indicated by fluid inclusions in ejected granitic blocks from Ascension Island, J. Petrol. 8, 417-451.

Roedder, E. and Weiblen, P.W., 1970, Lunar petrology of silicate melt inclusions, Apollo 11 rocks, Proc. Apollo 11 Lunar Science Conf., Geochim. Cosmochim. Acta, G.B., Suppl. I, pp. 801-837.

— 1971, Petrology of silicate melt inclusions, Apollo 11 and Apollo 12 and terrestrial equivalents, in Proc. Lunar Science Conf., 2nd Proc. v. 1, Geochim. Cosmochim. Acta, 2, 507-528.

Roggensack, K., 2001a, Sizing up crystals and their melt inclusions: a new approach to crystallization studies, Earth Planet. Sci. Lett. 187, 221-237.

— 2001b, Unraveling the 1974 eruption of Fuego volcano (Guatemala) with small crystals and their young melt inclusions, Geology 29, 911-914.

Roggensack, K., R.L. Hervig, S.B. McKnight and S.N. Williams, 1997, Explosive basaltic volcanism from Cerro Negro volcano: Influence of volatiles on eruptive style, Science 277, 1639-1642.

Self, S. and P.W. Francis, 1987, Volcanology, Rev. Geophys. 25, 1065-1078.

Shinohara, H., 1994, Exsolution of immiscible vapor and liquid phases from a crystallizing silicate melt: Implications for chlorine and metal transport, Geochim. Cosmochim. Acta 58, 5215-5221.

Signorelli, S., G. Vaggelli and C. Romano, 1999, Pre-eruptive volatile (H_2O, F, Cl and S) contents of phonolitic magmas feeding the 3550-year old Avellino eruption from Vesuvius, southern Italy, J. Volc. Geotherm. Res. 93, 237-256.

Sirbescu, M. C and P.I. Nabelek, 2000, Insights on internal differentiation of granitic pegmatites: A fluid inclusion approach, Geol. Soc. Am. Abstr. Prog. 32 (7) A-150.

Sisson, T.W. and G.D. Layne, 1993, H_2O in basalt and basaltic andesite glass inclusions from four subduction-related volcanoes, Earth Planet. Sci. Lett. 117, 619-635.

Skirius, C.M., J.W. Peterson and A.T. Anderson, Jr., 1990, Homogenizing rhyolitic glass inclusions from the Bishop Tuff, Am. Mineral. 75, 1381-1398.

Sobolev, A.V., 1996, Melt inclusions in minerals as a source of principle petrological information, Petrology 4, 209-220.

Sobolev, A.V. and L.V. Danushevsky, 1994, Petrology and geochemistry of boninites from the north termination of the Tonga Trench: constraints on the generation conditions of primary high-Ca boninite magmas, J. Petrol. 35, 1183-1211.

Sobolev, V.S. and V.P. Kostyuk, 1975, Magmatic crystallization based on a study of melt inclusions, Fluid Inclusion Research 9, 182-253 (translated from original publication in Russian).

Solovova, I, V. Naumov, A. Girnis, V. Kovalenko and A. Guzhova, 1991, High-temperature fluid heterogeneity: Evidences from microinclusions in Pantelleria volcanics, Plinius 5, 206.

Sommer, M.A., 1977, Volatiles H_2O, CO_2, and CO in silicate melt inclusions in quartz phenocrysts from the rhyolitic Bandelier air-fall and ash-flow tuff, New Mexico, J. Geology 85, 423-432.

Sommer, M.A. and L.S. Schramm, 1983, An analysis of the water concentrations in silicate melt inclusions in quartz phenocrysts from the Bandelier Tuff, Jemez Mountains, New Mexico, Bull. Volcanol. 46, 299-320.

Sorby, H.C., 1858, On the microscopic structure of crystals, indicating the origin of minerals and rocks, Geol. Soc. London Quart. J. 14 (1) 453-500.

Sowerby, J.R. and H. Keppler, 2002, The effect of fluorine, boron and excess sodium on the critical curve in the aplite–H_2O system, Contrib. Mineral. Petrol. 143, 32-37.

Stormer, J.C., Jr., 1975, A practical two-feldspar geothermometer, Am. Mineral. 60, 667-674.

Student, J.J. and R.J. Bodnar, 1996, Melt inclusion microthermometry: Petrologic constraints from the H_2O-saturated haplogranite system, Petrology 4 (3) 291-306.

Tait, S., 1992, Selective preservation of melt inclusions in igneous phenocrysts, Am. Mineral. 77, 146-155.

Takenouchi, S. and H. Imai, 1975, Glass and fluid inclusions in acidic igneous rocks from some mining areas in Japan, Econ. Geol. 70, 750-769.

Thomas, R., 2002, Determination of the H_3BO_3 concentration in fluid and melt inclusions in granite pegmatites by laser Raman microprobe spectroscopy, Am. Mineral. 87, 56-68.

Thomas, R. and J.D. Webster, 2000, Strong tin enrichment in a pegmatite-forming melt, Mineral. Deposita 35, 570-582.

Thomas, R., J.D. Webster and W. Heinrich, 2000, Melt inclusions in pegmatite quartz: complete miscibility between silicate melts and hydrous fluids at low pressure, Contrib. Mineral. Petrol 139, 394-401.

Touret, J.L.R. and M.–L. Frezzotti, 1993, Magmatic remnants in plutonic rocks, Bull. Soc. Geol. France, Huitieme Serie, 164, 229-242.

Tuttle, O.F., 1952, Origin of the contrasting mineralogy of extrusive and plutonic salic rocks, J. Geol. 60, 107-124.

Vaggelli, G., H.E. Belkin and L. Francalanci, 1993, Silicate-melt inclusions in the mineral phases of the Stromboli volcanic rocks: a contribution to the understanding of magmatic processes, Acta Vulc. 3, 115-125.

Van den Bogaard, P. and C. Schirnick, 1995, $^{40}Ar/^{39}Ar$ laser probe ages of Bishop Tuff quartz phenocrysts substantiate long-lived silicic magma chamber at Long Valley, United States, Geology 23, 759-762.

Veskler, I.V., R. Thomas and C. Schmidt, 2002, Experimental evidence of three coexisting immiscible fluids in synthetic granitic pegmatite, Am. Mineral. 87, 775-779.

Wallace, P.J., and A.T. Anderson, 1998, Effects of eruption and lava drainback on the H_2O contents of basaltic magmas at Kilauea volcano, Bull. Volcanol. 59, 327-344.

Wallace, P.J., A.T. Anderson, and A.M. Davis, 1995, Quantification of pre-eruptive exsolved gas contents in silicic magmas, Nature 377, 612-616.

— 1999, Gradients in H_2O, CO_2 and exsolved gas in a large-volume silicic magma systems: interpreting the record preserved in melt inclusions from the Bishop Tuff, J. Geophys. Res. 104, 20097-20122.

Watson, E.B., 1976, Glass inclusions as samples of early magmatic liquid: Determinative method and application to a South Atlantic basalt, J. Volc. Geotherm. Res 1, 73-84.

Watson, E.B., M.A. Sneeringer and A. Ross, 1982, Diffusion of dissolved carbonate in magmas: Experimental results and applications, Earth Planet. Sci. Lett., 61, 346-358.

Webster, J.D. and W.A. Duffield, 1994, Extreme halogen abundances in tin-rich magma of the Taylor Creek rhyolite, New Mexico, Econ. Geol. 89, 840-850.

Webster, J.D. and C.R. Rebbert, 2001, The geochemical signature of fluid-saturated magma determined from silicate melt inclusions in Ascension Island granite xenoliths, Geochim. Cosmochim. Acta 65, 123-136.

White, W.M. and A.W. Hoffmann, 1982, Sr and Nd isotope geochemistry of oceanic basalts and mantle evolution, Nature 296, 821-825.

Whitney, J.A., 1984, Fugacities of sulfurous gases in pyrrhotite-bearing silicic magmas, Am. Mineral. 69, 69-78.

Winick, J.A., W.C. McIntosh and N.W. Dunbar, 2001, Melt-inclusion-hosted excess ^{40}Ar in quartz crystals of the Bishop and Bandelier magma systems, Geology 29, 275-278.

Wones, D.R., 1972, Stability of biotite: A reply, Am. Mineral. 57, 316-317.

Wood, B.J. and S. Banno, 1973, Garnet-orthopyroxene and orthopyroxene-clinopyroxene relationships in simple and complex systems, Contrib. Mineral. Petrol. 42, 109-124.

Wyllie, P.J., 1979, Magmas and volatile components, Am. Mineral. 64, 469-500.

Yang, K. and R.J. Bodnar, 1994, Magmatic-Hydrothermal evolution in the "Bottoms" of porphyry copper systems: Evidence from silicate melt and aqueous fluid inclusions in granitoid intrusions in the Gyeongsang Basin, South Korea, International Geology Rev. 36, 608-628.

Yang, K. and S.D. Scott, 1996, Possible contribution of a metal-rich magmatic fluid to a sea-floor hydrothermal system, Nature 383, 420-423.

Zirkel, F., 1873, Die mikroscopische Beschaftenheit der Mineralien und Gesteine, Wilhelm Englemann, Leipzig, 502 p.

This Page Intentionally Left Blank

Estimating the Time scales of Magmatic Processes

Chris Hawkesworth[1], Rhiannon George[1], Simon Turner[1], and Georg Zellmer[2]

[1]Department of Earth Sciences, University of Bristol, Wills Memorial Building, Queens Road, Bristol BS8 1RJ, UK.
[2]Lamont Doherty Earth Observatory, Geochemistry Building, 61 Route 9W, Palisades, New York 10964, U.S.A.

Abstract

A number of techniques have been developed to estimate time scales from magmatic rocks. The techniques may be usefully subdivided into those that yield absolute ages, as from short lived isotopes of the U-series, and those that yield relative ages. The latter include major and trace element profiles modified by diffusion, and they are calculated on the basis of how long individual crystals have been at magmatic temperatures as inferred from the mineralogy of the host rock. They have the advantage that individual rocks can be characterised in terms of the age profiles of their crystal populations.

Age information can be obtained from crystals, the whole rocks and the groundmass, and each yield information on different aspects of the evolution of the magmatic system. They range from eruption ages, best determined on minerals from the groundmass, to the pre-eruption crystallisation history inferred from phenocrysts, the residence of magmas in the crust, and the time scales of magma differentiation. One way to assess the geological reliability of the calculated ages is to see if similar ages are obtained from other age dating systems. It is argued that if crystals are very young at the time of bulk rock crystallisation, there may have been insufficient time for fractional crystallisation to have taken place. The estimated time scales for magma differentiation range from 1000 years to 200,000 years, and if differentiation is linked to fractional crystallisation/crustal melting, it is likely to be thermally controlled. Longer time scales are inferred for magmas that crystallised deep in the crust, and there appear to be fewer evolved magmas in areas of high melt generation rates. It is less clear whether there is any link between different magma series and their time scales of differentiation.

Introduction

An understanding of how natural processes take place requires good estimates of the rates at which they occur. The average rates of plate tectonic movements, and the vastness of Geologic Time, led to a sense that many changes take place slowly. The counter view is that changes take place much more rapidly in short lived events as typified most dramatically in meteorite impacts, but also in flash floods, earthquakes and volcanic eruptions. One challenge is to determine such rapid rates of change from the geologic record.

In the study of magmatic processes, the ability to determine time scales of a few years to tens of thousands of years has revolutionised models for partial melting and melt extraction beneath mid-ocean ridges and ocean islands (e.g. McKenzie, 1985). In island arcs reasonable rates of melt generation need to reconciled with apparently rapid transfer of hydrous fluids from the mantle wedge (Turner et al., 2001). For studies of partial melting, much of the time information comes from the application of short-lived isotopes, which are

Table 1 - Age Information from Volcanic Rocks

Eruption ages

- Crystals formed at the time of eruption, typically in the groundmass (U-Th-Ra)
- Whole rocks or minerals for readily degassed systems (K-Ar, Ar-Ar)

Pre-eruption ages

- Accessory phases such as zircon (U-Th); often modeled as the onset of crystallisation and linked to temperatures of crystallisation
- U-Th-Ra isotopes in major phases, but these also may reflect contributions from inclusions of melt and accessory minerals
- Ages of highly evolved magmas (Rb-Sr)
- Ages of individual crystals from diffusion modified major and trace element profiles
- Crystal Size Distributions to estimate the ages of crystal populations

Magma crustal residence times

- Models of whole-rock short-lived isotope ratios in steady-state systems
- Estimates of amounts of radioactive decay since magmas entered the crust (U-Th-Ra)

Time scales of magma differentiation

- Changes of U-Th-Ra isotopes with indices of differentiation in whole-rocks and/or groundmass
- Rb/Sr ages of high Rb/Sr evolved glasses

increasingly well determined by high precision mass spectrometry. Once magmas have formed, entered the crust, and begun to cool and differentiate, time scales can be determined from short lived isotopes, but also from major and trace element profiles that have been modified by diffusion, from thermal modeling, and from the rates of changes in the volcanic stratigraphy. In this contribution we are concerned with how the time scales of crystallisation compare with those of magma differentiation, and the extent to which the latter may be different for different magmatic associations. Recent developments have provided new insights into the time periods associated with the magmatic records preserved in melt inclusions, and there is continuing debate over the insights available from the new information on the time scales of magmatic processes.

Magmas crystallize over a range in temperature, and in principle there is ample opportunity for early formed crystals to separate from the liquid, and for this to be the primary mechanism of differentiation in magmatic systems. Crystals form in response to cooling of the magma, decompression and degassing, and the time scales of crystallisation may be very different in such different regimes. The rate of crystallization can be a response to falling temperature, whereupon it increases with the rate of cooling, and hence with decreasing depth in the crust. In some cases this may take 10s to 100s of thousands of years (e.g. Davies and Halliday, 1998; Halliday et al. 1989, 1991; Reid et al., 1997; Charlier and Zellmer, 2000; Hawkesworth et al., 2000). Alternatively, if crystallization

occurs in response to decompression or magma degassing, it can be extremely rapid and take place over days or weeks (e.g. Nakamura, 1995; Brophy *et al.*, 1999; Blundy and Cashman, 2001) to a few hundred years (Zellmer et al., in press). Subsequently, the ease, and hence the time required for crystal-liquid separation to occur depends on the density contrast between the crystals and the liquid, the viscosity of the liquid, the size of the crystals and on the dynamics of the magma chamber system. Crystallization results in a build up of volatiles in the liquid, which may in turn trigger explosive eruptions; conversely, magma degassing can cause crystallization.

Thus, there is considerable interest in the links between crystallization and volcanic eruptions, and in the primary controls on magma differentiation. Critically, when crystallisation takes place in response to degassing and/or decompression, the time scales may be too short for efficient separation of the crystals and liquid, and hence for fractional crystallisation.

The presence of crystals of different sizes in igneous rocks highlights the fact that crystals form under different conditions, and that (a) different aspects of an igneous rock can be dated, and hence (b) they provide information on different magmatic processes (Fig. 1; Table 1). Crystals can be dated, either by *in situ* techniques or as mineral separates that may contain 10s to 100s of crystals. The larger crystals may yield information about the pre-eruption history of the magmatic system, or they may be unrelated xenocrysts. The ages of groundmass crystals provide the best information on the eruption age of the host magma

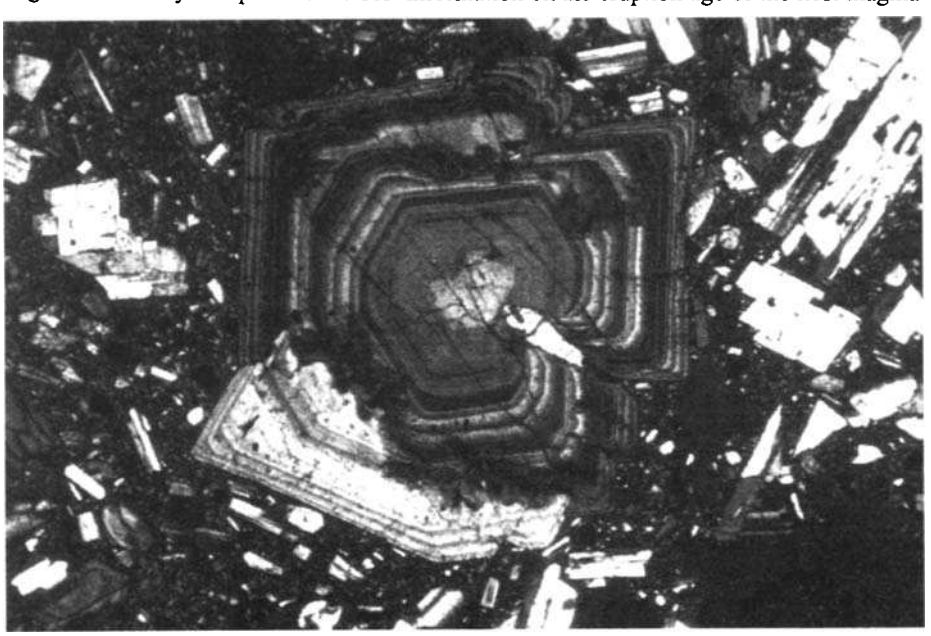

Fig. 1 A thin section of basaltic andesite highlighting the complex magmatic records preserved in plagioclase phenocrysts, and the different, much younger record in the microlites and groundmass. The latter will clearly yield ages much closer to that of eruption and whole rock crystallisation.

which has long been a principle goal of many geochronologic studies. Finally, it may be possible to estimate the 'age' of the liquid component of the magma, as for example preserved in the bulk groundmass, which should in turn reflect the age of the parental magma, and when magma differentiation took place. If the key question is 'how long did differentiation take for this magma' then it is much more robust to estimate the age of the differentiated magma, than the age of the crystals (Hawkesworth et al., 2001). Crystals yield spectacular records of how magmas have evolved, but (a) they are still in the host rock, and so they are not responsible for the differentiation of their host rock, and (b) it is difficult to determine whether they are xenocrysts, and hence perhaps not closely related to the differentiation processes being studied.

Dating techniques

Formally, dating techniques can be sub-divided into those that yield absolute ages, in essence dependent on an agreed half life for the isotopes in question, and those that yield relative ages. Short-lived radiogenic isotopes yield absolute ages, more so even than radiocarbon, since the latter is often sensitive to assumptions about ^{14}C fluxes, and the presence or absence of any 'old' carbon. In particular, the development of improved mass spectrometric techniques has prompted a significant increase in the number of U-series isotope analyses on volcanic rocks and separated minerals. The more widely used isotopes of ^{230}Th and ^{226}Ra have half lives of 75.4 ky and 1.6 ky respectively and they can be used to investigate processes operative within the last 300 ky. Other potentially useful isotopes in the study of magmatic processes have half lives of a few decades, or even days, such as ^{210}Pb, ^{210}Bi and ^{210}Po, and these are typically determined by counting techniques (see, for example, Lambert et al., 1986). Some of these shorter lived isotope systems are part of radioactive decay chains that involve a gaseous phase, and so in principle they provide information on the time scales of magma degassing processes.

Relative ages from igneous rocks include those of crystal populations inferred from crystal size distributions (CSD) (Marsh, 1998), and the ages and growth rates of individual crystals from major, trace element and Sr isotope profiles in crystals that may have been modified by diffusion (Nakamura, 1995; Knesel *et al.*, 1999; Zellmer *et al.*, 1999; Morgan *et al.*, 2002, Zellmer et al., in press). The latter rely on methods to predict the distribution of elements and isotopes in a crystal at the time of crystallisation, and then by comparison with the present day profiles to estimate the extent they have been modified by diffusion. That, in turn, constrains the length of time those individual crystals were present at high temperatures after formation, and the strength of the approach is that the histories of individual crystals can be unravelled. A weakness is that the approach yields no absolute ages, we infer the length of time the crystal was at high temperatures, but not when that was. Other approaches include the time scales over which isotope ratios and other chemical parameters change either within zoned eruptive units or between different units in an eruption sequence (Hobden et al. 1999). In general, these rely on models for distinguishing the emplacement of different parental magmas, and rocks that are related by fractional crystallisation from similar parental magmas.

U-series isotopes

The radiogenic isotopes of Pb are the end products of a decay chain of intermediate isotopes which have very short half lives relative to their parents, and so can be used to date rocks and minerals formed within the last few hundred thousand years. Their distinctive feature is that they involve intermediate isotopes that are parts of decay chains, and so both the parent and the daughter isotopes are radioactive. Thus, in a uranium-bearing system that has been left undisturbed for a few million years, a state of secular equilibrium is established such that the rate of decay, or the 'activity', of the daughter nuclide in the chain is equal to that of the parent. If that decay chain is disturbed by the fractionation of a parent from a daughter nuclide it takes time for secular equilibrium to be restored by radioactive decay. In that period before secular equilibrium is restored, the age of the fractionation event can be determined from the measured isotope ratios (see Gill *et al.*, 1992, and Dickin, 1995, for fuller discussions of the short-lived isotope dating techniques).

U-Th and Ra-Th isotope results are usually presented on an isochron, or equiline, diagram (Fig. 2), in which the parent and the daughter isotopes are normalised to an isotope not involved in the decay scheme. The isotope ratios are expressed as activity ratios, and so in secular equilibrium the activity ratios involving the parent and the

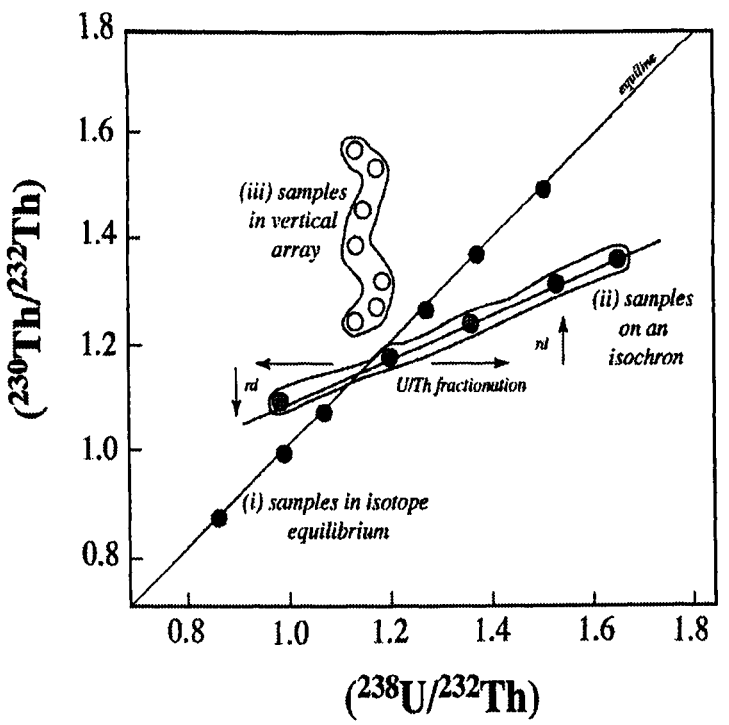

daughter isotopes are unity. All samples in secular equilibrium therefore plot on the 1:1 line on an isochron diagram (Fig. 2), and this line is known as the equiline (Allègre & Condomines, 1976). Secular equilibrium is disturbed by any process that fractionates the parent from the daughter nuclides, in this case U from Th, and when that process took place is determined by the difference between the initial and the present day Th isotope ratios. The initial Th isotope ratio is that of the magma at the time of the event that is being studied. It may therefore be significantly different from the Th isotope ratios of magmas at the time of eruption, and in practice age information is often obtained in one of two ways.

First, samples with different U/Th ratios may plot on a positive linear array, an isochron (Figs. 2 & 3), and the slope of that array will correspond to an age. That age will be the time of formation of the different U/Th ratios, and the age will be geologically meaningful if the samples had the same initial Th isotope ratio, and their U/Th and Th isotope ratios have remained in a closed system subsequently. In igneous systems, the samples with different U/Th ratios may be suites of comagmatic whole rocks or mineral separates. However, U and Th are highly incompatible in most common igneous minerals, and so closed system differentiation processes usually do not result in significant variations in U/Th ratios. Exceptions include magnetite, which appears to have very variable U/Th ratios, and other parent/daughter ratios, such as Ra/Th, are fractionated by, for example, the feldspars (e. g. Reagan et al., 1992). Accessory minerals, such as apatite and zircon may also show strong ^{230}Th-^{238}U disequilibria, and if these minerals crystallised at the time of eruption their U-Th isotope compositions can be used to determine the ages of volcanic rocks (e.g. Condomines, 1997).

Second, while many comagmatic igneous rocks have similar U/Th ratios, in some cases they have very different Th isotope ratios. Thus, they plot in a near vertical array on a U-Th equiline diagram (Fig. 2). In primitive rocks such vertical arrays may reflect dynamic melting processes (e.g. McKenzie, 1985), but in rocks related by fractional crystallization they may reflect the time taken for fractional crystallization to occur. In the latter

Fig. 2. A U-Th equiline, or isochron, diagram illustrating the kind of age information that can be obtained for three different sets of samples. ^{238}U decays through a number of intermediate isotopes to ^{230}Th, and ^{230}Th decays to ^{226}Ra with a half life of 75.4 ky. Samples that are older than ~5 times the half life, i.e. ~350 ky, plot on the equiline with (^{230}Th/^{232}Th) ratios that reflect their (^{238}U/^{230}Th) ratios (group i), and the only age information that can be obtained is that these samples are older than 350 ky. If samples plot off the equiline and define an isochron (group ii), their age can be calculated since the slope = 1-e? t (see also Fig. 3). The assumptions are that at time t all the samples had the same Th isotope ratio, and different U/Th ratios, and that they would therefore have plotted on a horizontal line on the U-Th equiline diagram. If samples plot to the right of the equiline they are said to have excess ^{238}U, and if they plot to the left they have excess ^{230}Th. Samples with excess ^{238}U and excess ^{230}Th migrate vertically towards the equiline at a rate that depends on the half life of ^{230}Th, and hence the slope of the isochron = 1-$e^{\lambda t}$. The samples in group (iii) have variable (^{230}Th/^{232}Th) and almost constant (^{238}U/^{230}Th), and so the time needed to move from the sample with the greatest to the least (^{230}Th-^{238}U) can also be calculated from the decay equation (e.g. Dickin, 1995). (rd = radioactive decay.)

interpretation it is envisaged that the parental magma had high ($^{230}Th/^{232}Th$) and that the lower values are due to radioactive decay during magma differentiation (see discussion in Hawkesworth et al., 2000). U-Th-Ra isotopes are the most widely used in the study of igneous rocks, but there is also considerable potential to exploit isotopes with even shorter half lives, including ^{210}Pb (22 years), ^{210}Bi (5 days) and ^{210}Po (138 days), in addition to ^{231}Pa (32,000 years).

What magmatic events or processes can be dated?

Traditionally the main target of geochronology was the eruption or emplacement ages of igneous rocks. These were easy to date, and they provided key time markers in developing the chronology of particular areas. For Ar-Ar and Rb-Sr systems ages were obtained using whole rock samples, and a key underlying assumption was that the time periods over which the crystals grew and the rocks crystallised were short relative to the half-life of the isotope system. However, for systems with shorter half lives measured in 1000s of years, this assumption is less likely to be valid (e. g. Reid et al., 1997; Charlier and Zellmer, 2000), and that influences the sampling strategy. The shorter the half life, the more this will be an issue, since commonly invoked crystallisation times for phenocrysts are in the range of years to a few thousand years (Cashman and Marsh, 1988).

Ages on groundmass crystals

Short-lived isotopes can be used to determine eruption ages, but because the whole rocks often have similar parent/daughter element ratios, most studies have relied on mineral-whole rock isochrons. The minerals analysed must have crystallized at, or very close to, the time of eruption, and so the most reliable ages are those obtained on groundmass crystals. In practice the crystals are often accessory phases because they provide greater fractionation of, for example, U/Th ratios (Fig. 3a, Peate *et al.*, 1996; Condomines, 1997; Black *et al.*, 1998a).

Absolute ages on phenocryst minerals

The most striking minerals in volcanic rocks are phenocrysts (Fig. 1), with the term used loosely here because it is not always easy to recognise which individual crystals are xenocrysts. Phenocrysts provide spectacular records of magmatic processes that can now be unravelled for trace elements and isotope ratios (Tepley et al., 1999), as well as for major elements. The difficulty is in determining which liquids were responsible for the records in the crystals, and even the relationship between individual crystals and the host rock, if there is one.

Crystal ages are typically obtained by analysis of mineral separates that may contain 10s to 100s of grains. Thus it is difficult to be sure of the textural affiliation of each grain, and a few old grains, for example, can bias the measured age. Moreover, if these crystal ages are to be compared to the age of eruption of the host rock, the latter must be known independently.

There have now been a number of studies that have yielded a wide range of ages on recent volcanic rocks (e.g. Fig. 3b, Heath et al., 1998a). Most of the ages have been obtained from U-Th isotopes, but some are from Rb-Sr and Ar-Ar in high silica rocks, and

there is increasing information from Ra-Th isotopes (Cooper et al., 2001). Figure 4 summarises some of the available data on the ages of crystal separates in recent volcanic rocks at the time of eruption, plotted against an index of differentiation, molar Si + Al (after Hawkesworth *et al.*, 2000). These are framework forming elements in the liquid,

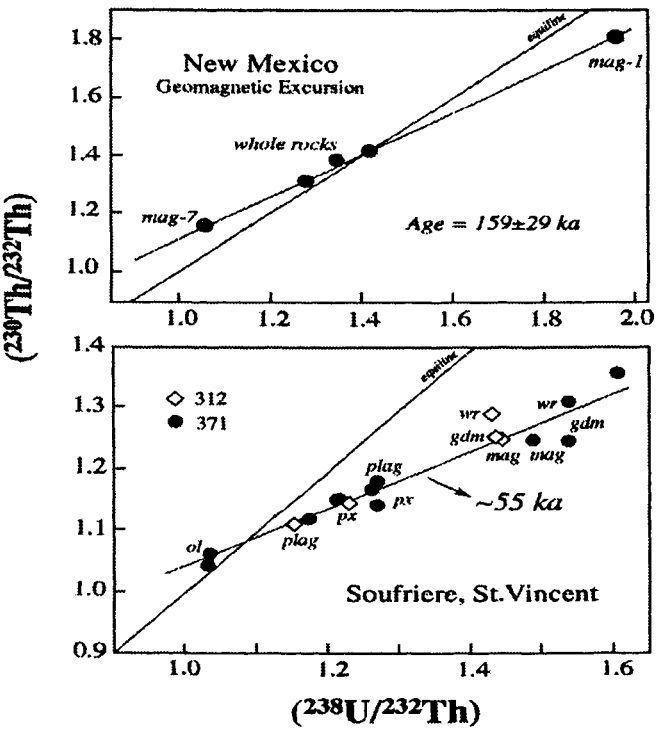

Fig. 3 Mineral-whole rock/groundmass isochrons from (a) New Mexico (Peate *et al.*, 1996) and (b) the Soufriere on St. Vincent in the Lesser Antilles (Heath et al., 1998a). In (a) an isochron on groundmass minerals yields an age of eruption for the host rock (the errors are two sigma). In (b) the apparent ages of ~55 ka is much older than the eruption ages (within the last 4ky), and the linear array may reflect mixing processes, and have no age significance, or it may indicate the ages of older minerals in this magmatic system.

there is a marked increase in the viscosity of liquids at Si + Al = ~66 (e.g. McBirney, 1984). Critically, most of the old pre-eruption mineral ages are from rocks with relatively high Si + Al values. Thus the simplest observation is the intuitive one that the likelihood of erupted magmas containing old crystals is much greater in the higher viscosity liquids.

It illustrates how most of the old mineral ages have been obtained from rocks with relatively high Si + Al contents, and these will also have higher viscosities. By contrast,

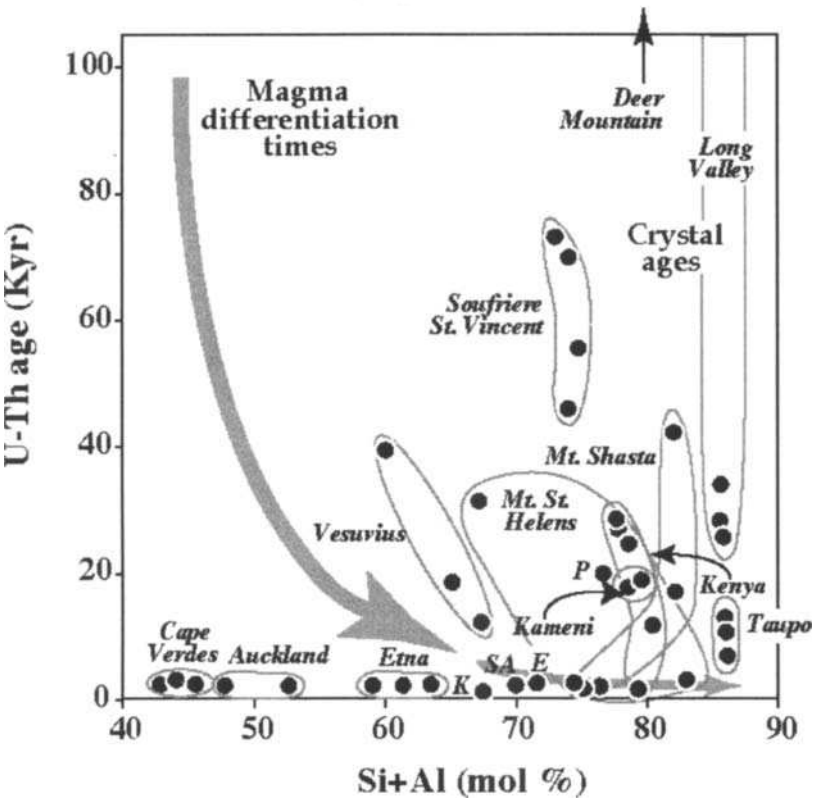

Fig. 4. A plot of age information, in many cases from internal ^{238}U-^{230}Th mineral isochrons, from recent volcanic rocks versus the Si + Al contents of the bulk rock (after Hawkesworth et al., 2000).

studies of the variations in U-Th isotopes in bulk rock samples of different major and trace element compositions (grey arrows) suggest that differentiation from basanitic parental magmas to more intermediate compositions can take 10s to ~200 ky. Moreover, the results of similar studies, principally using whole rock Ra-Th isotopes, suggest that the inferred differentiation times for more evolved liquids are very much shorter, perhaps 10s to 100s of years. Overall, such observations are consistent with slower rates of crystallisation and differentiation in more mafic magmas at greater depths, and much faster rates of differentiation in more evolved magmas at shallower depths. E denotes Erebus in Antarctica, K is Kilauea, 1955, P is Parinacota, Chile, and SA is Sangeang Api (data sources: Black et al., 1998a, b; Bourdon et al., 1994; 2000; Charlier and Zellmer, 2000; Cooper et al., 2001; Heath et al., 1998; Heumann and Davies, 2002; Heumann et al., 2002; Reagan et al., 1992; Reid et al., 1997; Turner et al., 2002; Volpe, 1992; Volpe and Hammond, 1991).

Simple cooling and crystal settling models also imply that primitive basalts affected solely by cooling in a chamber will contain a small proportion of near-liquidus phenocrysts

whereas more evolved magmas will have an increasing proportion of phenocrysts inherited from early stages of the magma's history. In detail it is difficult to evaluate the role of these 'old' crystals in the differentiation of the erupted magmas, not least because particularly in calc-alkaline rocks only the rims of phenocrysts may be in equilibrium with the host magma (e.g. Heath et al. 1998a & b). Non-equilibrium minerals with old ages may be xenocrysts incorporated by the magma en route to the surface, and as such provide little insight into magma residence times, or the time scales of magma differentiation. Alternatively, they may be minerals that crystallised from earlier magma batches, and so constrain the length of time over which a particular magma system has been active, but that is difficult to resolve.

Ra-Th isotopes offer the advantage of investigating the time scales of processes that occurred in the last few 1000 years. However, both elements are highly incompatible in the phases that crystallise from basaltic and intermediate magmas, and so their abundances measured in such mineral separates contain significant contributions from melt inclusions. Cooper et al. (2001) overcame this problem by calculating how the Ra-Th isotope ratios of magmas in equilibrium with the minerals would have changed with time, and hence when the magmas in equilibrium with the analysed minerals and the host magma had the same isotope composition. This is then the best estimate of the age of the crystals, and a minimum magmatic residence time of ~550 years was obtained for a relatively evolved magma from Kilauea on Hawaii (Cooper et al. 2001). Using the same approach, mineral ages up to 3000 years have been determined on rocks from Sangeang Api in Indonesia and from the Tonga arc (Turner et al., in press; George and Turner, unpublished). However there are still difficulties in that (a) these ages can be much less than those estimated from U-Th isotopes on the same samples, and the reasons are unclear. (b) In some cases the isotope ratios of the magmas in equilibrium with the minerals are not the same as those of the host rock, and no useful age can be obtained.

High Rb/Sr glasses and co-existing minerals

The old pre-eruption ages summarised in Figure 4 offer a tantalising glimpse of relatively long lived magmatic records. But a difficulty with all straight lines on isochron plots is that they may also be mixing lines, whose slopes need not have any age significance, and there remains the question of how their geological reliability should be assessed. One longstanding test of the reliability of geochronologic data has been to obtain similar, and hence concordant, ages from different radioactive decay schemes. For U-Th isotopes this can be done with highly evolved magmas that have very high Rb/Sr ratios, and hence yield Rb-Sr ages with very small errors. The latter were used to investigate the time scales of differentiation in the Bishop Tuff, where it was inferred that feldspar phenocrysts were stored in the chamber for 300 ka before eruption, and that there were also xenocrystic feldspars that were up to 1.3 Ma old at the time of eruption (Davies and Halliday, 1998). However, the Bishop Tuff was erupted at 760 ka, and so it is too old for U-series isotope analyses. But Heumann and Davies (2002) reported Sr and U-Th isotopes on separated glasses and mineral phases from peralkaline rhyolites from the Olkaria complex in Kenya.

The Olkaria rocks were erupted in the last 20 ka, and the glasses have Rb/Sr ratios up to ~600. They may therefore be dated with errors of 1 ka by conventional Sr isotope determinations. A mineral-glass Rb-Sr isochron age of 24±1 ka, and a U-Th age of 25±10

ka were obtained from a rhyolite erupted 8 ka ago. These concordant ages therefore provide confidence in the conclusion that the crystals and the high Rb/Sr liquids formed ~15 ka before eruption (Heumann and Davies, 2002). However, the results also highlight the very different characteristics of the two decay systems, in that the Rb-Sr age depends on the high Rb/Sr ratios of the glasses, and yet the glasses are in secular equilibrium for U-Th isotopes. In contrast, U/Th ratios are not readily fractionated between common major igneous minerals, and the observed spread of U/Th ratios is primarily attributed to accessory phases, in this case chevkinite, as inclusions in the major minerals. Thus, concordant ages have been obtained, even though the processes responsible for the Rb-Sr and U-Th ages are very different. The small error on the Rb-Sr age can also be used to constrain magma fractionation rates, and it was concluded that these were high at 2.5×10^{-3} km^3 of magma per year (Heumann and Davies, 2002).

Dating zircons using U-Th isotopes

Zircons are widely used in geochronology because they have high concentrations of U and Th, they are robust, and they are often zoned and can preserve records of a number of events. Thus, zircons may contain unique information on the timing of pre-eruption events in magmatic systems. Small amounts of zircon can be analysed, and as analytical techniques have evolved it is now possible to measure U and Th isotopes *in situ*. Obtaining precise absolute *in situ* ages is a major objective for such magmatic studies because it is much easier to ascertain what is being dated. The temperatures of zircon solubility, and hence of when zircon will crystallise can be calculated (Harrison and Watson, 1983), but it may be more difficult to establish how the timing of crystallisation of accessory phases such as zircon fits into the crystallisation history of the major phases, and hence with magma differentiation.

Rhyolite eruptions from the Taupo Volcanic Zone in North Island, New Zealand, are hazardous, and so they have been the subject of a number of studies to evaluate the volcanic risk. A key issue is the length of time that magma resides at shallow levels in the build up to major eruptions, since that influences the monitoring strategy. Charlier and Zellmer (2000) investigated the time scales of crystallisation in the 26.5 ka Oruanui eruption by analysing U-Th isotopes in different size fractions of zircons, because their U and Th concentrations were too low to allow *in situ* analyses. Somewhat unexpectedly they found that the zircon-whole rock U-Th ages were different in the three different zircon size fractions, ranging from 5.5 ka to 12.3 ka at the time of eruption (Fig. 5). Thus, there appeared to have been crystallisation ~10 ka before eruption, but was it an accurate estimate of the time scale of crystallisation? There were two useful observations; first, the larger zircons had the older zircon-whole rock ages, and the smaller zircons had the youngest ages, and second, cathodoluminescence showed that the zircon crystals typically have euhedral cores and rims, suggesting two components. The observed ages might therefore be modeled by mixing an older (~27 ka at the time of eruption) population of zircons with new zircons that crystallised shortly before eruption.

In practice it is therefore difficult to resolve whether the zircons crystallised continuously or not. A more useful question may therefore be to tie down when crystallisation started. Charlier and Zellmer (2000) argued that the overall ingrowth of ^{230}Th in a continuously growing crystal depended on the crystal growth rate. Using the estimated ($^{230}Th/^{232}Th$) value in the zircon cores, they calculated a zircon growth rate for

the cores of 2.1μm/kyr, implying that crystallisation started ~ 170 ka before eruption for the largest observed zircon core. This age is more than an order of magnitude older than the 12 ka conventional zircon-whole rock age for the largest size fraction, and oldest zircon fraction. Thus, zircons may have been present for 100-200 ka before eruption, and similar results were also obtained from an ion probe study of zircons from Long Valley Caldera in eastern California (Reid et al., 1997). In Long Valley the zircons yielded whole rock-zircon ages that clustered about 230 ka in two suites that were erupted 115 ka and 0.6 ka ago. Zircon saturation temperatures indicate that the magmas cooled to below 815°C more than 200 ka ago, but there is some uncertainty over whether the magmas solidified then and were subsequently remelted, or whether they had been crystal mushes since these zircons crystallised. This is a general problem with interpreting pre-eruption ages, and it may be that the change in ages with grain size in the Taupo rocks (Charlier and Zellmer, 2000) is the best evidence yet for long periods of crystallisation, irrespective of whether that was continuous or in discrete stages.

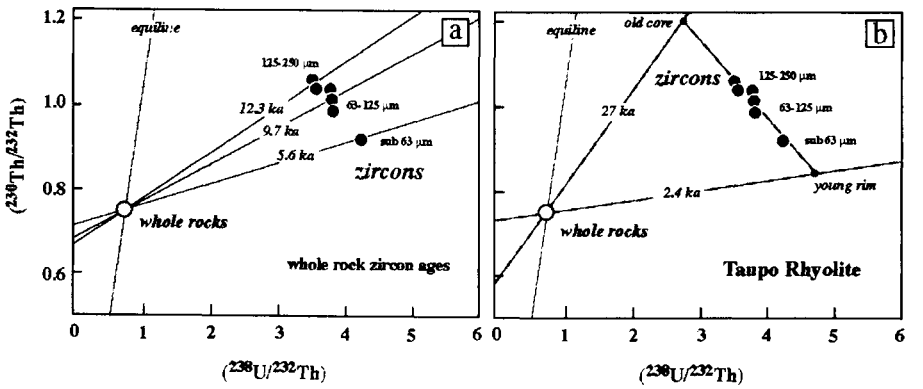

Fig. 5a Summary of the U-Th isotope results on whole rock and zircons of different size fractions from the 26.5 ka Oruanui rhyolite in the Taupo Volcanic Zone, New Zealand (Charlier and Zellmer, 2000). Zircon samples of different sizes have different calculated zircon-whole rock ages, which may reflect mixing between old and young zircon, as illustrated in Fig 5b.

In summary, there is relatively little U-Th fractionation between the common major igneous minerals, and melt inclusions contain U, Th and Ra contents that are much higher than the host minerals. Thus, many U-series mineral 'isochrons' may be dating the age of the inclusions, whether they are melt inclusions or accessory phases. The exceptions are Ra-Th in feldspar where the contribution from the melt inclusions can be corrected for (Cooper et al., 2001), and U-Th in zircons. There is now good evidence that zircons crystallised up to 100-200 ka before eruption (Reid et al., 1997; Charlier and Zellmer, 2000). Zircons only crystallise from evolved magmas, and so these are minimum ages for magmatic sytems in which the acid rocks formed by differentiation from more mafic precursors.

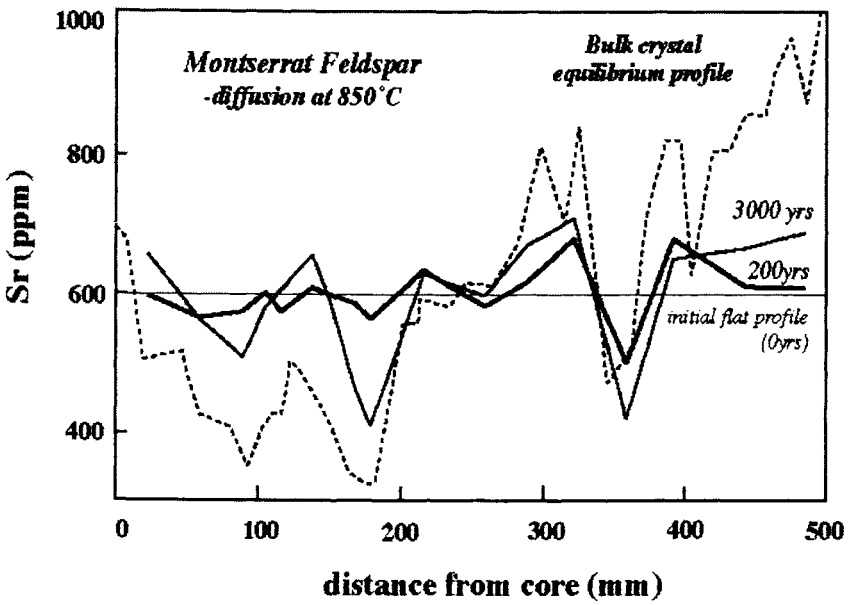

Fig. 6 Model showing the diffusive equilibration of an initially flat Sr profile towards bulk crystal equilibrium in plagioclase phenocryst MVO152-p7 at 850°C (Zellmer et al, in press). The calculated Sr contents are shown after 200 and 3000 yrs, and the equilibrium profile reflects the variation in An contents across the crystal.

Relative ages on 'phenocryst' minerals

Two similar approaches have been developed involving diffusive re-equilibrium across the boundaries of chemical zones that formed during crystallisation. One involves diffusion of Sr and Ba in plagioclase feldspars (Zellmer et al., 1999; in press), and the other diffusion of Fe and Mg in clinopyroxenes (Morgan et al., 2002). Zellmer et al. (in press) investigated plagioclase residence times at the Soufrière Hills volcano on Montserrat, West Indies, which has erupted andesitic lava since 1995. The andesites of the current eruption are very similar in mineralogy and geochemistry to the products of previous eruptions, and contain abundant inclusions of mafic magma which they show evidence for having been molten when incorporated into the andesite (Murphy *et al.*, 1998). The Montserrat plagioclase phenocrysts have (a) crystal growth surfaces with abundant melt pockets that were included into the crystal during growth, (b) multiple resorption surfaces characterised by rounded edges and truncation of growth surfaces, (c) large zones of partial resorption, and (d) multiple zones of partial resorption. Resorption surfaces and zones of partial resorption may also be intimately associated, suggesting that they were formed by the same process. In general, the plagioclase feldspars have complex growth histories consistent with periodic magma heating and remobilization.

The diffusion of Ca and Na in plagioclase is slow compared to that for Sr and Ba (Morse, 1984). Thus the present day variations in An contents are used to calculate the

initial variations in Sr and Ba at the time of crystallisation (Fig. 6). The initial Sr profiles were approximately flat, consistent with closed system crystallisation of the andesites. The partition coefficient for Sr is greater than 1 and it increases with decreasing X_{An}, but the increase in the proportion of Sr taken up into the growing crystal is balanced by the reduction of Sr in the liquid such that the Sr concentration within the crystal remains approximately constant (Zellmer et al., in press). The present day Sr and Ba element profiles indicate that they have not reached intracrystalline diffusive equilibrium (e.g. Fig. 6). There is no systematic variation in the degree of local disequilibria with distance from the crystal cores, and so it is inferred that the time scale for crystal growth is much shorter than the crystal residence times at magmatic temperatures. The crystals would appear to have grown rapidly in short bursts, and then stayed perhaps at magmatic temperatures, before the next period of crystal growth. The approach was in two steps, first to describe equilibrium between trace elements in adjacent zones of the crystals with variable An contents. If, as in the case of the Montserrat samples, equilibrium was not achieved, the second step was to investigate the time taken for a trace element profile to reach diffusive equilibrium. The latter depends on the temperature and the diffusion coefficients, which in turn vary with the An content of the feldspar.

The magmatic temperatures for the Montserrat andesites are ~860°C from pyroxene geothermometry (Murphy et al., 2000), and the magma would have crystallised completely at temperatures of ~ 800°C. Thus, plagioclase phenocryst residence times at 850°C were calculated using finite difference modelling of Sr diffusion, with both equilibrium partitioning and diffusion coefficients varying across each crystal due to the dependence of these parameters on anorthite content (Zellmer et al., in press). The calculated residence times range from ~1220 to ~10 years in 12 crystals of 6 samples from prehistoric and currently erupting andesites. These ages are relative ages, in the sense that the calculated ages are for the lengths of time the crystals resided at high temperatures, and not *when* that was. There is no link between the calculated residence times and the age of the host magma. The complex crystal growth histories, rapid crystal growth, and variable crystal residence time can be reconciled if small volumes of andesite are intermittently intruded into the upper crust where they crystallise rapidly, e.g. due to degassing. In such a model, differentiation to form the andesite magma took place deep in the crust, subsequent crystallisation of the observed minerals was fast, and the crystals were apparently too short lived for further differentiation to have taken place at shallow levels. Influx of mafic magma then led to amalgamation of the andesitic intrusives by remobilisation and convection, ultimately leading to eruption. Significantly, the shallow level magma residence times were short compared with the longevity of the volcano, and this is consistent with generation and long-term storage of andesite deep in the crust. It is concluded that the episodic ascent of deeply stored magma leads to formation of ephemeral magma reservoirs and episodes of intense volcanic activity.

In an analogous study Morgan et al. (2002) exploited the diffusional broadening of originally sharp discontinuities in clinopyroxene to calculate the magma residence times of individual clinopyroxene crystals. However, rather than analyse just one or two minerals from the same rock, they analysed 23 crystals from the same unit, the 1944 eruption from Vesuvius, and obtained a spread of ages that reflected the magma chamber volume. The strengths of this approach are, first, that the effects of diffusion are seen in the distribution of major elements, in this case Fe and Mg, and these can be determined to high spatial resolution using back-scattered electron images. The magmatic temperature for this

eruption was ~1080°C, and the time the different crystals were at this temperature ranged from 0 to 19 years before eruption. Second, this is the first study to determine the ages of a number of crystals from the same eruption, and the distribution of ages can be used to evaluate the nature of the magmatic processes. Vesuvius erupted every year from 1913 and 1944, and modeling the erupted volumes suggests a magma chamber volume of ~10^8 m^3. Moreover, the cumulative crystal residence curve implies that the near surface chamber was full from 1913 to 1944, awaiting only a large enough triggering input to cause an eruption.

Melt inclusions offer exceptional insights into the compositions of more primitive magmas, and into magma volatile contents prior to degassing. Sequences of melt inclusions across individual crystals may in principle chart the composition of the host magma during crystallisation, and the time period can be inferred from estimated crystallisation rates. Recently, however, Danyushevsky et al. (2002) developed a quantitative technique of estimating the time that high Fo olivines resided at high temperatures, from the time scale of re-equilibration of olivine crystallised from melt inclusions with the host olivine. Cooling of a melt inclusion after trapping in olivine results in crystallisation of olivine from the trapped melt, forming an olivine rim on the walls of the inclusion. Since the rim olivine has lower Fo contents than the host olivine, the degree of re-equilibration in Fe and Mg between the inclusion and the host can be used to estimate the time the olivine crystal was at high temperatures. Danyushevsky et al. (2002) concluded that re-equilibration is rapid, and that partial re-equilibration of up to 85% occurs within 3-5 months. They concluded that such short residence times are consistent with crystallisation from primitive, low viscosity magmas and efficient removal to cumulate zones at the base of the chamber. Olivines contain extremely small amounts of U, Th and Ra, and so their measured abundances in olivine separates will reflect the contributions from melt inclusions. In principle this offers an exciting new window into the short lived isotope disequilibria of the more primitive magma compositions preserved in melt inclusions in olivines.

Magma time scales and differentiation processes

If the degree of isotope disequilibrium of a magma when it leaves its melt zone is known, its isotope composition at the time of eruption can be used to constrain how long it took to move through the crust. This will vary depending on the thickness of the crust and the amounts of extension, and it may be accompanied by variable amounts of differentiation. In principle, the rate of magma transfer, and the rate of differentiation are different, and it may be possible to determine them separately (Table 1).

Figure 7 is a plot of ($^{226}Ra/^{230}Th$) activity ratios plotted against Th abundances as an index of differentiation for a number of magmatic suites. Samples are in secular equilibrium when ($^{226}Ra/^{230}Th$) = 1, and higher and lower values will evolve to ($^{226}Ra/^{230}Th$) =1 by radioactive decay. Thus diagrams such as Figure 7 can be used to infer the time scales of differentiation because they combine age information with indices of differentiation. Analogous diagrams for U-Th isotopes against indices of differentiation can also be plotted to investigate differentiation over longer time scales (e.g. Hawkesworth et al., 2000). In Figure 7 ($^{226}Ra/^{230}Th$), and hence the amount of Ra-Th isotope disequilibria, decreases with increasing Th contents in several selected volcanic suites, suggesting that the more evolved magmas are 'older' than the less evolved magmas. The initial point is

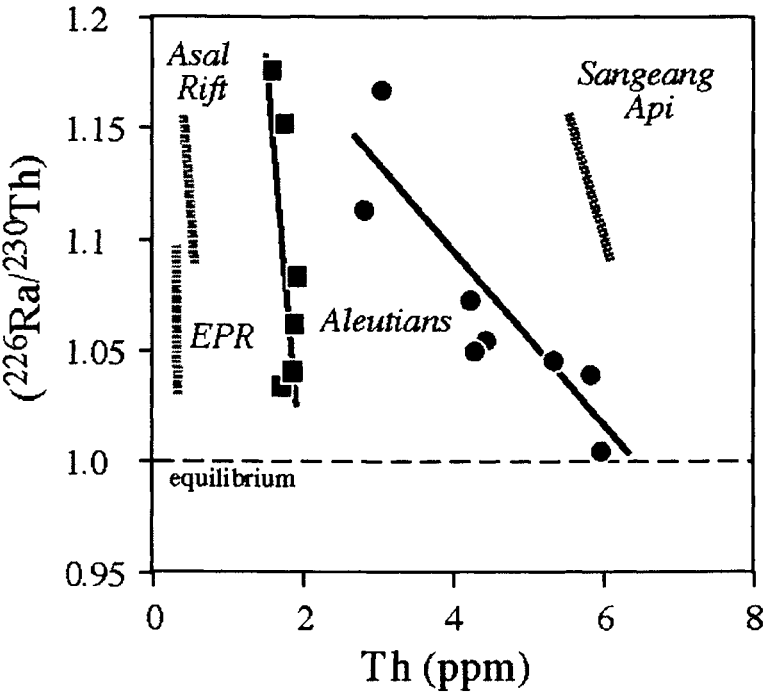

Fig. 7 A plot of ($^{226}Ra/^{230}Th$) versus Th contents for selected magmatic suites, after George et al. (2002). In particular, the tholeiitic lavas from Akutan and the calc-alkaline lavas from Aniakchak in the Aleutian-Alaskan arc preserve a similar range in ^{226}Ra-^{230}Th disequilibria even though the Aniakchak rocks (circles) experienced significant differentiation, and the Akutan (squares) have not. The slope of the Akutan lavas is similar to those of other tholeiitic lavas from extensional settings e.g. the Asal Rift (Vigier et al., 1999) and the East Pacific Rise (EPR; Sims et al., 2002), while the Aniakchak lavas have shallower slopes more akin to the Sangeang Api lavas (Turner et al., in press). If the rate of differentiation is proportional to the slope of the arrays, then the shallower the slope, the more differentiation was achieved per unit of ^{226}Ra decay, or time.

that the lower silica rocks have ($^{226}Ra/^{230}Th$) values of ~ 1.2 at the time of eruption. The highest known value from an island arc magma, for example, is ~6 (Turner et al., 2001), and even that may have already decayed by 50%. Such arguments indicate that magmas with ($^{226}Ra/^{230}Th$) of 1.2 were erupted within ~ 7,000 years of leaving the melt zone.

Obtaining more precise information on the time scales of differentiation from plots of ($^{226}Ra/^{230}Th$) versus an index of differentiation can be more difficult. In cases where differentiation is dominated by mixing with high silica materials, the variation in Ra-Th isotopes may also reflect mixing, and so no time information can be obtained. However, it is interesting that different magmatic suites have different slopes on the ($^{226}Ra/^{230}Th$)-Th

ppm diagram (Fig. 7), suggesting different rates of differentiation. Where the effects of magma mixing appear to have been minimal, time scales of differentiation range from 500 years up to 200,000 years using U-Th isotopes for phonolites differentiated from basanites at the base of the crust beneath Tenerife in the Canary Islands (Hawkesworth et al., 2001). George et al. (2002) undertook a detailed study of tholeiitic lavas from Akutan and calc-alkaline lavas from Aniakchak in the Aleutian-Alaskan arc. Strikingly, both lava suites preserve a similar range in ^{226}Ra-^{230}Th disequilibria even though the Aniakchak rocks experienced significant differentiation, and the Akutan have not (Fig. 7). It appears that the time scale of crustal residence of magmas beneath both these volcanoes was similar and on the order of a few 1000 years, despite their different differentiation histories. Such time scales are slow enough for differentiation to take place by cooling in crustal magma chambers rather than by faster decompression and degassing processes during ascent (e.g. Blundy and Cashman, 2001).

Early attempts to infer magma residence times from short lived isotopes developed models for steady state systems, such as Hawaii, Etna and Stromboli (Pyle, 1982; Albarede, 1993). Magma residence times of 10-100 years were obtained, and typically ~10% of the volume of the magma chamber was inferred to be erupted annually. More widely it appears that volcanoes that erupt semi-continuously have relatively small volumes of evolved magma types. In contrast, evolved magma types tend to be more common at volcanoes where eruptions are more episodic, and in western North America, for example, there is typically 200-300 ka of magmatic activity before caldera-related rhyolites are erupted. It would appear that significant amounts of time are required for the generation of evolved magmas. The implications are that differentiation is slow, and that it is therefore likely to be controlled by cooling, and/or that the differentiation processes include a significant amount of crustal melting (Annen and Sparks, 2002), or at least the remobilisation of crystalline mushes. An additional feature is that evolved magmas also tend to erupt late in the volcanic history of an individual eruptive centre. This may reflect decreases in the rate of cooling of the magma, allowing the establishment of long-lived magma reservoirs that are thermally buffered by hot host rocks.

Summary

As the number of dating techniques continue to grow it is important to isolate the process being dated (Table 1). Absolute and relative ages have been identified, the former have the advantage of yielding absolute ages, but the latter have the potential to yield ages for individual crystals, and hence information on the distribution of ages of crystal populations in a single whole rock. Crystals and liquids yield different ages, and the relative ages from individual crystals are often young, typically tens to hundreds of years. Crystals with very young ages may have formed during decompression and degassing, and they may be too young to have been involved in differentiation processes. Older ages are obtained from short lived isotopes, but these are on mineral separates and they are difficult to interpret. In some cases they may reflect older xenocrystic crystals that have little direct link to the magma in which they were erupted. Magma differentiation time scales are best evaluated from changes in short lived isotope ratios with increasing differentiation. It is important to use differentiation trends that cannot be simply attributed to mixing processes, since that may invalidate any calculated differentiation rates. Where this has been done it yields differentiation times of a few 1000 to 200,000 years, with the longer times being

inferred from systems where crystallisation and differentiation took place deep in the crust. In the case of Olkaria in the East Africa rift valley, the differentiated liquids themselves appear to have been 15,000 years old at the time of eruption.

Overall, it appears that when crystallisation is in response to decompression and degassing, the time scales are so short that it does not result in fractional crystallisation, and there is no time for whole rock differentiation. Conversely, when fractional crystallisation does take place it may be principally associated with crystallisation in response to cooling, which at one level simplifies attempts to model the process.

Acknowledgements

We thank Benedetto De Vivo and Robert Bodnar for organising a highly successful workshop on Melt Inclusions: Methods, Applications and Problems in the Sorrento area, Italy, in September 2002, and Patrick Allard and Rick Hervig for speedy and helpful reviews. We thank Steve Blake, Jon Blundy and Steve Sparks for many discussions on magma time scales and related topics, and gratefully acknowledge financial support from the Royal Society, the Leverhulme Trust and the NERC.

References

Albarède, F. 1993, Residence time analysis of geochemical fluctuations in volcanic series, Geochimica et Cosmochimica Acta 57, 615–621.

Allègre, C.J. and M. Condomines, 1976, Fine chronology of volcanic processes using ^{238}U-^{230}Th systematics, Earth and Planetary Science Letters 28, 395–406.

Annen, C. and R.S.J. Sparks, 2002, Effects of repetetive emplacement of basaltic intrusions on thermal evolution and melt generation in the crust, Earth and Planetary Science Letters, 203, 937-955.

Black, S., R. Macdonald, B.A. Barreiro, P.N. Dunkley and M. Smith, 1998a, Open system alkaline magmatism in northern Kenya: evidence from U-series disequilibria and radiogenic isotopes, Contributions to Mineralogy and Petrology 131, 364–378.

Black, S., R. Macdonald, B. De Vivo, C.R.J. Kilburn and G. Rolandi, 1998b, U-series disequilibria in young (A. D. 1944) Vesuvius rocks: Preliminary implications for magma residence times and volatile addition, Journal of Volcanology and Geothermal Research 82, 97-111.

Bourdon, B., A. Zindler, and G. Wörner, 1994, Evolution of the Laacher See magma chamber: Evidence from SIMS and TIMS measurements of U-Th disequilibria in minerals and glasses, Earth and Planetary Science Letters 126, 75–90.

Bourdon, B., G. Wörner and A. Zindler, 2000, U-series evidence for crustal involvement and magma residence times in the petrogenesis of Parinacota volcano, Chile, Contributions to Mineralogy and Petrology 139, 458–469.

Blundy, J. and K.V. Cashman, 2001, Ascent-driven crystallisation of dacite magmas at Mount St Helens, 1980-1986, Contributions to Mineralogy and Petrology 140, 631-650.

Brophy, J.G., C.S. Whittington and Y.R. Park, 1999, Sector-zoned augite megacrysts in Aleutian high alumina basalts: implications for the conditions of basalt

crystallization and the generation of calc-alkaline series magmas, Contributions to Mineralogy and Petrology 135, 277–290.

Cashman, K.V. and B.D. Marsh, 1988, Crystal size distribution (CSD) in rocks and the kinetics and dynamics of crystallisation II: Makaopuhi lava lake, Contributions to Mineralogy and Petrology 99, 292-305.

Charlier, B. L. A. and G.F. Zellmer, 2000, Some remarks on U-Th mineral ages from igneous rocks with prolonged crystallisation histories, Earth and Planetary Science Letters 183, 457-469.

Condomines, M., 1997, Dating recent volcanic rocks through ^{230}Th-^{238}U disequilibrium in accessory minerals: Example of the Puy de Dome (French Massif Central), Geology 25, 375-378.

Cooper, K.M., M.R. Reid, M.T. Murrell, and D.A. Clague, 2001, Crystal and magma residence at Kilauea Volcano, Hawaii: 230Th-226Ra dating of the 1955 east rift eruption, Earth and Planetary Science Letters 184, 703-718.

Danyushevsky, L.V., S. Solokov and T.J. Falloon, 2002, Melt inclusions in olivine phenocrysts: using diffusive re-equilibration to determine the cooling history of a crystal, with implications for the origin of olivine-phyric volcanic rocks, Journal of Petrology 43, 1651-1671.

Davies, G.R. and A.N. Halliday, 1998, Development of the Long Valley rhyolitic magma system; strontium and neodymium isotope evidence from glasses and individual phenocrysts, Geochimica et Cosmochimica Acta 62, 3561–3574.

Dickin, A.P. 1995, Radiogenic isotope geology. Cambridge University Press pp 490.

George, R., S. Turner, C. Hawkesworth, C. Nye, C. Bacon, P. Stelling, and S. Dreher, 2002, The time scales of magmatic differentiation at island arcs, Geochimica et Cosmochimica Acta 66, A270.

Gill, J.B., D.M. Pyle, R.W. Williams, M. Ivanovich, and R.S. Harmon, 1992, Igneous rocks. In Ivanovich, M. & Harmon, R.S. (eds.), Uranium-series disequilibrium: application to Earth, marine and environmental sciences, Clarendon Press, Oxford, pp. 207–259.

Halliday, A.N., G.A. Mahood, P. Holden, J.M. Metz, T.J. Dempster, and J.P. Davidson, 1989, Evidence for long residence times of rhyolitic magma in the Long Valley magmatic system – the isotopic record in precaldera lavas of Glass Mountain, Earth and Planetary Science Letters 94, 274–290.

Halliday, A.N., J.P. Davidson, W. Hildreth, and P. Holden, 1991, Modelling the petrogenesis of high Rb/Sr silicic magmas, Chemical Geology 92, 107–114.

Harrison, T. M. and E.B. Watson, 1983, Kinetics of zircon dissolution and zirconium diffusion in granitic melts of variable water content, Contributions to Mineralogy and Petrology 84, 66-72.

Hawkesworth, C., S. Blake, P. Evans, R. Hughes, R. MacDonald, L. Thomas, S. Turner and G.F. Zellmer 2000, Time Scales of Crystal Fractionation in Magma Chambers - Integrating Physical, Isotopic and Geochemical Perspectives, Journal of Petrology 41, 991-1006.

Hawkesworth, C.J., S. Blake, S.P. Turner and L.E. Thomas, 2001, Magma differentiation rates: combining isotopic constraints and thermal models, Eos 82, 261-265.

Heath, E., S.P. Turner, R. Macdonald, C.J. Hawkesworth and P. van Calsteren, 1998a, Long magma residence times at an island arc volcano (Soufriere, St. Vincent) in the Lesser Antilles: evidence from ^{238}U-^{230}Th isochron dating, Earth and Planetary Science Letters 160, 49–63.

Heath, E., R. Macdonald, H. Belkin, C. Hawkesworth and H. Sigurdsson, 1998b, Calc-alkaline magma genesis at Soufriere Volcano, St. Vincent, Lesser Antilles arc, Journal of Petrology 39, 1721–1764.

Heumann, A. and G.R. Davies, 2002, U-Th disequilibrium and Rb-Sr age constraints on the magmatic evolution of peralkaline rhyolites from Kenya, Journal of Petrology 43, 557-577.

Heumann, A., G.R. Davies and T. Elliott, 2002, Crystallisation history of rhyolites at Long Valley, California, inferred from combined U-series and Rb-Sr isotope systematics, Geochimica et Cosmochimica Acta 66, 1821–1837.

Hobden B.J., B.F. Houghton, J.P. Davidson and S.D. Weaver, 1999, Small and short-lived magma batches at composite volcanoes: time windows at Tongariro volcano, New Zealand, J. Geol. Soc. London. 156, 865-868.

Knesel, K.M., J.P. Davidson and W.A. Duffield, 1999, Evolution of silicic magma through assimilation and subsequent recharge: evidence from Sr isotopes in sanidine phenocrysts, Taylor Creek Rhyolite, N.M., Journal of Petrology 40, 773–786.

Lambert, G., M.-F. Le Cloarec, B. Ardouin, and J.-C. Le Roulley, 1986, Volcanic emission of radionuclides and magma dynamics, Earth and Planetary Science Letters 76, 185-192.

Marsh, B.D., 1998, On the interpretation of crystal size distributions in magmatic systems, Journal of Petrology 39, 553-599.

McBirney, A.R., 1984, Igneous Petrology. San Francisco: Freeman Cooper & Co., pp. 504.

McKenzie, D., 1985, Th^{230}-U^{238} Disequilibrium and the melting processes beneath ridge axes, Earth and Planetary Science Letters 72, 149–157.

Morgan, D., S. Blake and N. Rogers, 2002, Determination of crystal residence times and magma chamber volumes: Vesuvius 1944, Geochimica et Cosmochimica Acta 66, 15A, A525.

Morse, S.A. 1984, Cation diffusion in plagioclase feldspar, Science 225, 504-505.

Murphy, M.D., R.S.J. Sparks, J. Barclay, M.R. Carroll, A.-M. Lejeune, T.S. Brewer, R. Macdonald, S. Black and S. Young, 1998, The role of magma mixing in triggering the current eruption at the Soufriere Hills volcano, Montserrat, West Indies, Geophysical Research Letters 25, 3433-3436.

Murphy, M.D., R.S.J. Sparks, J. Barclay, M.R. Carroll and T.S. Brewer, 2000, Remobilization of andesite magma by intrusion of mafic magma at the Soufriere Hills volcano, Montserrat, West Indies, Journal of Petrology 41, 21-42.

Nakamura, M., 1995, Continuous mixing of crystal mush and replenished magma in the ongoing Unzen eruption, Geology 23, 807-810.

Peate, D.W., J.H. Chen, G.J. Wasserburg, D.A.Papanastassiou and J.W. Geissman, 1996, ^{238}U–^{230}Th dating of a geomagnetic excursion in Quaternary basalts of the Albuquerque volcanoes field, New Mexico (USA), Geophysical Research Letters 23, 2271–2274.

Pyle, D.M., 1992, The volume and residence time of magma beneath active volcanoes determined by decay-series disequilibria methods, Earth and Planetary Science Letters 112, 61–73.

Reagan, M.K., A.M. Volpe and K.V. Cashman, 1992, ^{238}U and ^{232}Th-series chronology of phonolite fractionation at Mount Erebus, Antarctica, Geochimica et Cosmochimica Acta 56, 1401–1407.

Reid, M.R., C.D. Coath, M. Harrison and K.D. McKeegan, 1997, Prolonged residence times for the youngest rhyolites associated with Long Valley Caldera: ^{230}Th-^{238}U ion microprobe dating of young zircons, Earth and Planetary Science Letters 150, 27–39.

Sims, K., S.J. Goldstein, J. Blichert-Toft, M.R. Perfit, P. Kelemen, D.J. Fornari, P. Michael, M.T. Murrell, S.R. Hart, D.J. DePaolo, G. Layne, L. Ball, M. Jull and J. Bender, 2002, Chemical and isotopic constraints on the generation and transport of magma beneath the East Pacific Rise, Geochimica et Cosmochimica Acta 66, 3481–3504.

Tepley, F.J.III, J.P. Davidson and M.A. Clynne, 1999, Magmatic interactions as recorded in plagioclase phenocrysts of Chaos Crags, Lassen volcanic center, California, Journal of Petrology 40, 787–806.

Turner, S.P., P. Evans and C.J. Hawkesworth, 2001, Ultrafast source-to-surface movement of melt at island arcs from ^{226}Ra-^{230}Th systematics, Science 292, 1363-1366.

Turner, S., J. Foden, R. George, P. Evans, R. Varne, M. Elberg and G. Jenner, 2002, Rates and processes of potassic magma generation at Sangeang Api volcano, east Sunda arc, Indonesia, Journal of Petrology in press.

Vigier, N., B. Bourdon, J.L. Joron and C.J. Allegre, 1999, U-decay series and trace element systematics in the 1978 eruption of Ardoukoba, Asal rift: timescale of magma crystallisation, Earth and Planetary Science Letters 174, 81-97.

Volpe, A. M., 1992, ^{238}U-^{230}Th-^{226}Ra disequilibrium in young Mt. Shasta andesites and dacites, Journal of Volcanology and Geothermal Research 53, 227-238.

Volpe, A.M. and P.E. Hammond, 1991, ^{238}U-^{230}Th-^{226}Ra disequilibria in young Mount St. Helens rocks: time constraint for magma formation and crystallisation, Earth and Planetary Science Letters 107, 475–486.

Zellmer, G.F., S. Blake, D. Vance, C. Hawkesworth and S. Turner, 1999, Plagioclase residence times at two island arc volcanoes (Kameni islands, Santorini, and Soufriere, St. Vincent) determined by Sr diffusion systematics, Contributions to Mineralogy and Petrology 136, 345-357.

Zellmer, G.F., R.S.J. Sparks, C.J. Hawkesworth, and M. Wiedenbeck, 2002, Remobilisation timescales beneath Montserrat: insights from Sr and Ba profiles across plagioclase phenocrysts, Journal of Petrology in press.

This Page Intentionally Left Blank

LIQUID TO GLASS: QUANTIFYING PROPERTIES AND STRUCTURE OF MELTS ACROSS THE GLASS TRANSITION.

Don B. Dingwell

Earth and Environmental Sciences, University of Munich, Theresienstr. 41/III, 80333 Munich, Germany

INTRODUCTION

The preservation of high temperature igneous liquids as glass in intrusive or eruptive rocks presents petrologists with the challenge or quantifying the temperature-dependent path of melt structure and properties from eruptive/emplacement temperature down to ambient temperature (i.e., far below the equilibrium crystallisation temperature range). Melts that experience such a transit appear 1) widely spread as a glassy matrix phase in many volcanic lithologies and 2) as glassy inclusions in crystals, so-called "melt inclusions", in an even wider range of igneous lithologies. This paper concerns the latter. A qualitative understanding of the conditions attendant on melt inclusions during their cooling presupposes a clear appreciation of the fundamental nature of the transition from liquid to glass, i.e. the so-called "glass transition". Quantification of those conditions must be based on a quantification of the temperature dependent properties of both the liquid and the glassy state. Only then can the P-T path of melt inclusions from near-liquidus conditions to room temperature be effectively partitioned into the temperature ranges corresponding to liquid-like and solid-like (i.e., glassy) properties and behavior.

Fortunately, great progress has been made in recent years in our understanding of the relevance of the glass transition for petrology and volcanology (Dingwell, 1995, 1996, 1998). As a result we are now better able to predict 1) the qualitative behavior of structure and properties across the glass transition, 2) the temperature of the glass transition as a function of chemical composition and cooling rate and the quantitative variation of melt properties from the liquid to the glassy state across the glass transition. This progress is briefly reviewed here.

BACKGROUND

In the first half of the 20th century, observations of inhomogeneity and variability in the refractive index and density of glasses led to an analysis of their origins via the thermal treatment of the glass (see review in Dingwell, 1995). These efforts led to the establishment of the concept of "fictive temperature" as a description of the physical state of a disequilibrium state, comparable to an order parameter in transition state theory. The fictive temperature was defined as the temperature at which the properties and structure of the glass would equal those of the equilibrium liquid. With this simple

statement we can use fictive temperature as a proxy for each thermodynamic property or structural element of a glass as it experiences the transition from the glassy to the liquid state, or vice versa. This fundamental behavior of the fictive temperature is illustrated in Fig. 1 where the variation of Tf versus temperature, is shown. For the liquid state, the structure and properties of the melt correspond to those of a metastable, supercooled liquid in local equilibrium with the temperature field. Thus Tf = T, as reflected in the upper right part of Fig. 1a. For the glassy state, the structure of the melt is not in equilibrium with the ambient temperature, rather it corresponds to a higher temperature where the structure was frozen in. Further, this structure does not change with temperature within the glassy range. Thus, the fictive temperature of the glass is a constant and higher than the ambient temperature. In the glass transition interval between purely glassy and purely liquid behavior, the fictive temperature is a transient whose value depends on the temperature dependence of the relaxation time of the system, the cooling history of the glass and the thermal history being applied during the measurement. This segment of the temperature-dependent properties of the melt, which corresponds to a mixture of solid-like and liquid-like (i.e. viscoelastic) response, is thus fundamentally path-dependent.

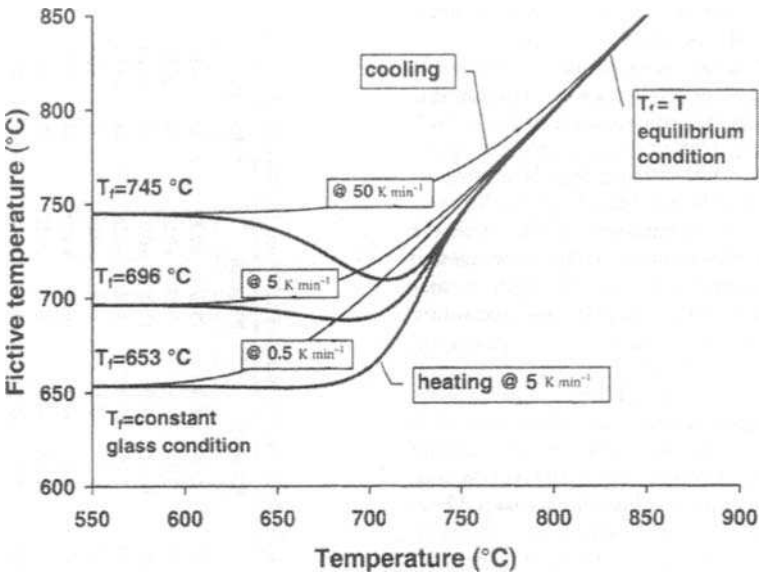

Fig. 1. Fictive temperature versus temperature for transects of the glass transition at rates of 0.5, 5 and 50 K/min. The cooling segments yield simple inflections from Tf = T to Tf = constant. The heating segments illustrate the hysteresis typical of glasses cooled very slowly in nature and then heated in the laboratory at a higher rate. In general, the variation in the transient value of melt properties across the glass transition is path-dependent. This means that there is information on the cooling path of natural glasses contained in their path-dependent behavior upon reheating across the glass transition (reproduced from Gottsmann and Dingwell, 2002).

Whether a 2nd order thermodynamic transition exists as a limiting case of the glass transition at long timescales is still being debated. Regardless of the outcome, for all practical purposes involving the quantification of property evolution through the glass transition, a fundamentally kinetic ansatz has been applied to the transition, with considerable success. Thus we understand and interpret the glass transition as a purely kinetic phenomenon. Given this premise it is clear that in addition to chemical composition, time scales must be defined in order to precisely predict the transition. If, on the other hand, the transition temperature is well defined, then we have a source of information on the timescales involved in cooling/quenching the melt inclusion.

Transition phenomenology

What is the phenomenological basis for such curves of Tf versus temperature? It comes to us from scanning calorimetric or dilatometric determinations of heat capacity and expansivity, respectively. Fig. 2a,b contains such illustrations of the experimental phenomenology of the glass transition. The transition is reflected in the temperature and/or pressure dependence of the properties of the system. Experimentally, the glass transition, defined as the transition in the molten state from liquid-like to solid-like behaviour, is most commonly observed during the determination of first or second order thermodynamic properties. For the case of first order thermodynamic properties such as volume and enthalpy, the transition is evident as the extrapolated intersection of the temperature-dependent properties of the liquid and glassy states (Fig. 2a).

Note that there is an inflection, but no discontinuity, in the temperature dependence of these properties across the glass transition. This is a fundamental distinction between the thermodynamics of melting/crystallisation versus those of crossing the glass transition. For the case of second order thermodynamic properties such as thermal expansivity or heat capacity, the transition impacts on the properties in the manner seen in Fig. 1b. Here the details of the property path from the glassy to the liquid state reveal a strong nonlinearity. The exact description of curves of the type seen in Fig 2b has been developed in the glass literature and recently applied in the geosciences. These curves contain information on the cooling rate, or, more generally, the thermal history, of the melt as it cooled across the glass transition temperature (see below). Every chemically pristine glass observed in nature thus contains information on its rate of cooling in nature. This information may be experimentally accessed. The liquid state is a metastable equilibrium state where properties are time independent and where the response of properties and structure to perturbations in intensive variables such as temperature appear to the observer as instantaneous. If phase transitions such as crystallization can be kinetically avoided, the metastable undercooled liquid transforms into a glass at the transition. The glass is a disequilibrium state. Properties of the glass may age over long timescales and the initial properties with which a glass is endowed upon cooling through the transition are path-dependent. That is to say the path through the glass transition determines glass properties, but not liquid properties.

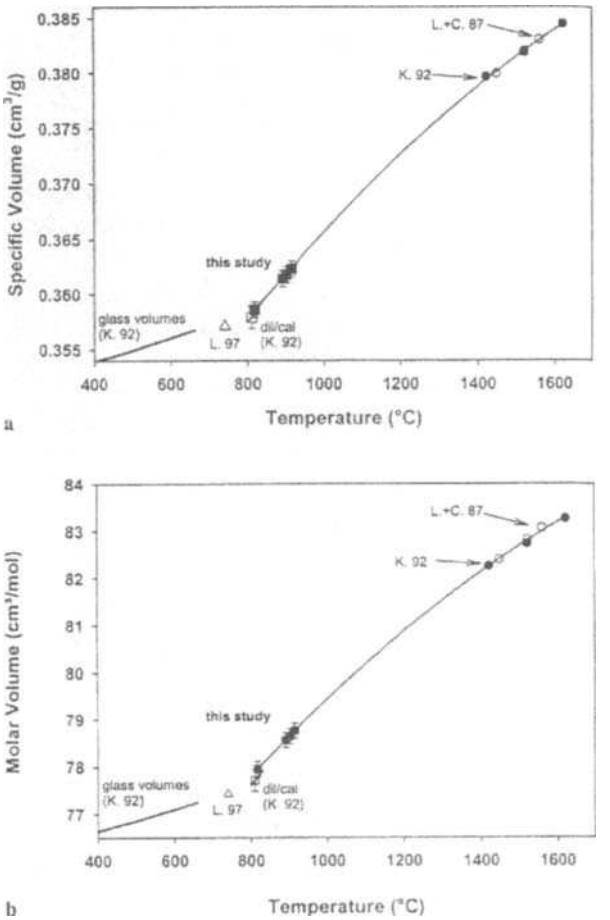

Fig. 2a. The variation of an integral thermodynamic property, the volume, across the glass transition. The specific and molar volumes of diopside melt from the glassy to the liquid state. The glass transition is clearly evident as the kink in the temperature dependence of the volume. At the glass transition the temperature dependence of volume increases from the glassy to the liquid state, (reproduced from Gottsmann and Dingwell, 2000)

Locating the glass transition

Prediction of the location of the glass transition of igneous melts has been accomplished by several methods. Conventions applied to the types of curves illustrated in Fig. 2b have been the position of the curve peak, or the extrapolated onset of the peak. Once it was realised however that the exact position of the glass transition phenomenon in calorimetry, dilatometry and a host of further property and structure determinations is controlled by the temperature dependence of the viscosity, it became clear that determining viscosity was perhaps the most reliable and effective way of

locating the glass transition. Perhaps the most straightforward method involves the Maxwell relation for viscoelasticity. The ratio of Newtonian viscosity to Hookean elasticity yields a quantity with the units of seconds. This time is the mean time required for the structure of the silicate melt to respond to perturbations of intensive variables. The structure defines the properties of the melts and so the transition occurs at this "relaxation" time for the given value of melt viscosity. A series of equations relating relaxation time, viscosity at the glass transition and cooling rate, have been developed, which allow prediction of the glass transition in time and temperature for a melt for which the Newtonian viscosity is well known (Dingwell and Webb 1989,1990).

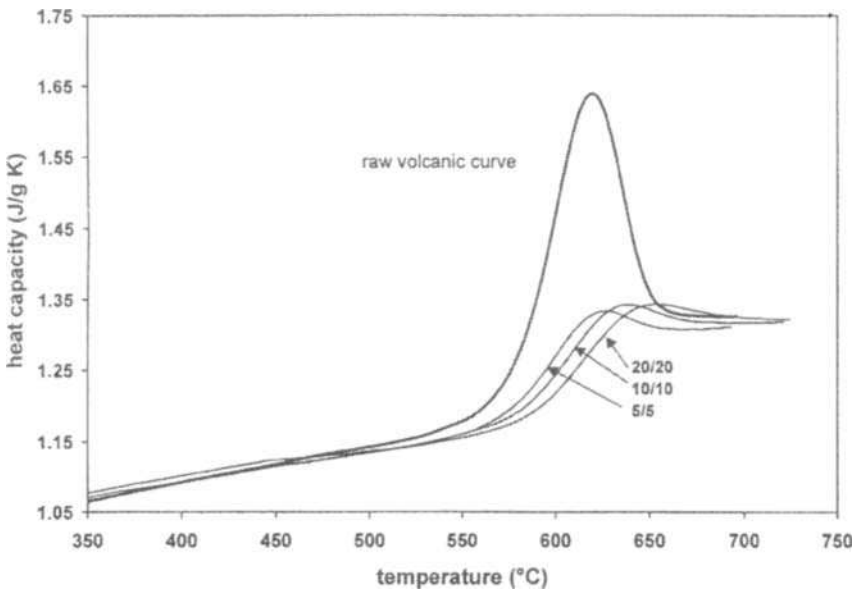

Fig. 2b. The variation of derivative thermodynamic property, the heat capacity, across the glass transition. The characteristic overshoot in the transient value of the heat capacity is often used to define the glass transition temperature. The extrapolated onset of the peak (the intersection of extrapolations of the low temperature heat capacity with the downward extrapolation of the maximum positive slope) is also often used for fixing the glass transition temperature in a consistent manner. The overshoot of the heat capacity is path dependent and depends thereby on the thermal history of the glass, (reproduced from Gottsmann and Dingwell, 2001).

Viscosity prediction

Given the last statement, the task of predicting the glass transition reduces to that of predicting the Newtonian viscosity (the elasticity is a near constant). Now we are in an arena where extensive ongoing experimental programs are increasingly in a position to provide us with multicomponent parameterisations of melt viscosity. An important step in this process, and one which serves well to illustrate the variation of glass transition temperature with chemistry and timescale is presented in Fig. 3 where the parameterisation of melt viscosities for hydrous calcalkaline rhyolites is presented (Hess

and Dingwell, 1996). From Fig. 3 and using the above equations we can derive the range of glass transition temperatures accessible by cooling hydrous calcalkaline rhyolites. Currently, models to obtain the same precision for the non-Arrhenian viscosity of multicomponent silicate melts are being developed (Giordano & Dingwell, 2003).

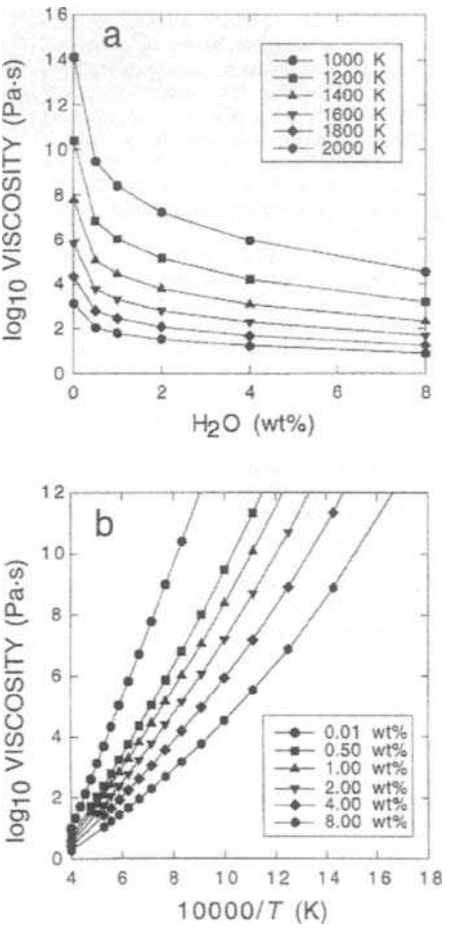

Fig. 3. The predicted viscosities of hydrous calcalkaline rhyolitic melts using the model of Hess and Dingwell (1996). This is the first nonArrhenian model for the variation of viscosity with temperature and water content. Such a model permits prediction of the viscosity, and together with the Maxwell relationship, the glass transition temperature, for any metaluminous granitic or calcalkaline rhyolitic melt composition, (reproduced from Hess and Dingwell, 1996).

Synthetic fluid inclusions in glass

The common presence of fluid-filled bubbles in glasses returned from petrological experiments at high pressure and temperature is a clear indication that fluid inclusions in glass are experimentally accessible. Given the appropriate experiment P-T-t

conditions, such inclusions contain fluids that are in chemical equilibrium with the surrounding melt phase at the temperature and pressure of the experimental dwell. If the experimental dwell is terminated by a quench that is sufficiently rapid to avoid substantial chemical reequilibration of fluid and melt, then the fluid inclusions contain information on the conditions of their "trapping" during the isobaric quench (Dingwell, 1993).

Based on this concept, an experimental program to investigate the nature of trapping of these fluid inclusions in glass was conducted in the mid-1990s. The principle of the method is illustrated in Fig. 4. The high-pressure, high-temperature experimental dwell is indicated by the point in the upper right quadrant of the diagram. The path of the isobaric quench of the sample is represented as the horizontal line emanating from that point to lower temperature at constant pressure.

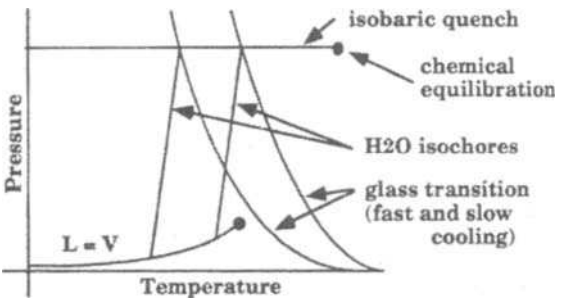

Fig. 4. The principle of the determination of the glass transition temperature using the method of synthetic fluid inclusions in glass. Homogenisation temperatures obtained on SFGs yield "trapping" temperatures corresponding to the glass transition temperature for the host melt in question. Varying quench rate affords an analysis of glass transition temperature versus quench rate, (reproduced from Dingwell, 1993)

Also included in Fig. 4 is a schematic indication of the two-phase liquid-vapour curve and critical point of pure water. Superimposed on these curves are two putative P-T projections of the kinetic glass transition of a water-saturated granitic melt. The curves have negative slopes, which steepen with pressure. The form of these curves results from the nonlinear dependence of water solubility on pressure and the nonlinearity of the decrease of Tg on that dissolved water. The two curves correspond to the glass transition for two cooling rates. Given a sufficiently rapid isobaric quench of the experimental charge, the decompression path of fluids included in bubbles in an increasingly viscous silicate melt will deviate qualitatively from that of the host melts. The contraction of the melt phase is controlled kinetically by the viscosity of the melt. This viscosity is an exponential function of the temperature. Thus a decrease in temperature leads to an exponential increase in viscosity and an exponential slowing of the response time required for the melt to contract in equilibrium with the temperature drop. At some intermediate temperature, the viscosity is so large that the melt density lags behind the equilibrium value for the ambient temperature. Once started, this lag is exacerbated by further temperature drop until no further viscous response of the volume is possible. The glass transition has been crossed at high temperature and pressure for

the given cooling rate. We are now left with a glass containing a fluid inclusion whose volume undergoes no further viscous changes. The resulting fluid inclusion follows a P-T path, which corresponds, to an isochore of the fluid system chemistry involved. For the case of water, the isochore terminates at the liquid-vapour curve.

Rehomogenisation of such fluid inclusions (Romano et al., 1994) yields homogenisation temperatures that serve as the points of departure for the isochores. Following the isochores to the pressure of the initial isobaric quench, we obtain temperature estimates of the "trapping" temperature corresponding to the volumes/densities of the inclusions, which are, in this system, the glass transition temperatures of the melts of interest.

Glass transition temperatures obtained using this method of synthetic fluid inclusions in glass (SFG method) are provided in Fig. 5a for the system albite-orthoclase-water. These were the first direct determinations of glass transition temperatures for hydrous melts at high pressure. The features exhibited by the variation of glass transition temperatures in this hydrous system reflect strikingly the variation in the dry albite-orthoclase system as well (Fig. 5b) The characteristic nonlinear deviation of the glass transition temperature from additivity towards lower temperatures is a reflection of the variation of viscosity in this binary mixed alkali system. Its origin probably lies in the contribution of the entropy of mixing of alkalis to the configurational entropy of the melts and the impact of that in reducing the viscosity of intermediate compositions. Despite the similar curve forms, the enormous fluxing affect of water in the binary albite-orthoclase system is evident as the decrease in Tg of up to 400°C. The orthoclase melt suffers a proportionally larger drop in Tg, despite the fact that it contains significantly less water in the saturated state. In this way fluid inclusions have given us the first direct insight into the glass transition in high pressure hydrous melts.

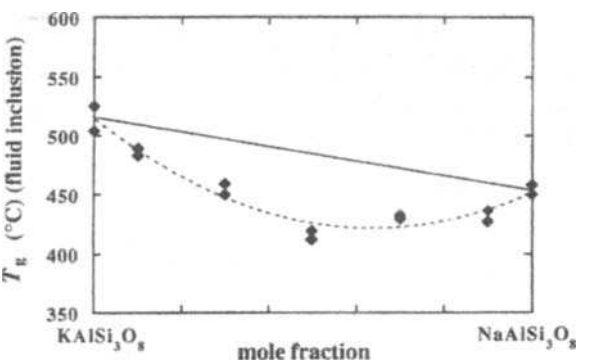

Fig. 5a. Glass transition temperatures obtained on water saturated orthoclase-albite melts using the method of SFGs. The glass transition temperatures exhibit the classic negative deviation from additivity, which is known as the mixed alkali effect. These are the first direct determinations of the glass transition temperature form hydrous melts at high pressure and temperature, (reproduced from Romano et al., 1994).

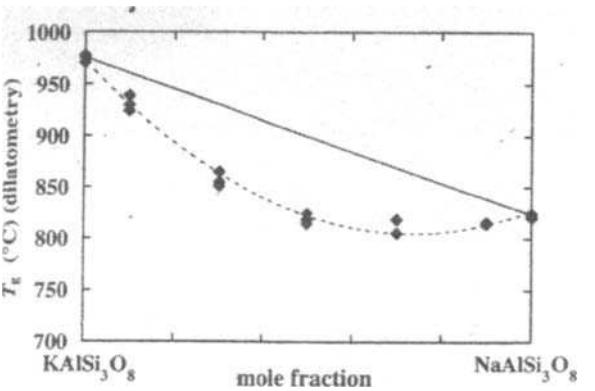

Fig. 5b. Glass transition temperatures of dry orthoclase-albite glasses obtained using dilatometry at 1 bar pressure. The mixed alkali effect is again observable. The dry glass transition temperatures are ca. 400K higher than those in the water-saturated system (Fig. 5a), (reproduced from Romano et al., 1994).

Properties from Synthetic fluid inclusions.

The most direct property information available from such experiments is the temperature of the glass transition, which may be expressed in terms of a viscosity-temperature data point. Thus high pressure – high temperature viscosity determinations in the high viscosity range are an automatic byproduct of the determination of the glass transition temperature. The results of determinations as described in Fig. 5 have in fact be compared with other direct experimental determinations and predictive models for melt viscosity have been based on both sorts of viscosity data. This is of particular assistance in the high water content range, which is otherwise experimentally difficult to access.

Further property data is provided via the determination of the density of the quenched glasses. The SFG samples may be cooled with different rates resulting in the generation of chemically identical glasses with differing fictive temperatures. Thermal expansivities of the glasses are relatively insensitive to thermal history. Thus the density differences obtained by varying the cooling rate, and thus T_f, correspond to liquid thermal expansivity-induced changes near the temperature of the transition interval. Thermal expansivities derived from the fictive temperature dependence of the density of SFG charges are illustrated in Fig. 6.

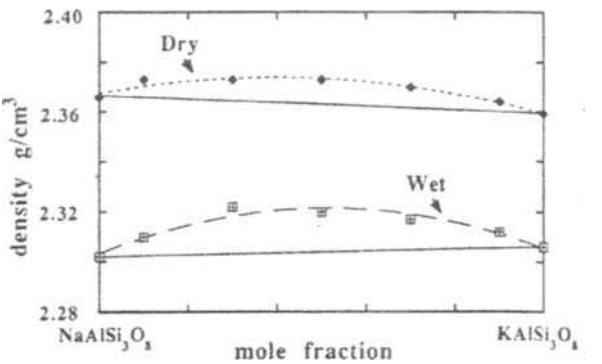

Fig. 6a. The variation of melt density with composition in the orthoclase-albite melt system as obtained from host glasses of samples from SFG experiments and from dry glasses of the same base compositions. The nonlinear variation of density results from the nonlinear "mixed alkali effect" in the glass transition temperature, (reproduced from Romano et al., 1994).

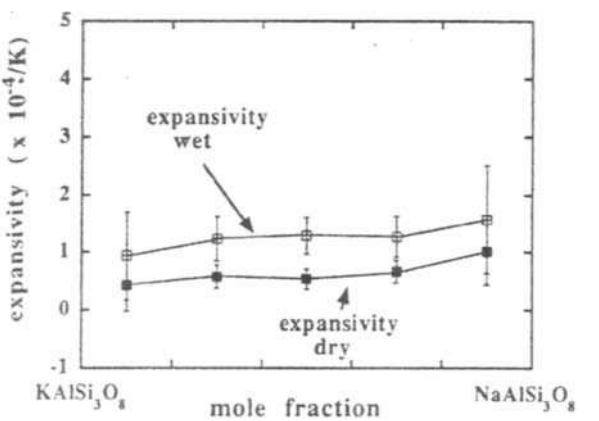

Figure 6b. The thermal expansivity of hydrous orthoclase-albite melts as obtained from the SFG analysis of the densities of host glasses, compared with the thermal expansivity of the dry melts, (reproduced from Romano et al., 1994)

The stability of SFG samples is also a source of information on the strength of the hydrous melts. Decrepitation experiments on SFG charges have revealed that water, in contrast to the sparingly soluble gases, CO_2 and Xe, drastically reduces the strength of vesicular glass (Fig. 7.). Investigations into the origin of this phenomenon via TEM studies of breached inclusion walls revealed the presence of microcracks that evolve away from the bubble walls from radial to concentric orientations (Romano et al., 1996). This observation precipitated numerical simulations of the stresses extant between bubbles and their host glasses during cooling in these experiments whose results suggested that microcracking around the bubbles was generated in response to stresses arising from the development of dehydration rims around the bubbles (Mungall et al., 1996).

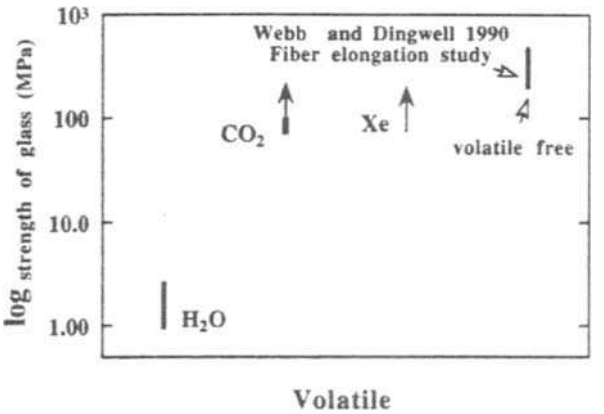

Fig. 7. Tensile strength estimates for vesicular glasses. The data are obtained from decrepitation experiments on samples from SFG experiments. The presence of Xe-bearing and CO_2-bearing fluid inclusions does not impact significantly on glass strength. The volatile free data represent the results of fiber elongation experiments. The presence of H2O-bearing inclusions in these glasses is accompanied by a drastic drop in tensile strength as recorded in decrepitation experiments, (reproduced from Romano et al., 1996).

The driving force for the dehydration is the development of a pressure gradient between the glass host and the included fluid below the glass transition. The pressure gradient impacts on the chemical potential of water, which is then substantially, lower in the bubble than in the glass. The result is diffusion of water from the glass rim leading to dehydration. The dehydrated glass is restrained from elastically adopting the higher density corresponding to a water poorer glass via its attachment to a further host reservoir of undehydrated glass. Eventually the stresses developed exceed the tensile strength of the glass in the rim and the microcracks ensue, radially oriented within the dehydrated zone and then concentric behind it (Fig. 8).

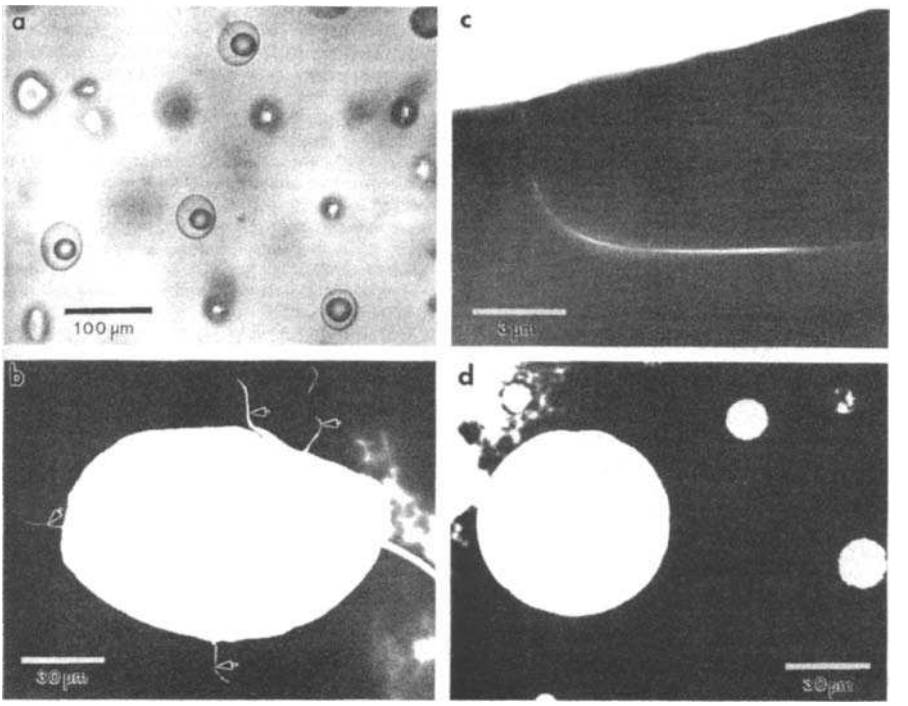

Fig. 8. A photomontage from SFG experiments, (a) Upper left - synthetic fluid inclusions in glass exhibiting typical homogeneously distributed two-phase inclusions at room temperature. (b) A TEM image of a single breached SFG exhibiting the presence of radial microcracks. (c) A single radial microcrack exhibiting the typical curving to a concentric geometry beyond a critical distance from the inclusion boundary, (d) Fluid inclusions from CO2-bearingexperiments exhibiting no microcracks. (reproduced from Romano et al., 1996).

Structure

Perhaps the most striking feature of glass transition behavior is that it provides a clear link between the kinetics of structure and properties in melts. The best-investigated aspect of melt structure in this regard is that of the role of water in melts. Since the 1980s the debate surrounding the role of dissolved water in silicate melts, and its impact on melt properties, has centered on the question of the dissociation constant of water in a silicate melt matrix. Infrared spectra of quenched silicate glasses illustrate clear evidence for the presence of significant fractions of total dissolved water both as molecular water and as hydroxyl groups (Stolper, 1982a,b). In the absence of a commonly accepted quantification of glass transition phenomena in the geoscientific community at that time, the question as to the nature of this coexistence in glasses and its possible role as a homogeneous equilibrium in high temperature melts was thermodynamically handled on the basis of glassy data in the 1980s with the assumption that the speciation observed simply reflected the state of the melt at the experimental

dwell temperature. In other words complete quenchability was assumed. In 1989 the first analysis of the fictive temperature dependence of water speciation was performed, based on the assumption that water speciation kinetics are controlled by glass transition kinetics (Dingwell and Webb, 1989). That study led to the immediate conclusion that the water speciation observed in hydrous rhyolitic glasses, reflected the speciation frozen into the glass at very low transition temperatures (400 – 600°C), that the temperature dependence of the speciation reaction yielded higher hydroxyl concentrations, and that the concentration dependence of the speciation was much less that initially inferred.

SFG experiments offer a special opportunity to perform a fictive temperature analysis of temperature-dependent speciation reactions. This is because the glass transition may be obtained using the methods described above on sample for which the infrared spectroscopic determination of water speciation has been performed. These measurements have been performed for example for the albite-orthoclase-water system described above. Fig. 9 describes the variation of the equilibrium constant of the water speciation reaction with composition in that system. All samples have been quenched identically. Composition however induces a strong nonlinear variation in the fictive temperature of the quenched hydrous glasses (Fig 9a). As a result a significant range of fictive temperature is accessible for the attribution of the temperature corresponding to each speciation data point.

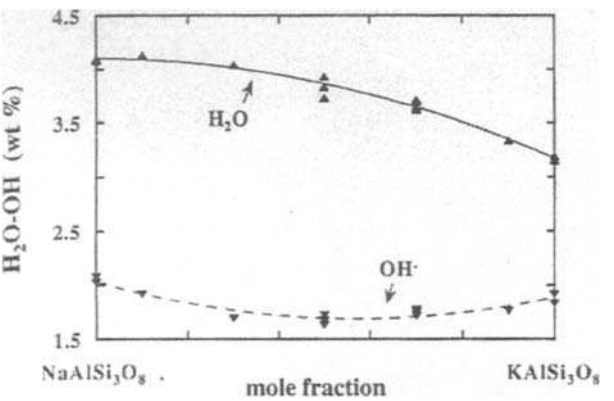

Fig. 9a. Infrared spectroscopic determinations of the concentration of hydroxyl and molecular water in host water saturated orthoclase-albite glasses from SFG experiments. The nonlinear variation in the concentration of the hydroxyl and molecular water species is a consequence of the "mixed alkali effect" in the glass transition temperature, (reproduced from Romano et al., 1995).

In Fig. 9c we are faced with the strikingly simple conclusion that the temperature dependence of the speciation of water dominates over the composition-dependence in this system. The nonlinearity in the composition-dependence of the fictive temperature is entirely responsible for the nonlinearity in the composition-dependence of the speciation data. The data is linearized by this fictive temperature calibration. The linear

array of equilibrium constant data points illustrated in Fig. 9c indicates that we can, within experimental error, exclude a significant composition dependence. This is a remarkable example of the kind of information on the thermodynamics of water solution in melts that can be obtained from fictive temperature analysis of quenched glasses.

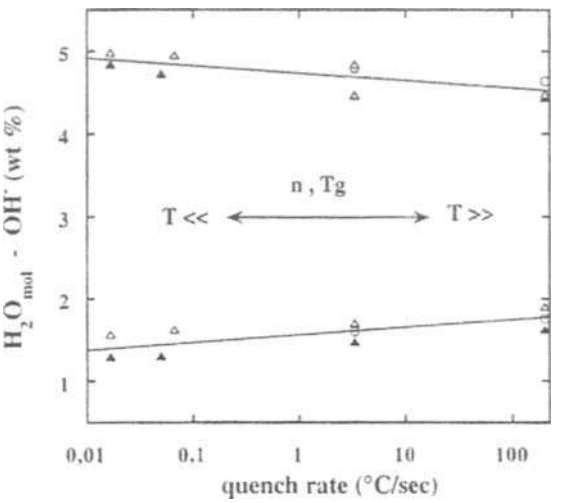

Fig. 9b. Infrared spectroscopic determinations of the concentration of hydroxyl and molecular water in host water saturated orthoclase-albite glasses from SFG experiments. The dependence of the species concentrations on the quench rate of the experiment is a clear indication of a relaxation process affecting the speciation. This means that fictive temperature analysis can be applied to quantifying the temperature-dependence of a reaction, (reproduced from Romano et al., 1995).

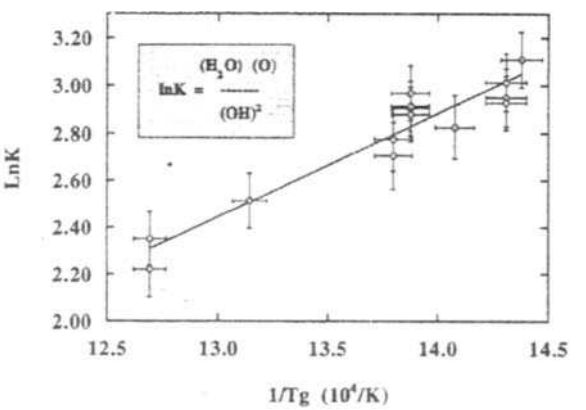

Fig.9c. The temperature dependence of the equilibrium constant of the water speciation reaction for the water-saturated orthoclase-albite melt system as derived from a fictive temperature analysis of the infrared spectra of host glasses from SFG experiments. The linear variation of the

equilibrium constant with reciprocal temperature (Arrhenian behavior) is a striking contrast to the initially nonlinear variation of species concentrations from the binary system as seen in Figure 9a. Linearisation of the reaction constant is obtained via normalisation of the speciation data to the glass transition temperatures as obtained in Figure 5a. This is a powerful example of the utility of fictive temperature analysis in conjunction with SFG experiments, (reproduced from Romano et al., 1995).

Direct, in situ determinations of water speciation (e.g., Nowak and Behrens, 1995) have confirmed that the kinetics of water speciation, and by inference perhaps of virtually all speciation kinetics in melts, are those of the glass transition. Fig. 10 illustrates the temperature dependence of water speciation in a granitic melt measured via in situ high-pressure spectroscopy. The inflection at intermediate temperature is evident both in the concentration data and the derived equilibrium constant data. By estimation of the inflection point in the equilibrium constant data we obtain a very precise estimate of the temperature of the glass transition, which is in excellent agreement with estimates from property determinations (see below).

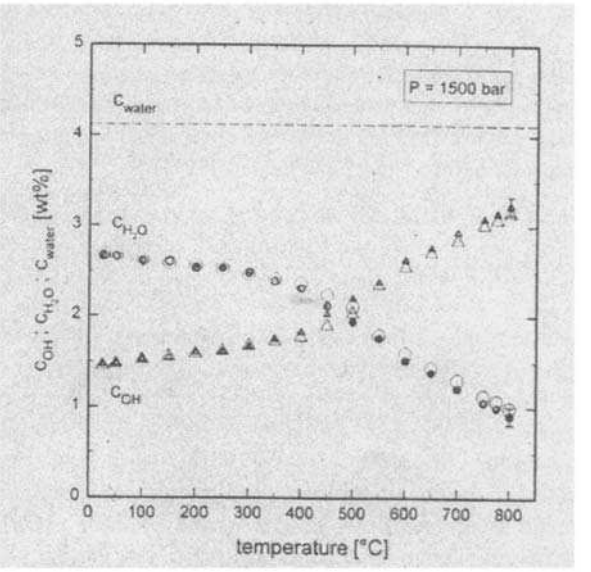

Fig. 10a. The variation in hydroxyl and molecular water species concentrations in a haplogranitic melt with temperature as obtained from "in situ" infrared spectroscopic determinations using a sapphire anvil cell. The glass transition is clearly visible as the temperature of the inflections in the concentration curves, (reproduced from Nowak and Behrens, 1995).

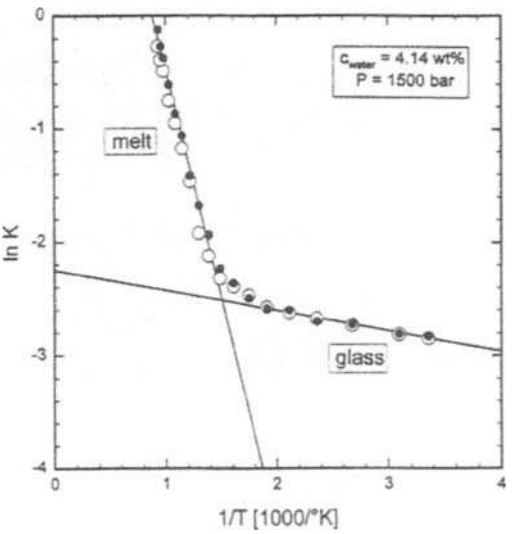

Fig. 10b. The equilibrium constant for the water speciation reaction as a function of reciprocal temperature for a haplogranitic melt with 4.14 wt.% total water dissolved in the liquid. The glass transition corresponds to the extrapolated crossover of the liquid and glassy trends of speciation the temperature, (reproduced from Nowak and Behrens, 1995).

Comparison of Tg estimates

Just how consistent the various methods of estimating Tg are, can be appreciated with the aid of Fig. 11. This is a summary of all Tg estimates for the viscosity of a haplogranitic melt as a function of water content. This comparison incorporates 3 completely different methods of obtaining the glass transition temperature. Data have been obtained using the Maxwell relationship and shear viscosity data, using the relaxation of water speciation data from high pressure experiments and using the method of synthetic fluid inclusions described above. Each experimental technique incorporates a different fundamental time scale. For the viscosity-based method the viscosity is fixed at a particular value for the glass transition. We chose a standard viscosity value of 1012.38 for this comparison. For the water speciation experiments, the intrinsic timescale relevant to the Tg determined from the inflection in the temperature dependence of water speciation is the effective dwell time per temperature step for the infrared spectroscopic determination of the speciation during what was effectively a slow step scan of the reaction progress variable. For the SFG method data the cooling rate during the quench is the intrinsic timescale. For the latter two cases the intrinsic timescales must be corrected to a value consistent with a viscosity of $10^{12.38}$ at the glass transition, the standard value that we chose above. A final input required for the correction of the experimental timescales is of course the temperature dependence of

the timescale of relaxation. This is available for the hydrous haplogranitic melt system e.g. via the temperature-dependence of the shear viscosity from the model of Hess and Dingwell (1996). Performing this correction results in temperature shifts of up to 15 °C and results in the fine correlation observed in Fig. 11.

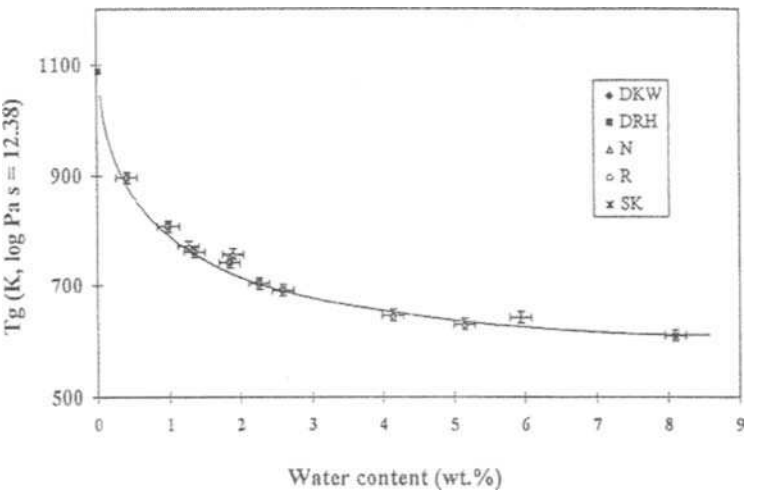

Fig. 11. The variation of the glass transition temperature with added water for a haplogranitic melt composition. Here, the results of glass transition temperature estimates from different sources compare very favorably. The three sources of glass transition temperatures are (1) viscosity data on highly viscous liquids, (2) inflection points of temperature dependent speciation in "in situ" measurements, and (3) the results of glass transition temperature determinations using the SFG method. The agreement of the three methods is remarkable. The effect of water on the glass transition temperature is very large a strongly nonlinear, (reproduced from Dingwell, 1998c).

OUTLOOK FOR MELT INCLUSION RESEARCH

Melt inclusions contain information on the thermal history of the rocks in which they are found. If methods for the determination of the relaxation properties of these melts can be developed then that information can be accessed. In order to quantify the temperature-dependence of the variations in the properties or structure which may be relevant to fictive temperature analysis of such inclusions one must either have a highly precise model for the temperature- and pressure-dependence of the property or structural aspect of interest, or obtain such a calibration on the sample of interest. If the model exists, the properties of quenched glasses (e.g. water speciation) may give direct indications of the cooling rates involved. If the property variations are not accessible from models of sufficient precision (e.g., density, refractive index) then the calibration of the samples must form a part of the experimental determination of the cooling rate. This has been performed with great success on vitrophyric matrix glasses from lava

flows (Wilding et al. 1995, Gottsmann et al., 2002) and should, in principle, be applicable to melt inclusions.

Analytical studies using SFGs have been attempted using both destructive (LA-ICP-MS) and non-destructive (SYXRF) methods (Lechtenberg et al., 1996, Schaefer et al, 1999). The success to date has been limited but the role of SFGs in constraining partitioning data and speciation information for experimental geochemistry remains open.

A number of further details remain to be clarified if reheating experiments on melt inclusions are to reveal cooling rates. These include the influence of pressure evolution during reheating and the effective exclusion of fluid-melt reequilibration during reheating to the glass transition. Nevertheless I remain optimistic that the fictive temperature analyses of melt inclusions can yield information on their thermal history and urge pursuit of such data in the near future.

REFERENCES

Dingwell, D.B. (1993) Experimental strategies for the determination of granitic melt properties at low temperature. Chemical Geology 108, 19-30.

Dingwell, D.B. (1995) Relaxation in silicate melts: some applications in petrology. Mineralogical Society of America Reviews in Mineralogy 32 [eds. Stebbins, J.F., Dingwell, D.B. and McMillan, P.W. Structure and Dynamics of silicate melts.] 21-66.

Dingwell, D.B. (1996) Volcanic Dilemma: Flow or blow? Science 273, 1054-1055.

Dingwell, D.B. (1998) A physical description of magma relevant to explosive silicic volcanism. „Physics of Explosive Volcanic Eruptions" Geological Society of London Special Publication 145, 9-26.

Dingwell, D.B. (1998) Magma degassing and fragmentation. Recent experimental advances. In: Freundt, A. and Rosi, M. (eds.) Explosive Volcanism: a physical description, Springer Verlag-Berlin, 318.

Dingwell, D.B. and Webb, S.L. (1989) Structural relaxation in silicate melts and non-Newtonian melt rheology in igneous processes. Physics and Chemistry of Minerals 16, 508-516.

Dingwell, D.B. and Webb, S.L. (1990) Relaxation in silicate melts. European Journal of Mineralogy 2, 427-449.

Giordano, D. and Dingwell, D.B. (2003) NonArrhenian Volcanic Melt Viscosities: A Model. (in press - Earth and Planetary Science Letters)

Gottsmann, J. and Dingwell, D.B. (2002) The thermal history of a rheomorphic air-fall deposit: The 8ka pantellerite flow of Mayor Island, New Zealand. Bulletin of Volcanology 64, 410-422.

Gottsmann, J., Dingwell, D.B. and Gennaro, C. (1999) Thermal expansion of silicate liquids: Direct determination of liquid expansivity using container-based dilatometry. American Mineralogist 84, 1176-1180.

Gottsmann, J. and Dingwell, D.B. (2000) Supercooled diopside melt: confirmation of temperature-dependent expansivity using container-based dilatometry. Contributions to Mineralogy and Petrology 139, 27-34.

Gottsmann, J. and Dingwell, D.B. (2001) Cooling dynamics of phonolitic rheomorphic fall-out deposits on Tenerife, Canary Islands. Journal of Volcanological and Geothermal Research 105, 323-342.

Hess, K-U. and Dingwell, D.B. (1996) Viscosities of hydrous leucogranitic melts: a non-Arrhenian model. American Mineralogist 81, 1297-1300.

Lechtenberg, F., S. Garbe, J. Bauch, D. B. Dingwell, J. Freitag, M. Haller,T. H. Hansteen, P. Ippach, A. Knöchel, M. Radtke, C. Romano, P. M. Sachs, H.-U. Schmincke, H.-J. Ullrich (1996) The X-ray fluorescence measurement place at beamline L of HASYLAB. Journal of Trace and Microprobe Techniques 14, 561-587.

Mungall, J., Romano, C., Bagdassarov, N and Dingwell, D.B.. (1996) Numerical modelling of stress generation and microfracturing of vesicle walls in glassy rocks. Journal of Volcanology and Geothermal Research 73, 33-46.

Nowak, M. and Behrens, H. (1995) The speciation of water in haplogranitic glasses and melts determined by in situ near-infrared spectroscopy. Geochimica et Cosmochimica Acta 59, 3445-3450.

Romano, C., Dingwell, D.B. and Sterner, S.M. (1994) Kinetics of quenching of hydrous feldspathic melts: quantification using synthetic fluid inclusions. American Mineralogist 79, 1125-1134.

Romano, C., Dingwell, D.B. and Behrens, H. (1995) The temperature-dependence of the speciation of water in NaAlSi3O8-KAlSi3O8 melts: an application of fictive temperatures derived from synthetic fluid inclusions. Contributions to Mineralogy and Petrology 122, 1-10.

Romano, C., Mungall, J., Sharp, T. & Dingwell, D.B. (1996) Tensile strengths of hydrous vesicular glasses: an experimental study. American Mineralogist 81, 1148-1154.

Schaefer, B., Frischknecht, R., Günther, D. and Dingwell, D.B. (1999) Determination of trace element partitioning between fluid and melt using LA-ICP-MS analysis of synthetic fluid inclusions in glass. European Journal of Mineralogy 11, 415-426.

Stolper, E.M. (1982a) The speciation of water ijn silicate melts. Geochim Cosmochim Acta 46, 2609-2620.

Stolper, E.M. (1982b) Water in silicate glasses: an infrared spectroscopc study. Contrib Mineral Petrol 81, 1-17.

Wilding, M., Webb, S.L. and Dingwell, D.B. (1995) Evaluation of a relaxation geothermometer for volcanic glasses. Chemical Geology 125, 137-148.

This Page Intentionally Left Blank

MAGMATIC INCLUSIONS IN THE SEARCH FOR NATURAL SILICATE-SALT MELT IMMISCIBILITY: METHODOLOGY AND EXAMPLES

Vadim S. Kamenetsky[1], Benedetto De Vivo[2], Vladimir B. Naumov[3], Maya B. Kamenetsky[1], Terrence P. Mernagh[4], Esme Van Achterbergh[5], Chris G. Ryan[5], Paul Davidson[1]

[1] *School of Earth Sciences and Centre for Ore Deposit Research, University of Tasmania, Hobart, Australia*
[2] *Dip. Di Geofisica e Vulcanologia, Università di Napoli "Federico II", Napoli, Italy*
[3] *Vernadsky Institute of Geochemistry, Russian Acad. of Sciences, Moscow, Russia*
[4] *Geoscience Australia, Canberra, ACT, Australia*
[5] *CSIRO Exploration and Mining, North Ryde, NSW, Australia*

ABSTRACT

Immiscible phase separation during the cooling and crystallisation of magmas is an inherently fugitive phenomenon and melt inclusions may provide the only remaining evidence of this process. We detail those features of such inclusions that can both prove the existence of immiscible phase separation, and constrain the compositional signature of the process. To do so requires the combination of traditional methods (petrographic examination, microthermometry, etc.) with state of the art microbeam analytical techniques (laser Raman spectroscopy and proton-induced X-ray emission). Examples of inclusions in phenocrysts from barren and mineralised rocks are provided to illustrate the approach and validate the interpretations.

INTRODUCTION

The most perplexing question concerning transition from magmas to hydrothermal fluids is the nature of the phases (melts, vapour- or liquid-rich fluids) that derive from magmas at the brink of solidification. It is widely believed (e.g., orthomagmatic model) that the phases exsolved late in the crystallisation of aluminosilicate magmas carry important amounts of volatile (e.g., H_2O, CO_2, Cl, S, F) and metallic elements that may subsequently enter hydrothermal systems and be responsible for formation of certain types of ore deposits (e.g., W-Sn skarns and greisens, pegmatites, and Cu-Mo-Au porphyries). Clearly underlying this thinking is the notion that the peculiar chemistry of the near-solidus magmatic fluids (CO_2- and H_2O-rich) or melts (essentially non-silicate – usually H_2O-bearing chloride, carbonate, sulphate, and phosphate, hereafter "salt melt", and sulphide-rich liquids) is related to the process of unmixing or direct immiscibility with parental aluminosilicate magmas.

Leaving aside the question of how magma-derived melts and fluids ultimately evolve into potentially ore-forming solutions, there are immediate problems about physical state and chemical compositions of these transitional phases. They appear to be released from solidifying magma in a murky window of temperatures between 750 and <500°C,

which remains largely uncovered by the geological research. The reason for this is twofold:

1. Historically, igneous petrology was segregated from studies into hydrothermal systems, although some overlap in the form of experimental and theoretical studies was always present;
2. Fluid and melt phases that could have been representative of natural compositions, leave virtually no record, as they are completely exhausted by crystallisation and degassing.

The second problem can be partially resolved by using melt and fluid inclusion studies for samples representative of magmatic-hydrothermal transition (see reviews in Roedder, 1992; De Vivo and Frezzotti, 1994; Lowenstern, 1995; Frezzotti, 2001). These are not necessarily intrusive or volcanic rocks that host mineralisation or bear hydrothermal alteration. In theory and in practice, any magma that is saturated in volatiles can further evolve by losing volatiles during degassing or separation of immiscible volatile-rich melts. At this point silicate melts and their immiscible volatile-rich products coexist and can be preserved if trapped as inclusions by crystallising minerals (e.g., Roedder and Coombs, 1967; Reyf and Bazheyev, 1977; Harris, 1986; Naumov et al., 1990; Lowenstern et al., 1991; Solovova et al., 1991; Frezzotti, 1992; Solovova et al., 1992; De Vivo et al., 1993; Lowenstern, 1993; Yang and Bodnar, 1994; De Vivo et al., 1995; Reyf, 1997; Kamenetsky et al., 1999; Thomas et al., 2000; Davidson and Kamenetsky, 2001; Fulignati et al., 2001). Such inclusions are still magmatic in nature but their compositions are much closer to hydrothermal solutions as potentially ore-forming elements preferentially partition into late magmatic immiscible phases (e.g., Candela and Holland, 1984; Shinohara, 1994; Webster, 1997).

However, in recent years the melt and fluid inclusion approach has become more attractive to growing numbers of researchers. Although there still remain limitations related to whether inclusions represent natural melts and fluids or to post-entrapment modification, the application of modern analytical tools to inclusions (FTIR and Raman spectroscopy, electron, ion and proton microprobes, scanning electron microscopy, laser ablation ICPMS etc) provides great advantages over conventional methods.

The aims of this paper are: 1) to describe unequivocal occurrences of late magmatic immiscibility using melt and fluid inclusions in phenocrysts from mineralised and unmineralised rock suites; 2) to recommend a set of methods and techniques that are most efficient in looking into magmatic-hydrothermal transition. Our test study covers inclusions in different minerals – quartz, clinopyroxene, leucite, and K-feldspar that crystallised from compositionally diverse magmas in different tectonic environments. Two of our examples represent clear association with economic mineralisation - Balut Dyke, Dinkidi Cu-Au porphyry deposit, Philippines (Kamenetsky et al., 1999) and Omsukchan Sn-granite, NE Russia (Naumov and Sokolov, 1981; Kamenetsky et al., 2002b), whereas in the other two examples (mafic to felsic xenoliths in alkaline lavas from Ventotene Island, Italy (De Vivo and Frezzotti, 1994; De Vivo et al., 1995) and dacite-rhyolite lavas from the 1.6 Ga Gawler Craton, S Australia (Kamenetsky et al., 2000)) this association is either hypothetical (so far) or does not exist.

METHODOLOGY FOR STUDYING MAGMATIC IMMISCIBILITY

Optical examination of inclusions

Optical examination at room temperature of phases present among magmatic inclusions is a prerequisite to and a keystone in the immiscibility studies.

Sample preparation: Samples can be prepared as double side polished sections on a soluble glue, with thickness comparable to the size of phenocrysts in order to preserve large inclusions intact. Whole rock sections are particularly useful for observing distribution of inclusions within a single crystal and constraining relationships (e.g., temporal) between different types or generations of inclusions. Double side polishing and the use of soluble glue are required if phenocrysts from a section are to be further used for experimental and analytical studies. If a rock is sparsely porphyric we recommend picking phenocrysts or their fragments from a crushed and sieved rock, followed by mounting grains in epoxy. Note that a few hundred grains can be placed in a standard mount, and this allows much broader examination of inclusions. Grains of interest can be later picked up from epoxy (with a hot needle), polished and studied individually.

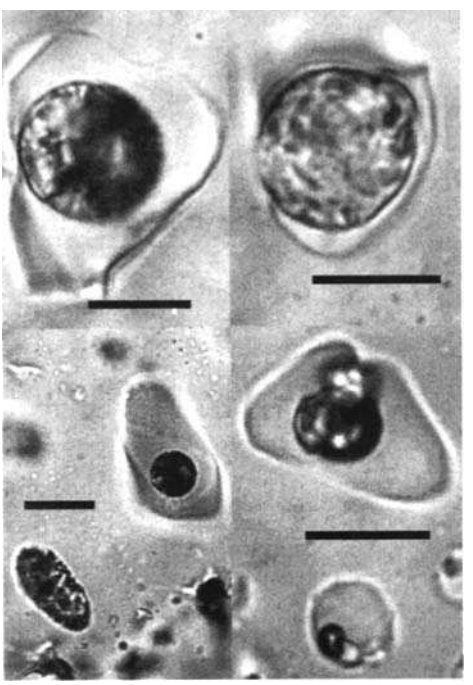

Fig. 1. Variable ratios between felsic glass and non-silicate globules in melt inclusions trapped in quartz from a granitic clast in a Gawler Range rhyolite. Scale bars are 10 μm.

Sample description: The task of finding and photographing inclusions under petrographic microscope, although laborious and time consuming, should be performed on as many phenocrysts as possible. It is important to identify temporal populations of inclusions and their genetic relationships. The criteria for recognising primary, pseudo-secondary and secondary inclusions are widely discussed in the literature (e.g., Roedder, 1979). For immiscibility studies the inclusions of primary and pseudosecondary origin (i.e., those trapped during the phenocrysts crystallisation) are a principal target as they characterise the magmatic phases. However,

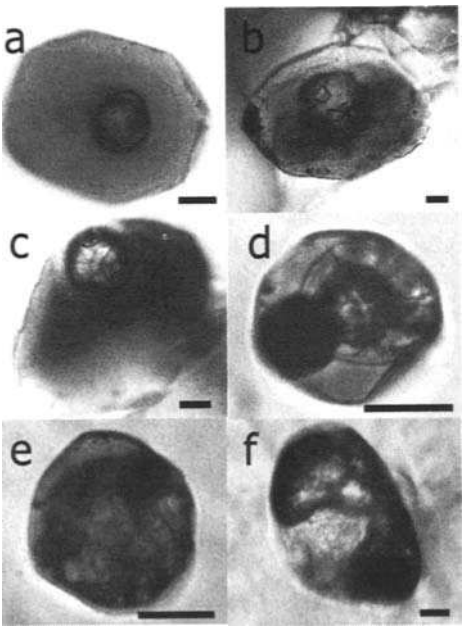

Fig. 2. Photomicrographs of melt inclusions in clinopyroxene from the Ventotene mafic xenolith showing variable proportion of silicate melt and volatile-rich, essentially non-silicate phases (see text for details). Scale bars are 10 μm.

secondary inclusions trapped in magmatic phenocrysts are not to be ignored if they may represent melts and fluids at temperatures just below the solidus of silicate magmas (Prokofiev et al., 1999).

To recognise magmatic immiscibility using inclusions a simple but stringent test was proposed by Edwin Roedder (1979). This test is to look for inclusions with variable amounts of two or more supposedly unmixed but coexisting phases. Commonly one or several phases in such inclusions have spherical shapes. As an example we refer to Fig. 1, which shows microphotographs of melt inclusions coexisting in a cluster in quartz from a granite xenolith in a Gawler Range rhyolite. Note the variable proportions of clear felsic glass and vapour-rich globules of essentially non-silicate phases represented by various carbon species (CO_2, carbonates and amorphous carbon). Another example is provided by inclusions in clinopyroxene from Ventotene xenoliths, shown in Fig. 2. In this case in the coexisting inclusions variable amounts of co-trapped brownish silicate glass (formerly melt), vapour ± crystal globules and sometimes Cu-rich, Fe-sulphide globule (Fig. 2d) can be seen. The proportion of glass in these inclusion ranges from >95 vol% (Fig. 2a) to <5 vol% (Fig. 2e). Glass-free inclusions are also present (Fig. 2f). Vapour-rich globules are also variable in terms of amount of crystals present. This amount varies from a few minute crystals decorating the walls (Fig. 2a) through large discrete euhedral crystals (Fig. 2b) to crystalline masses occupying the entire volume of the globules (Fig. 2 c-e).

However, in practical studies a researcher should be aware of the fact that inclusions of homogeneous melt or fluid may be trapped at temperatures above immiscibility, and unmixing may happen in such inclusions during cooling. If this is the case inclusions should show roughly the same proportions of in situ formed immiscible phases. This is best illustrated by numerous melt inclusions in leucite from Ventotene xenoliths (Fig. 3). Despite variable size these inclusions show approximately similar ratios of brownish

alkaline silicate glass, translucent crystalline mass of chlorides, carbonates, and sulphates (according to Raman spectroscopy; see below) and Cu-enriched Fe-sulphide globule usually on the meniscus between silicate and non-silicate melts.

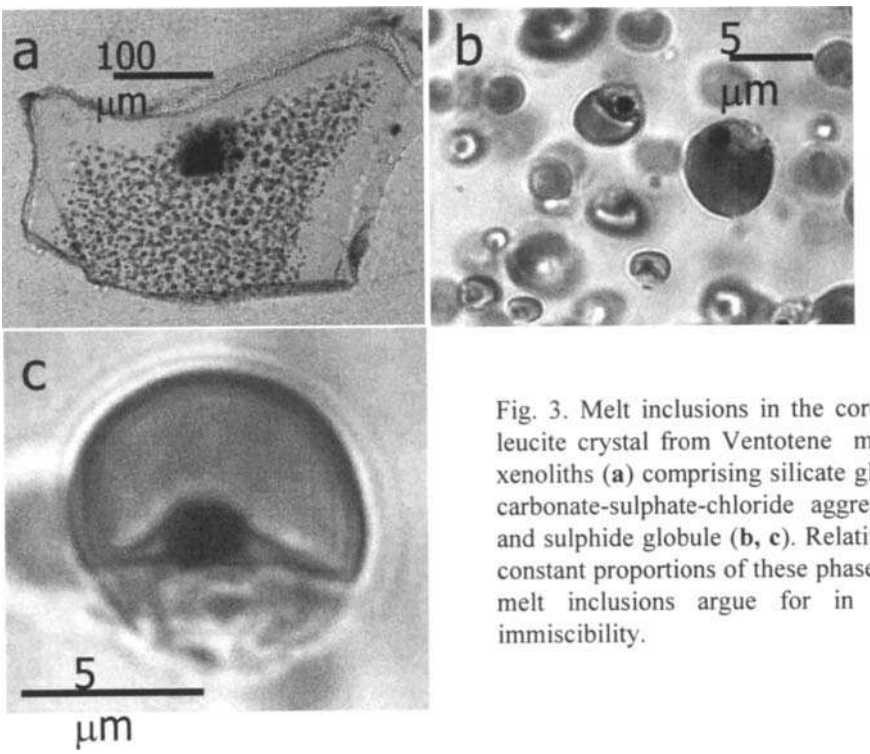

Fig. 3. Melt inclusions in the core of leucite crystal from Ventotene mafic xenoliths (**a**) comprising silicate glass, carbonate-sulphate-chloride aggregate and sulphide globule (**b, c**). Relatively constant proportions of these phases in melt inclusions argue for in situ immiscibility.

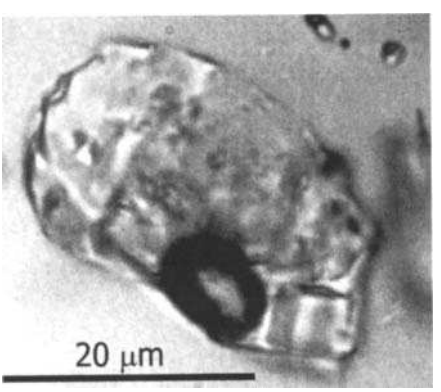

Fig. 4. Cubic salt mineral (halite ?) associated with a fluid phase in the silicate melt inclusion in quartz from the Omsukchan granite.

A researcher should be always on the lookout for non-silicate phases (such as salt crystals, CO_2 and H_2O vapours and liquids, sulphide globules, etc) in otherwise normal silicate melt inclusions. Occurrences of this phenomenon have been noted frequently in different magmatic suites (e.g., Roedder and Coombs, 1967; Lowenstern et al., 1991; Solovova et al., 1991; Tsareva et al., 1991; Andreyeva et al., 1995; Yang and Scott, 1996; Davidson and Kamenetsky, 2001; Kamenetsky et al., 2001; Kamenetsky et al., 2002a), and our Fig. 4 illustrates the presence of a cubic mineral (halite?) in a crystalline felsic melt inclusion from the Omsukchan granite.

Sometimes Roedder's test is not easy to exercise, especially at room temperature or prior to heating of melt inclusions in phenocrysts from slowly cooled rocks, because post-entrapment crystallisation may mask heterogeneously trapped immiscible phases within inclusions. To overcome this problem we recommend the use of heating and quenching techniques.

Thermometric experiments with inclusions

Aims: A lot of details of thermometric experiments with melt inclusions are available in the modern literature. In our immiscibility studies we use heating and subsequent quenching to pursue the following objectives:

1. Convert crystalline silicate daughter phases within devitrified inclusions into melt, and quench this melt into homogeneous glass. This makes heterogeneously trapped phases (including non-silicate, if present) available for observation and analysis;
2. Liberate immiscible salt melt and fluid phases heterogeneously trapped with the silicate melt and promote their coalescence into larger formations (globules or bubble) in order to successfully analyse them using microbeam techniques;
3. Initiate silicate melt – salt melt immiscibility within silicate melt inclusions that were trapped homogeneously and quenched in nature at temperatures above the temperature of immiscibility. The task is to exsolve non-silicate phases large enough for observation and subsequent analysis;
4. Observe and document (e.g., photographing or video recording) the behaviour (e.g., melting, homogenisation, crystallisation etc) inside immiscible non-silicate globules irrespectable of whether they were heterogeneously trapped or exsolved during heating.

Experimental techniques: Different heating stages and optical microscopes are available for this kind of work and various heating techniques are employed in practice. There are no generally accepted preferences as to the choice of heating setup or heating rate. In fact, every sample and every inclusion should be treated individually, and the alternating of heating and cooling in initiating in situ immiscibility must be applied wisely to achieve desirable results. In our studies we use a Linkam TS1500 heating stage with TMS 94 temperature control unit and an Olympus BX51 microscope. To prevent oxidation of Fe-bearing minerals at high temperatures we recommend maintaining an inert atmosphere inside the heating stage using high purity argon.

The laborious work with individual grains on a heating stage can be relieved if quantities of inclusion-bearing grains (e.g., >100) are first bulk heated in a furnace and

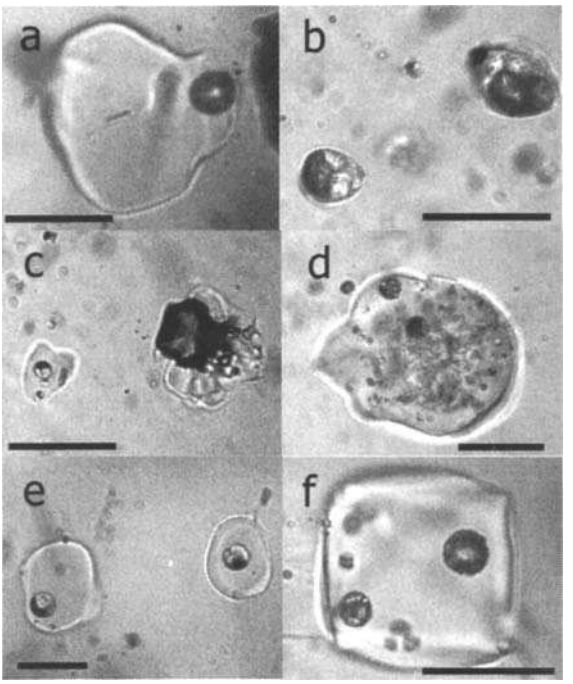

Fig. 5. Photomicrographs of heated and quenched melt inclusions in quartz from the Omsukchan granite (**a-e**) and the Gawler Craton rhyolite (**f**) showing variable amounts of silicate glass and volatile- and salt-rich phases. The immiscible endmembers are shown on Fig. 5a (silicate glass inclusion with shrinkage vapour bubble) and Fig. 5b (salt melt inclusions). Note microemulsion textures formed by globules of salt melt (**d, f**). Scale bars are 20 μm.

then quenched. The first aim of bulk heating is to convert the silicate content of inclusions into glass and initiate silicate-salt immiscibility that can be later enhanced and recorded properly in a heating stage with visual control. The second aim that a researcher may keep in mind is to provide plentiful samples for different microbeam analysis. Another aim is to identify those inclusions that have been already compromised (e.g., fractured) or decrepitated during bulk heating. This applies to inclusions in the vicinity of crystal deformations or invisible cracks and inclusions hosted by minerals with strong cleavage (e.g., plagioclase, clinopyroxene etc). A great number of inclusions in quartz cannot survive temperature-related volume change of host quartz (α to β quartz transition at ~573°C) and appear decrepitated after first heating. The appropriate combination of temperature and heating times in these preliminary experiments is to be derived from a series of heating runs on a few grains from each sample.

The bulk heating experiments are most suitable for those samples that record silicate-salt melt immiscibility that happened in a magma chamber during natural cooling. In this case the post-heating examination should reveal variable proportions of silicate glass and salt globules in a single inclusions. Commonly large numbers of inclusions may still represent homogeneous trapping of silicate or salt melt "endmembers" (Fig. 5 a, b). However, in such samples with inclusions representing both end-member compositions, the "mixed" varieties (Fig. 5 c-f) should also be

present, and actually these are vital if the immiscibility is to be proved (Roedder, 1979). Microemulsion texture in melt inclusions is also a good evidence for heterogeneous trapping of immiscible salt melt phases with the silicate melt (Fig. 5 d, f).

Silicate melt - salt melt immiscibility that may occur in homogeneously trapped silicate melt inclusions after entrapment during natural cooling, or during heating experiments with no visual controls can be distinguish from heterogeneous trapping by examining relative proportions of both silicate and salt phases. For example, after heating and quenching two coexisting inclusions from the Omsukchan granitic quartz (Fig. 5e) unlike other inclusions in this sample (Fig. 5) show a single, relatively small (~3.5 vol%) salt melt globule. These can be tentatively interpreted as exsolved from a silicate melt after entrapment. In another example from the Gawler Range rhyolite exceptionally rare occurrence of salt globules in glass (two coexisting inclusions in only one quartz grain out of several hundred heated grains) may suggest that immiscibility occurred during the experimental run (Fig. 5f).

Despite very short experimental times compared to the timescales of geological processes, in situ immiscibility within a given homogeneously trapped melt inclusions is still feasible. A few examples confirming this are given in recent literature. Thomas et al. (2000) reported the occurrence of immiscibility between two silicate melts with different concentration of volatiles in a single melt inclusion in the Ehrenfriedersdorf pegmatite quartz after quenching from 617°C. Experimental heating and cooling of melt inclusions in the Mt Vesuvius endoskarn minerals has revealed that unmixing and homogenisation between carbonate and chloride melts in a single inclusion could be repeatedly attained at ~690°C (Fulignati et al., 2001).

Heating stage experiments: Heating stage experiments with visual control are a prerequisite for the study of in situ separation of immiscible phases within a given inclusion and phase transformations (e.g., melting and crystallisation) within immiscible phases.

Figure 6 shows heating of salt melt immiscible globules trapped together with silicate melt in the Omsukchan granitic quartz. This originally devitrified inclusion was first heated in the furnace for 20 hrs at 950°C. After quenching, the silicate content formed a clear glass containing two large and a few smaller salt melt globules. Several subsequent heating experiments show that 1) salt globules remain constant in size, do not change their position with respect to silicate melt, and do not mix with silicate melt even at temperatures exceeding liquidus (900-1100°C); 2) first melting in salt globules happens at 150-190°C; 3) vapour and solid phases in salt globules acquire spherical and pseudocubic shapes, respectively, and decrease in size with further heating and melting; 4) the last solid phase melts at ~ 735°C; and 5) complete homogenisation within the salt globules (vapour bubble dissolution) happens at ~840°C. Note that the above phase transformations take place simultaneously in all entrapped globules, and also in salt melt inclusions (alike those on Fig. 5b) outside this composite inclusion. In this example silicate and salt components of the inclusion show no significant interaction with each other and their miscibility is not achievable at the conditions of experiment.

A different picture is observed in experiments with melt inclusions in K-feldspar from the Ventotene felsic xenolith. At room temperature two adjacent inclusions have

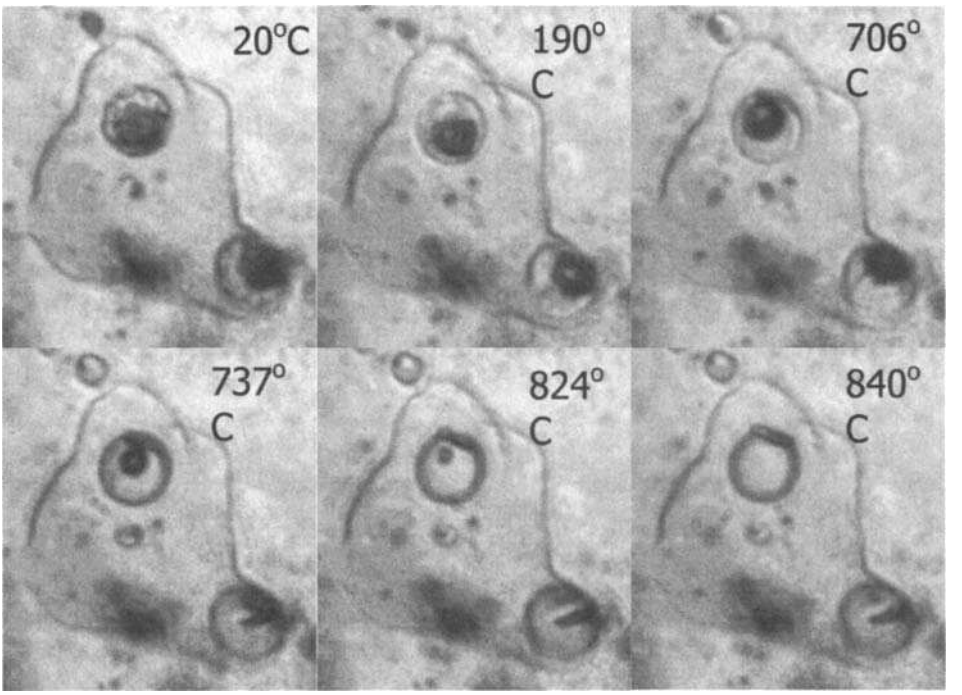

Fig. 6. Melting and homogenization during heating in the immiscible salt globules within a silicate melt inclusion hosted by quartz from the Omsukchan granite. Size of globules is ~12 μm.

rectangular shape and consist of crystalline phases and deformed vapour bubble (Fig. 7a). First melting, as evident from enhanced crystal boundaries, occurs at temperatures as low as 300-400°C. This suggests that daughter crystal belong to non-silicate species, and thus these inclusions can be classified as salt melts. Complete melting of daughter phases is achieved at 605-635°C, whereas the shape of inclusions becomes more round. The smoothness of shape and reduction in size of a bubble-bearing liquid are clearly noticeable at ~850°C. Close to this temperature a phase other than salt melt shows up outlining the original contours of the inclusions. With further transformation of a bubble-bearing melt phase into almost spherical globule at >900°C the presence of this phase (presumably silicate melt) is unambiguous. The bubbles in salt globules homogenised at 841 and 857°C on first heating, and at 919 and 938°C on second heating. Cooling below 850°C obscures the phase boundary between silicate and salt melt, causes spontaneous crystallisation of non-silicate crystals at ~400°C, and returns a rectangular shape to these inclusions.

Heating/cooling of the same inclusions in the third consecutive run caused simultaneous nucleation of bubbles in both silicate and salt liquids of the lower inclusion at 930°C, then the coalescence of bubbles in the silicate melt at 902°C, and

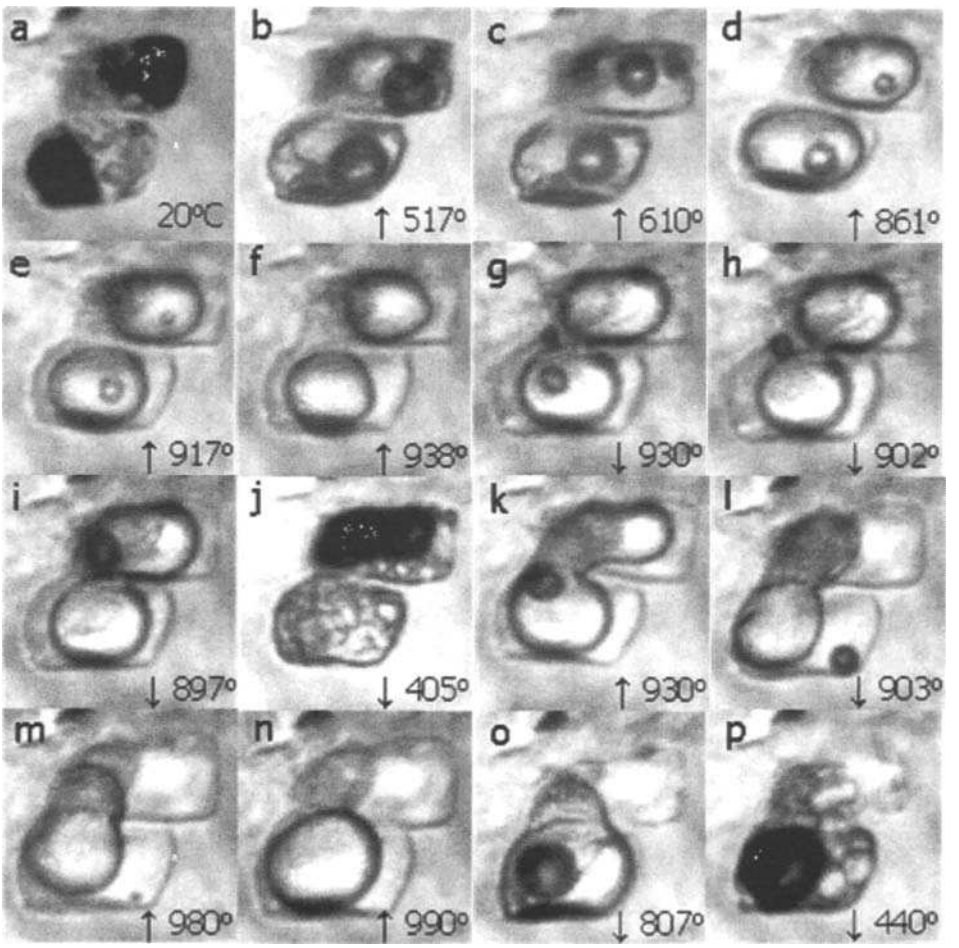

Fig. 7. Phase transformations (melting, immiscibility, crystallisation, homogenisation etc) during heating and cooling of two silicate-salt melt inclusions in K-feldspar from the Ventotene felsic xenolith. See text for details. Upwards and downwards arrows indicate heating and cooling events, respectively. Size of inclusions is ~25 μm.

migration of the bubble into the salt globule of the upper inclusion at 897°C (Fig. 7i). In this run a neck formed bridging between two inclusions possibly as a result of melting through the host feldspar. In a series of repeated experiments the salt melt content of the upper inclusion poured progressively into the lower inclusion, and eventually one large salt globule containing a vapour bubble formed (Fig. 7 n-p).

While most silicate-salt melt inclusions in the Ventotene feldspar show behaviour as described above due to very low silicate melt/ salt melt ratio, in some cases silicate melt prevails in composite inclusions, and thus the salt melt occurs in a spherical globule at room temperature (Fig. 8).

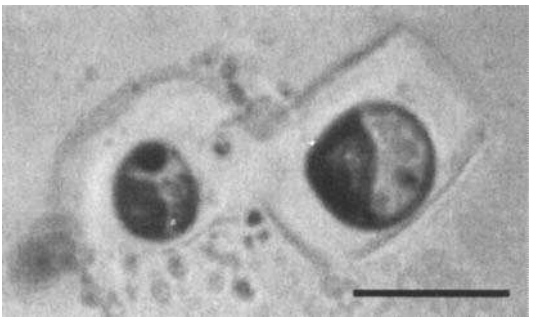

Fig. 8. Heated and quenched melt inclusions in K-feldspar from the Ventotene felsic xenolith showing separation of immiscible salt globule from the silicate melt (glass). Opaque rounded phase in salt globules is another immiscible phase represented by Cu-rich sulphide (see Fig. 10). Scale bar is 20 μm.

PHASE AND CHEMICAL COMPOSITIONS: ANALYTICAL TECHNIQUES

Once immiscible phases are recognised as individual inclusions or in composite inclusions the identification of their mineral constituents and bulk chemical composition is necessary. One endmember of the immiscibility – a silicate melt is usually quenchable into homogeneous glass that can be exposed by polishing and analysed by conventional microbeam techniques (e.g., electron microprobe, laser ablation ICPMS). Silica-poor and non-silicate, salt melts do not form glass even at very high quenching rates because of their extremely low viscosity. Consequently, at room temperatures these melts are represented by aggregates of crystals, a large volume vapour bubble(s) and possibly interstitial aqueous solution. The main problem in exposing such melt for analysis is in that some daughter minerals are unstable in the air or react with atmospheric moisture, and that aqueous and gaseous components are likely to be lost. The heterogeneous state of salt melt inclusions at room temperature poses a problem in calculating their bulk composition. Below we present a few suggestions as to how these problems are partially overcome in our studies.

Energy- and wavelength X-ray dispersive analysis (EDS and WDS)

The lapidary work is the most critical stage during the preparation of salt melt inclusions for the electron microprobe analysis. Grains with inclusion of interest should be ground individually by hand on very fine SiC abrasive paper, and the use of water must be avoided. Kerosene or any other light oil lubricant serves well, and once the inclusion is very close to the surface (< several microns) further grinding and ultimate polishing is done with 1μm diamond oil-based polishing paste on slowly rotating artificial silk disk such as Lamplan 450. The surface with exposed inclusion is cleaned with petroleum-based solvents like shellite, and the sample is immediately carbon (or gold)-coated and stored in a desiccator. Chemical composition of daughter minerals in exposed inclusions is then analysed routinely using an electron microprobe or scanning electron microscope equipped with the EDS or WDS detectors. For example, Fig. 9

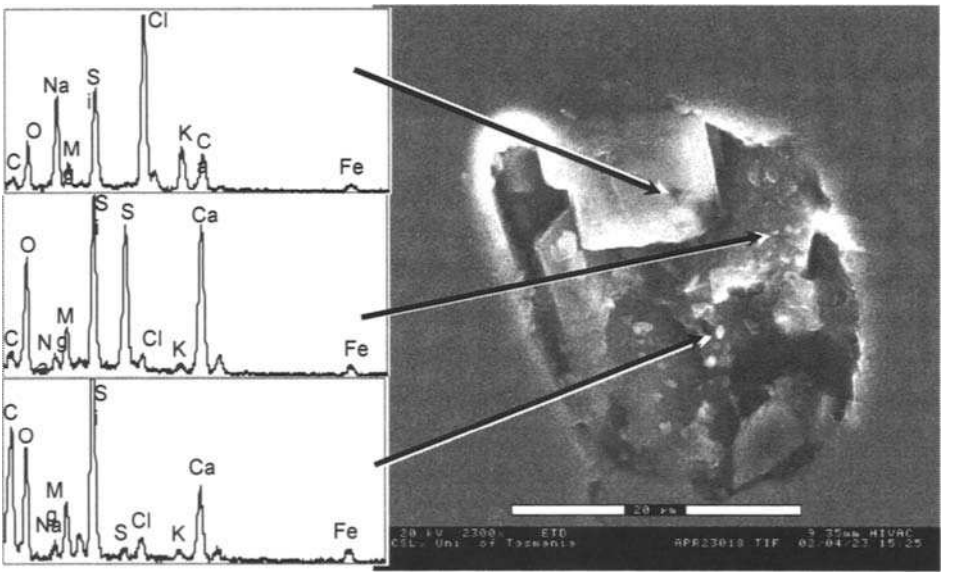

Fig. 9. Scanning electron photomicrographs and EDS spectra of phases in exposed salt melt inclusion in clinopyroxene from the Balut dyke, Didipio intrusive. Note that the sample is not carbon coated, and elevated abundances of Si, Mg, Fe and partly Ca in spectra are from host clinopyroxene

shows a secondary electron image of the exposed salt melt inclusion in clinopyroxene from the Balut dyke together with X-ray spectra obtained by EDS of some daughter phases (Na-K±Ca chlorides, Ca (±Na±K) sulphates and possibly carbonates) present in this inclusion. Large volume of voids in this inclusion (and other exposed salt melt inclusions) was formerly occupied by an aqueous solution and vapour.

Laser Raman spectroscopy

Laser Raman spectroscopy is a non-destructive, high spatial resolution (down to 1 μm) technique that can be used for the in situ analysis of individual daughter phases in unexposed salt melt and fluid inclusions within transparent host minerals. The Raman spectrum arises from inelastically scattered light resulting from the interaction of a monochromatic laser beam with the sample, which may be either a solid, liquid or a gas. It does not provide specific elemental information, but the Raman frequencies correspond to the vibrational modes of the sample, which means that it can provide important information on the molecular or crystalline structure of the sample. Furthermore, the narrowness of the Raman peaks and the common lack of overtones or combination bands means that the spectra of individual components are easier to identify as their bands can be separated from those of the host mineral.

The technique is well suited to the study of covalently bonded compounds and has proven particularly useful, in this study, for identifying carbonate, sulphate and sulphide minerals, which have their principle Raman bands in different regions of the spectrum. It can also detect graphite/carbon in various states of crystallinity and both free and crystalline water. Unfortunately, minerals with strongly ionic character have only weak Raman spectra, or no spectra at all. Therefore, laser Raman spectroscopy cannot provide any information on the chloride salts, which are present in salt melt inclusions.

Laser ablation inductively coupled plasma-mass spectrometry (LA-ICPMS)

LA-ICPMS is a fast developing technique in fluid and melt inclusion research (e.g., Kamenetsky et al., 1997; Taylor et al., 1997; Halter et al., 2002). This method can be used in analysis of unexposed inclusions, and the advantages are very high sensitivity of modern mass spectrometers (detection limits are better than a few ppm) and short acquisition times. However, the technique has the disadvantage that it is destructive of the sample. Currently this technique may produce element concentration ratios for salt melt and fluid inclusions, but it requires one of the measured elements to have been accurately quantified by some other method prior to LA-ICPMS in order to calculate absolute concentrations.

Proton-induced X-ray emission (PIXE)

The PIXE technique, especially as implemented using the CSIRO-GEMOC Nuclear Microprobe (North Ryde, Australia; see Ryan et al., 2001a;b), is an ideal tool for high spatial resolution analytical studies of melt inclusions. It is capable of simultaneous multi-element analysis of most of the periodic table, and can be applied to unexposed inclusions. This technology uses a high-energy proton beam (3 MeV) focussed to 1.3 μm diameter to penetrate the host mineral and excite characteristic X-rays and gamma-rays from elements within an inclusion. The beam is raster scanned across the sample, and the emitted X-rays are detected and used to create an element concentration map for each element in the sample. The element concentrations are calculated for individual phases accounting for sample geometry, density and depth below surface. Detection limit can be around 20 ppm, with accuracy for saturated aqueous fluids estimated at 30%. This technique is "standardless" in that no prior analysis is needed to normalise the data (as with LA-ICPMS), which is an enormous benefit when analysing unexposed salt melt inclusions. Also importantly, the technique is non-destructive, although interaction with the high-energy particles may cause some phases to nucleate, or change shape or colour (Kamenetsky et al., 2002b).

Examples of PIXE element maps for a melt inclusion comprising immiscible phases is shown on Fig. 10 in order to demonstrate preferential partitioning of volatile (e.g., Cl, S) and metallic (e.g., Cu, Zn, Pb) elements into non-silicate melts over the silicate glass.

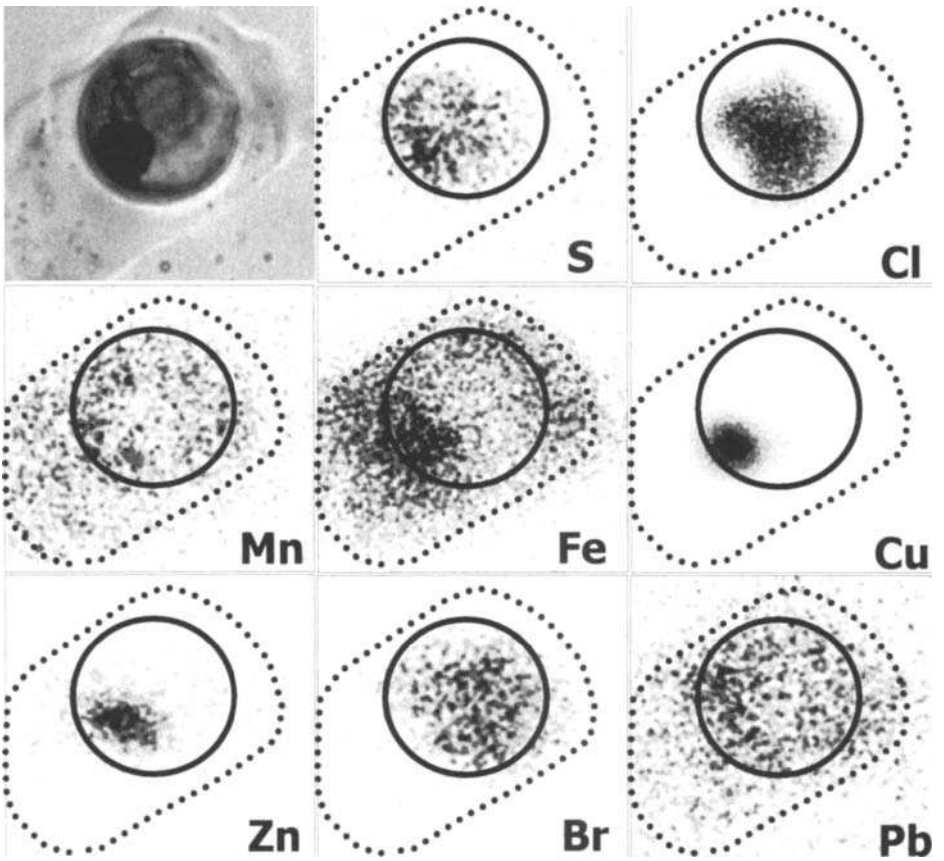

Fig. 10. Optical images and PIXE element maps of a silicate – salt – sulphide melt inclusion in K-feldspar from the Ventotene felsic xenolith (see also Fig. 8) Analysis was done using the new CSIRO-GEMOC Nuclear Microprobe (Ryan et al., 2001a;b). Intensity scale (from white to black) in each element image is normalised to its own maximum. Outlines on element maps mark boundaries of silicate glass and salt globule.

CONCLUSIONS

The pioneering work by Roedder and Coombs (1967) on the immiscibility between silicate melts and dense saline fluids in the Ascension Island granites was published thirty-five years ago. Since then amazingly little effort has been made by the international research community to tackle the problem of silicate – salt melt immiscibility by studying the late magmatic phases available in the form of phenocryst-

hosted inclusions. Instead great strides were made to approach the physical and chemical parameters of immiscibility by experimental and theoretical studies. The reasons for this imbalance are not discussed here in detail, but one thing is clear – the study of natural samples of immiscible melts and fluids is time-consuming, painstaking, and more importantly requires a lot of "know how". However, the great advantage of inclusion studies is in that they directly apply to natural melts and fluids, and the use of modern microbeam analytical techniques, promoted in this paper, can put solid constraints on the element partitioning and the fate of volatile and economic elements.

ACKNOWLEDGEMENTS

We are grateful to R. Wolfe and S. Allen for donating samples for this research, D. Steele for assistance in the electron microscope studies, and S. Stephens for advice in lapidary works. Thoughtful review by M. L. Frezzotti is greatly appreciated. Special thanks to Olympus Australia Pty. Ltd., without their microscopes and camera systems our successful research into melt and fluid inclusions would not have been possible. Financial support for this project came from the Australian Research Council, Centre for Ore Deposit Research (University of Tasmania) and Russian Foundation for Basic Research (grant 01-05-64109).

REFERENCES

Andreyeva, I.A., Naumov, V.B., Kovalenko, V.I., Listratova, E.N. and Kononkova, N.N., 1995. Magmatic celestite in melt inclusions in apatite from the Mushugay-Khuduk alkali volcano-plutonic complex in south Mongolia. Trans. (Doklady) USSR Acad. Sci., 339A: 154-159.

Candela, P.A. and Holland, H.D., 1984. The partitioning of copper and molybdenum between silicate melts and aqueous fluids. Geochim. Cosmochim. Acta, 48: 373-380.

Davidson, P. and Kamenetsky, V.S., 2001. Immiscibility and continuous melt-fluid evolution within the Rio Blanco porphyry system, Chile: Evidence from inclusions in magmatic quartz. Econ. Geol., 96: 1921-1929.

De Vivo, B. and Frezzotti, M.L., 1994. Evidence for magmatic immiscibility in Italian subvolcanic systems. In: B. de Vivo and M.L. Frezzotti (Eds), Fluid inclusions in minerals: methods and applications. Short course of the working group IMA. Virginia Tech., Pontignano-Siena, pp. 345-362.

De Vivo, B., Frezzotti, M.L. and Lima, A., 1993. Immiscibility in magmatic differentiation and fluid evolution in granitoid xenoliths at Pantelleria: Fluid inclusions evidence. Acta Vulcanol., 3: 195-202.

De Vivo, B., Torok, K., Ayuso, R.A., Lima, A. and Lirer, L., 1995. Fluid inclusion evidence for magmatic silicate/saline/CO_2 immiscibility and geochemistry of alkaline xenoliths from Ventotene Island, Italy. Geochim. Cosmochim. Acta, 59: 2941-2953.

Frezzotti, M.L., 1992. Magmatic immiscibility and fluid phase evolution in the Mount Genis granite (southeastern Sardinia, Italy). Geochim. Cosmochim. Acta, 56: 21-33.

Frezzotti, M.L., 2001. Silicate-melt inclusions in magmatic rocks: applications to petrology. Lithos, 55: 273-299.

Fulignati, P., Kamenetsky, V.S., Marianelli, P., Sbrana, A. and Mernagh, T.P., 2001. Melt inclusion record of immiscibility between silicate, hydrosaline and carbonate melts: Applications to skarn genesis at Mount Vesuvius. Geology, 29: 1043-1046.

Halter, W.E., Pettke, T., Heinrich, C.A. and Rothen-Rutishauser, B., 2002. Major to trace element analysis of melt inclusions by laser-ablation ICP-MS: methods of quantification. Chem. Geol., 183: 63-86.

Harris, C., 1986. A quantitative study of magmatic inclusions in the plutonic ejecta of Ascension Island. J. Petrol., 27: 251-276.

Kamenetsky, V.S., Binns, R.A., Gemmell, J.B., Crawford, A.J., Mernagh, T.P., Maas, R. and Steele, D., 2001. Parental basaltic melts and fluids in eastern Manus backarc basin: Implications for hydrothermal mineralisation. Earth Planet. Sci. Lett., 184: 685-702.

Kamenetsky, V.S., Crawford, A.J., Eggins, S.M. and Mühe, R., 1997. Phenocrysts and melt inclusion chemistry of near-axis seamounts, Valu Fa Ridge, Lau Basin: insight into mantle wedge melting and the addition of subduction components. Earth Planet. Sci. Lett., 151: 205-223.

Kamenetsky, V.S., Davidson, P., Mernagh, T.P., Crawford, A.J., Gemmell, J.B., Portnyagin, M.V. and Shinjo, R., 2002a. Fluid bubbles in melt inclusions and pillow-rim glasses: high-temperature precursors to hydrothermal fluids? Chem. Geol., 183: 349-364.

Kamenetsky, V.S., Morrow, N. and McPhie, J., 2000. Origin of high-Si dacite from rhyolitic melt: evidence from melt inclusions in mingled lavas of the 1.6 Ga Gawler Range Volcanics, South Australia. Mineral. Petrol., 69: 183-195.

Kamenetsky, V.S., van Achterbergh, E., Ryan, C.G., Naumov, V.B., Mernagh, T.P. and Davidson, P., 2002b. Extreme chemical heterogeneity of granite-derived hydrothermal fluids: An example from inclusions in a single crystal of miarolitic quartz. Geology, 30: 459-462.

Kamenetsky, V.S., Wolfe, R.C., Eggins, S.M., Mernagh, T.P. and Bastrakov, E., 1999. Volatile exsolution at the Dinkidi Cu-Au porphyry deposit, Philippines: A melt-inclusion record of the initial ore-forming process. Geology, 27: 691-694.

Lowenstern, J.B., 1993. Evidence for a copper-bearing fluid in magma erupted at the Valley of Ten Thousand Smokes, Alaska. Contrib. Mineral. Petrol., 114: 409-421.

Lowenstern, J.B., 1995. Applications of silicate-melt inclusions to the study of magmatic volatiles. In: J.F.H. Thompson (Ed), Magmas, fluids, and ore deposits. Mineralogical Association of Canada Short Course Series, pp. 71-99.

Lowenstern, J.B., Mahood, G.A., Rivers, M.L. and Sutton, S.R., 1991. Evidence for extreme partitioning of copper into a magmatic vapor phase. Science, 252: 1405-1409.

Naumov, V.B. and Sokolov, A.L., 1981. Genetic correlation of granites and the Industrialnoe tin ore deposits according to fluid inclusions data. Geol. Ore Depos., 4: 74-80.

Naumov, V.B., Solovova, I.P., Kovalenker, V.A., Rusinov, V.L. and Kononkova, N.N., 1990. Crystallization conditions and compositions of silicate and salt melts of the volcanoplutonic complex in the Angren area, Soviet Central Asia. Trans. (Doklady) USSR Acad. Sci., 312: 199-202.

Prokofiev, V., Kamenetsky, V.S., Kovalenker, V., Bodon, S.B. and Jelen, S., 1999. Evolution of magmatic fluids at Banska Stiavnica precious and base metal deposit, Slovakia -- Evidence from melt and fluid inclusions. Econ. Geol., 94: 949-956.

Reyf, F.G., 1997. Direct evolution of W-rich brines from crystallizing melt within the Mariktkan granite pluton, west Transbaikalia. Mineralium Deposita, 32: 475-490.

Reyf, F.G. and Bazheyev, Y.D., 1977. Magmatic chloride solutions and tungsten mineralizations. Geochem. Inter., 14: 45-51.

Roedder, E., 1979. Fluid inclusions as samples of ore fluids. In: H.L. Barnes (Ed), Geochemistry of Hydrothermal Ore Deposits. Wiley & Sons, New York, NY, pp. 684-737.

Roedder, E., 1992. Fluid inclusion evidence for immiscibility in magmatic differentiation. Geochim. Cosmochim. Acta, 56: 5-20.

Roedder, E. and Coombs, D.S., 1967. Immiscibility in granitic melts, indicated by fluid inclusions in ejected granitic blocks of Ascension Island. J. Petrol., 8: 417-451.

Ryan, C.G., McInnes, B.M., Williams, P.J., Dong, G., Win, T.T. and Yeats, C.J., 2001a. Imaging fluid inclusion content using the new CSIRO-GEMOC Nuclear Microprobe. Nuclear Instruments & Methods in Physics Research Sect. B, 181: 570-577.

Ryan, C.G., van Achterbergh, E., Griffin, W.L., Pearson, N.J., O'Reilly, S.Y. and Kivi, K., 2001b. Nuclear microprobe analysis of melt inclusions in minerals: Windows on metasomatic processes in the Earth's mantle. Nuclear Instruments & Methods in Physics Research Sect. B, 181: 578-585.

Shinohara, H., 1994. Exsolution of immiscible vapor and liquid phases from a crystallizing silicate melt: Implications for chlorine and metal transport. Geochim. Cosmochim. Acta, 58: 5215-5221.

Solovova, I.P., Girnis, A.V., Guzhova, A.V. and Naumov, V.B., 1992. Magmatic salt inclusions in minerals from eastern Pamirs alkaline basalts. Geokhimiya, 1: 68-77.

Solovova, I.P., Girnis, A.V., Naumov, V.B., Kovalenko, V.I. and Guzhova, A.V., 1991. Mechanism of degassing of silicic magmas: formation of two fluid phases during pantellerite crystallisation, Pantelleria. Trans. (Doklady) USSR Acad. Sci., 320: 982-985.

Taylor, R.P., Jackson, S.E., Longerich, H.P. and Webster, J.D., 1997. In situ trace-element analysis of individual silicate melt inclusions by laser ablation microprobe inductively coupled plasma-mass spectrometry (LAM-ICP-MS). Geochim. Cosmochim. Acta, 61: 2559-2567.

Thomas, R., Webster, J.D. and Heinrich, W., 2000. Melt inclusions in pegmatite quartz: Complete miscibility between silicate melts and hydrous fluids at low pressure. Contrib. Mineral. Petrol., 139: 394-401.

Tsareva, G.M., Kovalenko, V.I., Tsepin, A.I. and Naumov, V.B., 1991. Villiaumite in natural acid agpaitic magmas and its crystallization conditions (from the data of the study of melt inclusion). Doklady Akad. Nauk SSSR, 319: 1198-1201 (in Russian).

Webster, J.D., 1997. Exsolution of magmatic volatile phases from Cl-enriched mineralizing granitic magmas and implications for ore metal transport. Geochim. Cosmochim. Acta, 61: 1017-1029.

Yang, K. and Bodnar, R.J., 1994. Magmatic-hydrothermal evolution in the "bottoms" of porphyry copper systems: evidence from silicate melt and aqueous fluid inclusions in granitoid intrusions in the Gyeongsang Basin, South Korea. Inter. Geol. Rev., 36: 608-628.

Yang, K.H. and Scott, S.D., 1996. Possible contribution of a metal-rich magmatic fluid to a sea-floor hydrothermal system. Nature, 383: 420-423.

Analyzing hydrogen (H_2O) in silicate glass by secondary ion mass spectrometry and reflectance Fourier transform infrared spectroscopy

Richard L. Hervig[1], Frank K. Mazdab[1], Gordon Moore[2], and Paul F. McMillan[3,4,†]
[1] Center for Solid State Science, Arizona State University, Tempe, AZ 85287 USA
[2] Department of Chemistry and Biochemistry, Arizona State University, Tempe, AZ 85287 USA
[3] Department of Chemistry, Christopher Ingold Building, University College London, London, WCIH OAJ, UK
[4] Davy-Faraday Research Laboratory, Royal Institution of Great Britain, 21 Albermarle St., London, WIX 4B5
[†] PFM is a Wolfson-Royal Society Research Merit Award holder

ABSTRACT

The water contents of silicate glasses can be measured by secondary ion mass spectrometry (SIMS) and Fourier transform infrared (FTIR) spectroscopy. For SIMS, one of the impediments to quantitative analysis is uncertainty in the effect of sample chemistry on calibration, while for FTIR, sample preparation is often the most difficult step. A wide range of hydrogen-implanted silicate glasses was tested to see if a general relation between sample chemistry and calibration factors for SIMS could be formulated. The results show that while some compositions are suitable for H implantation (matching earlier calibrations based on experimentally hydrated samples), other H-implanted compositions show very low H signals. We suggest that the difference in atomic environment between implanted H vs. dissolved H may cause low count rates. Using the *reflected* IR spectrum simplifies sample preparation. Reflection IR measurements of experimentally hydrated glasses show that the H_2O content of basaltic, andesitic, and rhyolitic glasses can be quantified down to ~0.5 wt.%. Lateral resolution is limited by intensities of current IR sources to ~100μm.

INTRODUCTION

Secondary ion mass spectrometry (SIMS) and Fourier transform infrared (FTIR) spectrometry are two powerful techniques for measuring volatile species in silicate glasses. They effectively dominate the study of trapped melt inclusions because they allow the analysis of relatively small areas (tens of microns in diameter). Two general problems arise in applying these techniques: 1) the secondary ion signals measured in SIMS can be influenced in unknown ways by changing matrix chemistry, making quantification difficult; and 2) preparation of doubly polished wafers for infrared analysis can be difficult, and uncertainty in the measurement of sample thickness can introduce a significant error in the analysis. In this contribution we explore solutions to these problems: A) we have studied many hydrogen-implanted silicate glasses and minerals to test for a relation between sample chemistry and calibration for H using SIMS, and B) we show that measurements for H in basalts, andesites and rhyolites are possible using *reflection* infrared spectroscopy, thus greatly simplifying sample preparation.

Past work using SIMS

The use of SIMS for the analysis of volatile and trace elements in silicate glass has been discussed many times (e.g., Ihinger et al., 1994, Lowenstern, 1995, Hervig, 1996, Chaussidon et al., 1997, Hauri et al., 2002) and many melt inclusion researchers have used this technique (e.g., Kovalenko et al., 1988, Hervig et al., 1989, Dunbar, 1992, Sisson and Layne, 1993, Kovalenko et al., 1995, Webster et al., 1995). More recently, an issue of Chemical Geology (v. 183) was dedicated to melt inclusion research and SIMS analyses figure prominently therein.

While the sample matrix effects of electron-induced x-ray generation are well quantified by modeling absorption, fluorescence, and atomic number effects, there is no analogous theory applicable to SIMS. To convert the observed secondary ion intensity to a concentration, reference must be made to a previously characterized standard or set of standards of similar major element composition. Past efforts to create calibration curves for hydrogen have been very successful, but have also demonstrated that matrix effects for hydrogen are substantial (e.g., Ihinger et al., 1994, Hauri et al., 2002). Consequently, extrapolation of calibrations beyond a limited range of sample chemistry greatly increases analytical uncertainty. We present analyses of hydrogen-implanted materials covering a wide range of chemistry. These data show a weak relation between the mean atomic weight of the sample and the calibration factor for hydrogen, and also indicate that some compositions are not good candidates for hydrogen ion implantation.

Past work using FTIR

Since the early 1980s, the application of modern infrared spectroscopic techniques as a quantitative and nondestructive approach has been developed for the measurement of H_2O and CO_2 in natural samples (for review see Ihinger et al, 1994). In particular, the use of micro-Fourier transform infrared (FTIR) spectroscopy in the past decade has allowed the quantification of pre-eruptive volatile contents trapped in melt inclusions, thus greatly increasing our understanding of the role of H_2O and CO_2 in terrestrial volcanism (Dixon et al., 1995, Wallace et al., 1995). The most commonly used FTIR method to measure dissolved volatiles has been the transmission technique, where an IR beam is passed through a polished "plate" of glass, and the absorption of radiation is observed in the frequency region corresponding to the characteristic vibration of the dissolved volatile (e.g. O-H). By measuring the height of the absorption peak, and knowing the thickness of the sample (path length of the beam) and the density of the glass, the concentration of the volatile can be calculated using the Beer-Lambert law (Stolper, 1982, Ihinger et al., 1994). This technique has several practical disadvantages that were discussed in detail by Ihinger et al. (1994) and Grzechnik et al. (1996). For example, sample preparation is tedious due to the polishing necessary to produce plates with parallel faces. This is particularly challenging for melt inclusions, and also means that only one melt inclusion per mineral grain can usually be analyzed. Error is also introduced in the measurement of the plate thickness and density of the glass. Also, at high concentrations of volatile components that have a strong IR absorption such as H_2O, the plate necessarily becomes very thin in order to extract a precise number from the absorbance spectrum. This places a practical upper limit on the concentration that can be measured using the transmission IR method.

Given the suitability of FTIR spectroscopy for the measurement of CO_2 and H_2O in silicate glasses, it is desirable to develop a technique based on FTIR reflectance

spectroscopy (Hadni, 1967, Efimov, 1995, McMillan and Hofmeister, 1988) to provide an alternate method that does not have the previously discussed disadvantages of the transmission technique. The reflectance method relies upon an infrared beam reflected from a single polished surface of the glass sample, and thus eliminates preparation of the doubly polished plate necessary for the transmission experiment. This simple sample preparation step makes the reflectance method ideal for use on samples already prepared for SIMS or electron probe microanalysis, and is particularly adapted to studies needing both major and trace element data in conjunction with volatile concentration. The single polished surface also lends itself to the measurement of multiple melt inclusions in a single host mineral grain by successive polishing steps to different depths within the crystal. These measurements would then lead to a more robust statistical analysis of pre-eruptive volatile contents, as well as possibly giving information on the "history" of volatile concentration within the magma chamber (i.e. would allow the possibility of measuring volatile concentration as a function of host crystal growth). Earlier studies have shown that carbon-oxygen bearing species can be quantified using this approach (Grzechnik et al., 1996, Moore et al., 2000). In this contribution, we describe newly-developed applications to H_2O determination by reflectance IR in basaltic, andesitic, and rhyolitic glasses.

ANALYTICAL INSTRUMENTS AND APPROACHES

SIMS description

In SIMS, a primary beam of ions strikes a sample at energies of a few keV, progressively removing, or sputtering, atoms from the surface. Some sputtered atoms are ionized in the process and these are accelerated into a mass spectrometer for mass selection and counting. For most geological applications, the primary ion species chosen are O^-, O_2^-, Cs^+ or K^+, although Ar^+ and O_2^+ beams are also occasionally used. A duoplasmatron is used to generate ion beams from gases (O_2, Ar) while Cs^+ and K^+ ions are generated in thermal ion sources from a reservoir of the alkali metal or alkali metal oxide. Detailed information about ion sources can be found in Benninghoven et al. (1987). It is desirable to send the primary ion beam through a filter (either magnetic sector or Wien filter) to deliver an isotopically pure beam to the sample (e.g., eliminating H^- and $^{16}OH^-$ and other species from a $^{16}O^-$ primary beam). For typical microanalyses, the primary beam is focussed to a spot a few microns across and, with the aid of an optical microscope, directed at the area of interest on the sample. Commercially-available SIMS instruments currently achieve minimum beam diameters below 1 μm, but only at low primary ion currents. This results in low secondary ion intensities and extremely long counting times. A good balance with other analysis requirements is commonly achieved with beam diameters between 3 and 20 μm. Typical crater depths for analyses of hydrogen are less than 1 μm, but can become deeper if several other elements are measured.

Either positive or negative secondary ions can be accelerated into the mass spectrometer, the choice depending on the analytical problem under investigation. Halogens, P, As, and Au show high negative ion intensities under Cs^+ bombardment, while alkali metals, alkaline earths, and most transition metals give high positive ion count rates during sputtering with O^-. Hydrogen shows somewhat higher secondary ion yields for negative than positive ions (Wilson et al., 1989). In the Cameca ims 3f and 6f SIMS

instruments used in this study, the secondary ion beam is focussed by transfer optic lenses, energy filtered by an electrostatic analyzer and adjustable energy window, mass filtered by an electromagnet, and steered by a second electrostatic analyzer to an electron multiplier for ion counting. See Hervig (1996) and an online tutorial by Ron Fleming (www.cea.com) for more details.

Ion implantation approach for calibrating the SIMS

A common method of calibrating secondary ion signals in the semiconductor industry employs ion implantation. In this approach an ion beam of an isotope of the element of interest is generated and directed at the sample at high energy. The current densities of the implanted species are typically low, so that significant sputtering of the sample does not occur. The impact energy of the species is high (.01 to 1 MeV), so that the ions are buried to a depth between 200-1000 nm in the sample. By carefully measuring the implanted ion current and the exposure time of the sample to this beam, an accurate flux into the sample can be calculated. The implanted sample is subsequently analyzed by SIMS using depth profiling techniques. Most simply, the primary beam is rastered over an area from100 x 100 μm^2 to 250 x 250 μm^2 and the ion signal from the sample is monitored as a function of time (depth). A field aperture is placed in the path of the secondary ions to restrict admission to the mass spectrometer only to those ions originating from the center of the crater. This eliminates ions from the crater walls, which would compromise the depth resolution. After the analysis, the depth of the crater is measured by stylus profilometry (here, we used an Alphastep 200 instrument). While using ion implantation for calibrating the SIMS is common in the semiconductor industry (Leta and Morrison, 1980), it is rarely applied to problems in geochemistry (Wilson and Long, 1982, Streit et al., 1986, Kurosawa et al., 1992, Cabri and McMahon, 1995).

For this study, we mounted 29 glass and mineral samples into epoxy-filled holes in 5 drilled aluminum disks. Each disk contained a fragment of dry SiO_2 glass (H_2O content < 20 ppm by FTIR) and 6 other samples. Most of the glasses (provided by R. Lange, Department of Geol Sci., U. Michigan) came from the studies of Nelson and Carmichael (1979), Stein et al. (1986), and Lange and Carmichael (1987). Additional materials included crystalline olivine (Fo_{80}, Fo_{90}), Gore Mountain garnet (Valley et al., 1995), and glassy $LiAlSiO_4$, MORB basalt (Hervig et al., 2002), and Macusani rhyolite (Pichavant et al., 1987). The samples were sent to Los Alamos National Laboratory, where they were implanted with 1 x 10^{16} H/cm^2 at an impact energy of 40 keV (the error in the dose is $\leq \pm 3\%$). This dose was selected because the peak concentration of the implant would be < 1 atomic % H (corresponding to approximately 0.5 wt.% H_2O). This level is easily detectable, but is generally considered not so large as to influence the ion yields of the constituent atoms of the target (Wilson et al., 1989). The disks were coated with ~200Å Au prior to SIMS analysis, a standard practice to limit the charging of the sample under the primary ion beam.

Depth profiles were conducted using a primary beam of $^{16}O^-$ or $^{16}O_2^-$ and detection of positive secondary ions (quantification of negative secondary ions under Cs^+ primary bombardment is currently in progress). The raster size was 125 x 125 μm^2, and the primary currents were 70-100nA for $^{16}O^-$ and 35-45nA for $^{16}O_2^-$ beams, respectively. Secondary ions were accelerated to ~4.5 kV on the 3f SIMS and ~9kV on the 6f instrument. Hydrogen and $^{30}Si^+$ ions were measured by peak jumping the secondary magnet. Charging inside the crater during the profile was checked for frequently and was compensated by ramping the sample

voltage over a range of ~100 V while measuring the $^{30}Si^+$ signal, determining the centroid of the sample voltage *vs.* intensity plot, and returning the sample voltage to that value. Secondary ions with 0±20 and with 75±20 eV excess kinetic energy were monitored for both $^1H^+$ and $^{30}Si^+$. A 200μm diameter field aperture restricted the ions allowed into the mass spectrometer to a circular area 16 μm in diameter in the center of the crater.

Infrared instrument

The reflectance IR spectra were collected between 500 and 4000 cm^{-1} on polished glass samples using both a Bio-Rad FTS-40 spectrometer and a Bruker IFS-66v/s instrument. Reflectance measurements were duplicated on several identical samples using both spectrometers, providing spectra that were quantitatively indistinguishable between instruments. Both spectrometers were equipped with a Ge-coated KBr beamsplitter, a broadband MCT detector on a microscope attachment, and a Globar infrared source. In principle, only singly polished thick samples should be used for this technique, to avoid optical effects due to multiple reflections from both sides of the sample. Some interference effects were in fact observed in some samples that had previously been doubly polished and studied by the FTIR transmission technique.

The size of the microscope aperture used for all spectra was approximately 200 microns, with 1200 scans being taken for each spectrum at an effective spectral resolution of 4 cm^{-1} (fixed by the number of points sampled for the Fourier transform analysis), and with an interferometer speed of 20 kHz. At these conditions, each analysis set of scans (and FT conversion) took approximately 12 minutes. Backgrounds were taken on a silica glass slide thick-coated with gold before each sample was measured. The sample reflectance throughout the wavelength range is measured relative to that of the gold standard, which has a reflection coefficient of unity (100% reflectance) over the IR region measured in the experiment, and so the absolute value of the sample reflectivity is known with no further calibration. Unlike transmission measurements, there is no need for a sample thickness measurement because the optical constants giving rise to the reflectivity function are derived from reflection at a single surface, at the sample-air interface.

All of the andesitic samples and one of the rhyolites (SATCAM73-6) for this study (Table 1) derived from a suite of well-characterized natural volcanic compositions which have had water dissolved in them under high pressure H_2O-saturated conditions and their water contents subsequently measured by hydrogen manometry for a previous water solubility study (Moore et al., 1998). The basaltic samples were synthesized by Dr. S. Jakobsson (University of Iceland) using an icelandite starting material at high pressure and temperature with mixed volatile (CO_2 and H_2O) fluids present. The dissolved H_2O contents were subsequently determined using the FTIR transmission technique (as in Jakobsson, 1997). The remaining rhyolitic samples were synthesized and characterized for H_2O content by Dr. H. Westrich (Sandia National Laboratory) using Karl-Fischer titration (Westrich, 1987).

Table 1: Empirical change in reflectance spectra of hydrous glasses at ~3500 cm^{-1}

Sample No.	wt% H_2O	Average $\Delta R_{3500}/R_{4000}$	N (spectra)
rhyolite			
RR-1	0.0	0.006	1
RR-8	0.1	0.000(3)	2
RR-6	0.1	0.009(1)	2
RR-5	0.2	0.010(3)	2
RR-7	0.2	0.019(3)	3
RR-13	2.1	0.039(1)	2
RR-3	2.9	0.082(5)	2
RR-2	5.1	0.124(1)	2
SATCAM73-6	8.4	0.177(2)	2
andesite			
M12dry-1	~0.1*	0.002(5)	5
SATM12-1	2.62	0.038(7)	3
SATM12-2	5.03	0.095(6)	2
SATM12-4	6.76	0.133(2)	2
PEM12-20	6.82	0.135(4)	3
icelandite			
430	~0.1*	-0.004(5)	3
433	1.4	0.032	1
429	1.9	0.034(2)	2
426	2.5	0.047(9)	3
427	4.8	0.133(7)	3
425	6.2	0.140(4)	2

*- estimated H_2O contents for glasses held at ~1200°C for 24 hours at 1 atmosphere.
Standard deviation for averages given in parentheses.

RESULTS

SIMS analyses of H-implanted samples

At the time of this writing, all the implanted samples have been analyzed at least once on the Cameca ims 3f and several samples have also been analyzed on the Cameca ims 6f SIMS. Only the signals from ions with 75±20 eV excess kinetic energy are presented in this paper as the low energy ions (0±20 eV)showed a very high signal from adsorbed H derived from H species in the vacuum chamber (Ihinger et al., 1994). Two depth profiles of implanted silica glass are shown in Figure 1. The top one (Fig. 1A) shows a more-or-less ideal example; as the depth profile begins, the H^+ signal is very high as a result of sputtering through the surface H adsorbed on the sample. The signal decreases in the first 200 nm and then increases as the implanted hydrogen is encountered. The signal reaches a peak at a depth around 600 nm and then decreases to a signal representing a combination of the intrinsic H in the sample and the contribution from H in the residual vacuum of the SIMS landing in the crater and being sputtered. Note that the peak is not symmetric. Some H is backscattered during implantation, leading to this asymmetry toward the shallow side of the implant. The calibration is determined using the integrated signal of the implanted H and a matrix species ($^{30}Si^+$) in the following manner:

$$RSF = (\text{Dose (atoms/cm}^2) * \sum {}^{30}Si^+/0.0301)/(\text{Crater Depth (cm)} * \sum \text{H-background})$$

where RSF is Relative Sensitivity Factor, the dose is $1x10^{16}$, the factor of 0.0301 corrects the $^{30}Si^+$ signal for the presence of ^{28}Si and ^{29}Si, and the crater depth is that part of the crater used for the calculation (the first 200 nm or so are neglected as it is dominated by surface adsorbed hydrogen). The RSF is in units of atoms/cm^3 and multiplying it times the H^+/Si^+ ion signal measured in an unknown phase of the same composition (corrected to 100% Si isotopic abundance) directly gives the hydrogen atomic concentration in this phase. Dividing this by the atomic density of the sample (e.g, SiO_2 contains 7×10^{22} atoms/cm^3) gives atom fraction. The RSF values that we calculated were also normalized to the mole fraction of Si in the phase (RSF/Si). This allowed comparison between the RSF values determined on phases with different silica contents.

In contrast to the profile depicted in Figure 1A, the profile shown in Figure 1B shows a constantly decreasing signal for hydrogen, and so subtracting the background H signal from the implanted H signal becomes difficult. An attempt was made to draw a smooth curve from the shallow part of the crater to a depth below the implant, but if the implanted H is actually moving toward the surface, then this approach will give too low an integrated H signal. In some cases, a profile such as Figure 1B might represent a mis-registration of the field aperture and primary beam raster. That is, the field aperture was not selecting ions from the center of the crater, but rather from the crater edge. For these analyses, however, the raster size was 125 x 125 μm^2 and the field aperture defined a circular analysed area <20 μm in diameter, so significant misregistration is unlikely. The calculated RSF/Si values for the profiles in A and B are 5.23×10^{23} and 5.79×10^{23}, respectively, and indicate a lower integrated H signal from B.

The assumption that a 1% addition of H would have no affect on the yields of other ions was tested by monitoring the intensity of $^{30}Si^+$ during several analyses. In general, Si ion intensities did not change throughout the depth profile. Some profiles did show a small decrease in the Si signal at a depth corresponding to the peak in the implanted H signal. Usually, the decrease in Si was less than 5-8% of the original Si signal. The major difference in the analyses that showed variable Si ion intensities was that these profiles used the H^+ ion intensity to determine the extent of charge compensation required in the analysis (instead of the $^{30}Si^+$ intensity as described earlier). Positive hydrogen ions display an energy spectrum that is strongly affected by changing hydrogen contents (Ihinger et al., 1994) so that as the peak of the implant was approached, the sample voltage was over-corrected for charging, resulting in low silicon ion intensities where the H signal was highest. The Si intensity at depths below the implant were not affected and these signals were used for calculating RSF values (e.g., the "max Si" intensity indicated on Fig. 1A). Comparing the RSF/Si values on the SiO_2 glass mounted in the five sample disks (using only the profiles where the H signal intensity behaved as in Figure 1A) showed small variation in RSF/Si (1σ <5%).

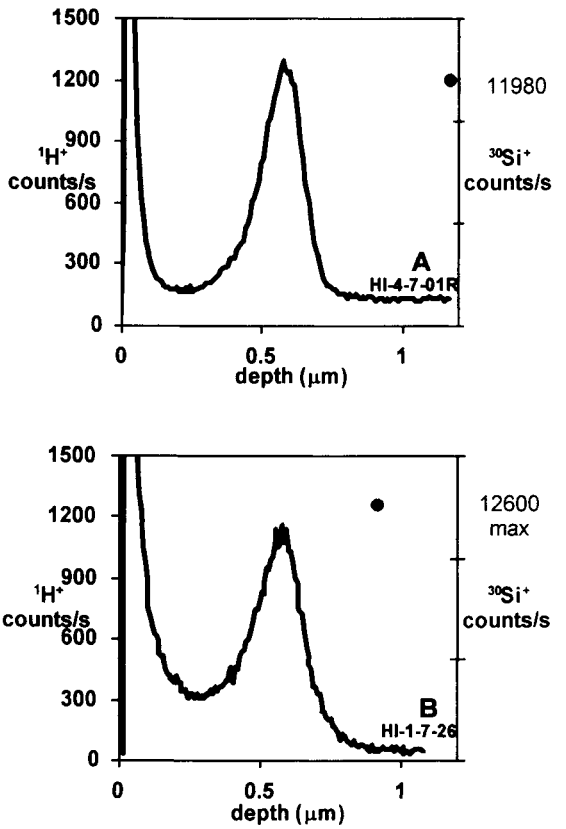

Figure 1. Depth profiles of hydrogen-implanted SiO_2 glass. Left and right axes show H^+ and $^{30}Si^+$ ion intensities (counts/s), respectively(A) Depth profile showing good behavior for H. (B) Depth profile showing poorer behavior for H in that the valley between the surface H and the implanted H peak is significantly higher than the H signal at ~1 μm depth.. The peak H signal corresponds to ~ 0.5 wt.% H_2O.

The RSF/Si values determined on all the H-implanted samples are listed in Table 2. No differences in RSF/Si between analyses using primary beams of $^{16}O^-$ and $^{16}O_2^-$ were observed. Some researchers have found relations between SIMS calibrations and the mass of the sample (Hervig et al., 1992, Eiler et al., 1997, King et al., 2002). For comparison with (King et al., 2002) we present the hydrogen calibrations in a similar manner on Figure 2 (see Fig. 7 for an example and Table 2 below for a description). There is a general decrease in the slopes (proportional to the relative H ion yield) with increasing sample mass, as observed by King et al. (2002). We have not found any simple relationship between any single element in the samples and the hydrogen calibration.

Table 2: Relative sensitivity factors (RSF) for H-implanted glasses and minerals.

sample	ref.	gfw*	average RSF (x 10^{23})	mole fraction Si	average RSF/Si (x 10^{23})	calculated calibration slope†
Nelson-10	(1)	71.32	1.69	0.224	7.56	**
Nelson-12	(1)	65.67	1.39	0.243	5.72	**
Nelson-15	(1)	68.85	1.25	0.211	5.91	**
Stein-2	(2)	68.39	1.92	0.220	8.73	0.17
Stein-10	(2)	70.22	1.99	0.188	10.56	0.14
Stein-12	(2)	68.45	1.93	0.183	10.55	0.14
Stein-15	(2)	73.37	2.16	0.169	12.77	0.12
macusanite glass	(3)	64.71	1.33	0.254	5.23	0.28
MORB glass	(4)	73.12	2.49	0.170	14.65	0.12
San Carlos olivine	(5)	73.49	2.56	0.145	17.64	0.12
Springwater olivine	(5)	75.99	3.64	0.137	26.55	0.08
Gore Mountain garnet	(6)	75.95	3.11	0.129	23.98	0.11
silica glass	(7)	60.08	1.64	0.333	4.93	0.29
eucryptite glass	(8)	63.00	1.17	0.173	6.74	0.20
Nelson-2	(1)	67.75	1.69	0.206	8.23	**
LC-2 glass	(9)	69.23	1.64	0.159	10.33	0.16
LC-3 glass	(9)	73.95	2.86	0.175	16.34	0.11
LC-4 glass	(9)	73.32	1.90	0.107	17.78	0.10
LC-6 glass	(9)	75.05	2.83	0.144	19.70	0.09
LC-9 glass	(9)	64.78	1.24	0.218	5.70	0.28
LC-10 glass	(9)	65.38	0.91	0.203	4.50	0.36
LC-11 glass	(9)	66.31	0.98	0.178	5.48	0.30
LC-12 glass	(9)	68.74	1.69	0.165	10.27	0.16
LC-13 glass	(9)	70.45	1.69	0.154	11.00	0.16
LC-14 glass	(9)	72.35	2.93	0.188	15.59	0.11

* gfw (gram formula weight) is calculated from a composition normalized to 2 oxygen atoms.

† calibration slope is the slope on a plot of H_2O (wt.%) vs $H^+/^{30}Si^+ * X_{SiO2}$, where X_{SiO2} is the weight fraction of silica in the sample. It was calculated by converting the RSF from a term that yields H concentrations in atomic density to a term that yields H_2O in wt. % (see Fig. 7).

** Slopes for these samples were not calculated due to lack of glass density data.

References to sample composition or preparation are given in: (1) Nelson and Carmichael (1979), (2) Stein et al. (1986), (3) Pichavant et al. (1987), (4) Hervig et al. (2002), (5) Hervig et al. (1992), (6) Valley et al. (1995), (7) from ASU glass shop, (8) Roy and Navrotsky (1984), (9) Lange and Carmichael (1987).

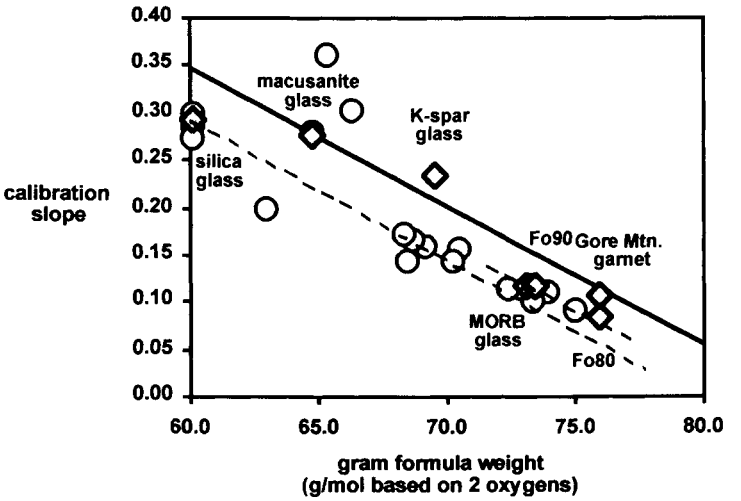

Figure 2. Sample formula weight vs. H calibration slope. Filled diamonds indicate 7 minerals and glasses from one sample mount (data from Table 2). Bold line is redrawn from (King et al., 2002). Dashed lines are parallel to the bold line and drawn to connect groups of samples.

Empirical calibration of reflectance IR for H_2O

A representative reflectance IR spectrum of an andesitic glass containing 6.8 wt. % H_2O is shown in Figure 3. The resonance due to the stretching vibration of dissolved H_2O in the glass is observed as a strong feature at 3650 cm^{-1}, superimposed on the slowly varying reflectivity function of the silicate glass above the frequency range of first-order glass phonons (these give rise to the strong increase in reflectivity below ~1300 cm^{-1}). Magnified views of the 3650 cm^{-1} feature for three andesite glasses containing from 0 to 6.8 wt% dissolved H_2O are shown in Figure 4.

At normal incidence, the reflectivity is related to the refractive index (n) of the silicate glass matrix through the Fresnel relation:

$$R = (|n - 1| / |n + 1|)^2 \qquad (1)$$

The frequency dependence of the refractive index ($n(\nu)$) in the "high frequency" range far from vibrational or electronic resonances is mainly determined by the interaction of light with the electron density in the sample. At a given frequency, n is then generally well-correlated with the glass density (Efimov, 1995).

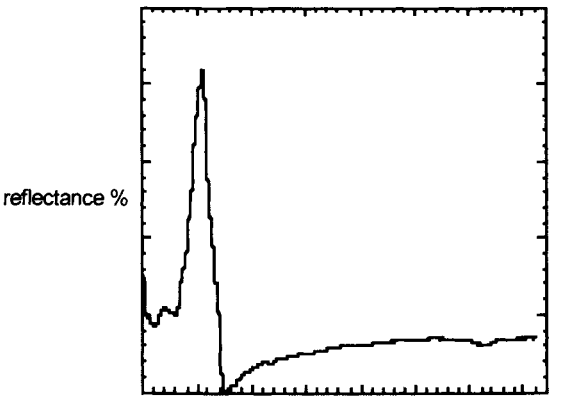

Figure 3. Reflectance IR spectrum on andesitic glass with 6.8 wt.% H_2O.

The feature due to H_2O at ~3650 cm^{-1} is clearly distinguishable from the smoothly varying glass reflectivity in this spectral region. In Figure 4, changes in the reflectance spectra in the 3000-4000 cm^{-1} region as a function of dissolved H_2O concentration are shown. There is an obvious variation in the amplitude of the H_2O resonance in the reflectivity function and the H_2O content. Due to the nature of the reflectivity function in the vicinity of the O-H resonance, the feature appears as a "negative" peak. To establish an easily used empirical relation between the contribution to the reflectivity curve from the H_2O resonance and the H_2O content, we have chosen to measure the maximum amplitude (ΔR_{3650}%) of the signal at ~3650 cm^{-1} resonance (e.g., the reflectivity at ~3200 cm^{-1} minus the reflectivity in the valley near 3650 cm^{-1}). The amplitude of this function is directly dependent upon the H_2O content for a given glass refractive index (correlated with its density). Because of instrumental variation that might occur, it is useful to normalize this value to a reflectivity taken close to, but distinct from, the region of resonance. We have chosen R_{4000} for convenience. The $\Delta R_{3650}/R_{4000}$ ratio measured remained constant within 10% for measurements taken on a given sample, although the absolute reflectivities show a much greater variation due to the reasons already described. The results for the samples studied here are given in Table 1, and in Figure 5 we plot the values of the normalized reflectivity ($\Delta R_{3650}/R_{4000}$)% for all of the compositions against wt. % H_2O to establish an empirical correlation. A best fit line and descriptive equation to the data for each composition is shown. The standard errors of the slopes are <6% (1σ) relative, and the regression error corresponds to approximately 0.4 wt% H_2O (2σ). Detection levels are $\leq$0.5 wt.%.

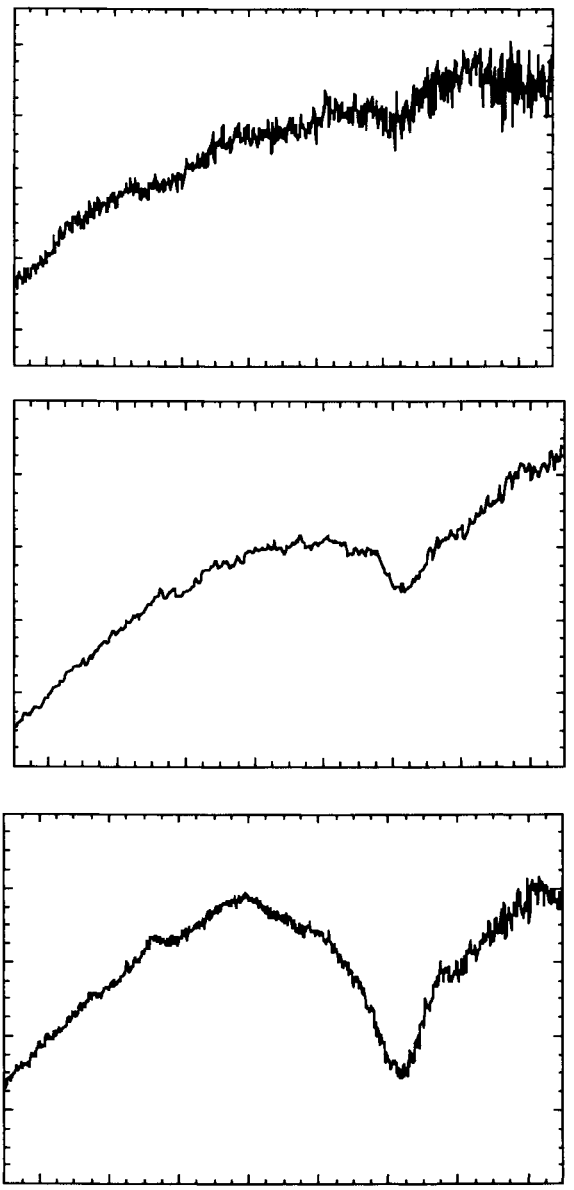

Figure 4. Reflectance spectra from 2500 to 4100 cm^{-1} on three andesite glasses containing from ~0 to 6.8 wt. % H_2O.

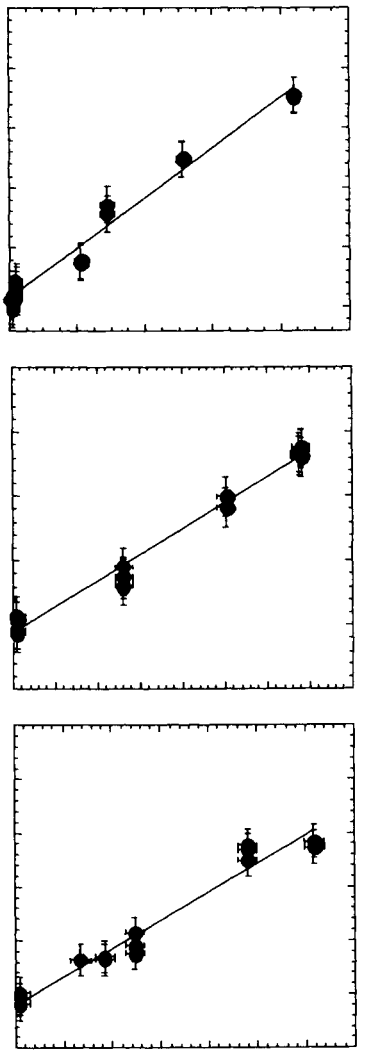

Figure 5. Infrared reflectance signal for O-H resonance (see text) as a function of total water content in hydrous rhyolite, andesite, and icelandite glasses.

DISCUSSION

Hydrogen analyses by SIMS

To convert secondary ion signals to absolute concentrations, most geochemists using SIMS apply a calibration based on the analysis of several standard materials. An example is shown on Fig 6, where three glass samples containing known amounts of Zr are compared to measured zirconium ion intensities. Following earlier conventions (Ihinger et al., 1994), the $^{90}Zr^+$ signal is normalized to a matrix signal (in this case, $^{30}Si^+$) and the matrix element abundance (in this case the weight fraction of SiO_2). The correlation in this example is very good and linear over a wide range of concentrations. Such a calibration allows accurate analysis for Zr in other high silica glasses. In this case and in certain others (e.g., boron, Hervig, 1996, Chaussidon et al., 1997), the calibration is not overly sensitive to composition so can be applied to samples with different amounts of silica (e.g., rhyolitic to basaltic compositions). Calibrations for a wide range of elements have been obtained, and these allow the determination of many elements in a single melt inclusion (e.g., Kovalenko et al., 1995).

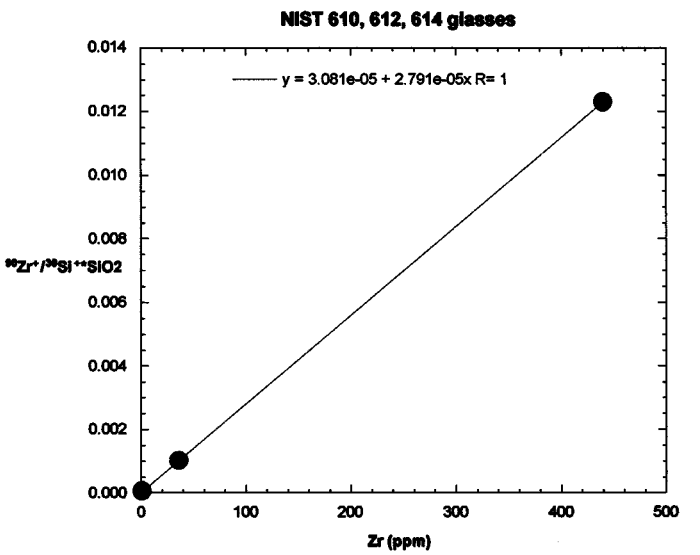

Figure 6. SIMS calibration for zirconium in three reference silicate glasses. Zr secondary ions with 75±20 eV initial kinetic energy were normalized to $^{30}Si^+$ and the wt. fraction silica.

The calibration of the SIMS for hydrogen represents a much different problem. Early studies (Steele, 1986, Hervig and Williams, 1988) found strong matrix effects on the measurement of hydrogen (as H^+ ions) in minerals and glasses sputtered with $^{16}O^-$ primary ions. Hervig and Williams (1988) determined that secondary electrons generated during sputtering were responsible for desorbing significant numbers of surface hydrogen atoms as H^+ ions, and these electron stimulated desorption (ESD) processes contributed to the matrix effects. Desorbed hydrogen can be eliminated from the mass spectrum by selecting secondary ions with >10-20 eV excess kinetic energy. Paillat et al. (1992) tested the effect

of selecting different energy ranges for hydrogen analysis by SIMS and concluded that the optimum secondary ion energies were >60 eV. However, even with the H^+ ions generated by ESD eliminated, matrix effects remain. For example, SIMS calibrations on peralkaline rhyolite, phonolite, basalt, humite minerals and hydrous Phase A are shown on Figure 7. The $H^+/^{30}Si^+$ ion ratio has been corrected for the silica content of the samples, but the slopes still vary by over a factor of 2 (ions with 75±20 eV excess energy were detected). Examining only the rhyolitic (~70 wt.% SiO_2) and basaltic (~50 wt.% SiO_2) glasses suggest that andesitic compositions (~60 wt.% SiO_2) might be expected to have an intermediate slope. However the phonolitic glasses (~59% SiO_2) are not distinguishable from the basaltic glasses on Figure 7, showing that the variation in relative ion yields for H^+ are not related only to silica concentrations. Measurements of H^- using $^{16}O^-$ primary ions have revealed similar matrix effects (Ihinger et al., 1994).

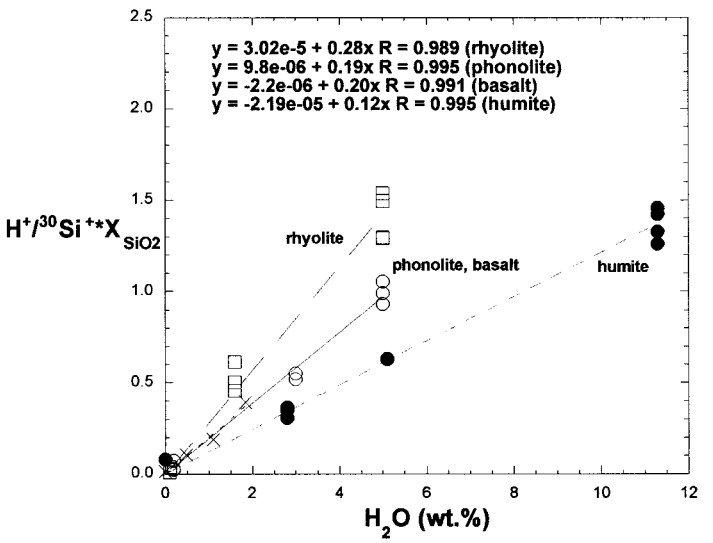

Figure 7. SIMS calibration for H in glasses of rhyolitic (open squares), phonolitic (open circles), and basaltic (crosses) glasses along with hydrous Phase A and humite minerals. Data from Kawamoto et al. (1995).

When a Cs^+ primary beam is used to sputter negative H ions, different results are observed. Hauri et al. (2002) showed that: 1) H^-/Si^- ratios increased linearly from 0-1.5 wt. % H_2O for basalt, andesite, and rhyolite glasses and 2) the calibrations overlapped without correcting for silica abundance. At water contents > ~1.5 wt. %, the calibrations diverged and became nonlinear. If the H^-/Si^- ratios are normalized to the silica concentration of the sample (see Fig. 8), the calibrations stay linear up to ~3 wt.% H_2O and there are only small differences in the calibrations for the three compositions. We have also studied the yields of H^- ions from hydrous minerals sputtered with a Cs beam (ASU, unpublished data) and confirm the non-linear results shown by Hauri et al. (2002). If reliable standards are available, non-linearities do not impede the collection of high quality analyses.

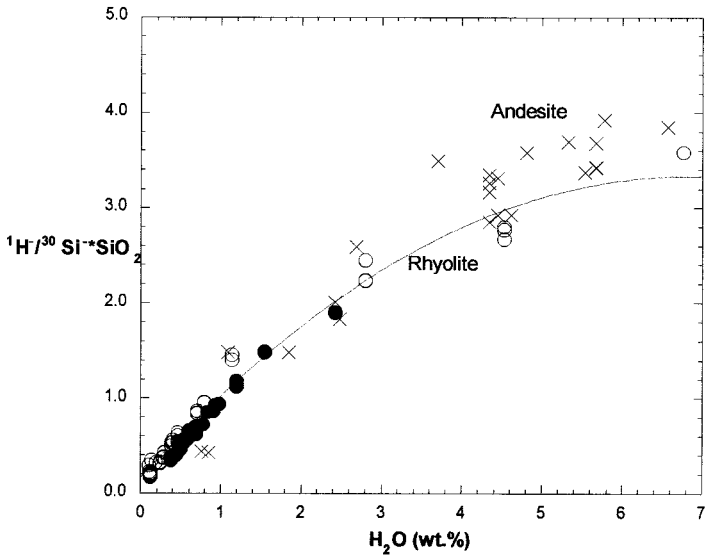

Figure 8. SIMS calibration for negative hydrogen ions sputtered from silicate glasses with a Cs^+ primary beam. Basaltic glasses shown as filled circles, andesitic glass as crosses and rhyolitic glass as open circles. Curve through rhyolite data is a second order polynomial regression. Redrawn from Hauri et al. (2002).

Application to melt inclusions

The trend in H calibrations displayed by the implanted samples (Fig. 2) suggests that it may be possible to estimate a calibration for H^+ ions on any glass sample for which an electron probe analysis is available (to calculate the mass of the sample). But first such an approach must be tested to see if implanted samples give the same calibration for H as working curves such as in Figure 7. When hydrogen is added to a nominally dry glass by implantation, it is not in the same atomic positions as when dissolved in a liquid at high P and T. It is thus important to consider if this causes a change in hydrogen ion yields. During the depth profile analysis, the primary beam penetrates the sample to a depth ranging from 30-60 nm, rearranging the atoms to some new configuration during this stirring effect before the surface is exposed and secondary ions are ejected. Because samples containing implanted or dissolved H experience this ion beam mixing and atomic rearrangement, we would predict that both types of samples would give the same calibration. To test this, we compare the H-implanted rhyolite and basalt to the calibrations derived from working curves (Fig. 7). The implanted rhyolite gives a calibration of 0.28 which matches the slope defined by the calibration curve for rhyolitic glasses on Figure 7 (0.28). A similar calculation using the implanted MORB glass gives a slope of 0.12, nearly one-half the slope determined for basaltic glasses on Figure 7 (0.2).

The reason for the H-implanted rhyolite glass matching well with the working curve on Figure 7 and the implanted MORB matching poorly is not known.. The implanted MORB glass gives relatively low integrated H signal compared to the basaltic glasses in

Figure 7. Perhaps the environment of the implanted H in the MORB glass is so different compared to hydrated basaltic glass that the yield of positive H ions is affected. Perhaps the negative charge build-up in the crater attracts protons to the surface and they escape into the gas phase. If the latter were true, then we might expect that the profiles would change as a function of primary beam intensity (changing the charge delivered to the sample). However, depth profiles conducted on the implanted basaltic glass at a wide range of primary currents do not give different results. The first explanation (different environment for implanted H vs dissolved H) is presently the most likely reason for the observed differences between the two approaches to calibration for basaltic glass. However, these differences do not appear in all compositions (e.g., rhyolitic glass). We note that many of the samples which give low integrated H^+ signals are Fe-rich. This potential relationship shall be investigated in the future. It is not yet clear which compositions will be suitable for H-implantation calibration techniques.

Summary of SIMS

In terms of calibrating the SIMS for H analyses, it is clear that the yield of positive hydrogen ions generated during sputtering with an O^- primary beam decreases with increasing mass of the sample. However, the trend in Figure 2 can not be used to predict calibrations on natural glasses in the general case because there is considerable scatter and the implanted basaltic glass fails to match the calibration for hydrated basaltic glasses determined independently. At this time, the relation between sample mass and H calibration may be more reliably determined by using experimentally hydrated liquids and hydrous minerals as presented in King et al. (2002).However, even in this case the trend from the latter study (reproduced on Fig. 2) would suggest a calibration for basaltic glass of ~0.17 instead of the measured 0.2.

Detecting negative hydrogen ions under Cs bombardment shows much smaller matrix effects than when positive hydrogen ions are studied (Fig. 8). It remains to be determined if the H^- ion yield from implanted samples under Cs bombardment will produce as good or better match with working curves than our present work on H^+ ions. Because the peak concentration of the implants is only ~0.5 wt.%, they represent concentrations in the linear region of Figure 8.

Despite the presence of matrix effects on positive and negative hydrogen ions, existing calibrations allow quantitative water contents to be determined on "typical" rhyolite, andesite, and basaltic compositions (Figs. 7, 8, Ihinger et al., 1994, King et al., 2002). The choice of polarity depends on the other interests of the analyst. When positive ions are studied, low detection levels are also achievable for many lithophile elements, such as Li, Be, B, Rb, Sr, Y, Zr, Nb, Mo, Cs, Ba, REE, Hf, Pb, Th, and U (e.g., Kovalenko et al., 1995). When negative ions are studied, several other volatile elements such as C, F, S, and Cl are accessible and show good detection levels (Hauri et al., 2002). It is also possible to measure appropriately sized melt inclusions using both approaches (on different sessions). Determination of H contents can potentially be coupled with δD, or with δ^7Li, $\delta^{11}B$, or Pb isotope ratios (in positive mode) or with $\delta^{12}C$, $\delta^{18}O$, $\delta^{34}S$, and $\delta^{35}Cl$ (in negative mode).

Comparison of reflectance and transmission IR calibrations

The results from the reflectance IR experiments on glasses with known total H_2O contents can be compared to previous calibrations for similar compositions that used the transmission technique by performing a Kramers-Kronig transformation procedure (Burns, 1990, Efimov, 1995) on the reflectance spectra. The details of the mathematical algorithm and the procedure used can be found in Moore et al. (2000). Our results show that the absorption coefficients for the total H_2O feature at ~3500 cm^{-1} calculated from the reflectance spectra compare very well to those for basalt and andesite. For example, we calculate an absorption coefficient for the icelandite of 51±9, while the value for basalt from Dixon et al. (1988) is 63±5. The absorption coefficient for andesite from reflectance IR is 63±9, compared to 62.3±0.4 by Mandeville et al. (2002). Our calculated value for rhyolite is 101±12, but no direct comparison with transmission IR can be made because the value given in Newman et al. (1986) is for the OH component only, while our high water rhyolite samples surely have significant amounts of molecular H_2O dissolved in them.

Application of reflectance IR to melt inclusions

Examination of the calibration for H_2O on rhyolite, andesite, and icelandite glasses in Figure 5 shows slopes of 0.021, 0.020, and 0.026, respectively. The apparent small effect of sample chemistry on the calibration is conducive to using reflectance IR to characterize a wide (chemical) range of melt inclusions for their water content, and contrasts strongly with the SIMS calibrations shown on Figure 7 and for the high water samples shown on Figure 8. However, all of the reflectance IR spectra shown here were measured using a 200 micron aperture on large (2-3 mm) pieces of glass. This size aperture allows a good signal to noise ratio with a reasonable counting time (1200 scans; ~10-12 minutes/spectra). Because melt inclusions are usually 50-100 microns in diameter (or smaller), this raises the question of the applicability of reflectance IR to this type of sample. Our experience has shown that it becomes problematic to obtain a pure glass spectra on inclusions less than ~100 microns in diameter. For smaller inclusions, it is difficult to place the beam only on the glass, and the strong signal from the host crystal (typically quartz for our samples) changes the overall shape of the reflectance spectrum and overwhelms the H signal. The requirement of smaller apertures in the spectrometer also significantly decreases the signal to noise, making longer scan times necessary. Very long scan times are not a problem if the atmosphere around the sample is stable and does not have fluctuations of H_2O and CO_2 content. For some spectrometers and laboratories, it may become necessary supply an inert atmosphere around the microscope using a glove bag or some other means (Moore et al., 2000). In summary, applying reflectance IR to melt inclusions requires fairly large inclusions or improvements in the IR source intensity.

CONCLUSIONS

Secondary ion mass spectrometry and reflectance infrared spectroscopy represent two useful techniques for the characterization of melt inclusions. As for all techniques, successful application requires the right samples. Water contents of melt inclusions <10 μm in diameter can be measured by SIMS, but for best results, the major element chemistry should be similar to that used as a standard. For reflectance IR analyses, inclusions larger than 100 μm in diameter are best, but matrix effects appear to be small enough so that

significant deviation of the unknown from the chemistry of the standard does not have a large effect on the calibration.

Acknowledgments. This material is based upon work supported by the National Science Foundation under Grant No. EAR-9975549 to R. Hervig and an NSF postdoctoral fellowship to G. Moore. The authors thank J. Barclay, H. Westrich, R. Lange, and S. Jakobsson for samples and E. Hauri for a preprint containing his data. Helpful reviews from Jim Webster and Graham Layne and comments on ion implantation from P. Williams are much appreciated.

REFERENCES

Benninghoven, A., Rüdenauer, F. G. and Werner, H. W. (1987) Secondary ion mass spectrometry: Basic concepts, instrumental aspects, applications, and trends., John Wiley & Sons, New York.

Burns, G. (1990) Solid State Physics, Academic Press.

Cabri, L. and McMahon, G. (1995) SIMS analysis of sulfide minerals for Pt and Au: Methodology and relative sensitivity factors (RSF)., Can. Mineral., 33, 349-359.

Chaussidon, M., Robert, F., Mangin, D., Hanon, P. and Rose, E. (1997) Analytical procedures for the measurement of boron isotope compositions by ion microprobe in meteorites and mantle rocks, Geostandard Newsletter, 21, 7-17.

Dixon, J. E., M., S. E. and Delaney, J. R. (1988) Infrared spectroscopic measurements of CO2 and H2O in the Juan de Fuca basaltic ridge glasses., Earth Planet. Sci. Lett., 90, 87-104.

Dixon, J. E., Stolper, E. M. and Holloway, J. R. (1995) An experimental study of water and carbon dioxide solubilities in mid-ocean ridge basaltic liquids, Part 1: Calibration and solubility models, J. Petrol., 36, 1607-1631.

Dunbar, N. W. a. H., R. L. (1992b) (1992) Volatile and trace element composition of melt inclusions from the Lower Bandelier Tuff: Implications for magma chamber processes, .

Efimov, A. M. (1995) Optical constants of inorganic glasses, CRC Press.

Eiler, J. M., Graham, C. and Valley, J. W. (1997) SIMS analysis of oxygen isotopes: Matrix effects in complex minerals and glasses, Chem. Geol., 138, 221-244.

Grzechnik, A., Zimmermann, H. D., Hervig, R. L., King, P. L. and McMillan, P. F. (1996) FTIR micro-reflectance measurements of the CO32- ion content in basanite and leucitite glasses, Contrib. Mineral. Petrol., 125, 311-318.

Hadni, A. (1967) Essentials of modern physics applied to the study of the infrared., Pergamon Press.

Hauri, E., Wang, J., Dixon, J. E., King, P. L., Mandeville, C. and Newman, S. (2002) SIMS analysis of volatiles in silicate glasses 1. Calibration, matrix effects and comparisons with FTIR., Chemical Geology, 183, 99-114.

Hervig, R. L. (1996) In Boron: Mineralogy, Petrology, and Geochemistry in the Earth's Crust (Rev. in Mineral. 33)(Eds, Grew, E. S. and Anovitz, L. M.) Mineral. Soc. Amer., Washington D.C., pp. 789-803.

Hervig, R. L., Dunbar, N., Westrich, H. R. and Kyle, P. (1989) Pre-eruptive water content of rhyolitic magmas as determined by ion microprobe analyses of melt inclusions in phenocrysts, J. Volc. Geother. Res., 36, 293-302.

Hervig, R. L., Moore, G. M., Williams, L. B., Peacock, S. M., Holloway, J. R. and Roggensack, K. (2002) Isotopic and elemental partitioning of boron between hydrous fluid and silicate melt., American Mineralogist, 87, 769-774.

Hervig, R. L. and Williams, P. (1988) In Secondary Ion Mass Spectrometry, SIMS VI(Eds, Benninghoven, A., Huber, A. M. and Werner, H. W.) J. Wiley & Sons, , pp. 961-964.

Hervig, R. L., Williams, P., Thomas, R. M., Schauer, S. N. and Steele, I. M. (1992) Microanalysis of oxygen isotopes in insulators by secondary ion mass spectrometry, Int. J. Mass Spec. Ion Proc., 120, 45-63.

Ihinger, P. D., Hervig, R. L. and McMillan, P. M. (1994) In Volatiles in Magmas (Rev. in Mineral. 30)(Eds, Carroll, M. R. and Holloway, J. R.) Mineral. Soc. Amer., Washington D.C., pp. 67-121.

Jakobsson, S. (1997) Solubility of water and carbon dioxide in an icelandite at 1400 °C and 10 kilobars., Contrib. Mineral. Petrol., 127.

Kawamoto, T., Leinenweber, K., Hervig, R. L. and Holloway, J. R. (1995) In Volatiles in the Earth and Solar System(Ed, Farley, K. A.) American Institute of Physics, New York, pp. 229-239.

King, P. L., Vennemann, T. W., Holloway, J. R., Hervig, R. L., Lowenstern, J. B. and Forneris, J. F. (2002) Analytical techniques for volatiles: A case study using intermediate (andesitic) glasses., American Mineralogist, 87, 1077-1089.

Kovalenko, V. I., Hervig, R. L. and Sheridan, M. F. (1988) Ion microprobe analyses of trace elements in anorthoclase, hedenbergite, aenigmatite, quartz, apatite and glass in pantellerite: Evidence for high water contents in pantellerite melts, Am. Mineral., 73, 1038-1045.

Kovalenko, V. I., Tsaryeva, G. M., Goreglyad, A. V., Yarmolyuk, V. V., Troitsky, V. A., Hervig, R. L. and Farmer, G. L. o., 90, 530-547. (1995) The peralkaline granites-related Khaldzan-Buregtey rare element (Zr, Nb, REE) deposit, Western Mongolia, Econ. Geol., 90, 530-547.

Kurosawa, M., Yurimoto, H., Matsumoto, K. and Sueno, S. (1992) In High Pressure Research: Application to Earth and Planetary Sciences(Eds, Syono, Y. and Manghnani, M.) Terra Scientific Publishing Co., Tokyo, pp. 283-287.

Lange, R. A. and Carmichael, I. S. E. (1987) Densities of Na2O-K2O-CaO-MgO-FeO-Al2O3-TiO2-SiO2 liquids: New measurements and derived partial molar properties., Geochim. Cosmochim. Acta, 51, 2931-2946.

Leta, D. P. and Morrison, G. H. (1980) Ion implantation for in-situ quantitative ion microprobe analysis., Anal. Chem., 52, 277-280.

Lowenstern, J. B. (1995) In Magms, fluids, and ore deposits., Vol. 23 (Ed, Thompson, J. F. H.) Mineralogical Association of Canada, Victoria, B.C., pp. 71-99.

Mandeville, C. W., Webster, J. D., Rutherford, M. J., Taylor, B. E., Timbal, A. and Faure, K. (2002) Determination of molar absorptivities for infrared absorption bands of H2O in andesitic glasses., American Mineralogist, 87, 813-821.

McMillan, P. F. and Hofmeister, A. M. (1988) In Spectroscopic methods in mineralogy and geology., Vol. 18 (Ed, Hawthorne, F. C.) Mineralogical Society of America, Washington, D. C., pp. 99-159.

Moore, G., Chizmeshya, A. and McMillan, P. F. (2000) Calibration of a reflectance FTIR method for determination of dissolved CO2 concentration in rhyoliite glass., Geochim. Cosmochim. Acta, 64, 3571-3579.

Moore, G. M., Vennemann, T. and Carmichael, I. S. E. (1998) An empirical model for the solubility of water in magmas to 3 kilobars., Amer. Mineral., 83, 36-42.

Nelson, S. A. and Carmichael, I. S. E. (1979) Partial molar volumes of oxide components in silicate liquids., Contrib. Mineral. Petrol., 73, 117-124.

Paillat, O., Elphick, S. C. and Brown, W. L. (1992) The solubility of water in NaAlSi3O8 melts: a re-examination of Ab-H2O phase relationsips and critical behaviour at high pressures., Contrib. Mineral. Petrol., 112, 490-500.

Pichavant, M., Valencia Herrera, J., Boulmier, S., Briqueu, L., Joron, J.-L., Juteau, M., Marin, L., Michard, A., Sheppard, S. M. F., Treuil, M. and Vernet, M. (1987) In Magmatic Processes: Physicochemical Principles., Vol. 1 (Ed, Mysen, B. O.) Geochemical Society, , pp. 359-373.

Roy, B. N. and Navrotsky, A. (1984) Thermochemistry of charge-coupled substitutions in silicate glasses: the systems M1n+/nAlO2-SiO2 (M=Li, Na, K, Rb, Cs, Mg, Ca, Sr, Ba, Pb)., J. Amer. Ceram. Soc., 67, 606-610.

Sisson, T. W. and Layne, G. D. (1993) H2O in basalt and basaltic andesite glass inclusions from four subduction-realted volcanoes., Earth Planet. Sci. Lett., 117, 619-635.

Steele, I. M. (1986) Ion probe determination of hydrogen in geologic samples, N. Jb. Miner. Mh., 1986, 193-202.

Stein, D. J., Stebbins, J. F. and Carmichael, I. S. E. (1986) Density of molten sodium aluminosilicates, J. Am Ceram. Soc., 69, 396-399.

Stolper, E. M. (1982) Water in silicate glasses: an infrared study., Contrib. Mineral. Petrol., 81, 1-17.

Streit, L. A., Hervig, R. l. and Williams, P. (1986) In Microbeam Analysis-1986(Eds, Romig, A. D., Jr. and Chambers, W. F.) San Francisco Press, San Francisco, pp. 91-94.

Valley, J. W., Kitchen, N., Kohn, M. J., Niendorf, C. R. and Spicuzza, M. J. (1995) UWG-2 a garnet standard for oxygen isotope ratios: strategies for high precision and accuracy with laser heating., Geochim. Cosmochim. Acta, 59, 5223-5231.

Wallace, P. J., Anderson, A. T. and Davis, A. M. (1995) Quantification of pre-eruptive exsolved gas contents in silicic magmas., Nature, 377, 612-616.

Webster, J. D., Congdon, R. D. and Lyons, P. C. (1995) Determining pre-eruptive compositions of late Paleozoic magma from kaolinitized volcanic ashes: Analysis of glass inclusions in quartz microphenocrysts from tonsteins, Geochim. Cosmochim. Acta, 59, 711-720.

Westrich, H. R. (1987) Determination of water in volcanic glasses by Karl-Fischer titration., Chemical Geology, 63, 335-340.

Wilson, G. C. and Long, J. V. P. (1982) SIMS analysis of lithium: ion implantation and matrix effects., Int. J. Mass Spec. Ion Phys., 42, 63-75.

Wilson, R. G., Stevie, F. A. and Magee, C. W. (1989) Secondary Ion Mass Spectrometry: A Practical Handbook for Depth Profiling and Bulk Impurity Analysis, J. Wiley & Sons, New York.

This Page Intentionally Left Blank

From Mantle to Atmosphere: Magma Degassing, Explosive Eruptions, and Volcanic Volatile Budgets

Paul J. Wallace

Department of Geological Sciences
University of Oregon
Eugene, OR 97403-1272

ABSTRACT

Over the past 25 years there has been a growing body of evidence based on petrologic, remote sensing, and volcanic gas data that andesitic, dacitic, and rhyolitic magmas in crustal reservoirs are saturated with a multicomponent C-O-H-S vapor phase before eruption. A key piece of evidence for magmatic vapor saturation is the "excess" S problem: the common observation that much more S is released by explosive eruptions than was originally dissolved in the erupted volume of silicate melt. If all of the "excess" S is derived from a magmatic vapor phase, then intermediate to silicic magmas must commonly contain several wt% exsolved vapor prior to eruption. The large amounts of volatiles implied by these estimates suggest that exsolved vapor accumulates in the apical regions of magma bodies during repose periods between eruptions. A major uncertainty in understanding volcanic SO_2 emissions has been lack of information on S partitioning between silicate melt and coexisting hydrous vapor. Recently published experimental data on melt-vapor partitioning show that S partitions strongly into the vapor phase under conditions relevant for most dacitic and rhyolitic magmas. Thermodynamic modeling based on these results suggest that the pre-eruptive magmatic vapor phase for dacitic to rhyolitic magmas typically contains 0.5 to 6 mol% total S. Andesitic, dacitic, and rhyolitic magmas in crustal reservoirs are probably vapor saturated due to recharge and underplating by vapor-saturated basaltic magma. CO_2 is particularly important because it is abundant in mantle-derived basaltic magma but has low solubility in silicate melts at crustal pressures. Understanding budgets of the major volatiles requires integrating remote sensing and volcanic gas data for volatile fluxes from volcanoes with petrologic data for both differentiated magma stored in crustal reservoirs and mafic magma recharging these systems. Comparison of repose times, eruptive volumes, and basaltic magma supply rates for a spectrum of volcanic systems suggests that the flux of S, CO_2 and H_2O from explosive eruptions is approximately balanced by the mantle-derived supply rate of these volatiles provided by mafic recharge into the crust.

INTRODUCTION

The volatile constituents, H_2O, CO_2, and S, play an important role in the generation, evolution and eruption of magma. Knowledge of the abundance and flux of

these volatiles is important for understanding explosive eruptive behavior of volcanoes, recycling of volatiles in subduction zones, formation of magmatic-hydrothermal ore deposits, fluxes of volcanic gases to Earth's atmosphere, and potential climatic impacts of large volcanic eruptions. Over the past two decades, new analytical techniques for measuring volatiles in melt inclusions from volcanic rocks and new developments in remote sensing technology used for analyzing volcanic emissions have led to major advances in our understanding of volatile fluxes from magmatic systems.

Sulfur dioxide (SO_2) is the easiest of the main magmatic volatiles to measure in volcanic plumes using ground- and satellite-based remote sensing techniques because of its relativevly high concentration in volcanic plumes relative to background values. However, CO_2 and H_2S can also be analyzed using airborne sensors (e.g., McGee et al., 2001) and H_2O and CO_2 can be measured using ground-based FTIR spectrometry (e.g., Burton et al., 2000). Numerous measurements of SO_2 fluxes from active volcanoes have been made using remote sensing techniques (see review by Symonds et al., 1994), including both ground and air-based use of the ultraviolet correlation spectrometer (COSPEC) and the satellite-based Total Ozone Mapping Spectrometer (TOMS). Comparison of such SO_2 emission data with petrologic studies of dissolved S in magmas based on analyses of quenched melt inclusions trapped inside phenocrysts has led to a conundrum, known as the "excess" sulfur problem, concerning sulfur mass balance during volcanic eruptions (Stoiber

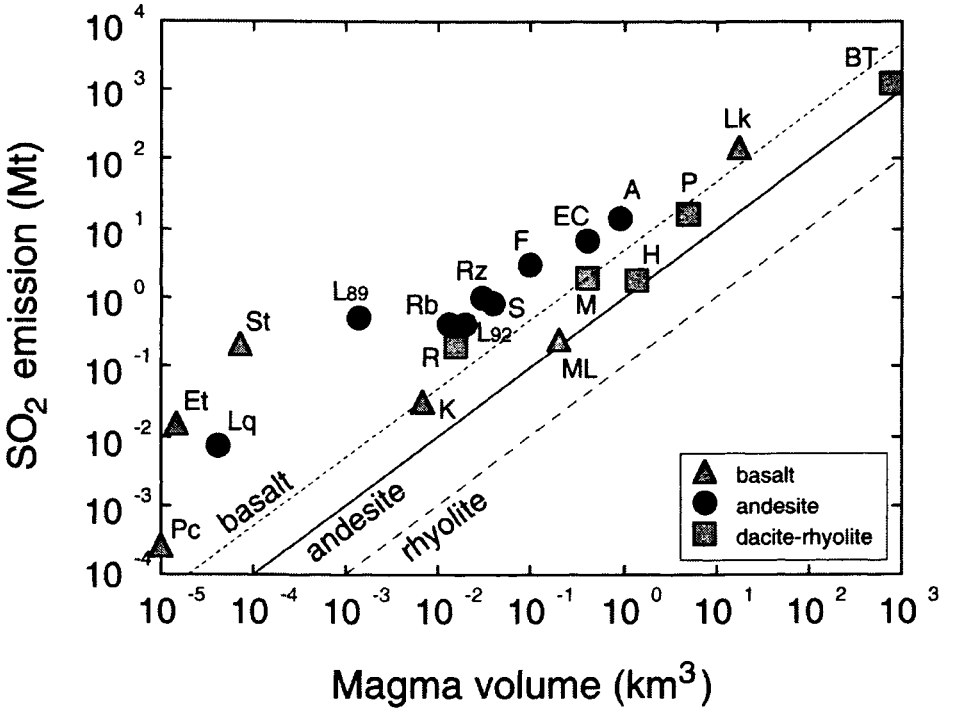

and Jepson, 1973; Rose et al., 1982; Andres et al., 1991). Concentrations of dissolved S in magmas before eruption, as estimated from melt inclusion data, are commonly far too low (by 1 to 2 orders of magnitude) to account for the total mass of SO_2 released during the eruption as measured by remote sensing techniques (Fig. 1). Excess eruptive S is observed in most eruptions for which remote sensing and melt inclusion data are available, and in particular, is characteristic of explosive eruptions of intermediate and silicic magma in subduction zone settings (Andres et al., 1991). In contrast, basaltic eruptions from divergent plate boundaries and hot spots, such as Hawaiian and Icelandic volcanoes, often do not show evidence of excess S emissions (Fig. 1).

Numerous lines of evidence from petrologic, remote sensing, and volcanic gas data suggest that the "excess" S problem is caused by the presence of an exsolved C-O-H-S vapor phase in the magma before the time of eruption (Anderson, 1975; Luhr et al., 1984; Sigurdsson et al., 1990; Andres et al., 1991; Lowenstern et al., 1991; Lowenstern, 1993; Gerlach et al., 1994; Wallace and Gerlach, 1994; Gerlach and McGee, 1994; Gerlach et al., 1996; Giggenbach, 1996; Wallace, 2001). As a result, eruptions of silicic magma can release large amounts of SO_2 derived from pre-eruptive exsolved vapor, despite the fact that such magmas generally have low concentrations of dissolved S. Techniques for quantifying the mass fraction of exsolved vapor in magma before eruption (Wallace et al., 1995; Scaillet et al., 1998; Wallace, 2001) are thus important for understanding SO_2 flux

---

Fig. 1. Volcanic SO_2 emissions, in megatons (1 Mt = 10^{12} g), vs. total volume of erupted magma. SO_2 emissions were measured using remote sensing methods except for the eruption of the Bishop Tuff (BT; see Wallace, 2001). Most of the remote sensing data are from the Total Ozone Mapping Spectrometer (TOMS), except for the data for Fuego (determined by COSPEC), Agung (estimated from stratospheric optical depth measurements), and Laki (estimated from information on atmospheric turbidity). Uncertainties of ±50% for both SO_2 emission and eruptive volume are less than to slightly greater than the size of the symbols. Uncertainties in SO_2 emission data are generally considered to be about ±30% for the TOMS data and ±20% to 50% for COSPEC (see discussion in Symonds et al., 1994). Data are shown for the following eruptions: (A) Agung, 1963, (EC) El Chichon, 1982, (Et) Etna, 1975, (F) Fuego, 1974, (H) Cerro Hudson, 1991, (K) Kilauea, annual average, (L89) Láscar, 1989, (L92) Láscar, 1992, (Lk) Laki, 1783-1784, (Lq) Lonquimay, 1989, (ML) Mauna Loa, 1984, (M) Mount St. Helens, 1980, (Pc) Pacaya, 1972, (P) Pinatubo, 1991, (Rb) Rabaul, 1994, (R) Redoubt, 1989-90, (Rz) Ruiz, 1985, (S) Spurr, 1992, (St) Stromboli, annual average. Data are taken from Gerlach and Graeber, (1985), Andres et al. (1991; and references therein), Bluth et al. (1993, 1997), Allard et al. (1994), Gerlach et al. (1994), Gerlach and McGee (1994), Miller et al. (1995), Self and King (1996), Roggensack et al. (1996), Thordarson et al. (1996), Naranjo and Stern (1998), and Calder et al. (2000). Shown for comparison are predicted relationships between SO_2 emission and eruptive volume for rhyolitic (dashed line), andesitic (solid line), and basaltic (short dashed line) melts calculated by assuming that the only SO_2 released during the eruption is from S that is originally dissolved in silicate melt. Note that the SO_2 emissions for all eruptions, with the exception of Mauna Loa, Kilauea, and Laki, are at least 1 order of magnitude greater than predicted for the appropriate bulk composition by syneruptive degassing of dissolved S only. This clear discrepancy over many orders of magnitude in eruptive volume indicates that a major additional source of S must be involved in all of these eruptions.

data used for forecasting eruptions and assessing the potential impacts of volcanic eruptions on Earth's climate and atmosphere. In addition, exsolved vapor in crystallizing magma bodies can trigger volcanic eruptions (Blake, 1984; Tait et al., 1989; Woods and Pyle, 1997) and contributes to some magmatic-hydrothermal ore deposits (Burnham, 1979; Hedenquist and Lowenstern, 1994; Kamenetsky et al., 2002). The purpose of this paper is to use melt inclusion and remote sensing data to quantify the abundance of pre-eruptive exsolved vapor in crustal magmatic systems. I then use these data to examine the sources and fluxes of the major volatiles by comparing the volatile contents and recharge rates of mantle-derived mafic magma with the output rates constrained from remote sensing and geochronologic data. In the following sections, I begin by reviewing petrologic evidence for pre-eruptive vapor saturation in magmas and methods for constraining the concentration of S in the vapor phase.

VAPOR SATURATION OF MAGMA

Volatile components occur as dissolved species in silicate melts, but they can also be present in an exsolved, multicomponent vapor phase if a melt is vapor saturated. The thermodynamic requirement necessary for vapor saturation is that the sum of the partial pressures of all dissolved volatiles in a silicate melt must equal the local confining pressure (Verhoogen, 1949). If a magma is vapor undersaturated, then volatiles will be present in solution only. During differentiation of vapor-undersaturated magma, concentrations of volatiles in residual melts are controled by crystal-liquid differentiation processes such that some volatiles behave as highly incompatible elements (e.g., CO_2, noble gases, N_2), others enter into crystallizing phases in small quantities (e.g., H_2O, Cl), and others may be strongly sequestered into solid or immiscible liquid phases (e.g., S). For a vapor-saturated magma, additional vapor is exsolved during isobaric crystallization (second or resurgent boiling). During this process, concentrations of volatiles in residual melts are controled largely by vapor-melt partitioning. Volatiles that partition strongly into the vapor phase are rapidly depleted from the melt whereas those that have low vapor-melt partition coefficients will increase in concentration in the residual melt. Exsolved vapor may also be redistributed within magma bodies due to its greater buoyancy relative to surrounding silicate melt and crystals (Vergniolle and Jaupart, 1990; Candela, 1991; Thomas et al., 1993; Shinohara and Kazahaya, 1995). As a result, the mass fraction of exsolved vapor is not strictly limited by pressure or solubility, and a vapor-rich magma can have a bulk volatile content that is greatly in excess of what could be dissolved in the melt at upper crustal pressures.

It has commonly been assumed that intermediate to silicic magmas only become vapor saturated during shallow ascent and emplacement, during eruptive decompression, or during advanced (pegmatitic) stages of plutonic consolidation. However, Holloway (1976) recognized that the very low solubility of CO_2 in silicate melts at crustal pressures could result in saturation with an H_2O-CO_2 vapor phase during all stages in the formation, ascent, and crystallization of granites. Anderson (1973) used data on Cl and K_2O in melt inclusions in olivine to infer that basaltic andesite and andesitic magmas in subvolcanic reservoirs are commonly vapor saturated. Anderson (1975) reached a similar conclusion using available CO_2 and SO_2 data for volcanic emissions.

Significant CO_2 in silicic melts has been detected using infrared spectroscopic techniques on melt inclusions in phenocrysts (Fig. 2). These data show that silicic magmas

have sufficient dissolved CO_2 to cause them to be vapor saturated at pressures of 1 to 3 kb. Relations between volatiles and incompatible trace elements in melt inclusions from some rhyolitic magmas provide additional strong evidence for vapor-saturated crystallization because they show that volatiles are being lost to a vapor phase during progressive crystallization (Lowenstern et al., 1991; Lowenstern, 1993; Wallace et al., 1995; 1999; Stix and Layne, 1996; Schmitt, 2001). The occurrence of high-temperature fluid inclusions in

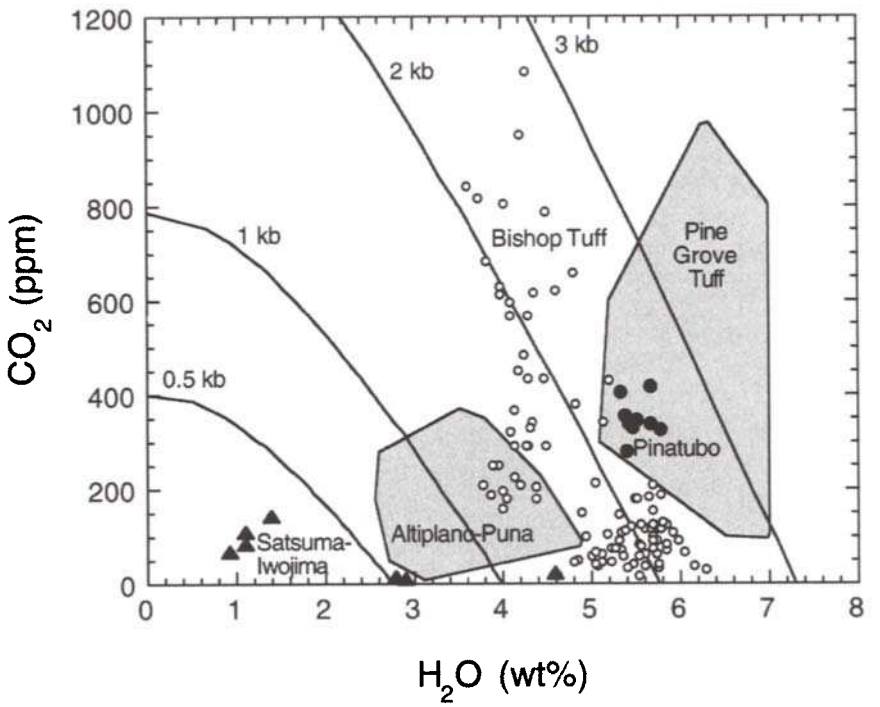

Fig. 2. H_2O vs. CO_2 in rhyolitic melt inclusions. Data are from the Bishop Tuff (Wallace et al., 1999), Tuff of Pine Grove, Utah (Lowenstern, 1994), Mount Pinatubo (Wallace and Gerlach, 1994), the Altiplano-Puna Volcanic Complex, northern Chile (Schmitt, 2001), and Satsuma-Iwojima Volcano, Japan (Saito et al., 2001).

phenocrysts from some silicic volcanic rocks also provides direct evidence that silicic magmas are vapor saturated during pre-eruptive crystallization (Roedder, 1992; Lowenstern, 1995).

In summary, there is strong evidence that many subvolcanic magma bodies contain significant exsolved vapor. To evaluate quantitatively the role of the vapor phase in volcanic SO_2 emissions requires information on the concentrations of various S species in the vapor phase and the total mass fraction of vapor. Although excellent thermodynamic models exist for predicting vapor-melt partitioning of H_2O and CO_2 (see

review by Newman and Lowenstern, 2002), a major uncertainty in understanding volcanic SO_2 emissions has been lack of information on S partitioning between silicate melt and coexisting hydrous vapor. In the following section I review recent experimental evidence, thermodynamic modeling, and volcanic gas data that provide information on vapor-melt partitioning of S.

VAPOR-MELT PARTITIONING OF SULFUR

The solubility behavior, activity-composition relations, and vapor-melt partitioning of S in silicate melts are complex due to multiple valence states (H_2S, S_2, SO_2, SO_3) and the occurrence of non-volatile S-rich phases (immiscible Fe-S-O liquid, pyrrhotite, monosulfide and intermediate solid solutions, anhydrite). Recently published experimental data on melt-vapor partitioning (Scaillet et al., 1998; Keppler, 1999) have shown that S partitions strongly into the vapor phase under conditions relevant for most dacitic and rhyolitic magmas. Vapor/melt partition coefficients for S determined experimentally by Keppler (1999) range from 47 under oxidizing conditions (NNO + 0.5; SO_2 dominant in vapor phase) to 468 under reducing conditions (CCO buffer; H_2S dominant). However, caution should be used in applying these results to other conditions because the concentrations of H_2S and SO_2 in the vapor phase are strongly dependent on oxygen fugacity (see Figure 6 in Carroll and Rutherford, 1985). The total S content of the vapor reaches a minimum around the NNO buffer but increases both with increasing oxygen fugacity above NNO (SO_2-rich vapor) and with decreasing oxygen fugacity below NNO (H_2S-rich vapor). Indeed, experimental studies by Scaillet et al. (1998) show that the vapor/melt partition coefficient for S increases rapidly as oxygen fugacity increases above the NNO buffer.

Thermodynamic modeling calibrated with the experimental partitioning results can be used to calculate the mole fractions of both SO_2 and H_2S in a magmatic vapor phase if temperature, pressure, oxygen fugacity, and dissolved H_2O and S contents of the silicate melt are known (Wallace, 2002). The model explicitly accounts for homogeneous equilibrium between oxidized and reduced S species dissolved in silicate melt and between H-O-S species in the vapor phase. The model allows prediction of melt-vapor partitioning of S through use of the heterogeneous equilibrium:

$$SO_2 \text{ (vapor)} + O^{2-} \text{ (melt)} + 0.5\ O_2 \text{ (vapor)} = SO_4^{2-} \text{ (melt)}.$$

The model is calibrated for dacitic to rhyolitic melts from 780-900 °C, 2-4 kbar, ? NNO from +0.5 to +2.6, and 30-1400 ppm dissolved S. However, nearly all of the experimental data are at 780 and 850 °C, so the temperature dependence is not well calibrated. Back calculation of the experimental data used for calibration yields an average deviation of ±24% in predicting the solubility of oxidized sulfur.

The vapor/melt partition coefficient for S varies strongly as a function of both temperature and relative oxygen fugacity (Fig. 3). Because S solubility decreases strongly with decreasing temperature, the partition coefficient increases from ~100 at 900 °C to ~1000 at 750-780 °C. As a result of the strong temperature dependence, S solubility in low temperature rhyolitic magma (~780 °C) is similar to that of CO_2. Degassing calculations indicate that the molar ratio [CO_2 / S_{total} (vapor)] / [CO_2 / S_{total} (melt)] is in the range

from 1 to 4 at 800 °C, making the CO_2 / S_{total} ratio in volcanic gases a potential guide to the ratio in the melt with which the gas last equilibrated (Wallace, 2002). Using this new thermodynamic model, the pre-eruptive magmatic vapor phase for dacitic to rhyolitic

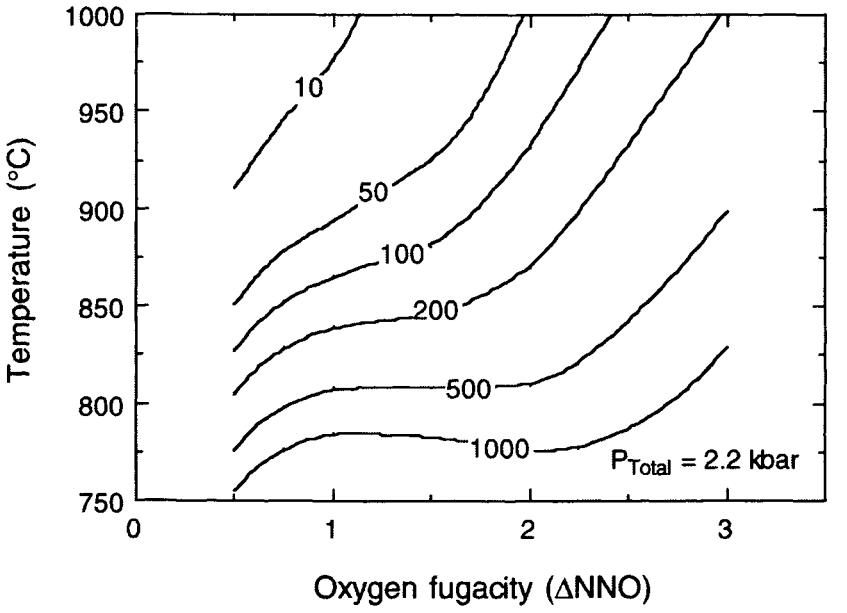

Fig. 3. Vapor-melt partitioning of S as a function of temperature and relative oxygen fugacity at 2.2 kb total pressure. Solid lines are isopleths of constant S_{vapor} / S_{melt} and are calculated using the thermodynamic model of Wallace (2002); see text for description.

magmas is estimated to contain 0.5 to 7.5 mol% total S (Fig. 4). However, the lowest values (Mount St. Helens, Ruiz, Krakatau) should be viewed with caution because they are at the upper temperature limit (~900 °C) of the calibration data.

Additional information about S in magmatic vapor comes from volcanic gas analyses. High-temperature gas discharges from convergent margin andesitic to dacitic volcanoes have mol% S_{total} [=100 $(SO_2+H_2S)/(H_2O+CO_2+SO_2+H_2S)$] that varies over two orders of magnitude from 0.04 to 7.3 (Symonds et al., 1994; Giggenbach, 1996). However, the lowest values are mostly samples collected from degassed lava domes (Symonds et al., 1994). Excluding these, most high-temperature volcanic gases have 0.3 to 7 mol% S_{total}, corresponding to CO_2 / S_{total} of about 0.2 to 10. This range is in good agreement with the results of the thermodynamic model described above and with the experimental determinations of S partitioning between melt and coexisting vapor at relevant oxygen fugacities (Scaillet et al., 1998; Keppler, 1999). This range of values is equivalent to ~1 to

20 wt.% SO_2 in the gas phase, because most of the gas is low-molecular-weight H_2O. It is important to note, however, that the ratio of SO_2 to H_2S in exsolved magmatic vapor is dependent on temperature, pressure, and the fugacities of oxygen and H_2O. Over the range of T, P, f_{O2}, and f_{H2O} conditions of most intermediate to silicic magmas (Carmichael, 1991), S in pre-eruptive vapor will either be predominantly H_2S or will occur as subequal

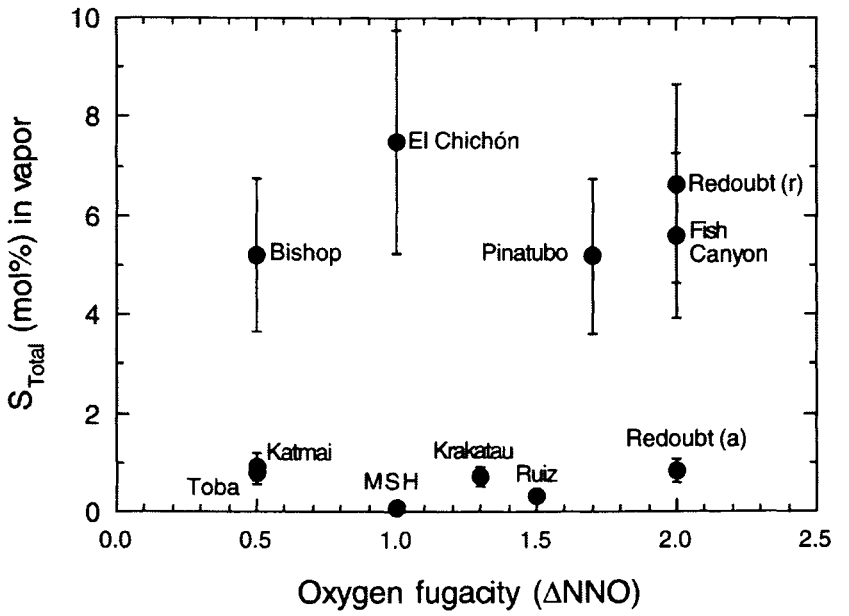

Fig. 4. Mol% S total predicted for pre-eruptive exsolved vapor in various andesitic, dacitic, and rhyolitic magmas. Calculations are based on the thermodynamic model of Wallace (2002).

amounts of H_2S and SO_2 (Carroll and Rutherford, 1985; Luhr, 1990). The reduced S in the vapor phase probably becomes oxidized to SO_2 during eruptive decompression and subsequent atmospheric transport (Varekamp et al., 1984; Gerlach and Casadevall, 1986; Bluth et al., 1995).

CAUSES OF "EXCESS" SO_2 EMISSIONS

One hypothesis to account for the discrepancies between remote sensing and petrologic (eruptive exsolution) estimates of SO_2 emissions (Fig. 1) is that magmas in crustal storage reservoirs are vapor saturated and that the vapor phase provides the "excess" S. If it is assumed that all of the SO_2 released during an eruption is originally contained, as both dissolved and exsolved species, within the volume of erupted magma, then the difference between remote sensing and petrologic estimates can be used to estimate the amount of SO_2 that is contributed by the vapor phase (Luhr, 1990; Gerlach

and McGee, 1994; Wallace and Gerlach, 1994; Scaillet et al., 1998; Wallace, 2001). The results suggest that intermediate to silicic magmas commonly contain about 1 to 5 wt.% exsolved vapor, equivalent to about 5 to 30 vol.%, before eruption (Fig. 5). Such large mass fractions of exsolved vapor are consistent with interpretations of trace element and volatile data for quartz-hosted melt inclusions from the Bishop Tuff (Wallace et al., 1995; 1999). Estimates on the order of 0.5 to 1 wt.% exsolved vapor have been made using similar evidence for the 1912 ignimbrite in the Valley of Ten Thousand Smokes, Alaska, and dacitic ignimbrites in northern Chile (Lowenstern, 1993; Schmitt, 2001). The large amounts of volatiles, particularly CO_2, implied by the exsolved vapor estimates based on remote sensing evidence exceed what could be dissolved at crustal pressures, suggesting that exsolved vapor accumulates in the apical regions of magma bodies during repose periods between eruptions.

Melt inclusion evidence and SO_2 emission data are also consistent with the hypothesis that magma chambers commonly have a vertical gradient in the mass fraction of exsolved vapor such that the vapor mass fraction is greatest in the roof zone of the

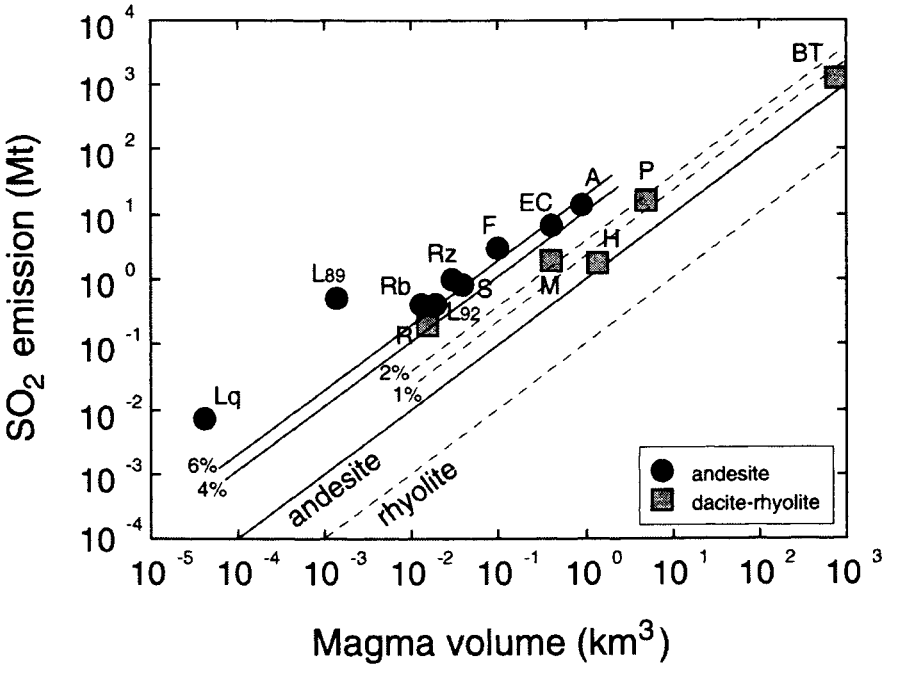

Fig. 5. Predicted effects of exsolved vapor on SO_2 emissions. Data for andesitic, dacitic, and rhyolitic magmas and eruptive exsolution estimates (dashed and solid line) are from Figure 1. Dashed and solid lines with % labels show the amounts of SO_2 that would be released per unit volume of erupted magma for magmas with pre-eruptive exsolved vapor contents of 1 and 2 wt.% (rhyolite; dashed lines) and 4 and 6 wt.% (andesite; solid lines).

chamber (Wallace, 2001). A key piece of evidence for the existence of such gradients is that smaller volume eruptions have higher ratios of exsolved vapor to mass of magma erupted. Such a pattern would be expected if the roof zones of magma chambers are vapor-enriched because smaller volume eruptions would preferentially tap the vapor-rich magma. The maximum volume fraction of exsolved vapor that can occur in a magma body may be limited by the percolation threshold (~30 vol.%) at which vapor bubbles become sufficiently interconnected to allow permeable flow of vapor (Candela, 1991; Garboczi et al., 1995; Rintoul and Torquato, 1997; Klug and Cashman, 1996).

An alternative hypothesis that has frequently been invoked to explain remote sensing data of SO_2 emissions is that unerupted magma at depth degasses dissolved volatiles during eruption, thereby contributing SO_2. This hypothesis and the one discussed above represent endmembers in a continuum of possibilities involving variable proportions of pre-eruptive exsolved vapor and syneruptive loss of dissolved volatiles from unerupted magma. Other potential sources of S, such as decomposition of phenocrystic anhydrite in an eruptive plume (Devine et al., 1984) or vaporization of S-rich hydrothermal brines, are not likely to be significant (Gerlach et al., 1996). It is well established that unerupted magma degasses during shallow emplacement and crystallization associated with activity before and after large explosive eruptions, during dome extrusion, and in persistently degassing, open vent systems such as Stromboli and Etna (e.g., Allard, 1997). At issue is the extent to which syneruptive loss of dissolved volatiles from unerupted magma during sustained Plinian and pyroclastic-flow-generating eruptions contributes to observed "excess" SO_2 emissions.

For many eruptions, a significant contribution from degassing of unerupted magma is unlikely based on volume considerations because it would require unreasonably large volumes of unerupted magma, far in excess of that permitted by geophysical estimates (Gerlach and McGee, 1994; Gerlach et al., 1994; Gerlach et al., 1996). An additional problem with the hypothesis that syneruptive degassing of unerupted magma is a significant source for SO_2 is the physical mechanism by which such gas loss could occur. Exsolution of dissolved volatiles is driven by decompression during magma ascent and eruption. This makes it difficult to envision a process by which gas could separate from deeply-stored but unerupted magma on eruptive timescales because of the very low pressures that would have to be sustained in the deep reservoir feeding the eruption (Wallace, 2001).

Another possible explanation for "excess" SO_2 emissions is that S is derived from mafic magma intruded into a silicic magma body shortly before eruption (Hattori, 1996; Kress, 1997). It is well documented that intrusion of mafic magma commonly triggers silicic volcanic eruptions (e.g., Sparks et al., 1977). Hattori (1996) proposed that exsolution of H_2O-CO_2-SO_2 vapor from newly intruded mafic magma at Mount Pinatubo was responsible for transferring S from mafic magma into the overlying dacitic magma body, resulting in oxidation of the dacitic magma and crystallization of anhydrite. Alternatively, Kress (1997) proposed that S was released from the newly intruded mafic magma as a result of redox reactions caused by magma mixing. However, it is not clear how much S would be released by such redox reactions because of uncertainties about the oxygen fugacity of the mafic magma (Wallace, 2001) and because reduction of the dacitic magma may actually cause crystallization of pyrrhotite instead of releasing S into the vapor phase (Scaillet et al., 1998). Regardless of how S is transferred from mafic magma into

silicic magma, the key questions that need to be resolved are issues of volume and timing. Specifically, it is unclear whether a single intrusion of mafic magma shortly before eruption provides all of the "excess" SO_2 or, as I argue in the following section, multiple, small injections of mafic magma during repose periods produce a gradual build-up of exsolved vapor. The first hypothesis requires a relatively large volume of mafic magma due to mass balance constraints. The second hypothesis does not require any single recharge event to be of large volume, but it does require that exsolved vapor accumulates at the top of a magma body rather than immediately leaking out into an overlying hydrothermal system.

Persistently active, open-vent basaltic volcanoes (e.g., Etna, Stromboli, Izu-Oshima) represent an interesting endmember case because they release large masses of SO_2 with little or no erupted material. Such open-vent systems commonly involve relatively low viscosity basaltic magma. The degassing behavior of these volcanoes has led to so-called "endogeneous growth" models, in which shallow-stored magma degasses without eruption, sinks to deeper levels of the magmatic system, and eventually solidifies to form a high density root beneath the volcano (Francis, et al., 1993; Kazahaya et al., 1994; Allard, 1997). Convection of magma in the open conduit is probably the main mechanism by which gas is transferred from a deeper magma body to the surface because gas separation from low viscosity basaltic magma probably occurs readily (Kazahaya et al., 1994; Stevenson and Blake, 1998). Conduit convection has also been suggested as an important mechanism for open-vent degassing in dacitic and rhyolitic systems (Stevenson and Blake, 1998; Kazahaya et al., 2002). However, the physical mechansim by which gas is released from ascending high-viscosity, silica-rich magma so that the magma convectively sinks along the conduit wall rather than erupting to form a dome is still unclear. Finally, it is important to note that although conduit convection and degassing may be the dominant processes in open-vent systems, they are unlikely to be important on the timescale of sustained Plinian or sub-Plinian eruptions because of the high magma conduit fluxes characteristic of such eruptions (Wilson et al., 1980).

In summary, the hypothesis that syneruptive degassing of unerupted silicic magma supplies the "excess" SO_2 observed in sustained explosive eruptions is unlikely for two main reasons. First, because of the very large volumes of unerupted magma that would have to degas, and second, because of the very low pressures that would have to be sustained in the deep reservoir feeding the eruption. Furthermore, new intrusion of mafic magma into a silicic magma reservoir just before eruption is also unlikely as the major source of "excess" SO_2 for most eruptions because of the mass of mafic magma required. In the following section, I discuss the ultimate sources of the major volatiles in silicic magmas and outline a hypothesis in which multiple small injections of mafic magma during repose periods produce a gradual build-up of exsolved vapor in a silicic magma body.

SOURCES AND FLUXES OF S, CO_2, AND H_2O IN CRUSTAL MAGMATIC SYSTEMS

Isotopic studies of S and CO_2 in intermediate to silicic magmatic systems have demonstrated that these volatiles are largely mantle-derived and are not dominantly related to crustal assimilation (Rye et al., 1984; Williams et al., 1990; McKibben et al., 1996;

Mandeville et al., 1998; Sorey et al., 1998). The ultimate source of S and CO_2 in these systems must therefore be from mafic magma, as suggested by Hildreth (1981), because it is well established that silicic magma reservoirs are created and sustained through long-term replenishment by mantle-derived basaltic magma during inter-eruption repose periods (Smith, 1979; Hildreth, 1981; Shaw, 1985). It should be noted, however, that in the case of subduction zones, some portion of the mantle S, C, and H_2O are recycled from subducted sediments and altered oceanic crust (e.g., Ito et al., 1983; Varekamp et al., 1992; Alt et al., 1993; Stolper and Newman, 1994; Métrich et al., 1999).

Andesitic, dacitic, and ryholitic magma in crustal reservoirs are probably vapor saturated due to recharge and underplating by basaltic magma that is saturated with multicomponent C-O-H-S vapor. In this regard, vapor saturation of intermediate to silicic magmas can be viewed as the inevitable consequence of the relatively high CO_2 contents of basaltic magmas coupled with relatively low CO_2 solubility in silicate melts at crustal pressures. Vapor transfer from underplated basaltic magma into an overlying silicic magma body is probably a slow process that occurs during the long repose periods that separate eruptive episodes. In systems where intrusion of basaltic magma into the crust generates silicic magma by partial melting (e.g., Huppert and Sparks, 1988), transfer of volatiles into mid to upper crustal silicic magma chambers may be a very complex process compared to systems in which basaltic magma intrudes directly into a silicic magma reservoir (Wiebe, 1996; Wiebe et al., 1997, 2001). However, in either case, if the S and CO_2 in crustal magmatic systems are ultimately derived from the mantle via basaltic magma, then the flux of these volatiles should be directly related to the basaltic magma flux.

The importance of mantle-derived basalt as a source of volatiles is exemplified by mafic cinder cones surrounding Popocatépetl volcano in central Mexico. Magnesian andesites erupted explosively from Popocatépetl volcano during the current eruption (December 1994 to 2002) have phenocryst assemblages and major- and trace-element systematics that indicate mixing of mafic and silicic magma (Straub and Martin del Pozzo, 2001). SO_2 and CO_2 emissions have been very high during the period Dec. 1994 to January 1998 (Gerlach et al., 1997; Delgado-Granados et al., 2001). Quaternary mafic cinder cones in the region surrounding Popocatepetl provide samples of possible mafic endmembers involved in mixing (Wallace and Carmichael, 1999). Olivine-hosted melt inclusions from these cones contain 1000-6000 ppm S, 250-2100 ppm CO_2, and 1.3-5.2 wt% H_2O (Cervantes and Wallace, 2003). The high S and CO_2 contents suggest that mafic magma recharging into the Popo system provides an abundant source of S and CO_2 that may explain the very large emissions from the current eruption. The H_2O and CO_2 contents are sufficiently high that these mafic magmas would be vapor saturated at the depths of a shallow crustal magma chamber beneath the volcano, so recharging mafic magmas could transfer significant volatiles during recharge events.

Based on the relationship between eruptive volumes and repose periods for intermediate to silicic magma systems spanning many orders of magnitude in eruptive volume, it has been estimated that a basaltic magma flux of ~0.01 km^3/year is required to sustain an individual long-lived crustal magmatic system (Shaw, 1985). If ~1000 ppm of S and 1000 ppm of CO_2 are degassed from mantle-derived basalt, then the basaltic magma flux for an individual magmatic system would yield a flux of 0.026 megatons (Mt) each of S and CO_2 per year. Similarly, if about 1 wt% H_2O is degassed from mantle-derived

basalt, then this results in a flux of 0.26 Mt of H_2O per year. In the mass balance model discussed below, I assume that a reservoir of silicic magma acts as a trap, intercepting volatiles released by mafic magmas regardless of whether the mafic magma is injected directly into the silicic chamber or transfers its volatiles indirectly by intrusion and crystallization at deeper crustal levels below the silicic chamber.

General relations between repose time and eruptive magma volume for silicic volcanic systems (Smith, 1979; Trial and Spera, 1990) can be used to estimate the length of the repose period preceding an eruption of a given volume. This in turn can be used to estimate the total amount of recharging mafic magma that is intruded into the crust during the repose period. This provides a means for comparing the flux of mantle-derived volatiles with the flux of S, CO_2 and H_2O released to Earth's atmosphere from explosive eruptions based on remote sensing techniques, volcanic gas analyses, and melt inclusion volatile data (Wallace, 2001). The results suggest that for a wide spectrum of magmatic system volumes, the fluxes of S, CO_2 and H_2O from explosive eruptions are approximately balanced by the mantle-derived supply rate of these volatiles, provided that mafic magmas degas ~1000 ppm S, ~2000 ppm CO_2, and ~2 wt% H_2O (Fig. 6). These values were chosen to make order of magnitude estimates of volatile fluxes from mafic magmas and are reasonable in light of analytical data for olivine-hosted melt inclusions in basalts, experimental solubility studies, and gas emissions from basaltic volcanoes (Fig. 7). The values of ~1000 ppm S and ~2000 ppm CO_2 are conservative estimates for volatiles degassed from mafic magmas. Mafic magmas commonly have higher S contents and volcanic gas data suggest higher primary CO_2 contents. Because of the low solubility of CO_2 in silicate melts, most magmas lose CO_2 by vapor exsolution during ascent, so melt inclusions only rarely trap melts with their primary CO_2 contents (e.g., Saal et al., 2002). The actual amounts of H_2O, CO_2, and S released by mafic magmas will undoubtedly be different for each magmatic system, but the general relations shown in Figure 6 suggest that the large amounts of exsolved vapor inferred from remote sensing data are supplied by the long-term recharge of basaltic magma from the mantle into the crust. For example (see Fig. 6), an andesitic eruption of 1 km^3 will be preceded by a ~300-year-repose period, during which time ~3 km^3 of basaltic magma is added to the system from below, contributing 16 Mt of SO_2. When the system erupts, ending the repose period, the systematics of Figure 6a indicate that associated with the 1 km^3 andesitic eruption is about 10 to 20 Mt of SO_2. Thus the mass of SO_2 released by the eruption approximately balances the mass of SO_2 added via mantle-derived basaltic magma during the repose period.

SUMMARY

Most volcanic eruptions have emissions of SO_2 that are 10 times or more greater than the amounts that could have been derived from syneruptive exsolution of dissolved S from the erupted volume of magma. The most notable exceptions to this pattern are Hawaiian and Icelandic volcanoes; other basaltic systems (Pacaya, Etna, Stromboli) are characterized by highly variable excess SO_2 emissions. A plausible hypothesis to explain excess SO_2 emissions is that magmas in crustal reservoirs are almost universally saturated with a multicomponent vapor phase consisting dominantly of H_2O, CO_2, and S species. Experimental studies and thermodynamic modeling show that S partitions strongly into the vapor phase under conditions relevant for most dacitic and rhyolitic magmas.

6A

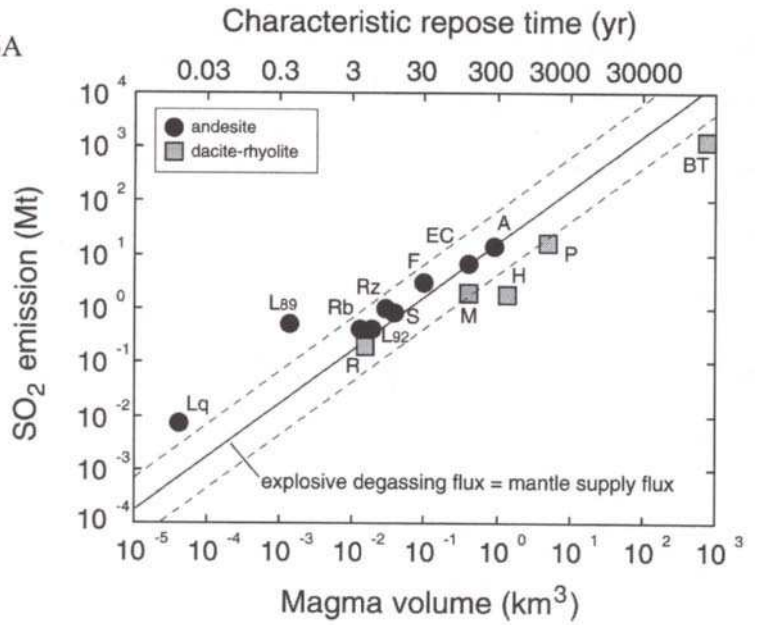
Characteristic repose time (yr)
0.03 0.3 3 30 300 3000 30000
andesite
dacite-rhyolite
BT
A
EC
F
P
H
Rz
Rb
S
M
L89
L92
R
Lq
explosive degassing flux = mantle supply flux
SO2 emission (Mt)
Magma volume (km3)

6B

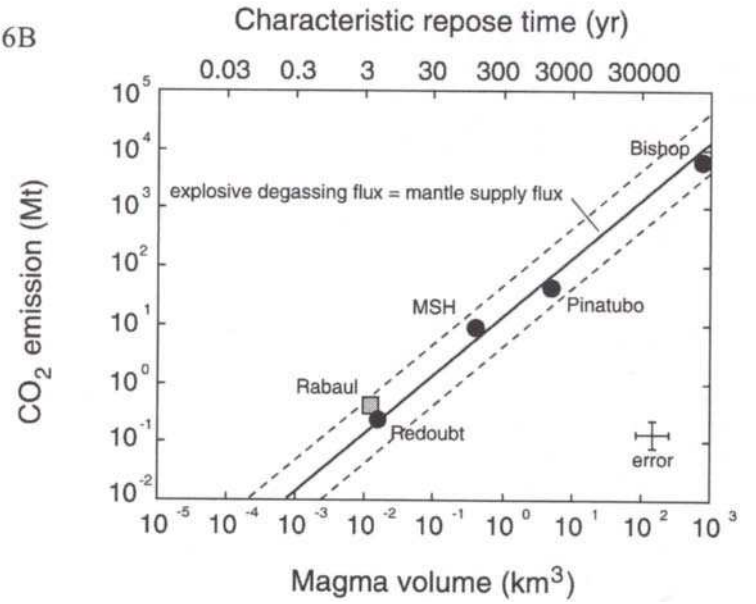
Characteristic repose time (yr)
0.03 0.3 3 30 300 3000 30000
Bishop
explosive degassing flux = mantle supply flux
MSH
Pinatubo
Rabaul
Redoubt
error
CO2 emission (Mt)
Magma volume (km3)

6C

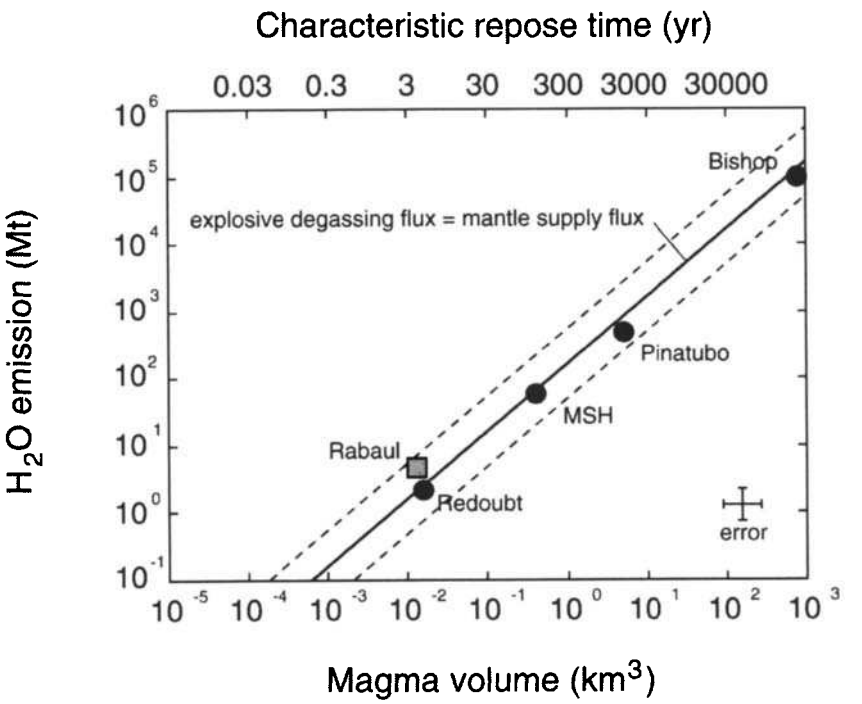

Fig. 6. Comparison of SO_2 emissions with estimates of the flux of volatiles from the mantle to the crust via basaltic magmatism as described in the text. **A.** Volcanic SO_2 emissions vs. total volume of erupted magma for the intermediate and silicic eruptions shown in Figure 1. The relationship between characteristic repose period (shown on upper horizontal axis) and volume of differentiated magma erupted (shown on lower horizontal axis) is based on Smith (1979) and Trial and Spera (1990) as described in Wallace (2001):

$$\log \text{repose time (yr)} = \log \text{magma volume } (km^3) + 2.5\ (\pm 0.5)$$

Solid line indicates a steady state balance between the amount of S introduced by prolonged degassing of basaltic magma during the repose period preceding an eruption and the amount of SO_2 released by explosive eruption of differentiated magma at the end of the repose period. The solid line is calculated assuming that an individual magmatic system has a basaltic magma flux of 0.01 km^3/yr (Shaw, 1985) and 1000 ppm S degassed from basalt, yielding a S flux from the mantle of 5.2 Mt SO_2/km^3 of basalt. Dashed lines correspond to an uncertainty of ± one-half order of magnitude in the relationship between repose period and eruption size. B. Similar calculation for CO_2 assuming basaltic magmas degas 2000 ppm CO_2. CO_2 emission estimates are calculated from SO_2 emissions by using the CO_2 / SO_2 ratio of either melt inclusions or volcanic gases. Calculations were made using data from Gerlach and McGee (1994), Roggensack et al. (1996), Wallace and Gerlach (1994), and Wallace et al. (1999). C. Similar calculation for H_2O assuming basaltic magmas degas 2 wt.% H_2O.

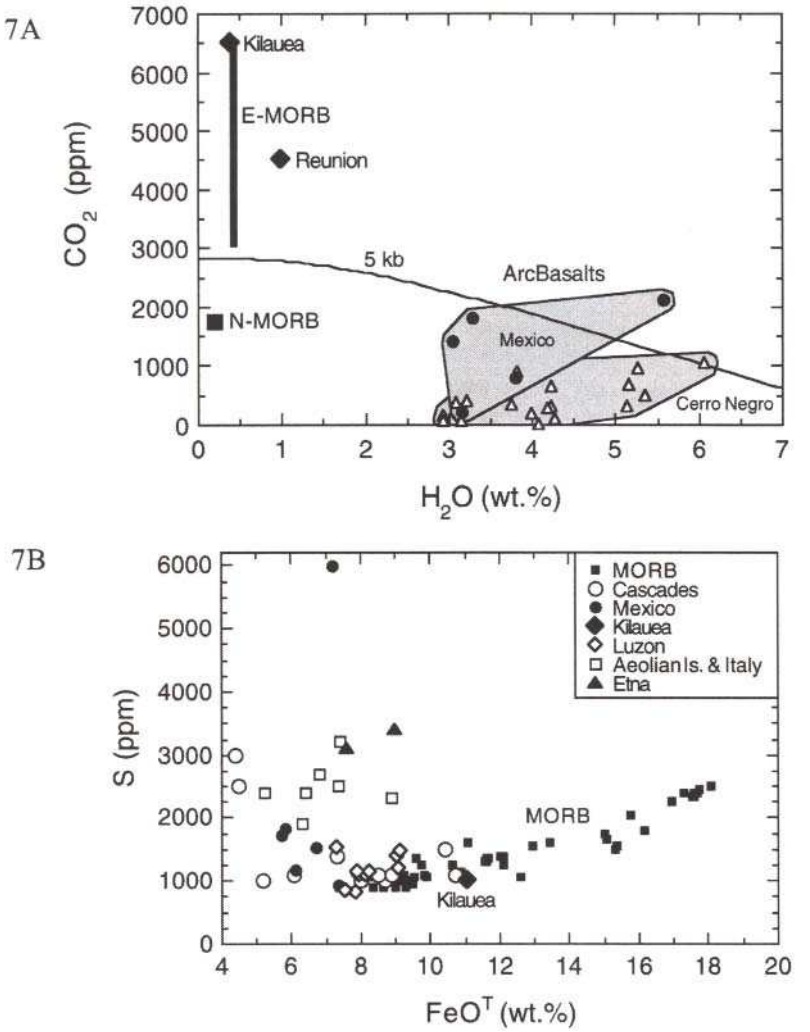

Fig. 7. A. H_2O vs. CO_2 for basaltic magmas based on melt inclusions, submarine basaltic glasses, and volcanic gas data. Melt inclusion data are from central Mexico (Cervantes and Wallace, 2003), Cerro Negro volcano in Nicaragua (Roggensack et al., 1997), and Reunion (Bureau et al., 1999). Estimates for primary H_2O and CO_2 in basaltic magmas include Kilauea (Gerlach and Graeber, 1985), normal MORB (Gerlach, 1989), and enriched MORB (Hekinian et al., 2000). B. FeO^T vs. S for basaltic magmas based on melt inclusions and submarine basaltic glasses. Data are shown for MORB (Wallace and Carmichael, 1992), central Mexico (Cervantes and Wallace, 2003), the Cascades (Anderson, 1974,), the Luzon volcanic arc, Philippines (Métrich et al., 1999), and Mt. Etna, the Aeolian Islands, and the Roman Volcanic Province (Métrich and Clocchiatti, 1996). Average S value for Kilauea is from Gerlach and Graeber (1985).

Andesitic, dacitic, and ryholitic magma in crustal reservoirs are probably vapor saturated due to recharge and underplating by basaltic magma that is saturated with multicomponent C-O-H-S vapor. During sustained Plinian and pyroclastic flow-forming eruptions, significant contributions of SO2 from syneruptive degassing of unerupted magma are unlikely given the mass balance and low pressures in the deep source reservoir that would be required for such gas loss. Future progress in understanding budgets of the major volatiles requires integrating remote sensing and volcanic gas data on fluxes of CO2, SO2, H2S, and H2O from volcanoes with petrologic data on temperature, pressure, oxygen fugacity, and dissolved volatiles in both differentiated magma stored in crustal reservoirs and mafic magma recharging these systems.

ACKNOWLEDGMENTS

I would like to thank B. De Vivo and R. Bodnar for organizing the melt inclusion workshop in Seiano, Italy, in September 2002 and for inviting this review. I would also like to thank J. Lowenstern and N. Métrich for their helpful reviews.

REFERENCES

Allard, P., 1997. Endogenous magma degassing and storage at Mount Etna. Geophys. Res. Lett., 24: 2219-2222.

Allard P., Carbonnelle, J., Métrich, N., Loyer, H., and Zettwoog, P., 1994. Sulphur output and magma degassing budget of Stromboli volcano. Nature, 368: 326-330.

Alt, J. C., Shanks, W. C., Jackson, M. C., 1993. Cycling of sulfur in subduction zones – The geochemisry of sulfur in the Mariana-island arc and back-arc trough. Earth Planet. Sci. Lett., 119: 477-494.

Anderson, A.T., Jr., 1973. The before eruption H_2O content of some high alumina magmas. Bull. Volcanol., 37: 530-552.

— 1974. Chlorine, sulfur, and water in magmas and oceans. Geol. Soc. Am. Bull., 85: 1485-1492.

— 1975. Some basaltic and andesitic gases. Rev. Geophys. Space Phys., 13: 37-55.

Andres, R. J., Rose, W. I., Kyle, P. R., deSilva, S., Francis, P., Gardeweg, M., and Moreno Roa, H., 1991. Excessive sulfur dioxide emissions from Chilean volcanoes. J. Volcanol. Geotherm. Res., 46: 323-329.

Blake, S., 1984. Volatile oversaturation during the evolution of silicic magma chambers as an eruption trigger. J. Geophys. Res., 89: 8237-8244.

Bluth, G. J. S., Schnetzler, C. C., Krueger, A. J., and Walter, L. S., 1993. The contribution of explosive volcanism to global atmospheric sulphur dioxide concentrations. Nature, 366: 327-329.

Bluth, G. J. S., Scott, C. J., Sprod, I. E., Schnetzler, C. C., Krueger, A. J., and Walter, L. S., 1995. Explosive emissions of fulfur dioxide from the 1992 Crater Peak Eruptions, Mount Spurr Volcano, Alaska. In: T. E. C. Keith (Editor), The 1992 Eruptions of Crater Peak Vent, Mount Spurr Volcano, Alaska. U. S. Geol. Surv. Bull., 2139: 37-45.

Bluth, G. J. S., Rose, W. I., Sprod, I. E., and Krueger, A. J., 1997. Stratospheric loading from explosive volcanic eruptions. J. Geol., 105: 671-683.

Bureau, H., Métrich, N., Semet, M. P., et al., 1999. Fluid-magma decoupling in a hot-spot volcano. Geophys. Res. Lett., 26: 3501-3504.

Burnham, C. W., 1979. Magmas and hydrothermal fluids. In: H. L. Barnes (Editor) Geochemistry of Hydrothermal Ore Deposits. Wiley, New York, 71-136.

Burton, M. R., Oppenheimer, C., Horrocks, L. A., et al., 2000. Remote sensing of CO_2 and H_2O emission rates from Masaya volcano, Nicaragua. Geology, 28: 915-918.

Calder, E. S., Sparks, R. S. J., and Gardeweg, M. C., 2000. Erosion, transport and segregation of pumice and lithic clasts in pyroclastic flows inferred from ignimbrite at Lascar Volcano, Chile. J. Volcanol. Geotherm. Res., 104: 201-235.

Candela, P. A., 1991. Physics of aqueous phase evolution in plutonic environments. Am. Mineral., 76:1081-1091.

Carmichael, I. S. E., 1991. The redox states of basic and silicic magmas: a reflection of their source regions? Contrib. Mineral. Petrol., 106: 129-141.

Carroll, M. R. and Rutherford, M. J., 1985. Sulfide and sulfate saturation in hydrous silicate melts. J. Geophys. Res., 90: C601-C612.

Cervantes, P. and Wallace, P. J., 2003. The role of H_2O in subduction zone magmatism: New insights from melt inclusions in high-Mg basalts from central Mexico. Geology, in press.

Delgado-Granados, H., Gonzalez, L. C., and Sanchez, N. P., 2001. Sulfur dioxide emissions from Popocatepetl volcano (Mexico): case study of a high-emission rate, passively degassing erupting volcano. J. Volcanol. Geotherm. Res., 108: 107-120.

Devine, J. D., Sigurdsson, H., Davis, A. N., and Self, S., 1984. Estimates of sulfur and chlorine yields to the atmosphere from volcanic eruptions and potential climatic effects. J. Geophys. Res., 89: 6309-6325.

Francis, P., Oppenheimer, C., and Stevenson, D., 1993. Endogeneous growth of persistently active volcanoes. Nature, 366: 554-557.

Garboczi, E. J., Snyder, K. A., Douglas, J. F., and Thorpe, M. F., 1995. Geometrical percolation threshold of overlapping ellipsoids. Phys. Rev. E., 52: 819-828.

Gerlach, T. M., 1989. Degassing of carbon dioxide from basaltic magma at spreading centers: II. Mid-oceanic ridge basalts. J. Volcanol. Geotherm. Res., 39: 221-232.

Gerlach, T. M. and Graeber, E. J., 1985. Volatile budget of Kilauea volcano. Nature, 313: 273-277.

Gerlach, T. M. and Casadevall, T. J., 1986. Fumarole emissions at Mount St. Helens Volcano, June 1980 to October 1981: degassing of a magma-hydrothermal system. J. Volcanol. Geotherm. Res., 28: 141-160.

Gerlach, T. M. and McGee, K. A., 1994. Total sulfur dioxide emissions and pre-eruption vapor-saturated magma at Mount St. Helens, 1980-88. Geophys. Res. Lett., 21: 2833-2836.

Gerlach, T. M., Westrich, H. R., Casadevall, T. J., and D. L. Finnegan, 1994. Vapor saturation and accumulation in magmas of the 1989-1990 eruption of Redoubt Volcano, Alaska. J. Volcanol. Geotherm. Res., 62: 317-337.

Gerlach, T. M., Westrich, H. R., and Symonds, R. B., 1996. Preeruption vapor in magma of the climactic Mount Pinatubo eruption: source of the giant stratospheric sulfur dioxide cloud. In: C. G. Newhall and R. S. Punongbayan (Editors), Fire and Mud: Eruptions and Lahars of Mount Pinatubo, Phillipines. Univ. Washington Press, 415-433.

Gerlach, T. M., Delgado, H., McGee, K. A., Doukas, M. P., Venegas, J. J., and Cardenas, L., 1997. Application of the LI-COR CO_2 analyzer to volcanic plumes: A case study, Volcan Popocatepetl, Mexico, June 7 and 10, 1995. J. Geophys. Res., 102: 8005-8019.

Giggenbach, W. F., 1996. Chemical composition of volcanic gases. In: R. Scarpa and R. I. Tilling (Editors), Monitoring and Mitigation of Volcano Hazards. Springer-Verlag, Berlin, 221-255.

Hattori, K., 1996. Occurrence and origin of sulfide and sulfate in the 1991 Mount Pinatubo eruption products. In: C. G. Newhall and R. S. Punongbayan (Editors), Fire and Mud: Eruptions and Lahars of Mount Pinatubo, Phillipines. Univ. Washington Press, 807-824.

Hedenquist, J. W. and Lowenstern, J. B., 1994. The role of magmas in the formation of hydrothermal ore deposits. Nature, 370: 519-527.

Hekinian, R., Pineau, F., Shilobreeva, S., Bideau, D., Gracia, E., and Javoy, M., 2000. Deep sea explosive activity on the Mid-Atlantic Ridge near 34°50'N: Magma composition, vesicularity, and volatile content. J. Volcanol. Geotherm. Res., 98: 49-77.

Hildreth, W., 1981. Gradients in silicic magma chambers: implications for lithospheric magmatism. J. Geophys. Res., 86: 10,153-10,192.

Holloway, J. R., 1976. Fluids in the evolution of granitic magmas: consequences of finite CO_2 solubility. Geol. Soc. Am. Bull., 87: 1513-1518.

Huppert, H. E., and Sparks, R. S., 1988. The generation of granitic magmas by intrusion of basalt into continental crust. J. Petrol., 29: 599-624.

Ito, E., Harris, D. M., Anderson, A. T., 1983. Alteration of oceanic crust and geologic cycling of chlorine and water. Geochim. Cosmochim. Acta, 47: 1613-1624.

Kamenetsky, V. S., Davidson, P., Mernagh, T. P., Crawford, A. J., Gemmell, J. B., Portnyagin, M. V., and Shinjo, R., 2002. Fluid bubbles in melt inclusions and pillow-rim glasses: High temperature precursors to hydrothermal fluids. Chem. Geol., 183: 349-364.

Kazahaya, K., Shinohara, H., Saito, G., 1994. Excessive degassing of Izu-Oshima volcano: magma convection in a conduit. Bull. Volcanol., 56: 207-216.

— 2002. Degassing process of Satsuma-Iwojima volcano, Japan: Supply of volatile components from a deep magma chamber. Earth Planets Space, 54: 327-335.

Keppler, H., 1999. Experimental evidence for the source of excess sulfur in explosive volcanic eruptions. Science, 284: 1652-1654.

Klug, C., and Cashman, K. V., 1996. Permeability development in vesiculating magmas: Implications for fragmentation. Bull. Volc., 58: 87-100

Kress, V., 1997. Magma mixing as a source for Pinatubo sulphur. Nature 389: 591-593.

Lowenstern, J. B., 1993. Evidence for a copper-bearing fluid in magma erupted at the Valley of Ten Thousand Smokes, Alaska. Contrib. Mineral. Petrol., 114: 409-421.

— 1994. Dissolved volatile concentrations in an ore-forming magma. Geology, 22: 893-896.

— 1995. Applications of silicate-melt inclusions to the study of magmatic volatiles. In: J. F. H. Thompson (Editor), Magmas, Fluids, and Ore Deposits. Mineral. Assoc. Canada Short Course, 23: 71-99.

Lowenstern, J. B., Mahood, G. A., Rivers, M. L., and Sutton, S. R., 1991. Evidence for extreme partitioning of copper into a magmatic vapor phase. Science, 252: 1405-1409.

Luhr, J. F., 1990. Experimental phase relations of water- and sulfur-saturated arc magmas and the 1982 eruptions of El Chichón Volcano. J. Petrol., 31: 1071-1114.

Luhr, J. F., Carmichael, I. S. E., and Varekamp, J. C., 1984. The 1982 eruptions of El Chichón, Chiapas, Mexico: mineralogy and petrology of the anhydrite-bearing pumices. J. Volcanol. Geotherm. Res., 23: 69-108.

Mandeville, C. W., Sasaki, A., Saito, G., Faure, K., King, R., and Hauri, E., 1998. Open-system degassing of sulfur from Krakatau 1883 magma. Earth Planet. Sci. Lett., 160: 709-722.

McGee, K. A., Doukas, M. P., Gerlach, T. M., 2001. Quiescent hydrogen sulfide and carbon dioxide degassing from Mount Baker, Washington. Geophys. Res. Lett., 28: 4479-4482.

McKibben, M. A., Eldridge, C. S., and Reyes, A. G., 1996. Sulfur isotopic systematics of the June 1991 Mount Pinatubo eruptions: A SHRIMP ion microprobe study. In: C. G. Newhall and R. S. Punongbayan (Editors), Fire and Mud: Eruptions and Lahars of Mount Pinatubo, Phillipines. Univ. Washington Press, 825-843.

Métrich, N. and Clocchiatti, R., 1996. Sulfur abundance and its speciation in oxidized alkaline melts. Geochim. Cosmochim. Acta, 60: 4151-4160.

Métrich, N., Schiana, P., Clocchiatti, R., and Maury, R. C., 1999. Transfer of sulfur in subduction settings: an example from Batan Island (Luzon volcanic arc, Philippines). Earth Planet. Sci. Lett., 167: 1-14.

Miller, T. P., Neal, C. A., and Waitt, R. B., 1995. Pyroclastic flows of the 1992 Crater Peak eruptions of Mount Spurr volcano, Alaska. In: T. E. C. Keith (Editor), The 1992 eruptions of Crater Peak Vent, Mount Spurr volcano, Alaska. U.S. Geol. Surv. Bull., 2139: 81-87.

Naranjo, J. A. and Stern, C. R., 1998. Holocene explosive activity of Hudson Volcano, southern Andes. Bull. Volcanol., 59: 291-306.

Newman, S. and Lowenstern, J. B., 2002. VolatileCalc: a silicate melt-H_2O-CO_2 solution model written in Visual Basic for excel. Computers Geosciences, 28: 597-604.

Rintoul, M. D. and Torquato, S., 1997. Precise determination of the critical threshold and exponents in a three-dimensional percolation model. J. Phys. A: Math. Gen., 30: L585-L592.

Roedder, E., 1992. Fluid inclusion evidence for immiscibility in magmatic differentiation. Geochim. Cosmochim. Acta, 56: 5-20.

Roggensack, K., Williams, S. N., Schaefer, S. J., and Parnell, R. A., Jr., 1996. Volatiles from the 1994 eruptions of Rabaul: understanding large caldera systems. Science, 273: 490-493.

Roggensack, K., Hervig, R.L., McKnight, S.B., and Williams, S.N., 1997, Explosive basaltic volcanism from Cerro Negro volcano: Influence of volatiles on eruptive style: Science, v. 277, p. 1639-1642.

Rose, W. I., Jr., Stoiber, R. E., and Malinconico, L. L., 1982. Eruptive gas compositions and fluxes of explosive volcanoes: Budget of S and Cl emitted from Fuego volcano, Guatemala. In: R. S. Thorpe (Editor), Andesites: Orogenic Andesites and Related Rocks. Wiley, New York, NY, pp. 669-676.

Rye, R. O., Luhr, J. F., and Wasserman, M. D., 1984. Sulfur and oxygen isotope systematics of the 1982 eruptions of El Chichón Volcano, Chiapas, Mexico. J. Volcanol. Geotherm. Res., 23: 109-123.

Saal, A. E., Hauri, E. H., Langmuir, C. H., and Perfit, M. R., 2002. Vapour undersaturation in primitive mid-ocean-ridge basalt and the volatile content of Earth's upper mantle. Nature, 419: 451-455.

Saito, G., Kazahaya K., Shinohara, H. Stimac, J., and Kawanabe, Y., 2001. Variation of volatile concentration in a magma system of Satsuma-Iwojima volcano deduced from melt inclusion analyses. J. Volcanol. Geotherm. Res., 108: 11-31.

Scaillet, B., Clemente, B., Evans, B. W., and Pichavant, M., 1998. Redox control of sulfur degassing in silicic magmas. J. Geophys. Res., 103: 23,937-23,949.

Schmitt, A. K., 2001. Gas-saturated crystallization and degassing in large-volume, crystal-rich dacitic magmas from the Altiplano-Puna, northern Chile. J. Geophys. Res., 106: 30,561-30,578.

Self, S. and King, A. J., 1996. Petrology and sulfur and chlorine emissions of the 1963 eruption of Gunung Agung, Bali, Indonesia. Bull. Volcanol., 58: 263-285.

Shaw, H. R., 1985. Links between magma-tectonic rate balances, plutonism, and volcanism. J. Geophys. Res., 90: 11,275-11,288.

Shinohara, H., Kazahaya, K., 1995. Degassing processes related to magma-chamber crystallization. In: J. F. H. Thompson (Editor), Magmas, Fluids, and Ore Deposits. Mineral. Assoc. Canada Short Course, 23: 47-70.

Sigurdsson, H., Carey, S., Palais, J. M., and Devine, J., 1990. Pre-eruption compositional gradients and mixing of andesite and dacite magma erupted from Nevado del Ruiz Volcano, Columbia in 1985. J. Volcanol. Geotherm. Res., 41: 127-151.

Smith, R. L., 1979. Ash-flow magmatism. In: C.E. Chapin and W.E. Elston (Editors), Ash-flow tuffs. Geol. Soc. Am. Spec. Pap., 180: 5-27.

Sorey, M. L., et al., 1998. Carbon dioxide and helium emissions from a reservoir of magmatic gas beneath Mammoth Mountain, California. J. Geophys. Res., 103: 15,303-15,232.

Sparks, R. S. J., Sigurdsson, H., and Wilson, L., 1977. Magma mixing: a mechanism for triggering acid explosive eruptions. Nature, 267: 315-318.

Stevenson, D. S. and Blake S., 1998. Modelling the dynamics and thermodynamics of volcanic degassing. Bull. Volc., 60: 307-317.

Stix, J. and Layne, G. D., 1996. Gas saturation and evolution of volatile and light lithophile elements in the Bandelier magma chamber between two caldera-forming eruptions. J. Geophys. Res., 101: 25181-25196.

Stoiber, R. E. and Jepson, A., 1973. Sulfur dioxide contributions to the atmosphere by volcanoes. Science 182: 577-578.

Stolper, E. M. and Newman, S., 1994, The role of water in the petrogenesis of Mariana trough magmas: Earth Planet. Sci. Lett., v. 121, p. 293-325.

Straub, S. M. and Martin-Del Pozzo, A. L., 2001. The significance of phenocryst diversity in tephra from recent eruptions at Popocatepetl volcano (central Mexico). Contrib. Mineral. Petrol., 140: 487-510.

Symonds, R. B., Rose, W. I., Bluth, G. J. S., and Gerlach, T. M., 1994. Volcanic-gas studies: methods, results, and applications. In: M. R. Carroll and J. R. Holloway (Editors), Volatiles in Magmas. Mineral. Soc. Am. Rev. Mineral., 30: 1-66.

Tait, S., Jaupart, C., and Vergniolle, S., 1989. Pressure, gas content and eruption periodicity of a shallow crystallising magma chamber. Earth Planet. Sci. Lett., 92: 107-123.

Thomas, N., Tait, S., and Koyaguchi, T., 1993. Mixing of stratified liquids by the motion of gas bubbles: application to magma mixing. Earth Planet. Sci. Lett., 115: 161-175.

Thordarson, Th., Self, S., Óskarsson, N., and Hulsebosch, T., 1996. Sulfur, chlorine, and fluorine degassing and atmospheric loading by the 1783-1784 AD Laki (Skaftár Fires) eruption in Iceland. Bull. Volcanol., 58: 205-225.

Trial, A. F. and Spera, F. J., 1990. Mechanisms for the generation of compositional heterogeneities in magma chambers. Geol. Soc. Am. Bull., 102: 353-367.

Varekamp, J. C., Kreulen, R., Poorter, R. P. E., Van Bergen, M. J., 1992. Carbon sources in arc volcanism with implications for the carbon cycle. Terra Nova, 4: 363-373.

Verhoogen, J., 1949. Thermodynamics of a magmatic gas phase. Univ. Calif. Bull. Dept. Geol. Sci., 28: 91-136.

Vergniolle, S., and Jaupart, C., 1990. Dynamics of degassing at Kilauea volcano, Hawaii. J. Geophys. Res., 95: 2793-2809.

Wallace, P., 2001. Volcanic SO_2 emissions and the abundance and distribution of exsolved gas in magmas. J. Volcanol. Geotherm. Res., 108: 85-106.

— 2002. A thermodynamic model for dissolution of oxidized sulfur in silicate melts: Formulation, calibration, and applications to volcanic SO_2 emissions. In preparation.

Wallace, P. and Carmichael, I. S. E., 1992. Sulfur in basaltic magmas. Geochim. Cosmochim. Acta, 56: 1863-1874.

Wallace, P. J. and Gerlach, T. M., 1994. Magmatic vapor source for sulfur dioxide released during volcanic eruptions: evidence from Mount Pinatubo. Science, 265: 497-499.

Wallace, P. and Carmichael, I. S. E., 1999. Quaternary volcanism near the Valley of Mexico: Implications for subduction zone magmatism and the effects of crustal thickness variations on primitive magma compositions. Contrib. Mineral. Petrol., 135: 291-314.

Wallace, P. J., Anderson, A. T., Jr., and Davis, A. M., 1995. Quantification of pre-eruptive exsolved gas contents in silicic magmas. Nature, 377: 612-616.

— 1999. Gradients in H_2O, CO_2, and exsolved gas in a large-volume silicic magma system: Interpreting the record preserved in melt inclusions from the Bishop Tuff. J. Geophys. Res., vol. 104, pp. 20,097-20,122.

Wiebe, R. A., 1996. Mafic-silicic layered intrusions: The role of basaltic injections on magmatic processes and the evolution of silicic magma chambers. Trans. Roy. Soc. Edin. 87: 233-242.

Wiebe, R. A., Smith, D., Sturm, M., King, E. M., and Seckler, M. S., 1997. Enclaves in the Cadillac Mountain granite (coastal Maine): Samples of hybrid magma from the base of the chamber. J. Petrol. 38: 393-423.

Wiebe, R. A., Frey, H., and Hawkins, D. P., 2001. Basaltic pillow mounds in the Vinalhaven intrusion, Maine. J. Volcanol. Geotherm. Res., 107: 171-184.

Williams, S. N., Sturchio, N. C., Calvache, M. L., Londono, A., and Garcia, N., 1990. Sulfur dioxide from Nevado del Ruiz volcano, Colombia: total flux and isotopic constraints on its origins. J. Volcanol. Geotherm. Res., 42: 53-68.

Wilson, L., Sparks, R. S. J., and Walker, G. P. L., 1980. Explosive volcanic eruptions IV. The control of magma properties and conduit geometry on eruption column behaviour. Geophys. J. R. Astr. Soc., 63: 117-148.

Woods, A. W. and Koyaguchi, T., 1994. Transitions between explosive and effusive eruptions of silicic magmas. Nature, 370: 641-644.

Woods, A. W. and Pyle, D. M., 1997. The control of chamber geometry on triggering volcanic eruptions. Earth Planet. Sci. Lett., 151: 155-166.

This Page Intentionally Left Blank

Volatile evolution of Satsuma-Iwojima volcano: Degassing process and mafic-felsic magma interaction

Genji Saito*, Kohei Kazahaya, Hiroshi Shinohara

Geological Survey of Japan, National Institute of Advanced Industrial Science and Technology, Central 7, 1-1-1 Higashi, Tsukuba, Ibaraki 305-8567, Japan
*: Corresponding author. Fax: +81-298-56-8725; email: saito-g@aist.go.jp

ABSTRACT

Petrological and geochemical studies of volcanic rocks and melt inclusions of Satsuma-Iwojima volcano, Japan, were carried out to investigate the volatile evolution of the magma chamber since its latest caldera-forming eruption. Petrological studies on basalts, rhyolites and mafic inclusions in the rhyolites from post-caldera eruptions suggest there is a stratified magma chamber beneath the volcano, which consists of a lower basaltic layer, upper rhyolitic layer and an episodically-present, thin middle-andesitic layer. Chemical analyses of 30 melt inclusions in plagioclase and pyroxene phenocrysts from the basaltic and rhyolitic eruptions showed large variations in the volatile concentrations (H_2O, CO_2, S and Cl) of the melts. This suggests the following volatile evolution processes in the magma chamber: 1) a gas-saturated condition due to pressure variation in the rhyolitic magma chamber just before the caldera-forming eruption; 2) low pressure degassing of the rhyolitic magma chamber by magma convection in the conduit during the active degassing period in the post-caldera stage up to the present; and 3) the addition of CO_2-rich volatile from the underlying basaltic magma in the stratified magma chamber to the upper gas-undersaturated (degassed) rhyolitic magma.

INTRODUCTION

Interaction of mafic magma with felsic magma is accepted not only as an important control on the chemical and textural diversity of igneous rocks, but also as one of the dominant processes leading to the eruption of felsic magma (Eichelberger, 1980) and excess degassing from volcanoes. In the 1991 Mount Pinatubo eruption, a gas phase in the magma chamber before eruption was inferred (Wallace and Gerlach, 1994; Gerlach et al., 1996), and the ultimate origin of the volatiles was considered to be underlying mafic magma beneath the dacite magma (Hattori, 1993). In the 1991-1995 dacite eruption of Unzen volcano, Japan, SO_2 flux observed during the eruption was several times larger than that calculated from the magma effusion rate and sulfur content of melt inclusions in the ejecta

(Hirabayashi et al., 1995), and the excess degassing was due to supply of volatiles from underlying mafic magma (Saito et al., 2001b).

Melt inclusions can preserve both volatile concentration and major element composition of melts when its host phenocryst forms (e.g., Anderson, 1973; Anderson et al., 1989; Johnson et al., 1994). Therefore, we can evaluate volatile evolution in a magma chamber where magma evolution process such as crystallization and magma mixing occurs by a combination of melt inclusion analysis and petrological studies of volcanic rocks from various eruption stages of a volcano. In addition, comparing the volatile concentration of melt inclusions and the chemical composition and flux of volcanic gas allows the estimation of the current degassing process and the source of the volcanic gas.

Satsuma-Iwojima volcano, Japan, is one of the best fields to study the volatile evolution with mafic-felsic magma interaction and the current degassing process because of bimodal volcanic activity of basalt and rhyolite during the post-caldera stage (Ono et al., 1982), its intense and long-term passive degassing activity, and its well studied magmatic gas composition and flux (Shinohara et al., 1993; Kazahaya et al., 2002). The degassing process and magma evolution of the magma chamber is summarized here based on petrological and geochemical studies of melt inclusions (Saito et al., 2001a), mafic inclusions in rhyolites and their host ejecta (Saito et al., 2002), and volcanic gas studies (Kazahaya et al., 2002) on Satsuma-Iwojima volcano. In addition, we discuss the volatile and magma evolution model of the chamber; the chamber was stratified with upper rhyolite and underlying basalt during the post-caldera stage, and degassing of the rhyolite continued together with CO_2-rich volatile contribution from the underlying basalt.

OUTLINE OF SATSUMA-IWOJIMA VOLCANO

Geology

Satsuma-Iwojima is a volcanic island located on the rim of the largely submerged Kikai caldera in southwestern Japan (Fig. 1). Its pre-caldera volcanic activity probably began at less than 0.7 Ma, producing basaltic and rhyolitic eruptions (Ono et al., 1982). Multiple large caldera-forming eruptions began at least 77,000 y.B.P. (Takamiya and Nishimura, 1986), and the latest caldera-forming eruption produced the Takeshima pyroclastic flow deposit about 6500 y.B.P. (Kitagawa et al., 1995). Its total volume is estimated to be more than 100 km^3 (Machida and Arai, 1978).

Both basaltic and rhyolitic eruptions occurred contemporaneously during the post-caldera stage along the northwestern part of the caldera, forming the rhyolitic dome of Iwodake, and the scoria cone and basaltic lava flows of Inamuradake (Fig. 1; Ono et al., 1982). Despite their contrasting whole-rock composition, these post-caldera volcanoes grew only 2 km apart. Eruptive activity at Inamuradake ceased about 3000 y.B.P., and that of Iwodake continued to 500 y.B.P. (Kawanabe and Saito, 2002). More recently, submarine eruption of rhyolitic magma occurred in 1934-1935 about 2 km east of the main island (Fig. 1). This eruption formed a small volcanic island named Showa-Iwojima.

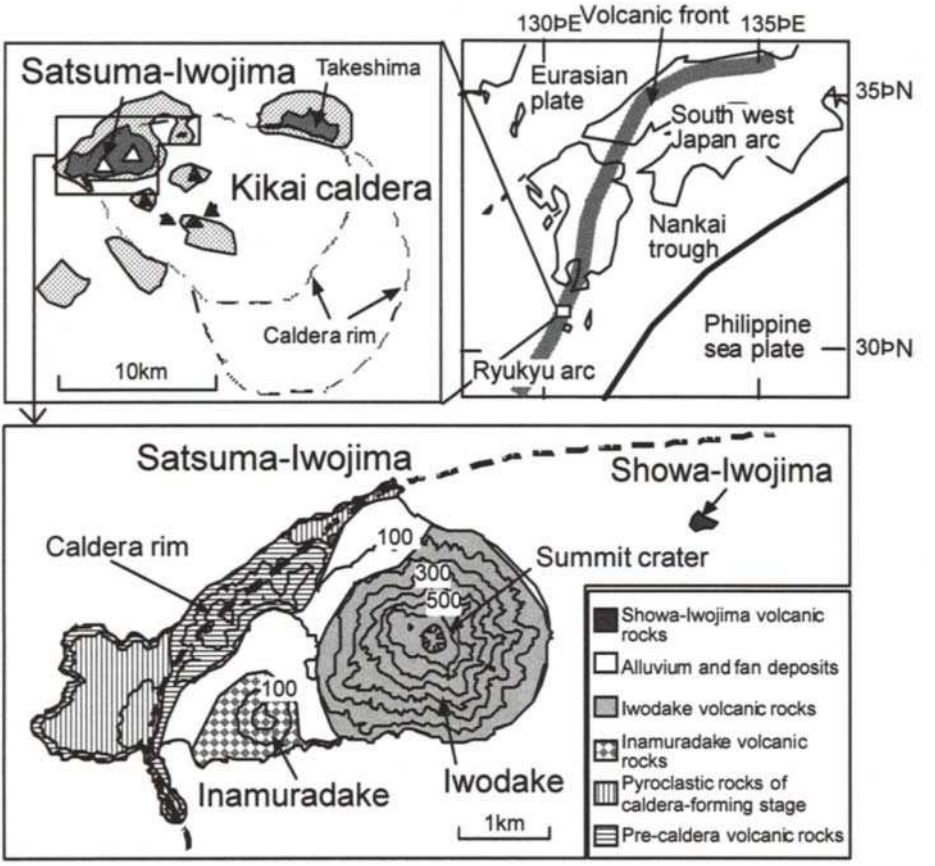

Fig. 1. Location maps of Kikai caldera and Satsuma-Iwojima volcano, Japan. The dark-shaded areas in the upper left figure indicate two islands on the caldera rim, and the dotted areas indicate a depth of less than 100 m beneath sea level. The closed triangles show submarine rises that are thought to be lava domes from the post-caldera stage. The lower figure shows post-caldera volcanoes and distribution of the volcanic rocks on Satsuma-Iwojima. After Saito et al. (2002).

Some submarine rises were observed on the floor of the Kikai caldera by bathymetry, and interpreted as submarine lava domes formed during the post-caldera stage (Fig. 1; Ono et al., 1982). The total volume of the magma erupted during the post-caldera stage (the last ~6000 years) is estimated to be more than 45 km^3 from topographic constraints (Saito et al., 2001a). This implies a magma effusion rate of ~7.5 km^3/1000 years, which is very high compared to the average eruption rates of late Quaternary volcanoes in the Japanese arc (0.1-1 km^3/1000 years; Ono, 1990) or the average worldwide rate of silicic magma production (1 km^3/1000 years; Shaw, 1985). The high apparent effusion rate suggests that there is still a large magma chamber beneath the caldera after the caldera-forming stage

(Saito et al., 2001a).

Satsuma-Iwojima volcano has been passively discharging a large quantity of high temperature volcanic gases from the summit crater of Iwodake. The maximum temperature of the volcanic gases has been almost constant for the past 10 years at about 900°C (Shinohara et al., 2002). Sulfur dioxide flux measured by COSPEC is almost constant with the average of 550 t/d since 1975 (Kazahaya et al., 2002). Most of the volatile components in the high temperature volcanic gases are believed to be of magmatic origin based on their chemical and isotopic compositions (Shinohara et al., 1993; Hedenquist et al., 1994; Goff and McMurtry, 2000). Intense fumarolic activity at the summit area of Iwodake has probably continued for more than 800 years according to old literature (Kamada, 1964); this is consistent with the strong silicification of the summit area of Iwodake by volcanic gas (Hamasaki, 2002).

Petrology

The volcanic rocks of the post-caldera stage show bimodal whole-rock chemistry consisting of basalts to basaltic andesites (SiO_2: 52-55 wt. %) and rhyolites (SiO_2: 70-73 wt. %; Saito et al., 2002). The rhyolites contain plagioclase as main phenocrysts (7-14 vol %) with clinopyroxene (<1.6 vol %), orthopyroxene (<1.1 vol %), and FeTi oxide (<1.1 vol %; Ono et al., 1982). The Showa-Iwojima rhyolitic lava has abundant quenched mafic inclusions (Goff et al., 1994). The Inamuradake basaltic scoria contains plagioclase (23 vol %), clinopyroxene (2.5 vol %), orthopyroxene (0.9 vol %), olivine (1.7 vol %), and FeTi oxide (0.8 vol %; Ono et al., 1982). Plagioclase phenocrysts in the rhyolites and the Inamuradake basaltic scoria and lava have core anorthite contents ranging from An#44 to An#70, and from An#74 to An#96, respectively (Saito et al., 2002). Core compositions of the clinopyroxene and orthopyroxene phenocrysts in the rhyolites (Wo_{41-44} En_{41-43} Fs_{14-16} and Wo_{2-3} En_{62-66} Fs_{31-35}) are a little different from those of the Inamuradake basalt (Wo_{39-41} En_{44-47} Fs_{13-16} and Wo_4 En_{70-75} Fs_{21-27}). Saito et al. (2002) applied two-pyroxene thermometry to intergrown pyroxene phenocrysts in the basalt and the rhyolites, obtaining magma temperatures of 1125 ± 27 (1σ)°C for the Inamuradake basalt, 960 ± 28 (1σ)°C for the Iwodake rhyolite, and 967 ± 29 (1σ)°C for the Showa-Iwojima rhyolite, respectively. The thermometry applied to intergrown pyroxene phenocrysts in the Takeshima pumice gave 961 ± 21 (n = 2)°C for the latest caldera-forming rhyolite (Saito, unpublished data). Coexisting FeTi oxide pairs from the Iwodake and Showa-Iwojima rhyolite also gave 942 ± 50 (1σ)°C for the Iwodake bomb and pumice, and 880 ± 24 (1σ)°C for the Showa-Iwojima lava, respectively (Saito et al., 2002). These estimates indicate that the magma temperature of the rhyolites has remained at 960-970°C since the latest caldera-forming eruption.

MAFIC INCLUSIONS

This section introduces a mafic-felsic magma interaction model for the post-caldera magma chamber proposed by Saito et al. (2002) based on petrological descriptions and

geochemical analysis of mafic inclusions in rhyolites (Fig. 2). The inclusions in Showa-Iwojima rhyolite are spherical to oblate, up to 20 cm in length, fine-grained with a diktytaxitic groundmass and vesicles of up to 5 mm in diameter at their cores. These features are similar to mafic to intermediate inclusions described from other silicic lava flows and domes, and indicate that the inclusions were predominantly liquid when they were engulfed by the rhyolitic magma (e.g., Heiken and Eichelberger, 1980; Bacon and Metz, 1984; Bacon, 1986; Linneman and Myers, 1990; Clynne, 1999). Some small mafic inclusions (up to 5 cm in length), which have similar shapes and textures to those of the Showa-Iwojima rhyolites, were also found in Iwodake volcanic bombs, but they are rare (<1 vol%) compared to those in the Showa-Iwojima lava.

Iwodake mafic inclusions have a similar or slightly SiO_2-richer composition (SiO_2: 53-55 wt.%) than that of the Inamuradake basalt. Their major element compositions plot between Inamuradake scoria and its scoria groundmass. These results suggest magma similar to Inamuradake basaltic magma being the source of the mafic inclusions, but that some fractional crystallization of the basaltic magma may have occurred before it was entrained in the Iwodake magma (Fig. 2a). The presence of plagioclase phenocrysts with Ab-rich cores and orthopyroxene phenocrysts with Fe-rich cores in the mafic inclusions provides some evidence for the mixing of the basalt and rhyolite, although the ratio of rhyolite to basalt would be very small. Most plagioclase and pyroxene phenocrysts in the Iwodake mafic inclusions have unzoned cores, and changes in the composition of their rims suggest that mixing take place just prior to eruption (Fig. 2a). These features are consistent with the spatial and temporal association and overlapping periods of activity for Iwodake and Inamuradake. The high temperature of the Iwodake rhyolite (960°C) may be due to heat supply from the underlying basalt.

Showa-Iwojima mafic inclusions have SiO_2-richer compositions (SiO_2: 56-61 wt.%) than Iwodake mafic inclusions and Inamuradake basalt. They have a large variation of chemical compositions, not only between inclusions, but also within single inclusions. Their major element compositions lie along mixing trends between Inamuradake magmas and the Showa-Iwojima rhyolite. There is also large variation in core anorthite content from An#47 to An#96 of plagioclase phenocrysts in the mafic inclusions; this also suggests the magma mixing of basalt and rhyolite. Saito et al. (2002) proposed the input of basaltic magma to rhyolitic magma, and the formation of large compositional variation within a mixed layer due to the mixing process (Fig. 2b). According to their model, basaltic magma with a similar or less evolved composition than Inamuradake magma intruded into the base of the rhyolite after the Iwodake eruptions, forming an andesitic layer (Fig. 2b). The injection and mixing process continued until the Showa-Iwojima eruption, resulting in the formation of a relatively thick mixed layer. Significant compositional variation in the mixed layer may be present depending on the mixing ratio of basalt to rhyolite, and/or on the extent of fractional crystallization. During the Showa-Iwojima eruption, the compositionally varied andesitic magma in the mixed layer was withdrawn along with the rhyolite to form Showa-Iwojima mafic inclusions (e.g., Blake and Ivey, 1986; Koyaguchi, 1986). Their model suggests that mafic-felsic magma interaction in the chamber proceeded from 1300 y.B.P. to the Showa-Iwojima eruption (1934-1935).

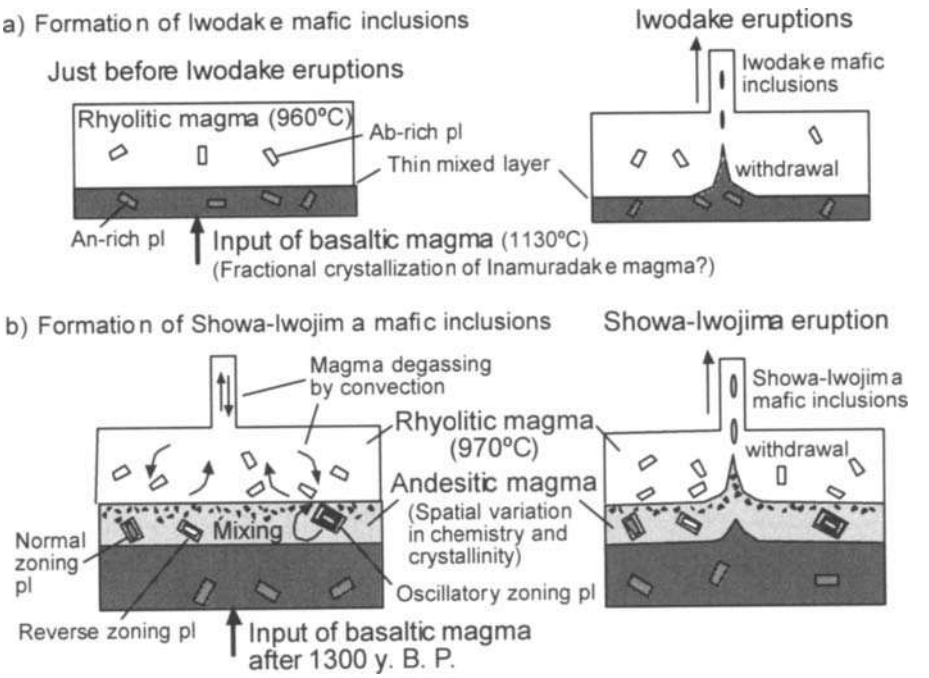

Fig. 2. Diagrams showing conceptual models for mafic-felsic interactions in the Satsuma-Iwojima magma chamber during the post-caldera stages: a) Just before the Iwodake eruptions, basaltic magma having a similar chemical composition to Inamuradake magma intruded into the base of the rhyolitic magma chamber. b) After 1300 y.B.P., basaltic magma with composition similar to less evolved Inamuradake magma intruded into the base of the rhyolitic magma chamber. Mixing of the basalt and rhyolite proceeded to form an intermediate layer of andesitic magma until the Showa-Iwojima eruption (1934-1935). pl = plagioclase. Redrawn after Saito et al. (2002).

VOLATILE CONTENT AND GAS SATURATION PRESSURE OF RHYOLITIC AND BASALTIC MAGMAS

To investigate the volatile concentration of rhyolitic and basaltic magmas in the magma chamber, Saito et al. (2001a) carried out chemical analysis of 30 melt inclusions in pyroxene and plagioclase phenocrysts of four different eruptive products since the latest caldera-forming eruption. The eruptive products are; plagioclases in pumices in the Takeshima pyroclastic flow deposit of caldera-forming eruption (ca. 6500 y.B.P.), pyroxenes in basaltic scoria of Inamuradake eruption (~ 3000 y.B.P.), plagioclases in pumices in a small pyroclastic flow deposit of Iwodake eruption (ca. 1300 y.B.P.), and plagioclases in Showa-Iwojima lavas (1934-1935). Most melt inclusions in these samples were composed of a single glass phase with/without tiny bubbles. The major elements, S and Cl of the

inclusions were analyzed by an electron microprobe. Water and CO_2 were analyzed by FTIR micro spectroscopy. Major element compositions of the melt inclusions of each ejecta closely agreed with those of the matrix for each sample. This agreement indicates that the chemical composition of these melt inclusions represents that of a melt in the magma chamber. Melt inclusions of the Takeshima pumice, the Iwodake pumice, and the Showa-Iwojima lava have rhyolitic chemical compositions that tend to become SiO_2-richer with time. Saito et al. (2001a) concluded that these rhyolites are derived from a common magma chamber whose plagioclase content increase with time by crystallization, based on identical major and trace element composition and strontium isotopic composition among their rhyolites, and an increase in plagioclase content from the Takeshima pumice to the Showa-Iwojima lava.

A large variation in volatile concentration was found among the melt inclusions of rhyolitic and basaltic products since the latest caldera-forming eruption (Fig. 3). The water concentration of the rhyolites (Takeshima pumice, Iwodake pumice and Showa-Iwojima lava melt inclusions) ranges from 4.6 wt.% to 0.7 wt.%, and the CO_2 concentration ranges from <10 ppm to 140 ppm, in spite of the belief that these rhyolites derived from the same chamber. On the other hand, Inamuradake scoria melt inclusions have higher CO_2 and S, but lower Cl concentrations than the rhyolites. In addition, the large variation in water and CO_2 concentrations was observed not only among these products but also in each ejecta. Saito et al. (2001a) discussed the origin of these variations considering several magmatic processes, including degassing due to decompression, isobaric crystallization, and gas supply from an external-source (Fig. 3a; Anderson et al., 1989), as summarized below.

1) High and varied water concentrations were measured for the Takeshima pumice melt inclusions (3.0 to 4.6 wt.%), whereas most of their CO_2 concentrations were below detection limit (Fig. 3b). Degassing with pressure decrease is more likely to result in variation in water concentration.

2) Water and CO_2 concentrations of the basaltic to andesitic melt of Inamuradake are 1.2-2.8 wt.% and $\leq$ 290 ppm, respectively (Fig. 3b). The CO_2 concentrations inversely correlate with H_2O concentrations along a gas saturation curve at about 100 MPa, suggesting that the variation was created by an isobaric process in a gas-saturated condition near 100 MPa.

3) Two of the Iwodake pumice melt inclusions have similar volatile concentrations to those of the Takeshima pumice melt inclusions (Fig. 3), and another is a H_2O-poor inclusion. As mentioned above, the Iwodake pumice is believed to have derived from a remnant of the magma chamber that ejected the Takeshima pumice. This hypothesis is also consistent with the similarity in their volatile concentrations.

4) The Showa-Iwojima lava melt inclusions are characterized by a distinctively H_2O-poor and CO_2–rich composition compared with those of the Takeshima pumice and the Iwodake pumice melt inclusions (Fig. 3b). Assuming that the H_2O-rich Iwodake melt (H_2O = 2.8 wt.%) is a source of the Showa-Iwojima melt, not only the addition of CO_2 but also exsolution of water from the melt should have occurred after the Iwodake eruption (1300 y.B.P.). Saito et al. (2001a) conclude that the H_2O-poor and CO_2–rich Showa-Iwojima melt was caused by decompressive degassing of the Iwodake magma followed by the addition of CO_2-rich volatile from an external source. Degassing by magma convection in a conduit

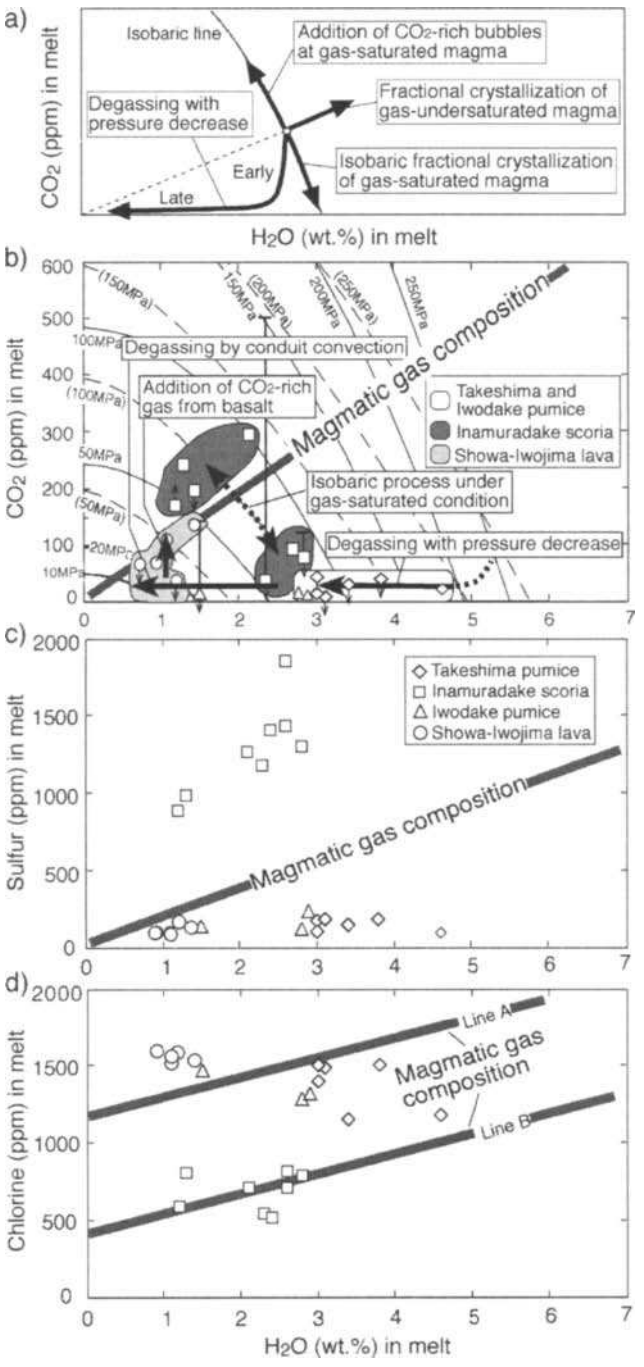

Fig. 3. a) Possible evolution processes of H_2O and CO_2 in a magma chamber. b) H_2O and CO_2 concentrations of melt inclusions of Satsuma-Iwojima volcano and suggested processes responsible for volatile evolution in the rhyolitic and basaltic magmas. The small arrows indicate that the plotted values are either the maximum or the minimum estimate of CO_2 concentration. Solubility of mixed gas of H_2O and CO_2 in the basaltic melt (dashed curves) and the rhyolitic melt (solid curves) are also plotted. Solubility data are cited from Miyagi et al. (1997) for H_2O in rhyolite at 1000°C, Burnham (1979) for H_2O in basalt at 1100°C, Fogel and Rutherford (1990) for CO_2 in rhyolite at 1200°C, and Stolper and Holloway (1988) for CO_2 in basalt at 1200°C. c) Sulfur and water concentrations of Satsuma-Iwojima melt inclusions. d) Chlorine and water concentrations of the Satsuma-Iwojima melt inclusions. The straight lines labeled "magmatic gas composition" show the chemical composition of magmatic gas currently discharged from the summit crater of the Iwodake ($H_2O:CO_2:S:Cl$ = 97.5:0.38:0.98:0.58 in vol %; Shinohara et al., 1993) assuming that the volatile concentration of degassed magma is equal to zero, except for chlorine. Lines A and B are obtained from the magmatic gas composition, assuming that chlorine concentration of the degassed magma is equal to that of rhyolitic matrix glass (1180 ppm) and of Inamuradake matrix glass (410 ppm), respectively. Redrawn after Saito et al. (2001a)

is more likely as the degassing process of the Iwodake magma, and addition of CO_2-rich volatile from basalt as the external source. This process will be discussed in next section.

Saito et al. (2001a) also estimated the gas saturation pressure of each magma, based on water and CO_2 concentration of melt inclusions from each ejecta (Fig. 4). The gas saturation pressure of Takeshima rhyolite is in the range of 80-180 MPa, corresponding to a depth of 3-7 km. The gas-saturation pressure of the two Iwodake pumice melt inclusions is 70 MPa, and that of the Showa-Iwojima melt is calculated to be 20-50 MPa (Fig. 4). The results indicate that the gas saturation pressure of the rhyolites has decreased since the latest caldera-forming eruption. On the other hand, the gas-saturation pressure of the Inamuradake scoria melt inclusions ranges from 70 to 130 MPa (Fig. 4), which is a similar or higher gas saturation pressure than the Iwodake rhyolite.

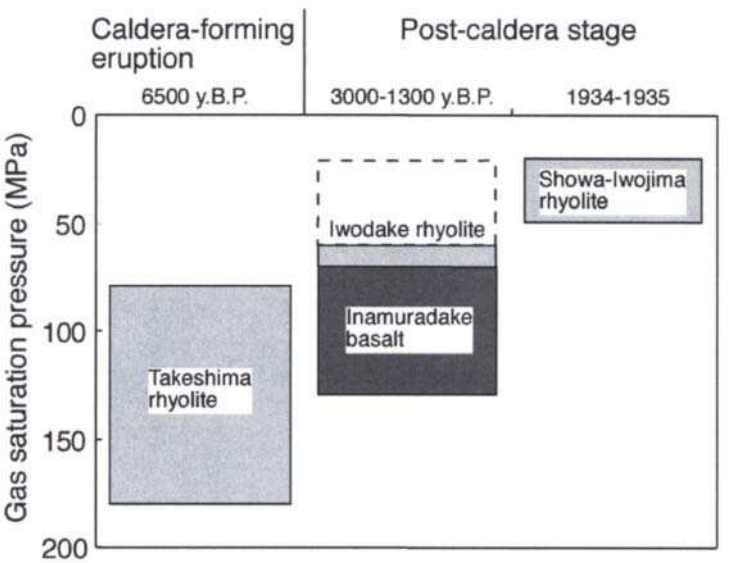

Fig. 4. Variation in gas saturation pressures of the rhyolitic and basaltic magmas of Satsuma-Iwojima volcano since 6500 y.B.P., estimated from H_2O and CO_2 concentrations of melt inclusions. The broken line shows gas saturation pressure of Iwodake magma estimated from the H_2O-poor Iwodake pumice melt inclusion. After Saito et al. (2001a).

VOLATILE EVOLUTION IN THE MAGMA CHAMBER

Previous sections introduced the mafic-felsic magma interaction model in the post-caldera magma, and variation in volatile concentration and gas saturation pressure of each rhyolite and basalt. This section discusses how the variation occurred and shows one possible volatile evolution model of the magma chamber of Satsuma-Iwojima volcano,

derived from combination of petrological studies and melt inclusion analyses (Fig. 5).

Takeshima pumice melt inclusions have 3 to 4.6 wt.% H_2O, and the cause of the large variation was considered to be degassing with a pressure decrease (Fig. 3; Saito et al., 2001a), indicating pressure variation in the magma chamber under gas-saturated conditions. Because the gas-saturation pressure of the Takeshima rhyolite ranges from 80 to 180 MPa (Fig. 4), a rhyolitic magma chamber is located at a depth of 3-7 km just before the latest caldera-forming eruption (6500 y.B.P.; Fig. 5). The large variation in water concentration of Takeshima pumice melt inclusions resulted from exsolution of volatile in the magma prior to the caldera-forming eruption is consistent with other research on plinian eruptions that concluded the existence of a vapor phase in a magma chamber (Anderson et al., 1989; Gerlach et al., 1996).

After the caldera-forming eruption, a remnant of the caldera-forming rhyolitic magma still existed to cause the Iwodake eruption and submarine dome eruptions (Fig. 5). The water concentration of the Iwodake melt is about 3 wt.%, and its gas- saturation

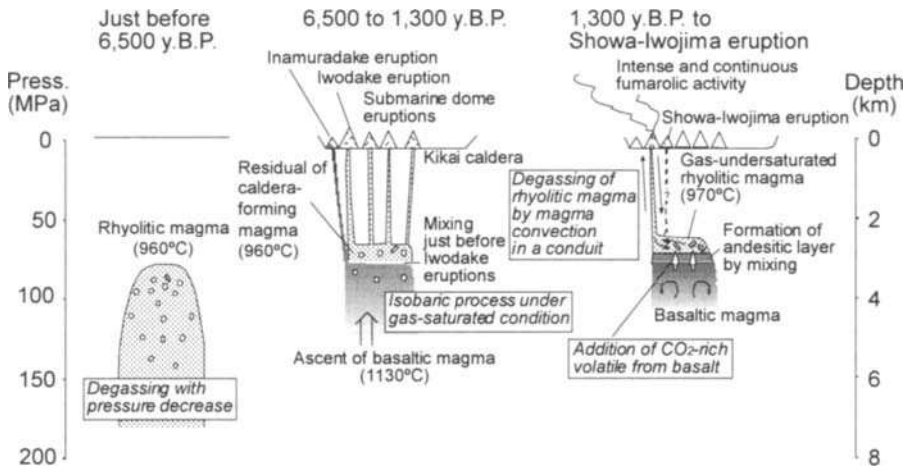

Fig. 5. Schematic illustration of volatile evolution and mafic-felsic magma interaction in the magma chamber of Satsuma-Iwojima volcano (see text).

pressure is 70 MPa. This suggests that the rhyolitic magma chamber located at a depth of ~3 km.

During the post-caldera-stage, a basaltic magma ascent to the base of the rhyolite and both magma reservoirs coexisted beneath the volcano, suggested by contemporaneous eruption of basaltic and rhyolitic magmas in a small area (Fig. 1). Mafic inclusions in Iwodake rhyolite indicate that the underlying basaltic magma was intermittently in contact with the upper rhyolitic magma in the magma chamber. Inverse correlation between water and CO_2 concentrations of the Inamuradake scoria melt inclusions along a gas

saturation curve at about 100 MPa (Fig. 3) indicates that the Inamuradake basalt was gas-saturated near 100 MPa. Saito et al. (2001a) proposed that the addition of CO_2-rich bubbles to the melt in isobaric conditions may shift the volatile composition of a melt to CO_2-rich/H_2O-poor composition along an isobaric-gas saturation curve (Fig. 3a). However, this possibility could not be evaluated because more detailed petrological and melt inclusion studies on the Inamuradake basalt are required. The gas-saturation pressure of the Inamuradake scoria melt inclusions ranges from 70 to 130 MPa (Fig. 4), corresponding to a 3-5 km depth of the basaltic magma. The estimates of magma chamber depth for the Iwodake rhyolite and the Inamuradake basalt agree well with the above stratified magma chamber model, which was suggested from the petrological studies on mafic inclusions in rhyolites. The very high eruption temperature of the rhyolites is also consistent with evolution of the rhyolite in the presence of basalt as a heat source.

From 1300 y.B.P. to the Showa-Iwojima eruption (1934-1935), basaltic magma with a composition similar to less evolved Inamuradake magma was continually injected at the base of the rhyolitic chamber (Fig. 5), suggested from petrological studies on Showa-Iwojima mafic inclusions (Fig. 2). This produced an intermediate layer between the upper rhyolite and the lower basaltic chambers until the Showa-Iwojima eruption (Fig. 5).

Melt inclusion analyses showed that the Showa-Iwojima magma has lower water (0.7-1.4 wt.%) but higher CO_2 (up to 140 ppm) concentrations than the Iwodake magma (1.5-2.9 wt.% H_2O and <14 ppm CO_2). The decrease in water concentration is unlikely to be caused by degassing due to pressure variation in the magma chamber because the water concentration of 1 wt.% corresponds to a very shallow part of a volcano (~400 m; 10 MPa). Such degassing of magma chamber could occur by magma convection in a conduit that is proposed as a mechanism responsible for rapid volatile transport from a deep magma chamber to the earth's surface (Fig. 5). Kazahaya et al. (2002) demonstrated that the convection of high-temperature rhyolitic magma (Showa-Iwojima rhyolite) in a conduit currently occurs, causing huge volcanic gas emission from the Iwodake summit of Satsuma-Iwojima volcano as discussed in next section. According to their model, the density difference between a volatile-rich and a volatile-poor magma is the driving force of the convection. The water content of the Iwodake rhyolite is higher than Showa-Iwojima magma, while their effective parameters on the convection mechanism, such as chemical composition and temperature of the magmas, are similar. Therefore, degassing of the Iwodake magma by magma convection in a conduit can also occur if a conduit similar to the present one existed since 1300 y.B.P. The intense fumarolic activity at the summit area of Iwodake is suggested to have continued longer than 800 years. This degassing process may have started to work after 1300 y.B.P. to decrease the water concentration of magma in the chamber from the Iwodake rhyolitic melt (~3 wt.%) to the Showa-Iwojima melt (~1 wt.%). This degassing process caused the rhyolitic magma in the magma chamber to be gas-undersaturated. One Iwodake pumice melt inclusion has a water concentration of 1.5 wt.%, though the other Iwodake inclusions have about 3 wt.% H_2O (Fig. 3). The decrease in water concentration to 1.5 wt.% may be caused by magma convection in a conduit because it requires magma degassing in a shallow part of the volcano (~800 m depth; 20 MPa). This indicates that degassing by magma convection in a conduit may have started

before 1300 y.B.P.

The addition of CO_2 supplied from an external source to the degassed Iwodake rhyolitic magma is also required to form the CO_2-rich Showa-Iwojima rhyolitic melt from the CO_2-poor Iwodake melt (Saito et al., 2001a). As mentioned above, it is suggested that basaltic magma is located beneath the Showa-Iwojima rhyolitic magma in the same chamber (Fig. 5). Since the Inamuradake scoria melt inclusions are CO_2-rich compared with rhyolitic melt (Fig. 3b), the source of CO_2 is likely to be the underlying basaltic magma. The increase in CO_2 concentration of the rhyolitic melt from Iwodake to Showa-Iwojima may be caused by the addition of CO_2-rich volatile from the underlying basaltic magma to the upper gas-undersaturated rhyolitic magma (Fig. 5). The degassed magma ponded at bottom of the rhyolitic magma reservoir as a gas-undersaturated magma was supplied with CO_2 from an underlying basaltic magma, forming the CO_2-rich Showa-Iwojima melt (Fig. 5).

CURRENT DEGASSING PROCESS

The current degassing process of the magma chamber can be quantitatively estimated by a combination of magmatic gas flux and composition obtained by volcanic gas observations, and the volatile content of the melt inclusions. This section discusses how degassing currently occurs in the stratified magma chamber beneath Satsuma-Iwojima volcano (Fig. 6).

As described in previous section, the magma chamber beneath Satsuma-Iwojima volcano is currently at least more than 3 km in depth and consists of upper rhyolitic layer, lower basaltic layer and thin middle layer of andesite (Fig. 6). The lower basaltic magma has a chemical composition of Inamuradake basalt (SiO_2 = 52-55 wt.%) and a temperature of 1130°C. The upper rhyolitic magma has a chemical composition of Showa-Iwojima rhyolite (SiO_2 = 70-73 wt.%), a temperature of 970°C and gas-undersaturated conditions. The andesite has a chemical composition of Showa-Iwojima mafic inclusions (SiO_2 = 56-61 wt.%). The hot underlying basalt may produce not only endmember of the mixing in the intermediate layer, but may also heat the upper rhyolite through the andesite layer.

At the surface, a large amount of volcanic gas (H_2O = 16000 t/d, CO_2 = 150 t/d SO_2 = 550 t/d) is currently discharged from the summit crater of Iwodake (Kazahaya et al., 2002). Most of the volatile components in the gases are of magmatic origin and are water-rich (>97%) (Shinohara et al., 1993). This indicates that the degassing pressure must be low enough to degas water efficiently from the magma. The maximum temperature of the magmatic gases (900°C) is fairly close to the temperature of the Showa-Iwojima rhyolitic magma (970°C), also suggesting that the gases are derived from magma close to the surface. Considering that such intense magmatic gas emission is believed to have continued for at least 800 years, the magmatic gas must come from a large magma chamber. However, petrological and melt inclusion studies indicate that the magma chamber is currently at more than 3 km in depth. Therefore, a huge amount of magmatic volatiles must be transported from the deep magma chamber to the surface.

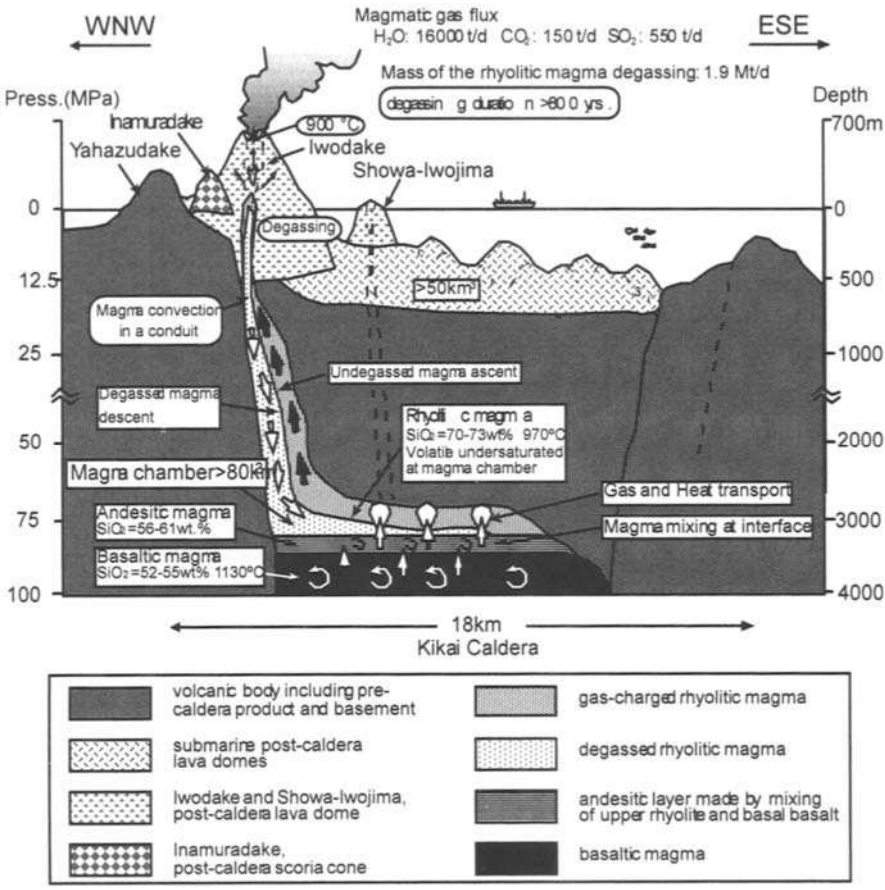

Fig. 6. Schematic illustration of current magma system of Satsuma-Iwojima volcano (vertically exaggerated). Redrawn after Kazahaya et al. (2002).

Kazahaya et al. (1994) first proposed degassing by magma convection in a conduit as a mechanism responsible for rapid volatile transport from a deep magma chamber to the earth's surface, causing intense and continuous degassing of Izu-Oshima volcano, a basaltic volcano in Japan. According to their model, the density difference between volatile-rich and volatile-poor magma is the driving force of theconvection, and the rate of magma (therefore volatile) transport was calculated based on simple fluid-dynamic models sufficient to cause the observed degassing rate for the volcano. Since gas-separation from the convecting magma occurs at the top of the magma column near the surface, water can be efficiently exsolved from the magma, and the water concentration of the degassed magma can be quite low. Kazahaya et al (2002) extended their model to Showa-Iwojima rhyolitic magma (Fig. 6) using revised fluid dynamic equations for the convection provided by

Stevenson and Blake (1998). Kazahaya et al (2002) showed that the density difference by degassing of 1 wt. % H_2O from the Showa-Iwojima rhyolite is 50 kg/m^3. They also calculated that a magma column diameter of 50 m is required to convect the rhyolitic magma with viscosity of $10^5 - 10^6$ Pas (1000°C), with a sufficient rate to explain the huge flux of volcanic gas currently discharged at the Iwodake summit. They indicate that this required diameter of the conduit is realistic, compared to estimations at other volcanoes (80-120 m for Mt. St. Helens in 1980; Stevenson and Blake, 1998).

Two geophysical and geochemical observations support this model. First, recent observation of regular oscillation of tremor magnitude with a period of about 50 minutes and a shallow source of long-period seismic pulses at about 40 m below the surface also suggests that replacement of the dense degassed magma by the ascent of fresh gas-rich magma in the conduit occurs near the surface (Ohminato and Ereditato, 1997). Second, if gas-separation from magma occurs at low pressure, the ratios of H_2O to CO_2 and H_2O to S in the magmatic gas should be similar to that in the magma before degassing because most of H_2O, CO_2 and S in the magma is exsolved. The composition of the magmatic gas discharging from the summit of Iwodake is similar to that of the Showa-Iwojima rhyolitic melt (Fig. 3). Concentrations of chlorine in the Showa-Iwojima lava melt inclusions are also consistent with the above hypothesis (Fig. 3d). The similarity between the volatile compositions of Showa-Iwojima melt inclusions and present magmatic gas composition indicate that the magmatic gas emission is caused by the degassing of Showa-Iwojima rhyolitic magma by convection in a conduit (Fig. 6).

The degassed rhyolitic magma descends to the bottom of the rhyolitic magma reservoir through the conduit. The degassed magma is supplied with CO_2-rich volatile from the underlying basalt as described previously (Fig. 6). The transport mechanism of the CO_2-rich volatile from the basalt to upper rhyolite is not clear, but may result from bubble migration or diffusion in the deep chamber (Kazahaya et al., 2002). The concentration of CO_2 in the CO_2-rich volatile supplied from the basalt is considered to be about 1 wt.% based on the magmatic gas composition, assuming that the water and CO_2 concentration of the degassed magma is almost zero. The concentration of CO_2 in the gas phase equilibrated with Inamuradake scoria melt inclusions having 1.3 wt.% H_2O and 240 ppm CO_2 is calculated to be 84 wt.% of CO_2 in H_2O-CO_2 gas. Supply of this gas efficiently increases the CO_2 concentration of the degassed magma to the Showa-Iwojima magma, but does not increase water concentration. This indicates that gas bubbles equilibrated with water-rich Inamuradake scoria melt inclusions having 2-3 wt.% H_2O and <100 ppm CO_2 is more likely if bubble migration occurs. On the other hand, if the chemical exchange between basaltic and rhyolitic magmas by diffusion modeled by Snyder and Tait (1998) occurs, volatile transport from the basalt to the rhyolite occurs (Kazahaya et al., 2002). In this case, the basaltic magma represented by the CO_2-rich Inamuradake melt having 1.3 wt.% H_2O and 240 ppm CO_2 may be a source of the CO_2-rich volatile. Saito et al. (2002) suggest that after 1300 y.B.P., the mixing of the basalt and rhyolite forms an intermediate layer of andesitic magma, and compositional gradient may have existed across the layer just before the Showa-Iwojima eruption (Figs. 5 and 6). The andesitic magma layer may act as volatile transporter from the basalt to rhyolite. To discuss the mechanism of volatile transport from the basalt to rhyolite, petrological and melt inclusion studies of the mafic

inclusions and related basalt is necessary, together with theoretical and experimental studies on the volatile behavior of the mixing process (e.g., Thomas et al., 1993).

Kazahaya et al. (2002) estimated the degassing rate of the Showa-Iwojima rhyolitic magma of 8 – 13 m^3/s (~1.9 Mt/d) based on the volatile concentrations (H_2O = 1 wt.%, CO_2 = 100 ppm, S = 110 ppm) of the Showa-Iwojima melt and the magmatic gas flux from the Iwodake summit crater (H_2O = 16000 t/d, CO_2 = 150 t/d, S = 550 t/d; Fig. 6). Assuming that similar degassing continued for about 800 years, the total volume of the degassed rhyolitic magma was estimated to be 250 km^3. The estimated volume does not represent the real volume of the rhyolite in the chamber because the degassed rhyolitic magma is supplied with volatiles from the underlying basalt. Assuming that all the water flux was supplied from the basalt with an H_2O content similar to the Inamuradake melt (2-3 wt.%), the total volume of the basaltic magma degassed in the past 800 years is estimated to be 80-120 km^3 (Fig. 6). Similar to the above estimation, assuming that all the CO_2 and S flux was supplied from the basalt with a CO_2 and S content similar to the Inamuradake melt (<290 ppm CO_2 and 900-1900 ppm S), the total volume of the degassed basaltic magma is estimated to be >90 km^3 from CO_2, and 14-30 km^3 from sulfur, respectively. The total volume of the degassed basaltic magma estimated from sulfur is smaller than that from water. This difference may be caused by a different transport process of sulfur from the basalt to rhyolite from that of water. On the other hand, the total volume of the degassed basaltic magma estimated from CO_2 is consistent with that from water, but these estimates could be smaller if the basaltic magma is gas-saturated at the time of melt inclusion entrapment. To discuss the volatile budget of the volcano quantitatively, volatile evolution process of basaltic magma chamber should be investigated. In particular, volatile analysis of melt inclusions in olivine phenocrysts is essential because the initial volatile contents of the less evolved basaltic magma can be recognized.

The above estimation on the total volume of degassed magma indicates that the basaltic magma with a volume comparable to that erupted at the latest caldera-forming eruption (>100 km^3) still exists beneath the volcano. This degassing model suggest that intense gas emission will continue until the underlying basaltic magma in the magma chamber is degassed. The degassing mechanism of the underlying basaltic magma is not yet clear, but magma convection in the basaltic magma reservoir such as the upper rhyolite may work.

CONCLUDING REMARKS

Melt inclusion analyses give the volatile concentration of a melt in a magma chamber. The degassing process in the chamber can be estimated from variation in water and CO_2 concentration of the melt inclusions. On the other hand, the magma evolution process in the magma chamber, such as crystallization and magma mixing, can be discussed by petrological studies systematically conducted on the volcanic rocks from various stages of a volcano. The chemical composition and flux of gas by magma degassing are important parameters for quantitatively estimating the current degassing process, and can be directly obtained by volcanic gas studies. This paper shows that a volatile evolution model of a magma chamber beneath Satsuma-Iwojima volcano, where mafic-felsic magma interaction

occurs, can be constructed by a combination of melt inclusion analyses, petrological studies on mafic inclusions and their host ejecta from different eruptions and volcanic gas studies. This model suggests that the chamber has stratified with upper rhyolitic, lower basaltic and episodically-present thin middle andesitic magmas during the post-caldera stage, and degassing of the rhyolite by magma convection in a conduit has continued together with the addition of CO_2-rich volatile from the underlying basalt during the active degassing period in the post-caldera stage and at present. This case study indicates that mafic magma underlying felsic magma contributes excess degassing of the volcano, not only during eruptions (e.g., 1991 Mount Pinatubo eruption), but also during passive degassing activity.

Acknowledgements

Thanks are extended to Drs. B. De Vivo and R. J. Bodnar for their invitation to participate in this short course.

REFERENCES

Anderson, A.T., 1973, The before-eruption water content of some high-alumina magmas, Bull. Volcanol. 37, 530-552.

Anderson, A.T., S. Newman, S.N. Williams, T.H. Druitt, C. Skirius and E. Stolper, 1989, H_2O, CO_2, Cl, and gas in plinian and ash-flow Bishop rhyolite, Geology 17, 221-225.

Bacon, C.R. and J. Metz, 1984, Magmatic inclusions in rhyolites, contaminated basalts, and compositional zonation beneath the Coso volcanic field, California, Contrib. Mineral. Petrol. 85, 346-365.

Bacon, C.R., 1986, Magmatic inclusions in silicic and intermediate volcanic rocks, J. Geophys. Res. 91, 6091-6112.

Blake, S. and G.N. Ivey, 1986, Magma-mixing and the dynamics of withdrawal from stratified reservoirs, J. Volcanol. Geotherm. Res. 27, 153-178.

Burnham, C.W., 1979, Magmas and hydrothermal fluids, In: Barnes, H.L. Ed., Geochemistry of Hydrothermal Ore Deposits 2nd ed. John Wiley & Sons, New York, 71-136.

Clynne, M.A., 1999, A complex magma mixing origin for rocks erupted in 1915, Lassen Peak, California, J. Petrol. 40, 105-132.

Eichelberger, J.C., 1980, Vesiculation of mafic magma during replenishment of silicic magma reservoirs, Nature 288, 446-450.

Fogel, R.A. and M.J., Rutherford, 1990, The solubility of carbon dioxide in rhyolitic melts: a quantitative FTIR study, Amer. Mineral. 75, 1311-1326.

Gerlach, T.M., H.R. Westrich and R.B. Symonds, 1996, Pre-eruption vapor in magma of the climatic Mount Pinatubo eruption: source of the giant stratospheric sulfur dioxide cloud. In: Newhall, C. G., Punongbayan, R. S. (eds.), Fire and mud: eruptions and lahars of Mount Pinatubo, Philippines. Univ. Washington Press., 415-433.

Goff, F., G.M. McMurtry, J.A. Stimac and A.I Adams, 1994, Stable isotopes and tritium of magmatic water at Satsuma-Iwojima volcano, Japan, EOS trans. American Geophys. Union. 1994 Fall meeting.

Goff, F. and G.M. McMurtry, 2000, Tritium and stable isotopes of magmatic waters, J. Volcanol. Geotherm. Res. 97, 347-396.

Hamasaki, S., 2002, Volcanic-related alteration and geochemistry of Iwodake volcano, Satsuma-Iwojima, Kyushu, SW Japan, Earth, Planets and Space 54, 217-229.

Hattori, K., 1993, High-sulfur magma, a product of fluid discharge from underlying mafic magma: Evidence from Mount Pinatubo, Philippines, Geology 21, 1083-1086.

Hedenquist, J.W., M. Aoki and H. Shinohara, 1994, Flux of volatiles and ore-forming metals from the magmatic-hydrothermal system of Satsuma-Iwojima volcano, Geology 22, 585-588.

Heiken, G. and J.C. Eichelberger, 1980, Eruptions at Chaos Crags, Lassen Volcanic National Park, California, J. Volcanol. Geotherm. Res. 7, 443-481.

Hirabayashi, J., T. Ohba, K. Nogami and M. Yoshida, 1995, Discharge rate of SO_2 from Unzen volcano, Kyushu, Japan, Geophys. Res. Lett. 22, 1709-1712.

Johnson, M.C., A.T. Anderson and M.J. Rutherford, 1994, Pre-eruptive volatile contents of magmas. In: Carroll, M.R. and J.R. Holloway, Eds., Volatiles in magmas, Reviews in Mineralogy 30, 281-330.

Kamada, M., 1964, Volcanoes and geothermy of Satsuma-Iwojima, Kagoshima prefecture, J. Japan Geothermal Energy Assoc. 3, 1-23 (in Japanese).

Kawanabe, Y. and G. Saito, 2002, Volcanic activity of Satsuma-Iwojima area during the past 6500 years, Earth, Planets and Space 54, 295-302.

Kazahaya, K., H. Shinohara and G. Saito, 1994, Excessive degassing of Izu-Oshima volcano: magma convection in a conduit, Bull. Volcanol. 56, 207-216.

Kazahaya, K., H. Shinohara and G. Saito, 2002, Degassing process of Satsuma-Iwojima volcano, Japan: Supply of volatile components from a deep-magma chamber, Earth, Planets and Space 54, 327-335.

Kitagawa, H., H. Fukuzawa, T. Nakamura, M. Okamura, K. Takemura, A. Hayashida and Y. Yasuda, 1995, AMS ^{14}C dating of varved sediments from Lake Suigetsu, central Japan and atmospheric ^{14}C change during the late Pleistocene, Radiocarbon 37, 371-378.

Koyaguchi, T., 1986, Evidence for two-stage mixing in magmatic inclusions and rhyolitic lava comes in Niijima island, Japan, J. Volcanol. Geotherm. Res. 29, 71-98.

Linneman, S.R. and J.D. Myers, 1990, Magmatic inclusions in the Holocene rhyolites of Newberry volcano, central Oregon, J. Geophys. Res. 95, B11, 17677-17691.

Machida, H. and F. Arai, 1978, Akahoya ash-a Holocene widespread tephra erupted from the Kikai caldera, south Kyushu, Japan, The Quaternary Res. 17, 143-163 (in Japanese with English abstract).

Miyagi, I., H. Yurimoto and E. Takahashi, 1997, Water solubility in albite-orthoclase join and JR-1 rhyolite melts at 1000°C and 500 to 2000 bars determined by micro-analysis with SIMS, Geochem. J. 31, 57-61.

Ohminato, T. and D. Ereditato, 1997, Broadband seismic observations at Satsuma-Iwojima, Japan, Geophys. Res. Lett. 24, 2845-2848.

Ono, K., 1990, Long-term forecast of volcanic eruptions, Bull. Volcanol. Soc. Japan. 34, S201-S214 (in Japanese).

Ono, K., T. Soya and T. Hosono, 1982, Geology of Satsuma-Io-jima district. Quadrangle Series, Scale 1:50,000 Tanegashima (16) No.2, Geol. Surv. Japan (in Japanese with English abstract).

Saito, G., K. Kazahaya, H. Shinohara, J. A. Stimac and Y. Kawanabe, 2001a, Variation of volatile concentration in a magma system of Satsuma-Iwojima volcano deduced from melt inclusion analyses, J. Volcanol. Geotherm. Res. 108, 11-31.

Saito, G., H. Satoh, H. Shinohara and Y. Yamaguchi, 2001b, Sulfur-rich melt inclusions in pyroxene phenocrysts of Unzen 1993 dacite: Evidence for excessive volatile supply from mafic magma, EOS trans. American Geophys. Union. 2001 Fall meeting.

Saito, G., J. A. Stimac, Y. Kawanabe and F. Goff, 2002, Mafic-felsic magma interaction at Satsuma-Iwojima volcano, Japan: evidence from mafic inclusions in rhyolites, Earth, Planets and Space 54, 303-325.

Shaw, H.R., 1985, Links between magma-tectonic rate balances, plutonism and volcanism, J. Geophys. Res. 90, 11275-11288.

Shinohara, H., W.F. Giggenbach, K. Kazahaya and J.W. Hedenquist, 1993, Geochemistry of volcanic gases and hot springs of Satsuma-Iwojima, Japan: Following Matsuo, Geochem. J. 27, 271-285.

Shinohara, H., K. Kazahaya, G. Saito, N. Matsushima and Y. Kawanabe, 2002, Degassing activity from Iwodake rhyolitic cone, Satsuma-Iwojima volcano, Japan: Formation of a new degassing vent, 1990-1999, Earth, Planets and Space 54, 175-185.

Stevenson, D.S. and S. Blake, 1998, Modelling the dynamics and thermodynamics of volcanic degassing, Bull. Volcanol. 60, 307-317.

Stolper, E. and J.R. Holloway, 1988, Experimental determination of the solubility of carbon dioxide in molten basalt at low pressure, Earth Planet. Sci. Lett. 87, 397-408.

Snyder, D. and S. Tait, 1998, The imprint of basalt on the geochemistry of silicic magmas, Earth Planet. Sci. Lett. 160, 433-445.

Takamiya, H. and S. Nishimura, 1986, Thermoluminescence ages of some volcaniclastic materials, Nucl. Tracks Radiat. Meas. 11, 251-257.

Thomas, N., S. Tait and T. Koyaguchi, 1993, Mixing of stratified liquids by the motion of gas bubbles: application to magma mixing, Earth Planet. Sci. Lett. 115, 161-175.

Wallace, P.J. and T.M. Gerlach, 1994, Magmatic vapor source for sulfur dioxide released during volcanic eruptions: Evidence from Mount Pinatubo, Science 265, 497-499.

Degassing process of Miyakejima volcano: Implications of gas emission rate and melt inclusion data

Hiroshi Shinoara [1)*], Keiichi Fukui [2)],
Kohei Kazahaya [1)], and Genji Saito [1)]

1) Geological Survey of Japan, AIST, 1-1-1 Higashi, Tsukuba 305-8567, Japan
2) Meteorological Research Institute, JMA, 1-1 Nagamine, Tsukuba, 305-0052, Japan
*: Corresponding author: Fax +81-298-56-8725, e-mail: shinohara-h@aist.go.jp

ABSTRACT

Various techniques of volcanic plume studies were applied to monitor degassing activity of Miyakejima volcano, Japan, including SO_2 emission rate measurement with COSPEC, heliborne-CO_2/SO_2 ratio measurements, Cl/S ratio measurements with alkaline-trap methods. The degassing activity of Miyakejima, that started mid-2000, was characterized by its larger emission rate (up to 40 kt/d SO_2), gradual decrease of the emission rate and constant composition even during the emission decrease. Composition of the volcanic gas was estimated by combination of these plume studies. Volatile contents of the magma were estimated by the analyses of melt inclusions in the Miyakejima 2000 basalt, and close similarity was found between the estimated melt composition and composition of the volcanic gas, indicating a shallow degassing of the magma. The results of volcanic plume and melt inclusion studies were integrated to evaluate the degassing process of the volcano, and the intense degassing was modeled based on the volatile-transport through a convecting magma conduit

INTRODUCTION

Magma degassing is one of the topics in volcanology that significantly advanced in the last few decades. Although volatile components have been recognized as the major energy source of explosive eruptions for a long time, poor constraints on volatile contents in magmas and gas emission rates from volcanoes have obscured quantitative evaluation of the degassing processes. These deficiencies were overcome by accumulation of data obtained by application of the modern micro-analytical techniques on melt inclusions and various techniques to study volcanic plumes, including COSPEC, TOMS, FT-IR and airborne sampling. Combinations of the studies on melt inclusions and volcanic plumes showed quantitative evaluation of degassing processes during explosive and non-explosive eruptions (Wallace, 2001; Satoh et al., 2002). Comparison of erupted magma volume and that of the degassed magma estimated from the volatile content and gas emission rate revealed that the gas emissions are supplied not only from the erupted magma but also often from magmas that degassed but never erupted. Such an excess degassing is obvious in particular at non-erupting degassing volcanoes such as Izu-Oshima, Etna, Stromboli and Satsuma-Iwojima, whose long-term and continuous degassing activities imply degassing of a large magma chamber (Allard et al., 1994; Allard, 1997; Kazahaya et al., 1994; 2002). A gigantic degassing activity of Miyakejima volcano is an another well studied example of such a continuous degassing activity. A variety of studies on volcanic plume and melt inclusions were performed to understand the process in operation. We summarize here the results of those studies and discuss the mechanism of the degassing activity as a demonstration of the importance of comprehensive studies of volcanic gases and melt inclusions.

MIYAKEJIMA 2000 ERUPTION AND SUBSEQUENT DEGASSING ACTIVITY

Miyakejima is a small volcanic island of a basaltic magma located 200 km south of Tokyo (Fig. 1). The island is 8-km-across and 800-m-high (before the 2000 eruption) but the volcanic edifice is 25 km in diameter and 1200 m in height as measured from the sea bottom. The volcano repeated 14 flank fissure eruptions with lava flows for recent 500 years and the eruptions have become more frequent with recurrence intervals of about 20 years (1940, 1962 and 1983). Although very weak steaming activity located at the summit, appreciable degassing activity has not been observed except those during the magmatic eruptions.

The Miyakejima 2000 volcanic activity is characterized by formation of a large collapsed caldera at the summit, and intense and continuous degassing activity started after eruptive activities. The eruptive activities started with a minor submarine eruption on 27 June 2000, preceded by an earthquake swarm and crustal deformation. The earthquake swarm started beneath the island on 26 June, then migrated to 20 km NW from the island, continuing for more than two months with five M>6 events and fifty M>5 events (Japan Meteorological Agency, 2000). The crustal deformation and the hypocenter distribution indicated intrusion of a dyke of 15 km length and 0.7 km^3 in volume at 20 km NW of Miyakejima (Nishimura et al., 2001). The intruded magma is suggested to be tapped from a magma chamber beneath Miyakejima.

Subsidence of the summit area started on 8 July with a minor phreatic eruption and the subsidence continued until mid-August forming a collapsed caldera of 1.6 km in diameter, 450 m in depth and 0.6 km^3 in volume (Geshi et al., 2002). Several phreatic and phreatomagmatic eruptions occurred during the subsidence. The eruptive activity culminated with a phreatomagmatic eruption on 18 August with an eruption column reaching 15-km height, and major eruptions ceased at the end of August. Total erupted volume is 0.007 km^3 that amounts to only 1% of the caldera volume, and only 20-40% of the erupted materials are fresh basalt. The collapsed caldera is concluded to have been created by subsidence of piston-cylinder-like materials into a magma chamber that caused magma ascent by stoping mechanism resulting in the phreatomagmatic eruptions (Uto et al., 2001; Kumagai et al., 2001). Diameter of the stoping column was estimated to be 600-700 m based on analyses of collapse caldera development processes (Geshi et al., 2002). The depression in the magma chamber might be caused by magma intrusion to the NW region out of the island.

Continuous emission of volcanic gases from the summit caldera was not observed in July in spite of the several phreatic and phreatomagmatic eruptions and caldera collapse. The volcanic gas emission started in mid-August and the emission intensity increased with time (Nakada et al., 2001) in contrast with the decrease in the eruptive activity. The high gas emission rate corresponding to more than 10 kt/d of SO_2 continued since the end of August to the present (May, 2002; see below for details). Because of the low altitude of the volcano and the high emission rate of the gases, the volcanic gases rich in SO_2 often attack to residential areas along the coast. The island residents (~4,000 people) were evacuated in early September because of the possible risk of further eruptions. Although large eruptions are no longer expected, the evacuation still continues because of the high SO_2 concentration over several ppm sometimes observed in the residential areas. Although small ash plumes were sometimes observed during this degassing stage, the ash amount is small and the ashes do not contain any fresh basaltic fragments.

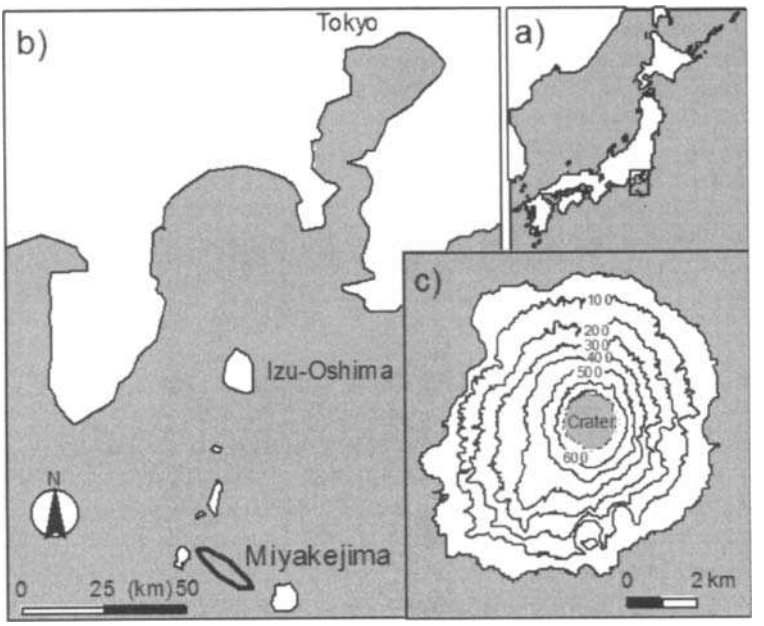

Fig. 1 Location and topographic map of Miyakejima volcano. a) Map of Japan islands. The square shows the area in the map b). b) Location of Miyakejima. Ellipse shows the region of the earthquake swarm that occurred from early July to late August 2000. c) Topographic map of Miyakejima volcano after formation of the collapsed caldera shown by the gray area outlined by the dotted curve in the center. Contour interval is 100 m.

MONITORING THE DEGASSING ACTIVITY

SO_2 emission rate

The COSPEC measurements of SO_2 emission rates are repeated to monitor variation of the gas emission rate (Kazahaya et al., 2001; 2002). Because of the large plume and the small size of the island, all the measurements were made with a helicopter-mounted COSPEC-V (Resonance Ltd.), except for the first two data on 26 and 27 August, when tripod-based measurements were performed on the island. The typical traverse course of the heliborne measurement is 8-16 km downwind of the summit at 90-m height. Wind direction and velocity was measured at 90-m and about 1000-m height. The volcanic plume was quite dense with steam and sometimes containing ash during early stages of the degassing activity, in particular in early September, 2000. The dense plume that does not pass UV light causes underestimation of SO_2 concentration in the atmosphere because most UV light detected by COSPEC was likely reflected at outer rim of the plume and little passed through the plume. Therefore, the estimated emission rate before mid-September can be significantly underestimated (Kazahaya et al., 2002; Fig. 2a). The daily average emission rates show a large variation in a short term such as in a week or a month, but multiple estimates obtained in

a single day commonly agree well. Therefore the short-term variation is the real fluctuation of the emission rate but not due to errors of the estimate.

Very large emission rates of SO_2 over 10 kt/d started to be observed only a few weeks after beginning of the gas emission in mid-August, in spite of the possible underestimation in early September. In late 2000, the SO_2 emission rate was quite large ranging from 10 to 200 kt/d with an average of 42 kt/d. The average emission rate gradually decreased in early 2001 to one-third of the peak value, and became more or less stable after the late 2001 with an average of 10 kt/day. Although the SO_2 emission rate can be slowly decreasing even after late 2001, the large short-term fluctuation obscures the possible long-term trend. The SO_2 emission rates of Miyakejima are one of the largest values observed during such a continuous degassing without explosive eruptions. The peak average of 42 kt/d far exceeded the global SO_2 emission rate from non-erupting volcanoes that was estimated as 26 kt/d before Miyakejima activity (Andres and Kasgnoc, 1998). Total SO_2 emission during the 20 months amounted to 15 Mt and is comparable with the SO_2 emitted by the explosive Pinatubo eruption in 1991.

CO_2/SO_2 ratio

Carbon dioxide is another major constituent of volcanic gases after water. Because of the low solubility in magma, CO_2 is possibly saturated even under magma chamber conditions and the CO_2-rich bubbles likely affects the eruption and degassing processes (e.g., Wallace, 2001). The CO_2 content in the volcanic plumes were monitored by heliborne measurement of CO_2/SO_2 ratio of the plume (Shinohara et al., 2002). Concentration of CO_2 and SO_2 were measured during plume traverses crossing the wind direction by CO_2 and SO_2 analyzers mounted on a helicopter. The CO_2/SO_2 ratio of the plume was obtained by comparing the CO_2 and SO_2 peaks during the plume traverses. As the common volcanic CO_2 concentration in the plume is a few ppm, that is much less than the atmospheric background of about 360 ppm, slight fluctuation of the atmospheric background value causes a large error in the estimation. Therefore, quality of each datum was evaluated based on the ratio of volcanic CO_2 peak and background noise and was classified into different levels as shown by the size of the symbols on Fig. 2b (Shinohara et al., 2002). The low quality data (small circles) due to the noisy background show a large scatter, whereas the high quality data are consistent. The CO_2/SO_2 mole ratio are constant at about 0.75 throughout the whole observation period, in spite of the large decrease in the SO_2 emission rate (Fig. 2b). Emission rate of CO_2 calculated with the mole ratio and the SO_2 emission rate also decreased from 21 kt/d in the late 2000 to 7 kt/d in late 2001.

Cl/S ratio and other ratios

Because of the low altitude of the volcano, the volcanic plume often comes down to the residential areas along the coast, in particular under strong wind conditions. We installed alkaline traps containing 0.1-1N KOH solution open to the air under a rain shield to absorb the acid gases (Noguchi and Kamiya, 1963; Italiano et al., 1991). The alkaline solution left for a certain period was analyzed for Cl and SO_4 ions with an ion-chromatograph after oxidation. Sodium content of the KOH solution was also analyzed to evaluate the amount of Cl derived as NaCl from the ocean. The estimated Cl/S mole ratio is almost constant at around 0.09 (Fig. 2d). As the acid gases were passively absorbed by the alkaline solution in this method, there could be fractionation depending on the species during the absorption process due to kinetic effects. In order to evaluate such errors, the volcanic gases were sampled by bubbling the air through the alkaline solution in March 2000 while the plume came down to the residential areas. The compositions analyzed for the pumped gases were similar with the results obtained by the alkaline trap method, indicating reliability of the latter method (Fig. 2c).

Concentrations of SO_2, H_2S and HCl in the air were measured also with gas detector tubes (GASTEC Corp.) in March 2002. The estimated mole ratios of HCl/SO_2 and SO_2/H_2S are 0.08 and 12, respectively. Emission rate of H_2O was estimated by the method of Fukui (1995) with the infrared video images of the volcanic plume (Matsushima and Nishi, 2001). The estimated H_2O emission rates are largely scattered but show similar variation with the SO_2 emission rate with the H_2O/SO_2 ratio of about 10 in weight ratio.

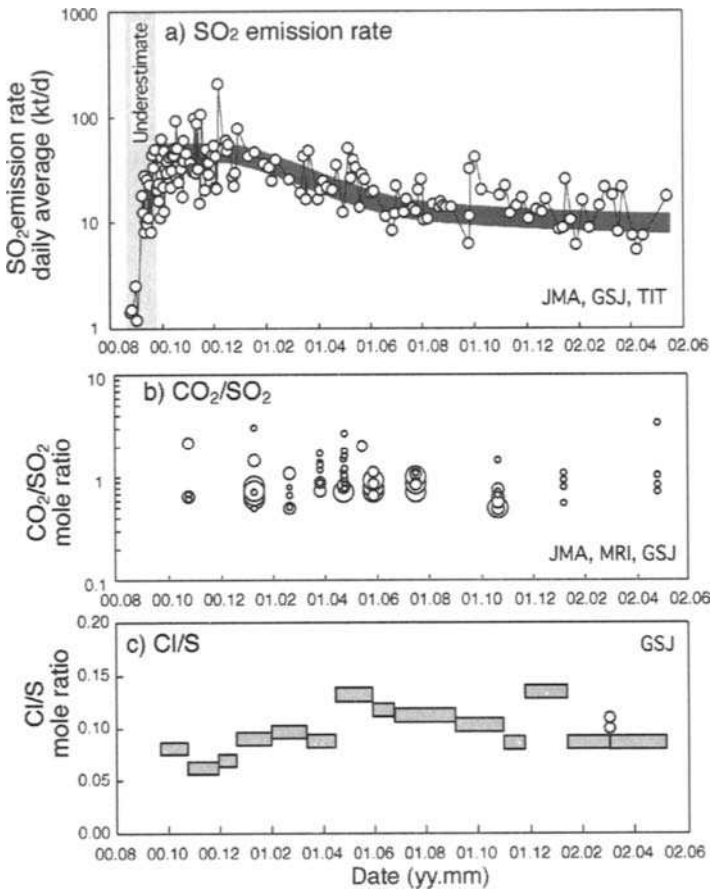

Fig. 2 Variation of emission rates and compositions of volcanic plume. a) Daily average of SO_2 emission rate (Kazahaya et al., 2002). The emission rates are likely underestimated during the early stages of the measurements marked with light gray. The thick curve shows long-term trend. b) Mole ratio of CO_2/SO_2 measured by the heliborne surveys (Shinohara et al., 2002). Size of the circles shows reliability of the data (Larger circle implies more reliable). c) Mole ratio of Cl/S of the volcanic plume. The ratio was analyzed for the alkaline solution left on the island to absorb the volcanic plumes during the period indicated by the bar. Circles shows the ratio in the alkaline solution through which the volcanic plumes were absorbed by pumping. The surveys were performed in cooperation of various organizations including;

Geological Survey of Japan, AIST (GSJ), Japan Meteorological Agency (JMA), Meteorological Research Institute, JMA (MRI) and Tokyo Institute of Technology (TIT).

Volcanic gas composition

We can calculate the composition of volcanic gas emitted from Miyakejima based on the gas component ratios obtained above (Table 1). This volcanic gas composition is consistent with the reported range of subduction-related volcanic gases (Giggenbach, 1996), but plot at the S-rich end of the composition range. The composition range is estimated based mainly on high-temperature volcanic gases from dacitic or andesitic volcanoes and few reliable data exist for basaltic volcanoes. Therefore this estimate should be regarded as a rare example of the volcanic gas composition from basaltic volcanoes in convergent margins. As S-contents in magma is commonly larger in basaltic magmas than in dacitic or andesitic magmas (Sigurdsson, 1990), the S-rich feature of Miyakejima volcanic gas is likely a characteristic of basaltic volcanoes. Hydrogen is the only major volcanic gas components which were not

Table 1 Composition of volcanic gas estimated based of the plume measurements at Miyakejima volcano (mol %)

H_2O	CO_2	SO_2	H_2S	HCl
94.9	2.0	2.7	0.21	0.24

measured at Miyakejima, and commonly consists about 1% of the water content in high-temperature gases (Giggenbach, 1996). The composition seems to be constant regardless of the emission rate decrease.

VOLATILES IN MAGMA

Melt inclusion analyses are the only direct tool to estimate composition of gas components dissolved in magmas before near-surface degassing. As little magma discharged during the continuous degassing activity, magmatic components discharged during preceding eruptive activities are used for the melt inclusion analyses with an assumption of a common magma for the eruptive and degassing activities.

Miyakejima 2000 Magma

The phreatomagmatic eruption on 18 August 2000 is the largest in the series of eruptions in 2000 and produced 8×10^9 kg of erupted materials. The juvenile basaltic magma consists of 40% of the eruption products and the remainders are fragments of old lavas, scorias, and hydrothermally altered rocks (Uto et al., 2001). The juvenile products include bombs, lapilli, and ashes that have similar texture, whole rock chemical composition and mineral composition. Their whole rock composition is distinct from the composition trend of historical eruption products. The juvenile products contain plagioclase, olivine and clinopyroxene as phenocrysts and their groundmass contains microlites of plagioclase, pyroxene and magnetite less than 20 μm in size with little glassy part. The plagioclase phenocrysts (0.1-1 mm) have homogeneous cores with An83-93 composition and Ab-rich (An65-90) rims 20-30 μm thick. Microlite plagioclase has the same composition as the Ab-rich rim indicating syn-eruptive growth of these plagioclases. Clinopyroxene phenocrysts also have homogeneous cores of Mg#77 with Mg-poor rim 20-30 μm thick. Olivine phenocrysts also show zoning with homogeneous cores of Mg#68-82 and Mg-poor rims of Mg#67-71. Olivine rims have relatively homogeneous compositions and the 100-300 μm

thickness, that is significantly larger than those of other phenocrysts. Considering the slower crystal growth rate of olivine than plagioclase, we inferred that the thick rims of olivine grew together with the core of other phenocrysts (Saito, et al., 2002).

Melt inclusions

Melt inclusions in bombs are commonly devitrified, whereas those in lapilli are mostly glassy. These contrasts are likely due to difference of cooling rates depending on ejecta size. Most analyses were made of inclusions in lapilli, except for one glassy inclusion found in a bomb. Melt inclusions are distributed in the core of plagioclase and clinopyroxene, and in the rims of olivine. Only one inclusion in the cores of olivine was analyzed (see below). Most inclusions are elliptical in shape with sizes ranging from 20-160 μm in plagioclase, 10-40 μm in pyroxene, and 10-80 μm in olivine. Rectangular inclusions are also found in plagioclase phenocrysts with the size ranging from 10 to 400 μm. About one-third of inclusions are bubble-free whereas others contain a bubble with various diameter ranging up to 0.5 of the inclusion diameter, corresponding to 10 vol % of the inclusion. Volume proportion of bubble to inclusion seems to have no correlation with inclusion size. Optical observation did not indicate any features typical of leaked inclusions such as fractures, melt channels or devitrification due to water-loss. Therefore the large bubbles in the inclusions are likely trapped bubbles, while small bubbles of less than a few vol % can be also formed by shrinkage. A few μm overgrowth of host minerals is commonly observed in the inclusions.

Major chemical composition and volatile contents of the melt inclusions were analyzed with EPMA and FTIR (Saito et al., 2002). Major elements were analyzed with a JEOL JXA-8900 Superprobe with an accelerating voltage of 15 keV, beam current of 12 nA, and defocused beam of 5 μm diameter. The analyses of S and Cl were made with the same EPMA with an accelerating voltage of 15 keV, 50 nA beam current, and beam diameter of 5 μm counted for 100 s. The search of SKα radiation wavelength was performed for precise analyses of sulfur. Water and CO_2 concentrations were determined for doubly polished melt inclusions with a Nicolet Magna-IR 550 FTIR spectrometer. Detailed analytical procedures, conditions and errors are given by Saito et al. (2001; 2002).

Major element compositions of melt inclusions overlap with the groundmass composition of the 18 August 2000 juvenile products, except for the one inclusion trapped in the core of olivine (Fig. 3). The agreement in compositions of groundmass and those of melt inclusions implies that these inclusions were trapped just prior to the eruption. In contrast, composition of the inclusion in the olivine core is more primitive, close to the whole rock compositions, and this inclusion likely represents the melt in an earlier stage of magmatic evolution. The major element composition also shows slight deviation from the groundmass composition depending on the host minerals. Inclusions in olivine tend to be more SiO_2-rich and MgO-poor than the groundmass, whereas inclusions in plagioclase tend to be enriched both in SiO_2 and MgO (Fig. 3a). As the host mineral overgrowth was observed, these tendencies are interpreted as the results of the host mineral overgrowth. Extent of the overgrowth was estimated for each inclusion by calculating melt composition with adding various amount of host mineral to the inclusion until reaching a composition close to the groundmass composition (Fig. 3). The extent of overgrowth was estimated to be 2-27 vol % in plagioclase, 2-9 vol % in olivine and 8-21 vol % in clinopyroxene. The analytical values of the volatile components were corrected for the host mineral overgrowth.

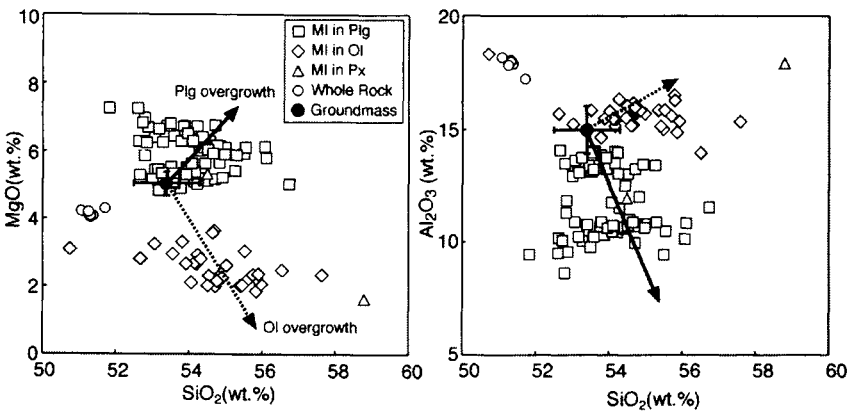

Fig. 3 Chemical composition of melt inclusions, groundmass and whole rock of the Miyakejima, Aug. 18, 2000 eruption products (Saito et al., 2002). a) MgO and SiO_2, and b) Al_2O_3 and SiO_2. All data are recalculated to water-free composition. The large cross shows one sigma scattering of groundmass composition. The solid and dashed arrows show the melt composition change by overgrowth of 30 vol % for plagioclase and 10 vol % for olivine, respectively. Extent of the overgrowth was estimated to best fit the MgO, K_2O and Al_2O_3 content with the groundmass.

Volatile contents

The number of melt inclusions analyzed with FT-IR is limited because of the relatively small sizes of inclusions for preparation of the doubly polished thin section. Water content was quantitatively measured for all the polished inclusions whereas only four of the polished inclusions contained enough CO_2 for quantification (Fig. 4a). The water content ranges from 1 to 2 wt. % and the CO_2 contents are less than 0.01 wt. %. Although the number of analyses is limited, there seems to be no difference in water content depending on the host minerals. Larger number of analyses was made for S and Cl content in melt inclusions. Distribution of S and Cl content of the inclusions analyzed with FT-IR is consistent with the range of all of the inclusion, indicating that there is no bias on the data due to selection of larger inclusions for the FT-TR analyses (Fig. 4d). There is no apparent correlation of the S and Cl contents with bubble size. The S and Cl content range overlaps for inclusions in plagioclase, olivine and pyroxene, but inclusions in olivine tend to have larger Cl content than those in plagioclase with similar S content. The inclusion in the core of olivine has the largest S content of 0.19 wt. %, whereas the others range from 0.05 to 0.17 wt. %.

Gas saturation pressure is calculated as a function of H_2O and CO_2 content in the melt with the VolatileCalc program (Newman and Lowenstern, 2002). The H_2O and CO_2 contents of inclusions indicate low saturation pressure ranging from 23 to 60 MPa, that corresponds to 1-3 km depth under lithostatic pressure gradient. The inclusions, however, contain bubbles with various volume proportion ranging from 0 to 10 vol %. Considering that a few % volume decrease is caused by cooling from 1150° to 1000°C, we infer that the bubbles with volume less than a few vol % can be shrinkage bubbles, whereas larger bubbles are likely trapped bubbles. We can estimate the original H_2O and CO_2 content in a inclusion containing

shrinkage bubbles with the method of Anderson et al. (1989) for a given set of H_2O and CO_2 content in the melt and volume proportion of bubble to inclusion. The two inclusions containing 0.010 and 0.007 wt. % CO_2 includes bubbles of 3.3 and 2.3 vol %, respectively. The original CO_2 contents and saturation pressures of these inclusions are estimated to be 0.12 wt. % (280 MPa) and 0.063 wt. % (150 MPa), respectively. In contrast, inclusions with 0.004 and 0.005 wt. % CO_2 contain very small bubbles of less than 1 vol % resulting in little changes due to the correction. These results suggest that the inclusions could have been trapped in the large pressure range from 23 to 280 MPa. By assuming the CO_2 detection limit as the CO_2 content in the melt, we can estimate the maximum trapping pressure of the other FT-IR measured inclusions to range from 17 to 150 MPa. The wide range in pressure at entrapment might indicate that the inclusions were formed during ascent of magma from a deep reservoir (Saito et al., 2002).

The variable bubble volume proportions down to zero even in large inclusions indicates that the shrinkage bubbles did not form in some cases, likely due to rapid cooling. The kinetic control of the shrinkage bubble formation suggests that the gas in the shrinkage bubble may not have been in equilibrium with the melt. In contrast, the above correction for the shrinkage bubbles assumes solution equilibrium of the volatile components between the gas and the melt after shrinkage. Therefore, the shrinkage bubble correction overestimates the trapping pressure in inclusions whose gas phase was not in equilibrium with the melt. If trapped bubbles are regarded as shrinkage bubbles that also causes overestimation of the trapping pressure. Consequently the upper values of the estimated trapping pressure of 280 MPa might be largely overestimated. The extent of overestimation, however, cannot be estimated without analyses of homogenized inclusions prepared by heating under pressure. Therefore, we should consider both the upper and lower estimates of the trapping pressure and CO_2 content for the present discussion (Saito et al., 2002).

The low saturation pressure down to 17 MPa as well as the wide range of the pressure implies that the inclusions were trapped during magma ascent under variable pressures. Because of its large solubility, water contents are not affected by the shrinkage bubble formation, and the variation in the water contents are likely the original variation or created by water exsolution during magma ascent in the low pressure range, less than 50 MPa (Fig. 4a). The wide variation in S content ranging from 0.05 to 0.15 wt. % with relatively constant Cl content, in particular for inclusions in plagioclase (Fig. 4d), suggests that the S content variation also formed by S-exsolution during magma ascent. As the S content variation does not show any correlation with the bubble volume, the S content does not seem to have been affected by the shrinkage bubble formation nor by the formation of the CO_2-rich bubble at high pressure (trapped bubbles). The variation of S-content is likely created in the low pressure range similarly as the H_2O content variation. The linear correlation among the H_2O, S and Cl content suggest similar behavior of these components during the shallow degassing. Therefore, we inferred that the upper values of H_2O, S and Cl contents, that is 2, 0.13, and 0.07 wt. %, respectively, likely represent the melt composition before the shallow degassing during magma ascent (Saito et al., 2002).

The composition of volcanic gas presently emitted from Miyakejima volcano (Table 1; gray lines on Fig. 4) show fairly good agreement with the variation of volatile contents in inclusions except for CO_2 content. Considering that Cl tends to remain in magmas even after shallow degassing, we conclude that the present volcanic gas emission likely originated from the same melt trapped in the inclusions. The disagreement in CO_2 content can be due to the effect of shrinkage bubble formation, however, is more likely due to super-saturation of CO_2 during inclusion entrapment.

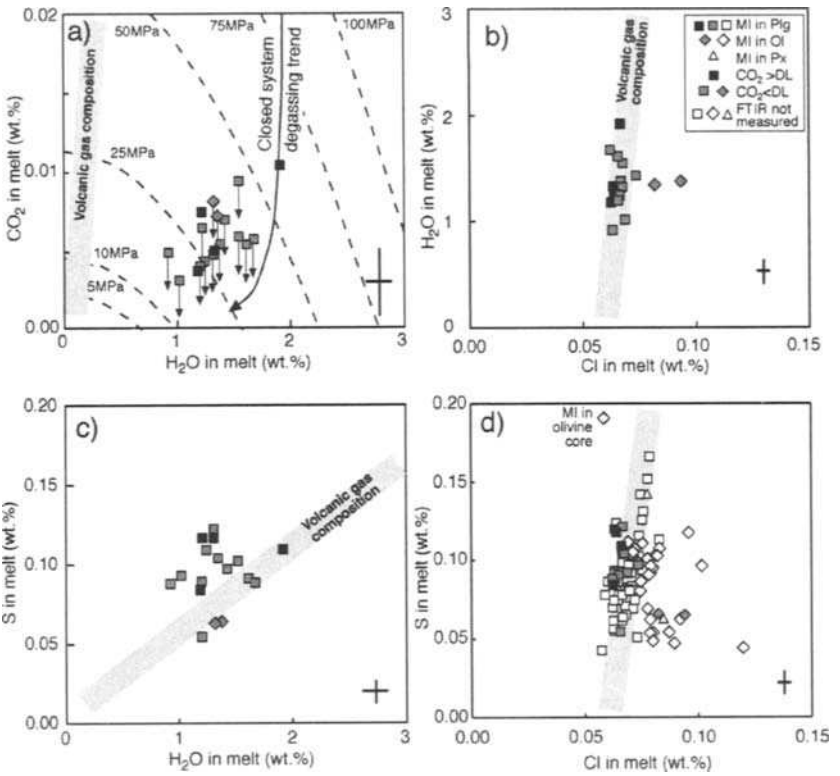

Fig. 4 Variation of volatile contents in melt inclusions in the Miyakejima, Aug. 18, 2000 eruption products (Saito et al., 2002). a) H_2O and CO_2, b) H_2O and Cl, c) S and H_2O, and d) S and Cl. All data are corrected for the host mineral overgrowth (Fig. 3). Squares, diamonds and triangles are inclusions in plagioclase, olivine and clinopyroxene, respectively. The filled symbols show inclusions whose H_2O and CO_2 contents were quantitatively measured and the gray symbols indicate inclusions which were analyzed with FT-IR but have lower CO_2 content than the detection limit. The gray symbols were plotted on the CO_2 detection limit value with an arrow to show that the value is the maximum of the possible CO_2 content. Crosses in each figure show one sigma error of analyses. Dashed curves and solid curve with an arrow in a) are isobars and degassing trend in a closed system calculated with the program by Newman and Lowenstern (2002). The degassing trend was calculated for basalt at 1150°C with initial H_2O and CO_2 contents of 2 and 0.12 wt. %, respectively. The gray straight lines show the estimated composition of volcanic gas (Table 1).

The CO_2 super-saturation is consistent with the observation of various size bubbles. Based on the volcanic gas compositions and H_2O and S contents of 2 and 0.13 wt. %, respectively in the melt before the shallow degassing, CO_2 content in the bulk magma (melt+bubbles) that supplies the volcanic gas is estimated to be 0.12 wt. %. Saturation pressure of this bulk magma with H_2O of 2 wt. % and CO_2 of 0.12 wt. % is calculated to be 280 MPa, corresponding to 11-km depth.

DEGASSING PROCESSES

Enormous amounts of volcanic gases are continuously discharging from Miyakejma volcano. Although little magma discharged after August 2000, the large gas emission rate implies that intensive magmatic degassing is occurring beneath the volcano. Quantitative comparison of the gas and melt inclusion studies, as well as other geophysical measurements, can provide an insight into the degassing processes, that is essential for evaluation of the present magmatic activity of the volcano.

Mechanism of the continuous degassing

The minimum amount of magma required to supply the gas emission is calculated from the SO_2 emission rate and the S content of the magma with an assumption of complete degassing. The daily emission rate of 42 and 14 kt/d of SO_2 during the peak period and the recent stages require magma degassing rate of 16 and 6.2 Mt/d, corresponding to 6.4 and 2.5 $x10^6$ m^3/d, respectively. The total amount of the degassed magma to supply 15 Mt of SO_2 is 5.8 Tt (2.3 km^3). Most likely mechanism to cause the continuous supply of the large amount of magma from a deep chamber to the shallow degassing site is magma convection through a conduit driven by the density difference between the volatile-rich and degassed magmas (Fig. 5; Kazahaya et al., 1994; 2002). Separation of the volcanic gas from the convecting magma at low pressure is necessary for efficient volatile discharge from the magma. Water content of Miyakejima magma ranges from 1 to 2 wt. %. Even if the original magma contains 2 wt. % of water, 50% water exsolution requires the gas-magma separation pressure lower than 10 MPa corresponding to 0.4-km depth, and much lower pressure is required for more efficient water discharge. As the large magma chamber of 2 km^3 is not expected to be located at such a shallow depth less than 0.4 km at Miyakejima, the convective magma transport from a deep magma chamber is necessary to cause the large volcanic gas emission.

The estimated rates of magma convection at Miyakejima volcano are from one to two orders of magnitude larger than the rates estimated for other basaltic volcanoes, such as Etna, Stromboli and Izu-Oshima (Allard, 1997; Allard et al., 1994; Kazahaya et al., 1994). The magma convection rate is controlled by the magma transport rate in the conduit and/or the rate of bubble separation at top of the magma conduit. The magma transport rate (Q) in the convecting magma column can be evaluated based on a simple fluid-dynamic equation given by Kazahaya et al. (1994) and revised by Stevenson and Blake (1998);

$$Q = \pi (R^*)^2 \, Ps \, (g \, \Delta\rho \, R^4/\mu_d) \qquad (1)$$

where R^* ($= R_a/R_d$) is the ratio of rising-flow and descending-flow radius, Ps is the Poiseuille flow number, g is the acceleration due to gravity, $\Delta\rho$ is the density difference between the rising and descending magmas, R is the conduit radius and μd is the viscosity of the descending magma, for a circular conduit flow. Considering that composition, water content and temperature are similar for basaltic magmas of Miyakejima and other volcanoes, we infer that the large magma degassing rate at Miyakejima is due to a larger conduit radius (R) at Miyakejima than in other systems. As the magma transport rate is proportional to R^4, only three times larger conduit radius can result in 100 times larger magma transport rate. For the following parameters; R^*=0.6, Ps=0.02, $\Delta\rho$ = 70 kg/m3 and μ_d=1000 Pas, the conduit radius required for a magma transport rate of 6.8 and 2.6 $x10^6$ m^3/d (that equals to 78 and 30 m^3/s) are 8.0 and 6.2 m, respectively. Although quantitative evaluation of the bubble separation rate is quite difficult, the larger surface at top of the conduit due to the larger conduit will also result in a greater bubble separation rate.

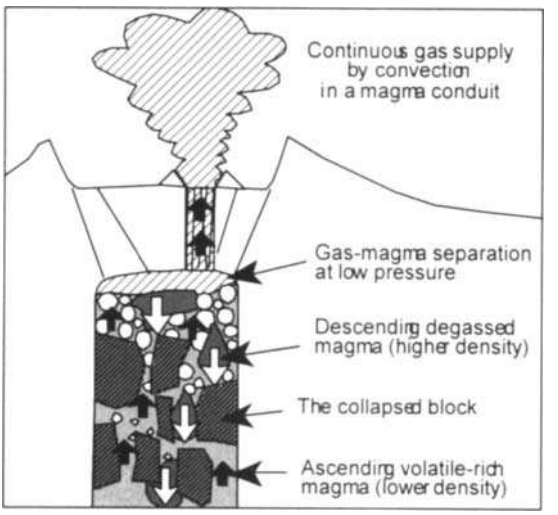

Fig. 5 Model of magma convection through the conduit. The large amount of volcanic gases are supplied as volatile-rich magma from a deep magma chamber by the magma convection. The convection is driven by density difference between the less-dense volatile-rich magma and the degassed magma with higher density. Gas-magma separation at low pressure enables effective degassing from the magma. The 2-km-subsidence of a large column of 600-700m diameter created large open fractures allowing magma ascent by stoping mechanism. The intensive magma convection is caused by the large magma flow channels through the large fracture system.

The large magma conduit system is likely created as the result of the collapsed caldera formation at Miyakejima. Geological, petrological and seismological studies concluded that the collapsed caldera was formed by subsidence of a piston-cylinder shaped column and the magma passively ascended from the chamber by magma stoping mechanism caused by the column subsidence (Kumagai et al., 2001; Uto et al., 2001). An intensive fracture system should have been formed in association with the 2-km subsidence of a 600-700 m diameter column (Geshi et al., 2002) and provided the space for the relatively large magma flow channels.

Evolution of magmatic systems

The volcanic gas emission rate decreased in early 2001, from the peak values of 42 to 14 kt/d SO_2, whereas little changes in the gas composition was observed (Fig. 2). The volcanic gas emission rate will be changed either by volatile content changes in the source magma, change in the gas-magma separation conditions or change in the magma transport rate controlled by Eq. (1). The constant composition of volcanic gases implies constant source magma compositions and gas-magma separation conditions. Therefore the gradual decrease of volcanic gas emission rate is likely the result of a decrease in the magma transport rate. As magma composition and gas-magma separation condition is constant, the magma densities and viscosities are likely constant and the magma transport rate decrease is likely caused by the decrease in the magma conduit radius. The magma transport rate is proportional to the fourth power of the conduit radius (Eq. 1), and a three fold decrease of the magma transport

rate can be caused by only 25% reduction of the magma conduit radius. The magma conduits were created filling the open space between the subsiding blocks and rearrangement of the blocks likely occurs resulting in narrowing of the magma conduit (Fig. 5).

The constant composition of volcanic gases indicates homogeneous distribution of volatile components in the magma chamber. The dissolved H_2O and CO_2 contents in the source magma are estimated to be 2 and 0.12 wt. %, respectively, with a saturation pressure of 280 MPa, corresponding to 11-km depth. In contrast, magma chamber depth of Miyakejima is suggested to be relatively shallow of >3 km based on hypocenter distribution during the collapsed caldera formation (Kumagai et al., 2001). If the magma chamber were located at 4-km-depth (100 MPa), 70% of CO_2 in the magma should be distributed in bubbles that accounts for 1 vol % in the magma. The bubbles ascend by their buoyancy through the magma resulting in a gradient in the bubble distributions. The bubble growth and ascent rate can be calculated as a function of magma viscosity, volatile content, pressure, diffusion coefficient and other parameters, with the assumption of Newtonian-fluid magma (e.g., Shinohara and Kazahaya, 1995). The model calculation predicts that bubbles formed at 100 MPa in a magma with 100-Pas viscosity and initial 0.12-wt. % CO_2 content ascend more than 100 m within a year, and more than 10 km after 10 years. The calculation implies that if the chamber were located at 4-km-depth, the CO_2-rich bubbles should have ascent to the chamber roof in a few years and the magma in the chamber cannot supply the volcanic gases of the constant composition for a few years. Therefore, the constant composition of volcanic gas for a few years implies the supply of the CO_2-rich magma from a source deeper than the saturation pressure (11 km). The calculation of bubble ascent, however, was made with an assumption of the Newtonian-fluid magma. If the magma has enough large yield strength, the small bubble will not ascend at all until they will grow large enough to overcome the yield strength. Since there are few estimates of the magma yield strength, we need to await the measurements of magma yield strength to confirm this conclusion.

It is difficult to estimate how the continuous degassing activity will come to an end. Empirical evaluation relies on the past examples, but there are few observation of termination of the non-erupting degassing activity. In contrast, the intense degassing is continuing for a long time at many volcanoes such as Etna, Stromboli, Sakurajima and Satsuma-Iwojima. The convective magma transport model suggests the conditions for the end of convection as: 1) exhaustion of a volatile-rich magma in a chamber, 2) reduction of the magma ascent driving force, or 3) closure of the magma conduit by external causes. The amount of the magma degassed since August 2000 is estimated to be 2 km^3. In contrast, volume of the magma chamber was estimated by analyses of the very-long-period earthquakes observed during the collapsed caldera formation to be 40 km^3, although this value might be overestimated due to neglect of bubbles that reduces bulk modulus of the magma (Kumagai et al., 2001). Although the volume estimate includes a large uncertainty, the large chamber of 40-km^3 volume can supply 20 times more magma for the degassing. The magma ascent driving force largely depends on the volatile content. The constant volcanic gas composition, however, indicates homogeneous distribution of volatile components in the chamber. The volcanic gas emission rate decreased by three times likely due to reduction of the magma conduit cross-section, although its process cannot be modeled for future evaluation yet.

CONCLUDING REMARKS

Emission rate and composition of volcanic gases show us the present state of magma degassing. Volatile composition analyses of melt inclusion help us to understand the source composition and the behavior of volatile components during magmatic processes. Although

each of these studies is important by themselves, only combination of both studies enables the quantitative evaluation of degassing processes, as they can constrain both the source and the results. The present example from Miyakejima volcano demonstrates the importance of the comprehensive studies to understand the origin of the volcanic gases, their degassing mechanism and evaluation of the state of volcanoes. There are still some technical difficulties for H_2O and CO_2 analyses in volcanic plumes and also in melt inclusions. Because of their well-understood solubility, however, the multi-volatile studies can provide quantitative evaluation of the degassing processes as shown here. Further experimental studies on S and Cl degassing at low pressures are also necessary for better constraints of the degassing processes based on the volcanic gas and melt inclusion studies.

Acknowledgments

We would like to thank Japan Meteorological Agency, Japan Self-Defense Force, Japan Coast Guard and Tokyo Metropolitan Government for their support for the heliborne and ground-based surveys. Thanks are also due to Drs. C. W. Mandeville and G. Chiodini for their constructive reviews.

REFERENCES

Allard, P., 1997, Endogenous magma degassing and storage at Mount Etna, Geophys. Res. Lett., 17, 2219-2222.

Allard, P., J. Carbonnelle, N. Metrich, H. Loyer and P. Zewttwoog, 1994, Sulfur output and magma degassing budget of Stromboli volcano. Nature, 368, 326-330.

Anderson, A. T., S. Newman, S. N. Williams, T. Druitt, C. Skirius and E. Stolper, 1989, H_2O, CO_2, Cl, and gas in plinian and ash-flow Bishop rhyolite. Geology, 17, 221-225.

Andres, R. J. and A. D. Kasngoc, 1998, A time-averaged inventory of subaerial volcanic sulfur emissions, J. Geophys. Res., 103, 25251-25261.

Geshi, N., T. Shimano, T. Chiba and S. Nakada, 2002, Caldera collapse during the 2000 eruption of Miyakejima Volcano, Japan, Bull. Volcanol., 64, 55-68.

Giggenbach W. F., 1996, Chemical composition of volcanic gases, in Monitoring and Mitigation of Volcanic Hazards, Eds. R. Scarpa and R. I. Tilling, pp. 221-256, Springer-Verlag.

Fukui, K., 1995, H_2O and Heat discharge from Aso volcano in Nonerupting stage, Kazan, 40, 233-248 (in Japanese with English abstract).

Italiano, G., P. M. Nuccio, G. Pecoraino and M. Valenza, 1991, Monitoring of acid gases at the crater of Vulcano using the method of the alkaline traps, Acta Vulcanologica, 1, 249-254.

Japan Meteorologica Agency, 2000, Recent seismic activity in the Miyakejima and Niijima-Kozushima region, Japan –the largest earthquake swarm ever recorded-, Earth Planet Space, 52, i-viii.

Kazahaya K., H. Shinohara and G. Saito, 1994, Excessive degassing of Izu-Oshima volcano: Magma convection in a conduit, Bull. Volcanol., 56, 207-216.

Kazahaya, K, J. Hirabayashi, H. Mori, M. Odai, Y. Nakahori, K. Nogami, S. Nakada, H. Shinohara and K. Uto, 2001, Volcanic gas study of the 2000 Miyakejima volcanic activity: Degassing environment deduced from adhered gas component on ash and SO_2 emission rate, J. Geogr., 110, 271-279 (in Japanese with English abstract).

Kazahaya, K., H. Shinohara, M. Odai, Y. Nakahori, H. Mori, K. Uto and J. Hirabayashi, Gigantic SO_2 emission from Miyakejima volcano, Japan, caused by caldera collapse, Geology, submitted, 2002.

Kumagai, H., T. Ohminato, M. Nakano, M. Ooi, A. Kubo, H. Inoue and J. Oikawa, 2001,

Very-long-period seismic signals and caldera formation at Miyake Island, Japan, Science, 293, 687-690.

Matsushima, N. and T. Nishi, 2001, H_2O emission rate of volcanic plume during the 2000-2001 Miyakejima volcanic activity, EOS, Trans. AGU, 82, Fall Meeting Supplement, F1371.

Nakada, S., M. Nagai, A. Yasuda, T. Shimano, N. Geshi, M. Ohno, T. Akimasa, T. Kaneko, and T. Fujii, 2001, Chronoloty of the Miyakejima 2000 Eruption: Characteristics of summit collapsed caldera and eruption products, J. Geogr., 110, 168-180 (in Japanese with English abstract).

Newman, S. and J. B. Lowenstern, 2002, VolatileCalc: a silicate melt-H_2O-CO_2 solution model written in Visual Basic for EXCEL: Comp. Geosciences, 28, 597-604.

Nishimura, T., S. Ozawa, M. Murakami, T. Sagiya, T. Tada, M. Kaizu and M. Ukawa, 2001, Crustal deformation caused by magma migration in the northern Izu Islands, Japan. Geophys. Res. Lett., 19, 3745-3748.

Noguchi, K. and H. Kamiya, 1963, Prediction of eruptions by measuring the chemical composition and amount of gases, Bull. Volcanol., 24, 367-378.

Saito, G., K. Kazahaya, H. Shinohara, J. Stimac and Y. Kawanabe, 2001, Variation of volatile concentration in a magma system of Satsuma-Iwojima volcano deduced from melt inclusion analyses, J. Volcanol. Geotherm. Res., 108, 11-31.

Saito, G., K. Uto, K. Kazahaya, H. Satoh and Y. Kawanabe, 2002, Petrological characteristic and volatile content of magma of August 18, 2000 eruption of Miyakejima volcano: Evidence for phreato-magmatic eruption and magma degassing, Bull. Volcanol, submitted.

Satoh, H., G. Saito, H. Shinohara H. and Y. Yamaguchi, 2002, Sulfur-rich mafic melt inclusions in pyroxene phenocrysts: Source of the excessive degassing during 1991-1995 dome-forming eruption at Unzen volcano, Geology, submitted.

Shinohara, H. and Kazahaya, K., 1995, Degassing processes related to magma-chamber crystallization. Ed., Thompson, J.F.H., Magmas, fluids and ore deposits, Mineral. Assoc. Canada Short Course, 23, 47-70.

Shinohara, H., K. Kazahaya, G. Saito, K. Fukui and M. Odai, 2002, Variation of CO_2/SO_2 ratio in volcanic plumes of Miyakejima: Stable degassing deduced from heliborne measurements, Geophys. Res. Lett., in press.

Sigurdsson, H., 1990, Assessment of the atmospheric impact of volcanic eruptions: Global catastrophes in Earth history; Geol. Soc. Am. Sp. Paper 247, 99-110.

Stevenson D. S., and S. Blake (1998) Modeling the dynamics and thermodynamics of volcanic degassing, Bull. Volcanol., 60, 307-317.

Uto, K., K. Kazahaya, G. Saito, J. Itoh, A. Takada, Y, Kawanabe, H. Hoshizumi, T. Yamamoto, I. Miyagi, A. Tomiya, H. Satoh, S. Hamasaki, and H. Shinohara, 2001, Magma ascending model of 2000 Miyakejima eruptions: Evidence from pyroclastics of August 18 and SO_2-rich volcanic gas, J. Geogr., 110, 257-270 (in Japanese with English abstract).

Wallace, P., 2001, Volcanic SO_2 emissions and the abundance and distribution of exsolved gas in magma bodies, J. Volcanol. Geotherm., Res., 108, 85-106.

This Page Intentionally Left Blank

Chemistry And Origin Of Zoned Haüyne In Tahitian Phonolite, With Implications For Magmatic Fractionation

Robert J. Tracy

Dept. of Geological Sciences
Virginia Tech
Blacksburg, Virginia USA 24061-0420

ABSTRACT

Unusually fresh, unaltered, chemically zoned nosean and haüyne pheno-crysts found in eight samples of phonolite, nepehelinite and trachyte from Tahiti have been studied in detail. All samples have abundant normative nepheline and modal feldspathoid, both as groundmass phases and as euhedral phenocrysts, commonly quite large. All contain microphenocrysts of titanian clinopyroxene, titanite, apatite and variably titanian magnetite. Some contain small laths of sodic plagioclase or potassic feldspar and most have abundant interstitial groundmass glass. Feldspathoids may be either nosean or haüyne, based on proportions of Ca and Na, but all are rich in SO_4 relative to Cl. Ca and Na variations are sympathetic with variations in bulk rock chemistry. Phenocrysts in all samples show consistent core-to-rim decreases in Ca and K that record shifts in the composition of the melt, indicating crystal fractionation processes in the pre-eruptive magma. Slight Cl enrichment at nosean or haüyne rims and ubiquitous discontinuous, apparently epitaxial, annular rims of end-member sodalite surrounding these crystals indicate exhaustion of magmatic sulfate during feldspathoid phenocryst crystallization and a cessation of haüyne or nosean crystalliza-tion. Sufficient Cl was present in the remaining strongly ne-normative melt to allow the abrupt shift from haüyne to sodalite crystallization.

Abundance of sulfate in these rocks (in nosean and haüyne crystals), coupled with absence of any trace of sulfide minerals or any S in ground-mass glass, indicates strong oxidation of magmatic sulfur and total deple-tion of sulfate in the melt during formation of feldspathoid phenocrysts. Cl enrichment in nosean and haüyne rims and the late shift from crystalliza-tion of nosean or haüyne to sodalite indicates a significant, probably syn-eruption increase in Cl/S ratio in the magma, possibly contamination by seawater but more likely related to sulfate depletion through feldspathoid crystallization. The bulk sulfur content of these rocks is high (1.5 to as much as 2 wt% SO_2), due to abundant sulfate feldspathoid phenocrysts, and probably is close to reasonable sulfur solubilities of such magmas, although data is sparse on S solubilities in phonolitic liquids. Model calculations of the potential effects of haüyne crystallization on residual melt compositions suggest that removal of 10 or 15 modal percent haüyne may significantly decrease magmatic Ca/Na ratio while dramatically increasing silica content, and may help to explain the unusual phonolite-trachyte trend observed in the Tahitian volcanic suite.

INTRODUCTION

The relatively uncommon minerals haüyne and nosean that occur in some alkalic volcanic and plutonic rocks are Si-poor, Al-rich tectosilicate members of the sodalite group. They are distinguished chemically from sodalite ($Na_8Al_6Si_6O_{24}Cl_2$) by the replacement of chlorine in sodalite with sulfate or even very minor sulfide, and by the replacement of substantial Na

with Ca (Taylor, 1967; Deer, Howie and Zussman, 1963). Nomenclature boundaries are not clear cut, but the mineral name sodalite is generally reserved for very Na- and Cl-rich varieties. The name *nosean* (end-member formula $Na_8[Al_6Si_6O_{24}]SO_4 \cdot nH_2O$) applies to Na- and SO_4-rich varieties and the compositionally complex nosean-haüyne solid solution series has the compositional range $(Na_{5-8}K_{0-1}Ca_{0-2}\square_{0-1})_8[Al_6Si_6O_{24}](SO_4)_{1-2} \cdot nH_2O$. The name *haüyne* has been used when Ca constitutes greater than 20 percent or more of the non-framework cations, and *lazurite* is used when significant sulfide rather than sulfate sulfur is present (this variety is more common in metamorphic than igneous occurrences). Na-rich nosean has space group $P\bar{4}3m$ and calcic haüyne is $P\bar{4}3n$, and this crystallographic criterion has been proposed by Taylor (1967) to distinguish nosean from haüyne, although he showed that distribution of the space groups may be dependent upon K content as well. The large size of the K^{+1} cation appears to preclude occurrence of a K-rich variety, although K is a significant minor constituent of many haüynes, particularly in potassic silica-undersaturated volcanics, as in the central and southern Italian potassic volcanic province. The literature contains several detailed structural investigations of nosean and haüyne (Hassan and Grundy, 1984, 1989, 1991; Hassan and Buseck, 1989a,b; Xu and Veblen, 1995).

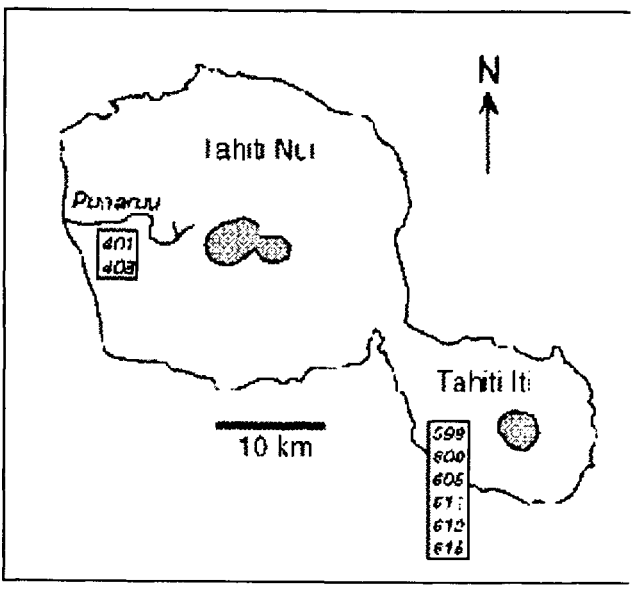

Figure 1 - Map of the island of Tahiti showing locations of samples discussed in this paper. Grayed areas in the ceter of Tahiti-Niu and Tahiti-Iti are the exposed plutonic cores of these two eroded volcanic cones (adapted from Duncan et al., 1994).

Because they are sulfate-rich, both nosean and haüyne are generally treated as parts of a solid solution series (Taylor, 1967) with fairly wide variations in Ca, Na and K contents that are assumed to reflect concentrations of these components in the host magmas. It has been suggested on the basis of TEM studies (Hassan and Buseck, 1989b, p. 179) that ordering of $[Na_4 \cdot SO_4]^{2+}$ and $[Na_4 \cdot H_2O]^{4+}$ clusters in nosean and $[Na_3Ca \cdot SO_4]^{3+}$ and $[K_2Ca \cdot OH]^{3+}$ clusters in haüyne precludes complete miscibility due to net charge differences. Data presented in this paper indicate substantial continuous solid solution, however, especially between Ca and Na end members.

As with other feldspathoids, minerals of the sodalite group form only in silica-undersaturated environments. There are rare meteoritic and meta-morphic occurrences but most reports of sodalite-group minerals are from silica-undersaturated volcanic and shallow plutonic rocks in alkaline igne-ous provinces such as southern Italy (e.g., Conticelli et al., 1997; Renzulli et al., 1998), the Eifel District of Germany (e.g., Sharygin, 1993), the volcanic province of central France (Montel and Gourgaud, 1992), the White Mountain - Monteregian plutons of the northeastern United States and adjacent Canada (e.g., Quinn, 1935; Mandarino and Anderson, 1988; Feininger and Goodacre, 1995) and the volcanic islands of Polynesia,

including Tahiti (e.g., McBirney and Aoki, 1968; Duncan et al., 1994).

In this study, microprobe analyses and compositional images of exception-ally fresh and unaltered zoned nosean and haüyne phenocrysts were obtained from a suite of eight haüyne/nosean-phonolite samples from Tahiti, along with analyses of other representative minerals and glasses in these rocks. The samples examined in this study were collected by Professor R.A. Daly in 1920-21 during an expedition through the Pacific, and are now in the Daly Collection at Harvard University. [The older and now obsolete volcanic rock name "tahitiite," referring to haüyne-bearing phonolite, trachyte or trachyandesite (Johannsen, 1939; McBirney and Aoki, 1968; LeMaitre et al., 1989), was coined around 1900 by Lacroix to acknowledge the typical occurrence of a blue feldspathoid mineral assumed to be haüyne as an unusually prominent phenocryst phase in numerous phonolites and other sodic, silica-undersaturated volcanics from Tahiti.] Data presented here documents a plausible petrogenetic mechanism to explain the limited occurrence of sulfate-rich haüyne phenocrysts, specifically the complete oxidation of magmatic sulfur in a strongly silica-undersaturated magma. The paper presents data on intracrystalline zoning in nosean and haüyne that is consistent with significant pre-eruption magmatic fractionation, and which indicates at least a theoretical possibility that physical removal of haüyne phenocrysts could explain the observed and previously unexplained phonolite-trachyte fractionation trend at Tahiti (McBirney and Aoki, 1968; Duncan et al., 1994).

PETROGRAPHY

The eight samples examined in detail are all either phonolite, tephritic phonolite, or phonolitic nephelinite as defined in the IUGS volcanic-rock classification (LeMaitre et al., 1989), and contain >10% normative or modal nepheline and roughly 10% or less Ca-plagioclase (see Table 6 below). As shown in Figure 1, two of the samples (T-401 and T-408) were collected from the Punaruu section of early shield-building lava flows on the western side of Tahiti-Nui, the main volcanic cone on Tahiti (Duncan et al., 1994). The remaining samples are from the southeastern peninsula of Tahiti-Iti, a slightly younger and smaller volcanic cone. Ages of the samples are not precisely known, but Duncan et al. (1994) reported ages of about 780 to 1200 Ka for flows at Punaruu and 500-1000 Ka for Tahiti-Iti. Some samples show a pronounced trachytic texture with a uniform fine groundmass of moderately to strongly aligned plagioclase laths and moderate proportions of phenocrysts.

In all but one sample, the only phenocrysts are of nosean or haüyne; the one exception contains rare phenocrysts of pale green Ti-poor clinopyroxene in addition to haüyne, although the unusual green color (due apparently to ferric iron and sodium) and Ti-poor character of these suggests they are xenocrystic. Nosean or haüyne also occur as small groundmass microphenocrysts in all samples. Phenocrysts of nosean or haüyne thus range from <100 micrometers up to 2 mm or more in a typical volcanic ground-mass in which crystals rarely exceed 50-100 micrometers in size, and are commonly smaller. Average haüyne and nosean compositions are given in Table 1 (but note that all grains are moderately to strongly chemically zoned).

In addition to nosean or haüyne, all samples contain microphenocrysts of Ti-rich calcic pyroxene, sphene (titanite), apatite, homogeneous (unexsolved) Ti-rich magnetite, and rare very small flakes of the native elements Cu and Ag. Three samples contain very sodic plagioclase and/or an Na-rich potassic feldspar (probably still or originally sanidine) as well as rare leucite microphenocrysts. Ilmenite or ilmenohematite has not been found in any

sample, nor has nepheline. Representative microprobe analyses of feldspars, pyroxenes and oxides are given in Tables 1-3. BSE examination of the groundmass (Fig. 2) indicates that nosean/haüyne, clinopyroxene and titanite crystals are typically euhedral, whereas titanian magnetite crystals are less commonly euhedral. Sodic plagioclase, leucite and sanidine crystals

Table 1. Mycroprobe analyses of feldspars.

Sample	599 (P)	599 (A)	600 (A)	611 (P)	611 (A)
SiO_2	63.40	65.59	66.69	66.76	66.93
Al_2O_3	21.39	18.69	19.16	20.24	19.20
FeO*	1.14	0.96	0.27	0.60	0.47
MgO	0.00	0.00	0.00	0.00	0.00
CaO	2.92	0.08	0.17	1.32	0.46
Na_2O	7.94	4.96	4.72	8.77	5.85
K_2O	2.31	9.43	9.41	3.05	7.57
BaO	0.66	0.00	0.20	0.39	0.14
TOTAL	99.76	99.71	100.62	101.13	100.62
Formulas on the basis of 8 oxygens					
Si	2.852	2.983	2.993	2.940	2.988
Al	1.134	1.002	1.013	1.050	1.010
	3.985	3.984	4.007	3.990	3.998
Fe	0.043	0.037	0.010	0.022	0.018
Mg	0.000	0.000	0.000	0.000	0.000
Ca	0.141	0.004	0.008	0.062	0.022
Na	0.692	0.437	0.411	0.749	0.506
K	0.133	0.547	0.539	0.171	0.431
Ba	0.012	0.000	0.004	0.007	0.002
	0.977	0.988	0.961	0.989	0.962
ab	71.7	44.2	42.9	76.2	52.8
an	14.6	0.4	0.9	6.3	2.3
or	13.7	55.4	56.3	17.4	44.9
	100	100	100	100	100

(P) - plagioclase

(A) - potassic feldspar

are interstitial and typically anhedral to subhedral, although elongated laths of strongly zoned feldspar form in some samples. Most samples contain well preserved glass in the groundmass, and microphenocrysts of all min-erals are typically embedded in and surrounded by this glass (see Fig. 2). Microprobe analyses of groundmass glass are given in Table 4. Fe-Cu-Ni sulfides constitute a mineral group that is prominently absent from all samples, reflecting the oxidized character of magmatic sulfur.

Many euhedral nosean/haüyne phenocrysts (Fig. 3) show optical color zoning in plane-polarized light with colorless cores and strongly blue rims, although not all colorless crystals have such blue rims and some phenocrysts are entirely blue. Nosean or haüyne phenocrysts in hand specimen typically show an intensely bright grayish azure-blue color, however.

Detailed micro-probe examination of several larger, optically zoned crystals for chemical zonation (see below) showed that these colored rims correlated only roughly with variations in cation ratios of Ca, K, Na and in Cl content, consistent with the proposition that such

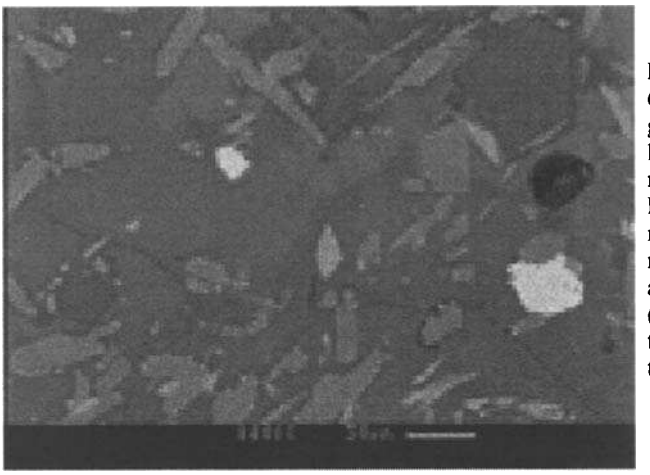

Figure 2. - BSE image from sample 605 showing typical appearance of groundmass in the phonolites. The larger subhedal grain in the upper right is a haüyne microphenocryst. Euhedral to subhedral microphenocrysts of Ti-rich magnetite (bright), titanite (inter-mediate brightness), Ti-Rich augite (bladed and blocky grains) and apatite (upper center) are set in a matrix of glass.

intense color variations in sodalite-group minerals are more likely due to slight shifts in the oxidation or molecular state of sulfur in the crystals than to variation in Cl content (Hogarth and Griffin, 1976; G. Rossman, pers. comm.). Most grains of nosean or haüyne show a modest increase in Cl (up to 1 wt%) immediately inside the rims, but typically not closely correlated with the boundary of colorless and blue parts of the crystal.

About a dozen randomly chosen nosean or haüyne crystals in several samples were compositionally imaged for various elements using the electron microprobe, and the Cl

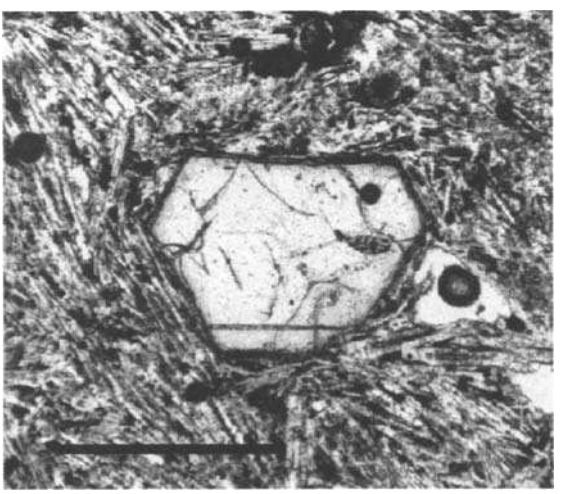

Figure 3. Transmitted-light photomicrograph of a large haüyne phenocryst in sample 401. Note the euhedral character and lack of alteration. The groundmass in this sample consists largely of feldspar laths and interstitial felsic minerals, including sanidine and leucite, along with very fine-grained clinopyroxene, titanite and Ti-rich magnetite (see Fig. 2). Scale bar is 1000 micrometers.

images reveal that virtually all of these crystals are surrounded by a thin epitaxial euhedral annulus of a mineral richer in both Cl and Na than haüyne, and upon analysis this turned out to be end-member sodalite, with no detectable Ca, K or SO_2 (Fig. 4). These overgrowths occur over the whole size range of haüyne phenocrysts, and it is likely that they reflect

exhaustion of magmatic sulfate due to haüyne crystallization and a concomitant late-stage increase in Cl/S ratio in the residual melt. Seawater penetration into the magma chamber or conduits immediately prior to eruption might also be invoked to help explain both the large amount of sulfate feldspathoid and the late jump to sodalite crys-tallization, but is not required (see discussion below on magmatic volatiles). Limited seawater contamination and

Table 2. Microprobe Analyses of Clinopyroxenes

Sample	401	408	599	600	605	611	612	615
SiO_2	41.77	45.39	50.89	45.22	46.43	51.85	44.68	44.92
TiO_2	5.65	4.58	1.82	2.49	3.92	1.33	4.91	4.75
Al_2O_3	8.71	6.27	2.70	6.33	5.89	2.09	7.14	6.98
Cr_2O_3	0.03	0.01	0.00	0.01	0.01	0.00	0.00	0.00
FeO*	11.80	9.58	9.57	15.36	9.48	9.00	10.94	10.12
MnO	0.29	0.29	0.97	0.91	0.29	0.96	0.36	0.29
MgO	8.72	10.91	11.75	7.02	11.07	12.21	9.69	10.22
CaO	21.05	21.54	20.17	20.12	21.96	20.36	20.84	21.50
Na_2O	1.04	0.88	1.72	1.75	0.89	1.61	1.25	1.02
TOTAL	99.05	99.45	99.59	99.20	99.95	99.42	99.81	99.80
Formulas on the basis of 6 oxygens								
Si	1.598	1.713	1.904	1.742	1.742	1.940	1.688	1.693
Al	0.393	0.279	0.096	0.258	0.258	0.060	0.312	0.307
	1.991	1.992	2.000	2.000	2.000	2.000	2.000	2.000
Al	0.000	0.000	0.023	0.029	0.002	0.032	0.005	0.003
Ti	0.183	0.146	0.058	0.081	0.125	0.042	0.157	0.152
Cr	0.001	0.000	0.000	0.000	0.000	0.000	0.000	0.000
Fe^{2+}	0.378	0.302	0.299	0.495	0.297	0.282	0.346	0.319
Mn	0.009	0.009	0.031	0.030	0.009	0.030	0.012	0.009
Mg	0.497	0.614	0.655	0.403	0.619	0.681	0.546	0.574
Ca	0.863	0.871	0.809	0.831	0.883	0.816	0.843	0.868
Na	0.077	0.064	0.125	0.131	0.065	0.116	0.092	0.075
	2.009	2.008	2.000	2.000	2.000	2.000	2.000	2.000
Fe/Fe+Mg	0.43	0.33	0.31	0.55	0.32	0.29	0.39	0.36

resulting oxidation may also be indicated by rare occurrence of very small groundmass grains of native metals (typically Ag or Cu) in most samples, which may form as a result of the absence of sulfides.

NOSEAN AND HAÜYNE CHEMISTRY

Microprobe Analytical Technique

All analyses and X-ray imaging were performed at Virginia Tech on a Cameca SX-50 electron microprobe. Minerals of the sodalite group are no-toriously difficult to analyze with the microprobe because of their extreme fragility under typical beam conditions (15 kV, 20

nA, ~1 micrometer spot). Most contain 15-20 wt% Na_2O or more, and some can contain molecular H_2O as well (Hogarth and Griffin, 1976). They can be observed to degrade phys-

Table 3. Microprobe Analyses of Ti-Rich Magnetites.

Sample	401	408	599	600	605	611	612	615
SiO_2	0.05	0.06	0.07	0.05	0.07	0.06	0.04	0.10
TiO_2	14.73	15.06	13.22	7.42	14.27	21.22	15.92	6.76
Al_2O_3	2.15	1.97	0.67	1.37	1.49	0.67	2.59	0.71
Cr_2O_3	0.03	0.04	0.00	0.00	0.04	0.03	0.00	0.00
FeO*	74.66	75.61	75.96	82.16	76.18	68.44	72.69	83.08
MnO	2.15	2.14	3.68	2.50	2.16	4.77	1.51	2.41
MgO	0.89	0.84	0.40	0.21	0.72	0.04	2.18	0.10
ZnO	0.20	0.13	0.17	0.12	0.13	0.10	0.16	0.21
subtotal	94.86	95.85	94.17	93.83	95.06	95.33	95.09	93.37
FeO	33.67	34.28	31.46	30.74	33.66	36.29	33.02	30.41
Fe_2O_3	45.55	45.94	49.45	57.14	47.25	35.73	44.09	58.53
TOTAL	99.42	100.45	99.12	99.55	99.79	98.91	99.51	99.23
Formulas on the basis of 24 cations/32 oxygens								
Ti	3.350	3.395	3.055	1.708	3.251	4.899	3.571	1.569
Al	0.766	0.696	0.243	0.494	0.532	0.242	0.911	0.258
Cr	0.007	0.009	0.000	0.000	0.010	0.007	0.000	0.000
Fe^{3+}	8.527	8.505	9.647	12.090	8.957	5.953	7.947	12.603
Fe^{2+}	3.350	3.395	3.055	1.708	3.251	4.899	3.571	1.569
	16.000	16.000	16.000	16.000	16.000	16.000	16.000	16.000
Fe^{2+}	7.004	7.053	6.820	7.229	7.092	6.719	6.614	7.276
Mn	0.551	0.543	0.958	0.648	0.554	1.240	0.381	0.630
Mg	0.401	0.375	0.183	0.096	0.325	0.018	0.969	0.046
Zn	0.045	0.029	0.039	0.027	0.029	0.023	0.035	0.048
	8.000	8.000	8.000	8.000	8.000	8.000	8.000	8.000
mag	53.29	53.16	60.29	75.57	55.98	37.20	49.67	78.77
usp	41.87	42.43	38.19	21.35	40.64	61.24	44.64	19.62
Al-spl	4.79	4.35	1.52	3.09	3.32	1.52	5.69	1.61
chr	0.04	0.06	0.00	0.00	0.06	0.05	0.00	0.00

ically (e.g., crater) under more than several seconds of beam exposureat the normal silicate analytical conditions. For this reason, analyses were performed at 15kV and 2.0 nA with a beam size of 5 μm for some analyses, and 2 μm for the traverses of zoned crystal discussed below. Amelia albite was used as the standard for Na, with the understanding that it was not the best possible choice due to having lower concentration of Na than the unknowns being analyzed. However, it was the highest-Na standard avail-able at the time. This potential standard problem prompted frequent checks of Na standardization using a number of Na-

bearing and Na-rich materials (including gem-quality, end-member sodalite from the Princess Mine, Bancroft, Ontario) as internal standards.

Hogarth and Griffin (1976) also noted significant analytical problems in microprobe analysis of lazurite due to the fragility of the material under the probe beam, and their study prompted careful examination of the issue of Na count loss. Loss of Na counts during quantitative

Table 4. Microprobe Analyses of Matrix Glass

Sample	401	408	599	605	612	615
SiO_2	60.70	59.39	57.99	59.36	61.61	57.2(
TiO_2	0.28	0.23	0.29	0.27	0.85	0.43
Al_2O_3	22.79	23.52	23.79	23.37	22.08	23.3:
FeO	1.58	1.64	1.61	1.61	1.94	1.68
MnO	0.05	0.07	0.07	0.06	0.09	0.06
MgO	0.03	0.02	0.26	0.10	0.03	0.03
CaO	0.26	0.45	0.40	0.37	0.54	0.39
BaO	0.09	0.16	0.00	0.08	0.17	0.00
Na_2O	8.10	9.66	11.97	9.91	7.75	10.4E
K_2O	6.91	5.10	3.62	5.21	3.63	6.68
S	0.00	0.02	0.04	0.00	0.01	0.06
Total	100.77	100.24	100.00	100.34	98.68	100.2E
CIPW Weight Norms						
or	40.79	30.11	21.37	30.75	19.83	39.4:
ab	38.31	42.99	42.79	41.26	65.51	24.0(
an	1.29	2.23	0.51	1.83	0.84	--
ne	16.34	20.95	31.65	23.04	--	31.8:
di	--	--	--	--	--	1.71
hy	--	--	--	--	1.63	--
ol	1.52	1.66	1.48	1.71	--	0.92
co	1.52	1.30		0.76	5.39	--
mt	0.34	0.36	0.35	0.35	0.42	--
ilm	0.53	0.44	0.55	0.51	1.62	0.82
qz	--	--	--	--	2.60	--
Norm An%	3.3	4.9	1.2	4.2	1.3	0.0
Atomic % Ca-Na-K						
Ca	2	4	3	3	6	3
Na	63	71	81	72	72	68
K	35	25	16	25	22	29

analysis in this present study proved not to be a problem down to spot sizes of about 2-5 μm at 2.0 nA beam current. Close observation with incident light showed no apparent beam damage on grain surfaces, and programmed tests were run to monitor changes in Na count

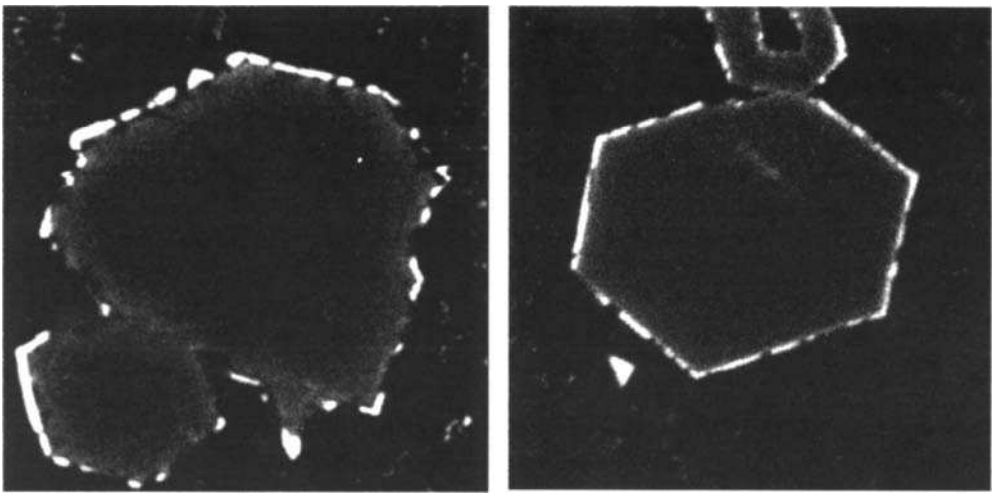

Figure 4. Electron microprobe X-ray intensity maps (analog concentration maps) for chlorine in euhedral haüyne phenocrysts from samples 408 (left) and 605 (right). The incomplete Cl-rich annuli surrounding each phenocryst rep-resent thin epitaxial rims of end-member sodalite. Field of view approximately 500 micrometers for both images.

rate over periods of up to 20 seconds (as typically used for analysis) on a spectrometer with a TAP crystal. The tests were run at 20 nA and spot size of 5 micrometers for Amelia albite (the current and beam diameter used for standardization) and 2.0 nA and 2 micrometers for nosean or haüyne (typical analytical conditions). Decrease in Na count rate over a 20 second counting time occurred with both standard and unknown, but neither was judged to be significant enough to affect analytical results strongly, particularly since percentage count rate loss patterns with time were very similar for both standard and unknown at respective beam conditions. The slopes of the regression lines in plots of Na count rate versus time indicate drops in cps/nA over 20 seconds of 9.8 for Amelia albite (at 20.0 nA) and 7.7 for nosean/haüyne (at 2.0 nA). By contrast, natural sodalite from Bancroft Ontario showed Na count-rate loss at 20.0 nA of over 20 cps/nA.

The Cameca SX-50 was also used to obtain two-dimensional X-ray-intensity maps of Na, K, Ca, S and Cl in several dozen nosean/haüyne crystals to document internal geometry of zoning patterns for comparison with quantitative traverses. These analog concentration maps (such as shown in Fig. 4) were made at a resolution of 512 x 512 pixels for square areas ranging from 80 to 750 micrometers across. Data was accumulated by beam-scanning or stage-scanning with a two-micrometer beam at 100 nA beam current.

Analytical Results for Nosean and Haüyne

About seven hundred spot analyses of nosean or haüyne in eight samples were obtained, including many analyses in traverses of zoned crystals from all samples. Acceptable analyses of multiple grains from each sample were averaged to produce the compositions reported in Table 5. The number of averaged analyses for each sample is reported in the table. Because of the presence of at least minor chemical zoning in nosean/haüyne in each sample, a statistical analysis would not produce a meaningful estimate of the quality of chemical analyses and thus was not performed, but as an example of compositional range, the spread of the whole dataset for sample 605 (in terms of cation concentrations of Ca, Na and K) was compared to

the mean composition. The range of this data is comparable to that found in the analyzed zoned crystals from all samples, and the mean composition appears to be representative of the sample as a whole.

Table 5. Average Microprobe Analyses of Haüynes and Noseans

Sample	401	408	599	600	605	611	612	615
SiO_2	31.79	34.63	33.76	33.90	32.96	33.78	33.88	32.77
Al_2O_3	27.93	29.02	27.90	28.78	27.90	28.25	28.53	27.41
FeO	0.39	0.84	0.50	0.30	0.37	0.47	0.60	0.42
MgO	0.11	0.13	0.02	0.01	0.08	0.03	0.09	0.11
CaO	8.22	4.22	5.20	4.16	8.07	4.42	7.07	8.10
Na_2O	16.14	17.50	17.82	19.61	16.65	17.99	15.83	15.51
K_2O	1.81	0.99	1.47	1.07	1.34	1.17	0.35	1.98
Cl	0.18	0.30	0.39	0.76	0.20	0.33	0.27	0.17
SO_2	13.12	11.35	12.74	10.97	13.22	11.95	13.27	13.27
S	0.00	1.44	0.00	0.00	0.00	0.61	0.00	0.00
O=S,Cl	0.04	0.79	0.09	0.17	0.05	0.38	0.06	0.04
TOTAL	99.65	99.63	99.71	99.39	100.74	98.63	99.83	99.69
Formulas normalized to 21 framework oxygens								
Si	5.895	6.037	6.078	5.998	6.007	6.042	6.022	6.042
Al	6.105	5.963	5.922	6.002	5.993	5.958	5.978	5.958
	12.000	12.000	12.000	12.000	12.000	12.000	12.000	12.000
Fe	0.121	0.246	0.150	0.089	0.112	0.140	0.179	0.129
Mg	0.030	0.034	0.006	0.002	0.022	0.008	0.023	0.030
Ca	2.377	1.146	1.459	1.149	2.293	1.232	1.961	2.329
Na	5.802	5.915	6.223	6.729	5.885	6.241	5.457	5.547
K	0.428	0.220	0.338	0.241	0.312	0.268	0.080	0.466
	8.758	7.561	8.176	8.211	8.623	7.889	7.700	8.501
Cl	0.057	0.088	0.118	0.227	0.063	0.100	0.082	0.053
SO_4	1.831	1.592	1.718	1.457	1.808	1.676	1.769	1.835
S	0.000	0.201	0.000	0.000	0.000	0.000	0.000	0.000
at% Ca	27.62	15.74	18.19	14.15	27.00	15.92	26.15	27.92
at% Na	67.41	81.24	77.59	82.88	69.32	80.62	72.78	66.49
at% K	4.97	3.02	4.21	2.97	3.68	3.46	1.07	5.59
Number of individual probe analyses averaged.								
	165	78	34	47	66	68	72	50

Formulas given in Table 5 have been recalculated using an Excel spread-sheet template that normalized cation contents to the 21 oxygens associated with the 3 Al_2O_3 + 6 SiO_2 (per formula unit) of the tectosilicate framework, as suggested by Deer et al. (1963), with modifications for estimation of S/SO_4 ratio as suggested by Hogarth and Griffin (1976). Sodalite-group minerals contain an aluminosilicate framework of approximately equal

numbers of AlO_4 and SiO_4 tetrahedra with each apical oxygen shared by two adjacent tetrahedra, generating clathrate-like 3-dimensional cubo-octahedral units with both six-membered and eight-membered rings constituting the faces. These 3-D units are joined by intersecting channels in three dimensions (Bragg, et al., 1965). The formula basis thus produces a hypothetically neutral framework with a composition of $Al_6Si_6O_{21}$ or a charged polyanionic unit $[Al_6Si_6O_{24}]^{6-}$. The larger cavities within the structure are occupied by Cl or SO_4 anions that are coordinated by Ca, Na or K: 3 Na_2O, 3 K_2O or 3 CaO, plus (in the sulfate members of the sodalite group) $Na_2(SO_4)$, $K_2(SO_4)$ or $Ca(SO_4)$. This results in these hypothetical ternary sulfate end-member formulas: $Na_6Al_6Si_6O_{24}{\cdot}Na_2SO_4$, $K_6Al_6Si_6O_{24}{\cdot}K_2SO_4$ and $Ca_3Al_6Si_6O_{24}{\cdot}CaSO_4$.

The nosean/haüyne/lazurite formula recalculation scheme suggested by Ho-garth and Griffin (1976) which uses a stoichiometric assumption and charge-balance to calculate SO_4^{2-} *versus* S^{2-} was adopted for this study. Their scheme arbitrarily normalizes numbers of cations based on an assignment of 12.000 Si + Al to the tetrahedral framework (Z-sites). Ideally, for sulfate end-members this should result in a positive charge of 48.000 to balance the 24.000 oxygens, so this number of oxygens are assigned proportionally to all cations (Si, Al, Na, Ca, K, Fe) exclusive of S^{6+}, with the charge for Cl subtracted. Remaining oxygen is assigned to S until ex-hausted. If S exceeds O, then the calculated formula results in some S^{2-} which Hogarth and Griffin suggested is replacing O^{2-} in anion sites. They reported S^{2-} in a number of analyzed metamorphic lazurites from Baffin Island and elsewhere, but it should be noted that lazurite, as a component of the semi-precious gemstone lapis lazuli, commonly coexists with abundant sulfide (either pyrite or pyrrhotite), so presence of reduced sulfur is not unexpected. None of the Tahitian rocks examined in this study contains any modal sulfide, and none of the nosean/haüyne formulas presented here shows any calculated S^{2-} in the formula recalculation.

Examination of the formulas in Table 5, however, shows that there are systematically less than 12 total framework cations per 21 oxygens (11.936 to 11.984 or 0.1 to 0.5% low) and that Si is systematically slightly in excess of the ideal value and Al is slightly deficient. There is thus a slight excess positive charge to the framework which may reflect that some of the sulfur in the analyses occurs as S^{2-} rather than SO_4^{2-}, well known in haüynes and lazurites, a discrimination which cannot immediately be determined from the microprobe analyses. As the effect is minor and because separating S and SO_4 would be arbitrary and highly speculative, the simplifying assump-tion has been made that all sulfur occurs as sulfate.

DISCUSSION OF ANALYTICAL RESULTS

Chemical Correlations

The primary variable cations in nosean and haüyne are Ca, Na and K, and a substantial range in proportions of these component is present within the group of samples analyzed. Nomenclature is loosely based on cation propor-tions: sodalite contains less than 5 atom% (Ca+K), nosean has up to 20% Ca replacing Na, and haüyne/lazurite has >20% Ca. Note that six of the Tahitian feldspathoids are thus classified as nosean, based on their Na/Ca ratios (408, 599, 600, 611, 612, 615) and two are barely across the boundary into the field of haüyne at >20 at% Ca (401 and 605). In fact, zoned phenocrysts from a number of samples (see Fig. 5) cross the nosean-haüyne boundary, so the cores of feldspathoid grains in most rocks are probably haüyne and the rims nosean, based on Figure 5. For convenience in

further discussion, these feldspathoids will all be referred to as "haüyne" for the rest of the paper.

There is a strong positive correlation of SO_4^{2-} with increasing Ca content and Cl^{1-} with Na content for all analyses, and converse negative correlations of Ca with Cl and Na with SO_4. These patterns are quite similar to the commonly observed correlations of Na with Cl^{1-}

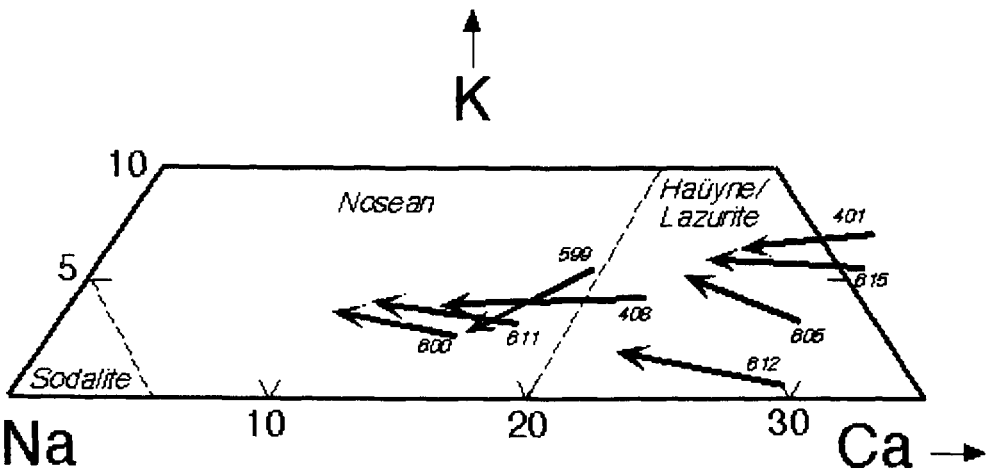

Figure 5. Na-rich portion of the Na-Ca-K ternary diagram for the sodalite-group minerals, showing suggested nomenclature boundaries. The bold arrows show extent and sense of zoning in nosean and haüyne discussed in this paper. In all cases, feldspathoid grains are more haüyne-rich in cores and more nosean-rich in rims.

and Ca with CO_3^{2-} in the scapolite solid solution, an Si-rich analog of nosean-haüyne solid solutions (Deer et al., 1963). In fact, given the common occurrence of anhydrite phenocrysts in strongly oxidized and S-rich silica-saturated felsic volcanics (dacites, rhyolites) at localities such as Mount Pinatubo and El Chichon, the presence of a $CaSO_4$ component in haüynes likely indicates that haüyne serves in part as a proxy mineral for anhydrite in strongly oxidized silica-undersaturated magmas.

Based on published crystal chemical studies of these feldspathoid minerals (e.g., Xu and Veblen 1995), this effect does not appear to be structurally controlled. Sulfate-rich nosean is well known and there is no reported struc-tural avoidance of Ca and Cl. The behavior of feldspathoid compositions reported here suggests that evolving ratios of Na to Ca and Cl to SO_4 in the magma controlled the feldspathoid compositions. This is further borne out by an observed pattern of fractionation and enrichment: strong fractionation of Ca from the melt at an early stage at virtually constant Cl to SO_4 ratio, followed by Cl enrichment as the melt became Ca-poor (see below).

Zoned Haüyne-Nosean Phenocrysts

Data from microprobe traverses of several haüyne-nosean phenocrysts in various samples are presented in Fig. 6. Inclusion-free euhedral phenocrysts typically show colorless cores and pronounced blue rims which originally inspired investigation of them for compositional zoning, as noted above. The variations of Ca, K, Cl and SO_4 across zoned grains are plotted;

data for Na indicate rather flat profiles, with perhaps slight enrichment toward rims. The color boundaries are not reflected by any compositional discontinuities and fall within the smoothly variable compositional regions near the rims.

Core-to-rim zoning is continuous in most of the analytical traverses. However, in sample 408 note a zoning pattern for Ca and K that suggests core and rim regions of the grain distinguished by zoning discontinuities. There is a relatively abrupt increase in both Ca and K across a boundary in the outer portion of the crystal at about 80 and 210 micrometers along the traverse. Ca, however, then continues a downward trend at both ends of traverse, whereas the K trend flattens out and K remains relatively constant until the last analyses at either crystal margin. Cl is flat (at about 0.2 wt%) across most of the grain (and unaffected by the suggested core-rim boundary) although there is a slight upward trend at the rim, especially on the left side of the diagram. SO_4 shows a very slight upward tendency within the core, but then is relatively constant in the rim until the last few micrometers near either rim, where a pronounced decrease in SO_4 roughly matches an increase in Cl. Data from these last analyses on either end of the traverse may be a bit suspect due to edge or secondary fluorescence effects, but the inverse trends of Cl and SO_4 suggest a late stage increase of Cl and decrease of sulfate in the melt. This is also strongly evidenced by the epitaxial rims of sodalite that are commonly observed (see Fig. 4).

PETROLOGIC INTERPRETATION

Implications of Haüyne Zoning

The zoning in the analyzed phenocrysts (Fig. 6) preserves a record of shifting melt composition, probably in a near-surface magma chamber immediately prior to eruption. The haüyne/nosean phenocrysts in all samples are generally significantly larger than any other crystalline phases now present (see Figs. 2 and 3), suggesting that they began crystallization in a magma chamber or conduit before the final eruptive event (unless their growth rate is far greater than that of the other silicates) and continued their growth through to the time of eruption or quenching.

The lack of a distinct chemical boundary between core and rim volumes in most of the zoned crystal suggests that the appearance or disappearance of one or more other phases on the liquidus does not cause a notable shift in haüyne zoning. The outward decrease in Ca in both core and rim regions could be due to crystallization of the haüyne itself (note below that there appears to be at least a slight fractionation of Ca from melt into haüyne), but is too pronounced to be due to haüyne removal alone. The presence of abundant clinopyroxene and titanite microphenocrysts suggests that these minerals co-precipitated with the more strongly zoned outer parts of the haüyne phenocrysts.

Implications for Magmatic Volatiles

The high sulfate content of haüyne phenocrysts (roughly 13 wt% SO_2) and the absence of reduced sulfur, either as sulfide microphenocrysts or as dissolved S in matrix glass, indicates that virtually all the sulfur in this magmatic system was present as sulfate. Sulfur speciation will clearly depend most strongly upon oxygen fugacity (e.g., Carroll and Rutherford, 1988; Carroll and Webster, 1994), and sulfur solubility will be highly depend upon melt composition, particularly on SiO_2 content. The presence of thin sodalite rims (with roughly 7 wt% Cl) on

haüynes indicates that Cl became important in magmatic crystallization at a late stage and overall behavior of Cl in the phonolite magmas should also be considered.

The oxygen fugacity range of the Tahitian phonolites (expressed as ΔFMQ) during haüyne crystallization may be estimated by assuming a reasonable T of crystallization (900 to 950

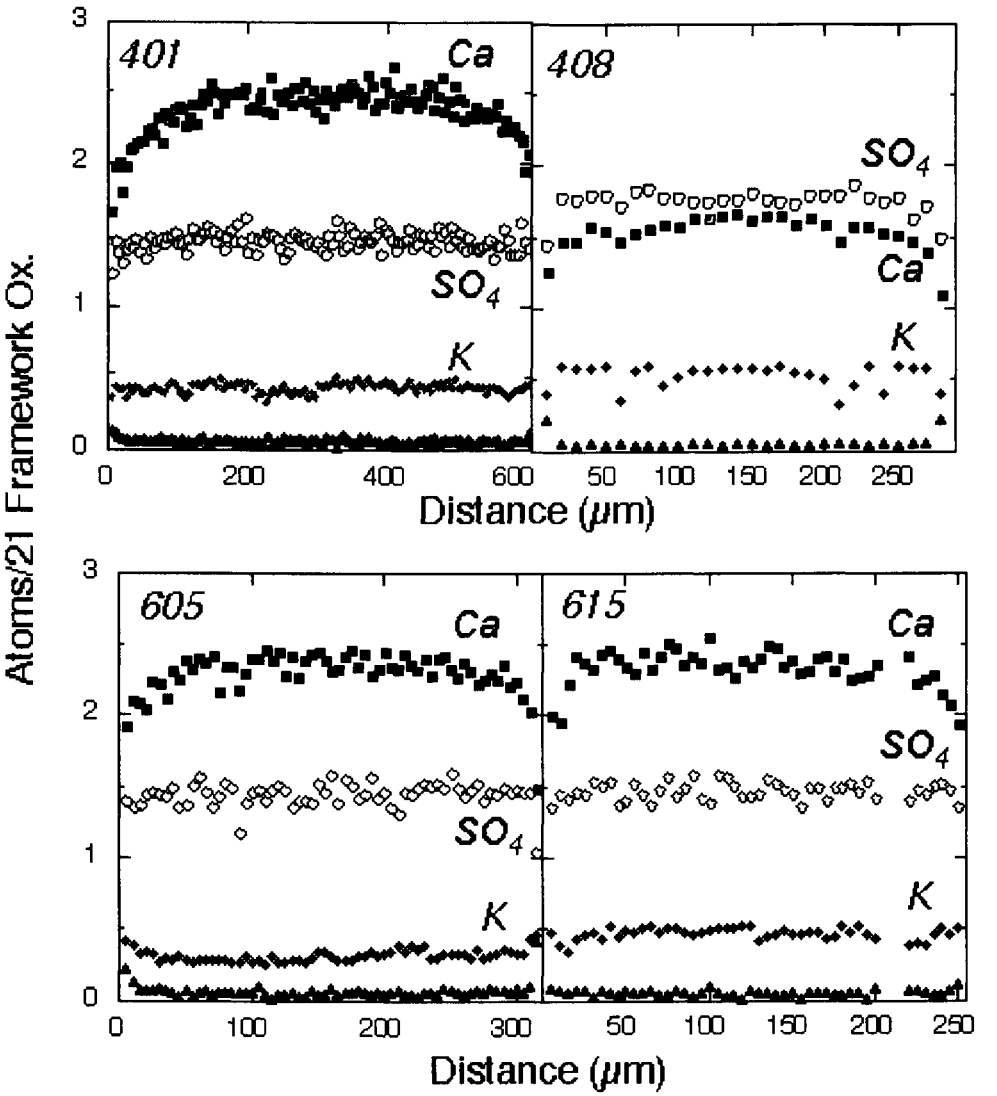

Figure 6. Microprobe traverses of zoned nosean or haüyne crystals in four samples, showing core-to-rim variations in Ca, K, SO4 and Cl (unlabeled, but at the bottom of each plot).

°C in this case). Using composition ranges of homogeneous Titanian magnetite microphenocrysts ($Mt_{53-80}Usp_{47-20}$) and the experimental data of Anderson and Lindsley (1988) on Fe-Ti spinel compositions as a function of T and fO_2 (Fig. 7), a range of ΔFMQ from +1.3 to +3.1 at 900 °C and +1.7 to +3.4 at 950 °C is indicated. Figure 7 also shows the location of the $H_2S - SO_2$ equilibrium (Burnham and Ohmoto, 1980, Fig. 4). At the range of oxygen

fugacity estimated for the Tahitian phonolites in Figure 7, most to all sulfur should be in the sulfate state.

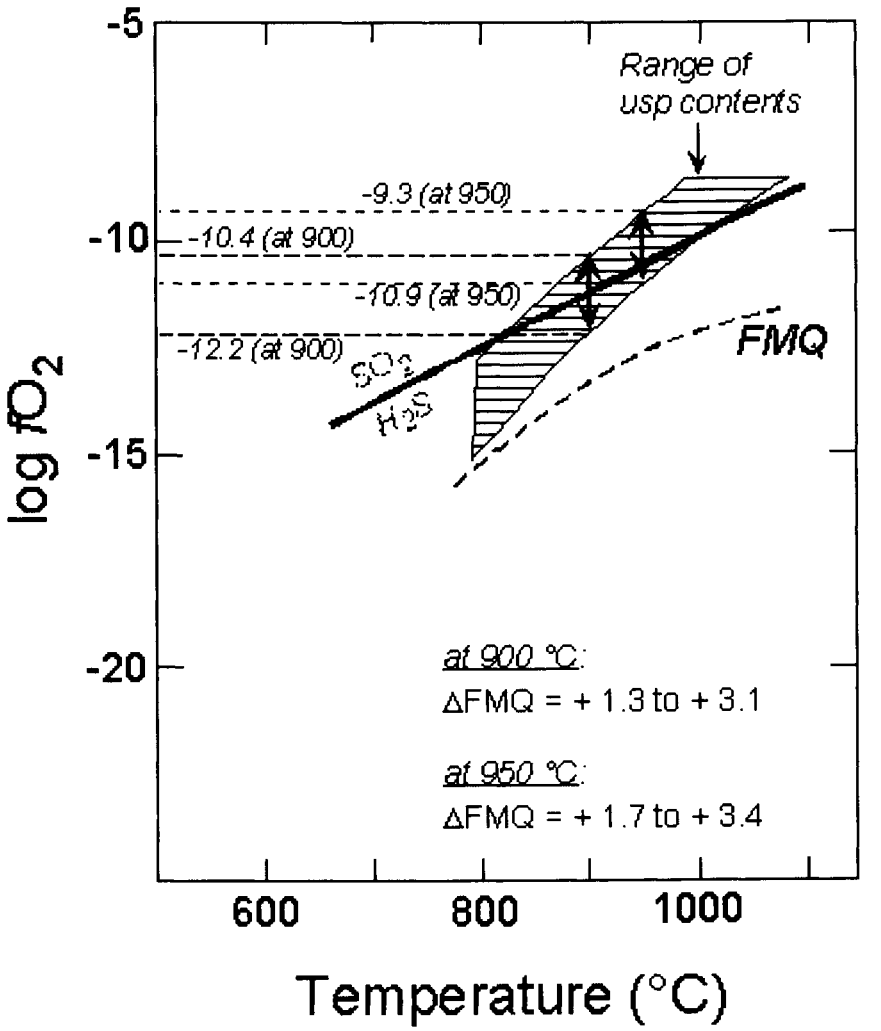

Figure 7. T – log fO_2 diagram for Tahitian phonolites. The T – fO_2 range for the phonolites is shown based on the range of usp contents of magnetites. This range, relative to FMQ, is shown at 900 °C and 950 °C. Also illustrated is the H_2S – SO_2 equilibrium of Burnham and Ohmoto (1980).

Another way of looking at sulfur speciation as a function of fO_2 was shown by Carroll and Webster (1994) in which they plotted the percentage of sulfate sulfur, relative to total sulfur, as a function of ?FMQ for various melt compositions. According to Carroll and Webster, for hydrous andesitic to dacitic melts complete oxidation of magmatic sulfur requires a ?FMQ anywhere from +3 to +4. Data from Nagashima and Katsura (1973) on unusually alkalic melts (molten sodium silicate) suggested a reduction in ?FMQ of 1 to 1.5 log units compared to those found in tholeiite to produce similarly high proportions of sulfate sulfur (>90%). This data for alkalic compositions may more adequately reflect the behavior of

sulfur in the Tahitian phonolites. Based on the sulfur speciation curve given by Carroll and Webster (1994, Fig. 3), at a ΔFMQ of +1.3 to +3.1 (at 900 °C), sulfate should constitute 60 to 100% of total sulfur for andesitic, tholeiitic and dacitic magmas, and probably > 90% at ΔFMQ above +1 for highly alkalic melts. At 950 °C, sulfur should be even more strongly oxidized, and should be virtually entirely sulfate, as in these phonolites.

Two questions raised by the high modal proportions of haüyne (10-20%) in these phonolites are: 1) Do they represent more sulfur than it is reasonable to assume could have crystallized isochemically from a sulfur-saturated magma; and 2) What is this source of the sulfur? 10 modal percent haüyne represents approximately 1.3 wt% SO_2 in the rock bulk composition, or approximately 6500 ppm S. Sulfate solubility is known to be greater than sulfide solubility in a range of magma compositions under oxidizing conditions (ΔFMQ of +1 to +4) (Carroll and Webster, 1994), but is still generally limited to several hundred to several thousand ppm, based on experimental studies. However, whole-rock magmatic sulfur contents of 0.1 to 1 wt% have been measured in recent eruptions of oxidized, anhydrite-bearing hydrous dacitic magmas at El Chichon and Mt. Pinatubo (Carroll and Webster, 1994).

Solubility data are sparse for strongly silica-undersaturated alkalic magmas, but given an inverse relationship between sulfur solubility and silica content (e.g., Wallace and Carmichael, 1992; Carroll and Webster, 1994) and a positive correlation of sulfur solubility and alkali content (Nagashima and Katsura, 1973) it is likely that SO_2 solubility in these phonolites should be at least as high as that reported at Mount Pinatubo, for example. In fact, in magmas like the Tahitian phonolites with large normative nepheline contents, as noted above, calcic haüyne could po-tentially be considered as a proxy mineral for the anhydrite that crystallizes in higher-silica magmas.

McBirney and Aoki (1968) and Duncan et al. (1994) suggested that the phonolites and trachytes at Tahiti represent an end-point of fractional crystallization of a mantle-derived alkali basaltic or even basanitic parent. Therefore it is reasonable that progressive fractionation of S into smaller proportions of progressively more oxidized magma could have produced the concentration of S in the phonolitic magmas (0.5 to 1 wt%) required to crystallize the large volumes of haüyne. Alternatively, any limited near-surface seawater contamination of the magmas could also be a potent source of sulfate, although addition of crustal or seawater sulfate appears not to be required. As far as the author is aware, there is no evidence reported of the existence of SO_2-rich gas emissions during the prehistoric eruption nor of any coexisting hypersaline melt.

Total chlorine contents of the Tahitian phonolites are much lower than those of sulfur, and based on modal estimates of the sodalite epitaxial rims on haüynes do not exceed a thousand parts per million. Cl is essentially undetectable in matrix glasses using the electron microprobe and relatively abundant apatite microphenocrysts also have low Cl (<0.3 wt% Cl). Total Cl is thus well within a normal range for alkalic and silica-undersaturated melts (Carroll and Webster, 1994), even considering potentially significant outgassing during eruption, and it does not seem necessary to call upon contamination to explain the late increase in Cl/S ratio.

Implications for Bulk Chemistry and Magma Evolution

Bulk rock compositions for five phonolites (408, 600, 605, 611 and 612) were determined by electron microprobe analysis of fused powders. Although less desirable than conventional bulk analysis techniques such as XRF, this technique was adopted because the very limited

sample size and historical nature of the samples precluded the more typical analytical procedures that require greater volumes of sample. Analyses were made by taking fractions of the rock hand samples, crushing them in a high-carbon steel mortar and milling the

Table 6. Microprobe Analyses of Phonolite Whole Rocks

Sample	**408**	**600**	**605**	**611**	**612**
SiO_2	48.83	56.95	49.98	60.69	50.29
TiO_2	2.70	0.40	2.95	0.66	2.97
Al_2O_3	19.38	22.54	18.40	20.10	18.60
FeO	7.17	2.42	7.28	2.68	7.30
MnO	0.26	0.12	0.21	0.13	0.23
MgO	2.02	0.38	1.98	0.47	1.86
CaO	6.38	1.65	6.36	1.46	6.27
Na_2O	8.37	8.61	7.80	7.87	7.94
K_2O	4.20	6.27	4.30	5.48	4.10
Total	99.31	99.34	99.26	99.54	99.56
CIPW Weight Norms					
or	24.5	36.5	25.4	32.1	24.2
ab	5.1	25.7	9.6	44.2	11.7
an	2.8	4.3	2.5	3.3	3.0
ne	35.1	25.0	30.5	11.8	30.0
di	24.0	3.3	24.5	3.4	23.8
ol	1.4	2.4	1.1	2.6	1.1
il	5.1	0.7	5.6	1.2	5.6
Norm. An%	36	14	21	7	20
Atomic % Ca-Na-K					
Ca	39	13	40	12	39
Na	46	59	44	60	45
K	15	28	16	28	15
IUGS Class.	phonolitic nephelinite	phonolite	phonolite	phonolite	tephritic phonolite

broken fragments to a fine powder in a Spex ball-mill with WC container and mullite ball. Similar materials of known composition were prepared and analyzed in the same way to test for contamination during crushing, which was found to be minimal. Although small, the pre-crushing sample volumes were judged to be adequate to be representative of rock bulk compositions, based on typical uniformly fine grain size of the rocks.

The powders were then fused without flux in sealed capsules at T in excess of 1000 °C, quenched and the resultant glass was mounted and analyzed by electron microprobe. All glasses were determined to be free of crystalline materials and homogeneous within normal precision limits of microprobe analysis. Analytical results are presented in Table 6. The

analyses are quite consistent with the XRF analyses for Tahitian phonolites and trachytes published by Duncan et al. (1994).

Phenocryst zoning data for Ca and K (see Fig. 6) indicate that the melt was being progressively depleted in these components as the haüyne phenocrysts grew. In the case of Ca, as noted above, it is possible but unlikely that haüyne removal alone from the melt could have caused the observed zoning; co-precipitation of clinopyroxene, titanite and apatite with haüyne are likely, and textural studies of the matrix with BSE confirm this. CaO data indicate positive fractionation of CaO from melt into haüyne in most cases. The behavior of Na_2O and K_2O are unequivocal in all cases, however: Na_2O is strongly fractionated into haüyne, whereas K_2O is fractionated into melt.

The hypothetical effects of removal of 1, 2, 5, 10, 15 and 20 volume percent haüyne from the bulk composition of sample 605 on compositions of residual liquids were calculated to show fractionation effects both as wt% oxide components and as wt% normative minerals. Calculation of CIPW weight norms for a modeled fractionated melt (Fig. 8) indicates decreased normative diopside content when Ca content of haüyne exceeds that of the melt. Results of model calculations for haüyne removal from phonolite, using compositions of haüyne and bulk rock from sample 605, indicate pronounced decreases in normative diopside and nepheline with progressive fractionation, and increases in orthoclase, albite, anorthite and olivine. Normative diopside decreases to zero at about 13% haüyne removal, producing an unusual algebraic normative consequence of the melt becoming peraluminous with the appearance of normative corundum, a rather unexpected effect in volcanic rocks with these compositions. A trend of increasing An% in normative plagioclase also reverses at

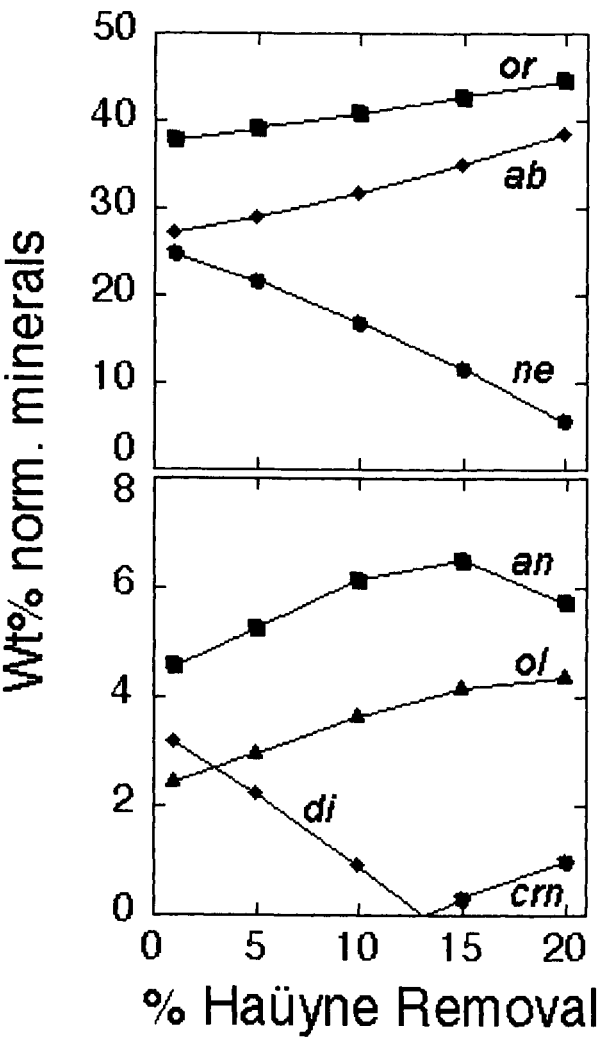

Figure 8. Results of fractionation modeling with progressive haüyne removal for sample 605.

this point at a maximum An% of about 16.5, decreasing as the normative anorthite decreases due to Ca decrease.

The CIPW norm therefore has the surprising characteristic of both norm-ative olivine and normative corundum. One possible *modal* mineralogic consequence of this might be the appearance of biotite or an aluminous, alkalic Ti-rich amphibole (kaersutite) in sufficiently hydrous melts, as observed in numerous Tahitian higher-P plutonic rocks (McBirney and Aoki, 1968).

One important implication of the fractionation models is that the decrease in normative nepheline produced by haüyne removal may produce a shift in magma chemistry from phonolite to trachyte, albeit feldspathoidal trachyte. One of the poorly explained peculiarities of the magmatic trends at Tahiti is the branching of the alkali basalt evolutionary parentage into trachyte and phonolite trends (McBirney and Aoki, 1968) in contrast to an expected simpler fractionation trend toward phonolite. The results of this modeling suggest that crystallization and removal of haüyne may sufficiently deplete Na_2O and increase SiO_2 in pre-eruptive phonolite magmas to produce a secondary trend toward trachyte.

This effect can be effectively illustrated in a diagram that shows the A-rich corner of the QAPF diamond from the IUGS volcanic-rock classification. Figure 9 shows the results of fractionation modeling for samples 408, 600, 611 and 612, as well as the analyzed groundmass

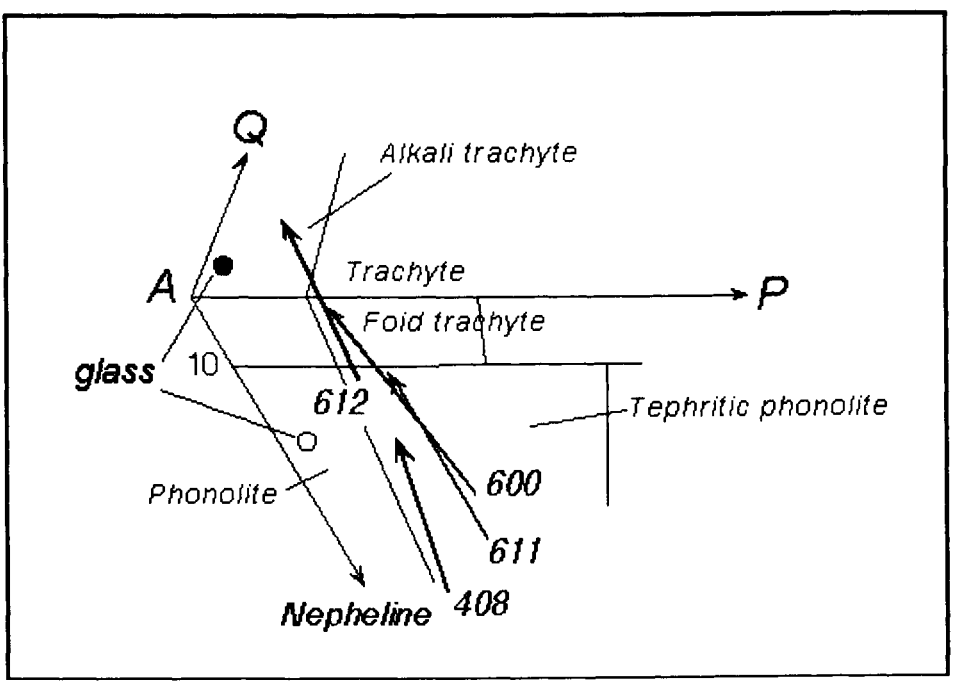

Figure 9. Alkali-rich corner of the QAPF quadrilateral from the IUGS Volcanic Rock Classification (LeMaitre, 1989). The results of modeled fractionation of four magma compositions are shown in terms of normative mineralogy. The open circle represents the composition of matrix glass in 611 and the filled circle that in 612. Note in particular the increase in degree of silica saturation, potentially even producing a silica-saturated trachytic composition (e.g., with 20% haüyne removal from sample 612).

glass compositions from samples 611 and 612. The beginning point of each arrow is the analyzed bulk composition of the rock and the arrow follows the calculated extent of

fractionation produced by haüyne removal. The shift of analyzed matrix glass compositions from the model trends toward the A(lkali) corner is of course due to the fractionation of one or more K-poor microphenocryst minerals, certainly including clinopyroxene, from the natural liquids. In any event, the trend toward silica enrichment upon haüyne removal is clear.

SUMMARY

Analyses of nosean or haüyne phenocrysts in eight Tahitian phonolites indicate that these minerals are strongly zoned in Ca and K, and weakly zoned in SO_4 and Cl. The Ca zoning in particular has a strong effect on evolution of residual melt compositions in magmas which are undergoing significant degrees of haüyne crystallization (>10%). Crystallization and removal of a silica-poor phenocryst phase like haüyne/nosean could potentially result in a silica-enrichment magmatic trend that could drive the evolution of phonolitic into trachytic liquids.

The zoning in Cl, and particularly the late jump from crystallization of a sulfate-rich feldspathoid to epitaxial rims of Cl-rich sodalite, combined with absence of sulfide minerals, illuminates several very important aspects of the chemistry of haüyne or nosean phonolite magmas. 1) The formation of sulfate-rich feldpathoids as primary phenocryst phases requires strong oxidation of the magma and the resultant shift in sulfur oxidation state from sulfide to dominantly to entirely sulfate. 2) Substantial $CaSO_4$ content of haüyne may indicate that this mineral serves as a proxy in strongly silica-undersaturated and strongly oxidized alkalic magmas for the an-hydrite that occurs in more silica-rich magmas. 3) End-stage depletion of magmatic sulfate by haüyne/nosean crystallization resulted in ultimate for-mation of minor volumes of sodalite rims due to dramatic increase in Cl/S ratio, reflecting the presence of sufficient Cl in the final melt and maintenance of nepheline-normative character of the magma. Sufficient Cl to crystallize sodalite rims on haüyne probably results from this simple increase in Cl/S, but may also indicate limited near-surface contamination of the magma by seawater, an event that could also have produced the strong oxidation of the magma.

ACKNOWLEDGEMENTS

The author thanks Dr. Carl Francis, Curator of Minerals in the Harvard Geological Museum, for access to the Daly samples in the Harvard collections. The author is grateful to Eric Essene and Mike Garcia for reviews of an earlier version of this paper, and especially to Jim Beard for a quick and helpful review of this current version, and to Bob Bodnar and Benedetto DeVivo both for organizing the Melt Inclusion Conference in Sorrento-Seiano in September of 2002, and also for coordinating and editing this Elsevier volume.

REFERENCES

Anderson, D.J. and Lindsley, D.H. (1988) Internally consistent solution models for Fe-Mg-Mn-Ti oxides. American Mineralogist, **73**, 714-726.

Bragg, W.L., Claringbull, G. F. and Taylor, W.H. (1965) Crystal Structure of Minerals. Ithaca, Cornell University Press. 408 p.

Burnham, C.W. and Ohmoto, H. (1980) Late-stage processes of felsic mag-matism. Mining Geology Special Issue (Japan), 1-11.

Carroll, M.R. and Rutherford, M.J. (1987) The stability of igneous anhydrite: experimental results and implications for sulfur behavior in the 1982 El Chichon trachyandesite and other evolved magmas. Journal of Petrology, **28**, 781-801.

Carroll, M.R. and Rutherford, M.J. (1988) Sulfur speciation in hydrous ex-perimental glasses of varying oxidation state: results from measured wavelength shifts of sulfur X-rays. American Mineralogist, **73**, 845-849.

Carroll, M.R. and Webster, J.D. (1994) Solubilities of sulfur, noble gases, nitrogen, chlorine, and fluorine in magmas. In: M.R. Carroll and J.R. Holloway, eds. Volatiles in Magmas. Reviews in Mineralogy, **30**, 231-279.

Conticelli, S., Francalanci, L., Manetti, P., Cioni, R. and Sbrana, A. (1997) Petrology and geochemistry of the ultrapotassic rocks from the Sabatini volcanic district, central Italy; the role of evolutionary processes in the genesis of variably enriched alkaline magmas. Journal of Volcanology and Geothermal Research, **75**, 107-136.

Deer, W.A., Howie, R.A. and Zussman, J. (1963) Rock-Forming Minerals. Vol. 4 - Framework Silicates. London, Longmans. 435 p.

Duncan, R. A., Fisk, M. R., White, W. M. and Nielsen, R. L. (1994) Tahiti: geochemical evolution of a French Polynesian volcano. Journal of Geophysical Research, B, Solid Earth and Planets, **99**, 24,341-24,357.

Feininger, T. and Goodacre, A.K. (1995) The eight classical Monteregian Hills at depth and the mechanism of their intrusion. Canadian Journal of Earth Sciences, **32**, 1350-1364.

Hassan, I. and Buseck, P.R. (1989a) Cluster ordering and antiphase domain boundaries in haüyne. Canadian Mineralogist, **27**, 173-180.

Hassan, I. and Buseck, P.R. (1989b) Incommensurate-modulated structure of nosean, a sodalite-group mineral. American Mineralogist, **74**, 394-410.

Hassan, I. and Grundy, H.D. (1984) The crystal structure of sodalite-group minerals. Acta Crystallographica, **B40**, 6-13.

Hassan, I. and Grundy, H.D. (1989) The structure of nosean, ideally $Na_8(Al_6Si_6O_{24})SO_4 \cdot H_2O$. Canadian Mineralogist, **27**, 165-172.

Hassan, I. and Grundy, H.D. (1991) The crystal structure of haüyne at 293 and 153K. Canadian Mineralogist, **29**, 123-130.

Hogarth, D.D. and Griffin, W.L. (1976) New data on lazurite. Lithos, **9**, 39-54.

Johanssen, A. (1939) A Descriptive Petrography of the Igneous Rocks. Vol. 1: Introduction, Textures, Classifications and Glossary. Chicago, University of Chicago Press. 318 p.

LeMaitre, R.W., Bateman, P., Dudek, A., Keller, J., Lameyre, J., Le Bas, M.J., Sabine, P.A., Schmid, R., Sørensen, H., Streckeisen, A., Woolley, A.R. and Zanettin, B., eds. (1989) A classification of igneous rocks and glossary of terms; Recommendations of the International Union of Geological Sciences Subcommission on the Systematics of Igneous Rocks. Blackwell Science Publications, Oxford, U. K. 193 pp.

McBirney, A.R. and Aoki, K. (1968) Petrology of the island of Tahiti. In, Coats, R.R., Hay, R.L., and Anderson, C.A., eds., Studies in Volcanology: A Memoir in Honor of Howel Williams. Geological Society of America Memoir 116, 523-556.

Mandarino, J.A. and Anderson, V. (1989) Monteregian Treasures - The Minerals of Mont Saint-Hilaire, Québec, Cambridge University Press, New York. 302 p.

Montel, J-M. and Gourgaud, A. (1992) Petrogenese des trachy-andesites a haüyne du massif de l'Aiguiller (Monts Doré; Massif Central Francais); hypothèse de mélange magmatique entre trachy-phonolite et hawaiite. Comptes Rendus de l'Academie des Sciences, Série 2, Mécanique, Physique, Chimie, Sciences de l'Univers, Sciences de la Terre, **314**, 791-797.

Nagashima, S. and Katsura, T. (1973) The solubility of sulfur in Na_2O-SiO_2 melts under various oxygen partial pressures at 1200, 1250, and 1300 °C. Bulletin of the Chemical Society of Japan, **46**, 3099-3103.

Quinn, Alonzo (1935) A petrographic use of fluorescence. American Mine-ralogist, **20**, 466-480.

Renzulli, A., Upton, B. G. J., Boyce, A. and Ellam, R. M. (1998) Petrology of quartz syenite and haüyne syenite clasts from the Pitigliano Formation, Latera Caldera, Vulsini District, Central Italy. European Journal of Mineralogy, **10**, 333-354.

Sharygin, V. V. (1993) Melt evolution during crystallization of haüyne phonolites of East Eifel (W. Germany). Russian Geology and Geophysics, **34**, 84-95.

Taylor, D. (1967) The sodalite group of minerals. Contributions to Miner-alogy and Petrology, **16**, 172-188.

Wallace, Paul and Carmichael, I.S.E. (1992) Sulfur in basaltic magmas. Geochimica et Cosmochimica Acta, **56**, 1863-1874.

Xu, Huifang and Veblen, D. R. (1995) Transmission electron microscopy study of optically anisotropic and isotropic haüyne. American Mineral-ogist, **80**, 87-93.

Magma ascent rates and depths of crustal magma reservoirs beneath the Aeolian volcanic Arc (Italy): inferences from fluid and melt inclusions in xenoliths

Maria Luce Frezzotti[1], Angelo Peccerillo[2], Rossana Bonelli[1]

[1] Dipartimento di Scienze della Terra, Università degli Studi di Siena, Via Laterina 8, I-53100 Siena, Italy , e-mail: frezzottiml@unisi.it
[2] Dipartimento di Scienze della Terra, Università degli Studi di Perugia, P.zza Università 1, I-06100 Perugia, Italy

ABSTRACT

Quartz-rich xenoliths in lavas and pyroclasts (basalts to rhyolites) from Alicudi, Salina, Filicudi Vulcano and Stromboli contain abundant fluid and melt inclusions, which bear striking similarities on a regional scale. Two main generations of CO_2-rich ($\pm$ H_2O or N_2) fluid inclusions are present in quartz grains: early (Type I) inclusions related to partial melting of the host xenoliths, and Type II inclusions trapped during xenolith ascent in the host magma. Homogenisation temperatures of fluid inclusions show a similar bimodal distribution, corresponding to two distinct density intervals: 0.9-0.5 (Type I) and 0.4-0.1 g/cm^3 (Type II). Early Type I fluid inclusions indicate trapping pressures between 0.6 and 0.3 GPa, which are representative for the levels of partial melting of crustal rocks and xenolith formation. Late Type II fluid inclusions show considerably lower trapping pressures, between 0.17 and 0.05 GPa, indicative for shallow magma rest and accumulation during ascent to the surface.

The present study indicates ponding of mantle-derived magmas at lower crustal depths and at shallow levels. Deep crustal reservoirs (25–12 km) are present beneath the whole archipelago and indicate that substantial melting processes occur at middle to lower-crustal conditions. The main stages of anatexis, occur at these depths approximating the Moho, and may have been induced by a regional heating during underplating and intrusion of the continental crust by mantle-derived basaltic magmas. The shallow magma chambers (6–4 km) are fed by the deep-sited crustal reservoirs and are the site of evolutionary processes such as fractional crystallisation and mixing.

INTRODUCTION

In the zones of active volcanism, understanding the role of shallow level evolutionary processes in magmas has important bearing on the way the various volcanoes work,

which is a necessary preliminary requirement to assess volcanic risk. The understanding of magma ascent rate, however, requires the determination of the residence depths of magmas (i.e. location magmatic chambers), based on reliable geo-barometers. Fluid inclusion studies in magmatic minerals and/or in xenoliths entrained in volcanic rocks represent a valuable technique to reach this objective (e.g. Roedder, 1965; Clocchiatti et al., 1994; Anderson and Neumann, 2001). Many studies have shown that fluid inclusions may be abundant in xenoliths, reflecting composition, pressure and temperature conditions of the fluid phases at the different stages during xenoliths ascent in host lavas (see Andersen and Neumann, 2001).

The Aeolian arc (southern Tyrrenian Sea) comprises seven volcanic Islands, some of which are active volcanoes (Vulcano, Stromboli, and, possibly, Lipari and Panarea). Volcanic rocks range from mafic to acid and have calc-alkaline (CA), high-K calc-alkaline (HKCA), shoshonitic (SHO) and potassic alkaline (KS) compositions (see De Astis et al. 1997, 2000). Magmas show variable enrichments in incompatible trace elements (ITE) and isotopic signatures; these latter range from typical mantle ratios (in some primitive CA rocks), to values that are intermediate between crust and mantle.

In spite of the many volcanological and geochemical studies carried out in the last decades, there is no or little information on the internal structure of Aeolian volcanoes and on the way the volcanic plumbing systems work. Such a goal is of paramount interest for gaining a much-needed insight into this active volcanic arc.

In the present study, we report on inclusions (fluid and melt) in quartz-xenoliths from Alicudi, Filicudi and Vulcano, and further compile data existing on fluid inclusions in xenoliths from Salina and Stromboli (Vaggelli et al., 2001; Zanon, 2000, 2002). New and literature data are discussed to trace the evolution of the magma plumbing system beneath the Aeolian Islands through time, and tentatively to relate it with the volcanic and petrologic evolution.

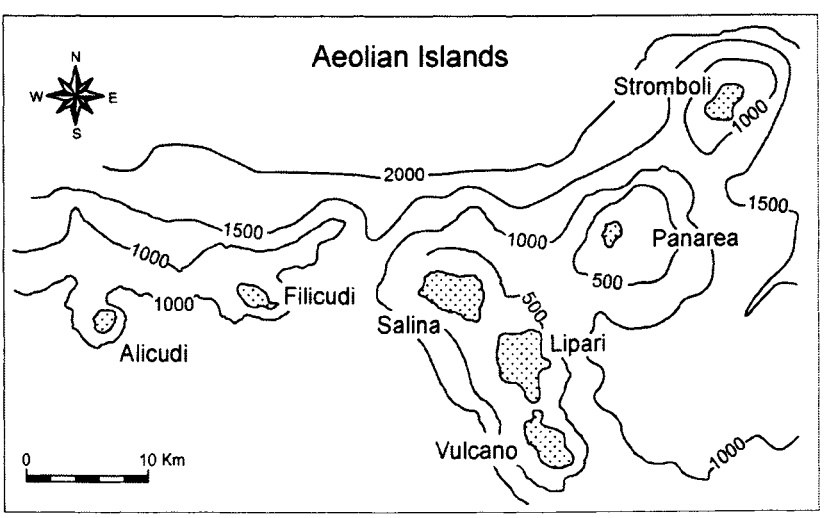

Fig. 1 Schematic map of the Aeolian Islands in the southern Tyrrenian sea.

GEOLOGICAL AND VOLCANOLOGICAL SETTING

The Aeolian volcanic arc is formed by seven islands (Alicudi, Filicudi, Salina, Lipari, Vulcano, Panarea and Stromboli; Fig. 1) and nine seamounts located about 25 km north of the Sicily coast (Beccaluva et al., 1985; Selli, 1985; Wezel, 1985). The volcanism initiated about 1 Million years ago, generated by subduction of the Ionian plate under the Calabro-Peloritani continental margin (Barberi et al., 1973, 1974; Ellam et al., 1988). The volcanic arc lies on the 18- to 25-km-thick Calabro-Peloritano basement (Calcagnile and Panza, 1979; Finetti, 1982; Beccaluva et al., 1985; Falsaperla et al., 1999) consisting of Hercynian and pre-Hercynian metamorphic and granitic rocks overlain by Mesozoic and Cenozoic sediments (e.g. Rottura et al., 1991). The oldest rocks occur in Sisifo, Eolo, Enarete western seamounts (1 – 0.8 Ma), Filicudi (> 1Ma, Santo et al., 1995) and Salina (430 - 32 ka). The younger volcanic activity has been concentrated at Alicudi (90 – 25 ka), Lipari (<150 ka), Vulcano (<120 ka), Panarea (60 ka) and Stromboli (< 90 ka) (Gillot, 1987; Calanchi et al., 2002). Stromboli and Vulcano are still active; historic eruptions were recorded at Lipari and vapour explosions recently occurred at Panarea.

A clear relationship exists between regional tectonics and volcanism. Alicudi, Filicudi and the oldest part of Salina define the western sector of the arc, where volcanism is extinct. Younger Salina, Vulcano and Lipari, which lie on the NW-SE Tindari-Letoianni dextral transcurrent fault, define the central part of the arc and divide the western islands from the eastern Panarea and Stromboli.

The western islands of Alicudi, Filicudi, and Salina are constituted mainly by CA magmas; basic to intermediate rocks largely dominate over more evolved compositions. Vulcano and Lipari are by far the most complex volcanoes with large calderas, abundant silicic eruptions and variable petrological affinity of the magmas (CA to SHO and KS). In the eastern arc, Stromboli shows a wide range of magma types (from CA to KS) but rocks are only basic to intermediate in composition. Panarea has geochemical and isotopic characteristics intermediate between Lipari and Stromboli.

Time-related evolution of the various islands shows that, in several volcanoes (e.g. Vulcano, Lipari, Salina, Filicudi and Alicudi), the lowest exposed products are mafic in composition (e.g., Peccerillo and Wu, 1992; De Astis et al., 1997; Crisci et al., 1990), whereas intermediate and acid volcanics dominate the younger activity.

CRUSTAL XENOLITHS IN AEOLIAN VOLCANIC ROCKS

A common character to most Aeolian-island lava and pyroclastic flows is the ubiquitous presence of crustal xenoliths. These are a very common feature and reveal an interaction of the crustal basement with the rising mafic magmas. The crustal xenoliths consist of four main types: 1) quartz aggregates (Fig. 2A), 2) garnet-cordierite and garnet-sillimanite gneisses, 3) vesuvianite- grossular-bearing skarns, and 4) metapelites, (Honnorez and Keller, 1968; Peccerillo and Wu, 1992).

The presence among crustal xenoliths of quartz-rich rocks is a peculiar feature of volcanoes of all the Aeolian Islands and of other volcanoes of the southern Tyrrenian sea (e.g. Etna; Michaud, 1995). Detailed geochemical studies of quartz-rich xenoliths present in the lavas of the island of Alicudi (Peccerillo and Wu, 1992; Peccerillo et al., 1993) found variable contents for both major and trace elements, except for Rb, Cs and K, which were invariably present at very low concentration levels. Such compositions were

interpreted to reveal that quartz xenoliths are residual lithologies of gneisses and or other quartz-rich metamorphic rocks that have undergone partial melting with extraction of various amounts of high-silica melts.

All the study samples consist of quartz-rich xenoliths, since these contain abundant CO_2-rich fluid and melt inclusions. Xenoliths have been collected in lavas and pyroclastic units of well-known chemical composition and age at Alicudi, Filicudi and Vulcano (Table I). Quartz-rich xenoliths generally have angular shapes, variable sizes (a few cm to a few dm) and a typical white colour, which makes them easily distinguished in outcrop (Fig. 2a). Contacts with host lavas are sharp but locally they appear to disaggregate within the host melt. Rocks consist of quartz (> 98 % modal) with subordinate amounts of zircon, apatite and sphene. Isolated K-feldspar and/or pyroxene and plagioclase grains are at times observed.

Textures are granular and most quartz grains show rounded or spongy contours, and are always surrounded by glass (Fig. 2b); μm-sized crystobalite external rims have been identified in some quartz grains by Raman spectroscopy. Additionally, quartz grains may form polygonal aggregates intersecting at 120°.

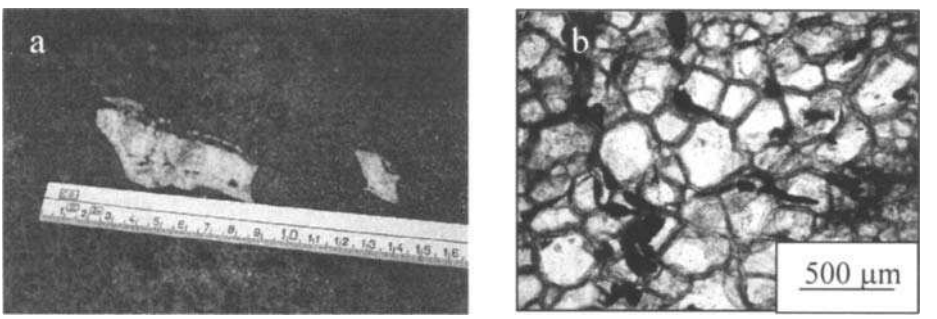

Fig. 2. a) Studied quartz xenoliths in basaltic lavas from Vulcano. b) Microphotograph of a quartz xenolith showing the presence of quartz rounded grains rimmed by glass (sample from Palaeovolcano lavas, Vulcano island).

Quartz xenoliths contain significant quantities of internal glass present both as intergranular veins (50 - 200 μm across) and as short trails or clusters of silicate-melt inclusions within single grains. The veinlets are clearly connected to each other (Fig. 2B, 3a), suggesting that the melt may have migrated along grain boundaries and microfractures. Glass from the host lava is distinguished petrographically from internal clear glass on the base of the brown - yellowish colour of the former.

Extensive evidence for melting, coupled with textural characteristics of the quartz grains allow us to exclude the possibility that the xenoliths may represent fragments of undisturbed metamorphic quartzites sampled by the ascending magmas. On the contrary, these features point to restitic rocks originated by different degrees of partial melting of an original fertile metamorphic rock such as a quartz-feldspatic gneiss and/or a mica-schist.

ANALYTICAL TECHNIQUES

Double polished, 100- to 200-μm-thick sections were prepared for microthermometric and Raman microspectroscopic investigations. Microthermometry was performed at the Università di Siena with a Linkam® THM 600 heating/freezing stage (Werre et al., 1979). Calibration was carried out by means of SYNFLINC® standard synthetic fluid inclusions, checking the temperature at the CO_2 and H_2O triple points (-56.6 °C and 0.1 °C respectively), and the CO_2 critical homogenisation temperature at 31.1 °C. Instrumental error at the reference standard points was ± 0.1 °C. For all the runs, the heating rate was 0.2°C/min. Isochores for fluid inclusions were calculated using the Mac Flincor® software package (Brown, 1989), using the equation of state provided by Holloway (1981). Density of CO_2 was derived from Angus et al. (1976).

Raman analyses were performed at the Università di Siena with a confocal Labram multichannel spectrometer of the Jobin-Yvon LTD. The excitation line at 514.5 nm was produced by a Ar^+ laser. The Raman intensity was collected with a Peltier-cooled CCD detector. The beam was focused to a spot size of about 1-2 μm using an Olympus 100x lens. The scattered light was analysed using a Notch holographic filter with a spectral resolution of 1.5 cm^{-1} and a grating of 1800 grooves/mm.

Table 1. Summary of fluid inclusions data

QUARTZ XENOLITHS					FLUID INCLUSIONS				
Island	Samples n.	Volcanic cycle	HOST LAVAS		Composition	Type I		Type II	
			Composition	Age (ka)		Th_L (°C)	d (g/cm^3)	Th_V (°C)	d (g/cm^3)
ALICUDI	6	1st cycle	basalts	90-60	$CO_2 \pm N_2 \pm CO$	-0.5 - 31	0.93 - 0.61	-6 - 31	0.08 - 0.42
ALICUDI	7	2nd cycle	basaltic andesites	55	$CO_2 \pm N_2 \pm CO$	-2.5 - 31	0.93 - 0.52	0 - 31	0.10 - 0.42
ALICUDI	6	3rd cycle	andesites	28	CO_2	-	-	6 - 18	0.12 - 0.18
FILICUDI	2	1st cycle	basalts	390	$CO_2 \pm H_2O$	18.1 - 31	0.79 - 0.52	24.2 - 31	0.23 - 0.42
FILICUDI	2	3rd cycle	basalts	390-230	$CO_2 \pm H_2O$	22.5 - 31	0.75 - 0.52	12 - 31	0.14 - 0.42
VULCANO	7	1st cycle	basaltic andesites	120	CO_2	18.1 - 31	0.79 - 0.52	18 - 30.9	0.18 - 0.40
VULCANO	6	2nd cycle	SHO basalts	24	CO_2	11.6 - 30.2	0.85 - 0.59	20.8 - 31.1	0.20 - 0.42
VULCANO	3	3rd cycle	rhyolites	24-15	CO_2	23.3 - 30.7	0.74 - 0.55	9.3 - 30.2	0.13 - 0.35
VULCANO	8	6th cycle	shoshonites	183 b.C.-1550 A.D.	CO_2	6.3 - 30.8	0.84 - 0.54	17 - 30.6	0.18 - 0.38

n.= total number of studied samples; ThL = Temperature of homogenisation to the liquid phase; ThV = temperature of homogenisation to the vapour phase; d = density.

FLUID- AND MELT-INCLUSION OCCURRENCE

In order to be able to relate composition and density data extracted from the fluid inclusions to the ascent history of quartz xenolith and host lavas, it is necessary to establish detailed inclusion trapping histories, and to characterise the processes which may have modified the composition and the physical properties of the fluid after trapping.

Two main generations of fluid inclusions (with and without associated melt inclusions) that can be related to temporally distinct trapping events are recognised in the study xenoliths from all the islands. The oldest fluid inclusion population (Type I) consists of early (i e. primary) $CO_2 \pm N_2 \pm H_2O$ inclusions often associated with silicate melt inclusions of high-silica composition, while younger fluid inclusions (Type II) are clearly secondary in origin, contain pure CO_2, and are never found associated to glass. For this reason, we subdivide the microstructural description below into distinct sections dealing with early and late features, respectively. The fluid inclusion data are summarised in Table 1.

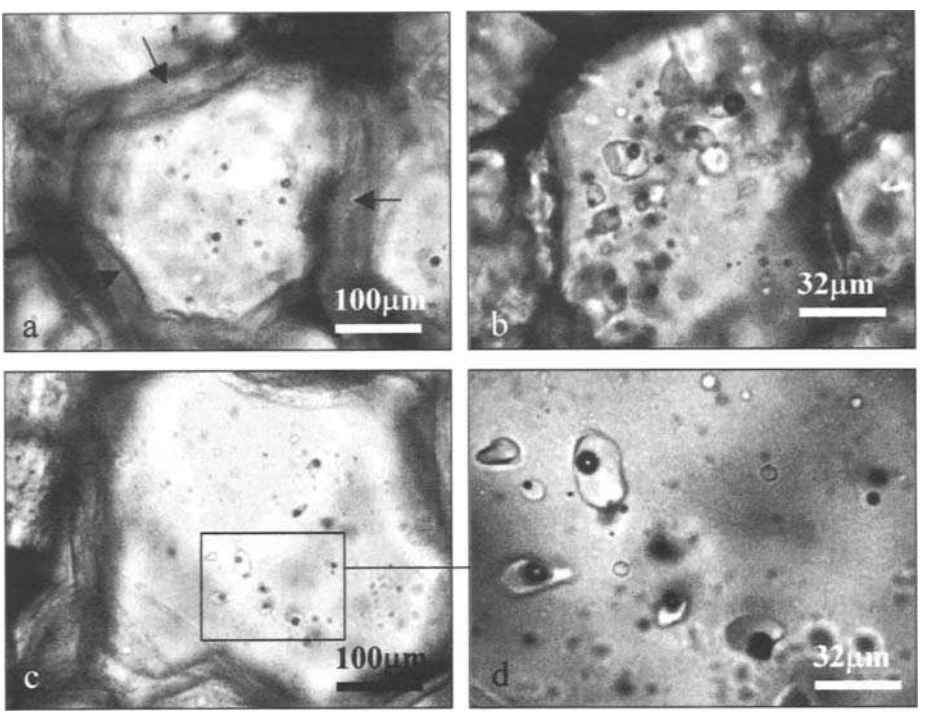

Fig.3 a) Quartz grain subtextures in a quartz xenolith from Vulcanello (Vulcano). Quartz grains are surrounded by rims of rhyolitic glass (arrows) and contain abundant fluid and melt inclusions. b) Cluster of texturally early Type I melt inclusions in a quartz grain from Alicudi quartz xenolith. c-d) silicic melt in the relic quartz crystals. Silicate melt inclusions of high-k, high-silica composition in a grain from Palaeovolcano quartz xenolith (Vulcano). Inclusions consist of glass, CO_2 and mixed CO_2 + glass inclusions, and indicate trapping of a CO_2 oversaturated silicate melt.

Early Type I melt inclusions

Silicate-melt inclusions are present only within quartz grains surrounded by glass (Fig. 3a) in clusters and/or as short trails originating at grain boundaries (i.e. secondary trapping; Fig. 3b and c). They have rounded morphologies often reaching negative crystal shapes and usually contain colourless glass and a bubble. Although true daughter minerals are absent, single crystals of wollastonite, pyroxenes, quartz, feldspars, sulphides or oxides may be present as incidentally trapped phases in different inclusions.

In some inclusions, a small shrinkage bubble is observed, but often large bubbles are present that contain immiscible CO_2, as low density (i.e. detected by Raman spectroscopy) or as high density fluids (Fig. 3d). In this last case, the presence of abundant fluid inclusions indicate that the melt trapped in Type I inclusions was volatile-rich and CO_2 oversaturated at some stage. The glass in silicate-melt inclusions is homogeneous and correspond to high-K_2O high-silica compositions (SiO_2 > 73 wt %; K_2O= 3-6.3 wt %) with low MgO (< 1 wt%) and alumina (Al_2O_3 = 10-12 wt%) contents, similar to interstitial glass veins lining quartz grains (Frezzotti et al., in press).

Early Type I fluid inclusions

Texturally early Type I carbonic inclusions occur isolated or in small clusters within most quartz grains (Fig. 4a). A few inclusions are distributed along short intragranular trails, both in the internal part of the grains and at grain boundaries. Inclusion size is in the range 3-10 μm and their shape is generally regular, with subordinate negative-crystal forms. At room temperature, Type I inclusions are single-phase (L) or may contain a vapour bubble (L+V) with a $df \leq 0.5$ ($df = V_{vapour}/(V_{liquid}+V_{vapour})$). No solid phases have been observed within these cavities. Many inclusions often show haloes of tiny fluid inclusions (∅ <0.1 μm) surrounding the inclusion cavity, and/or short cracks radiating from the inclusion walls, indicating that they have re-equilibrated during ascent of host xenoliths (Andersen et al., 1984).

Type I fluid inclusions may be associated with Type I silicate-melt inclusions, and mixed inclusions containing both CO_2 and glass inclusions are observed. Inclusions containing both glass and CO_2 show extremely variable fluid/glass ratios.

Late Type II fluid inclusions

Texturally late CO_2 inclusions of variable size (3-30 μm) are evenly distributed through the rocks and occur in trails reaching or crosscutting grain boundaries (Fig. 4b, c, d). At room temperatures, Type II inclusions are single-phase (V) or more commonly, two-phase vapour-dominated (V+L), with a df >0.7 (Figure 4b). They are never found associated with silicate-melt inclusions. Most Type II inclusions show little evidence for partial decrepitation.

In some quartz grains, late trail-bound Type II inclusions cut the clusters of early Type I inclusions. This indicates that Type II inclusions formed at a later stage, well after early fluid and melt entrapment.

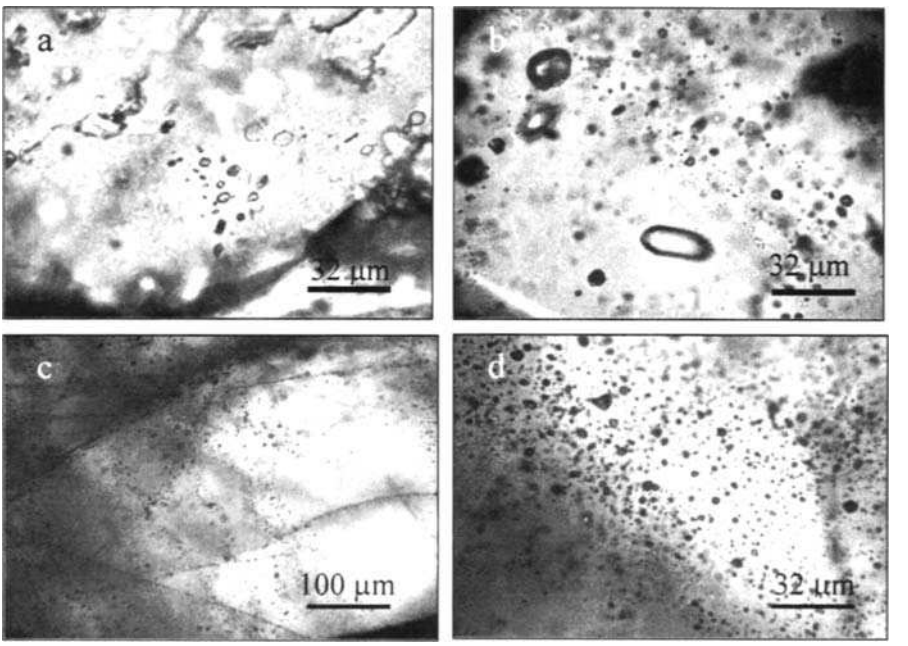

Fig. 4 - a) Cluster of early Type I inclusions in a quartz grain (Filicudi). Most inclusions are monophase (L) at room temperature. b) Particular of a trail of late Type II CO_2 inclusions (Alicudi). As shown here and in Fig. 4d almost all inclusions do not give textural evidence for partial decrepitation. c) Late trails of Type II CO_2 inclusions distributed along two main directions in a quartz grain from (Alicudi). d) Texturally late Type II inclusions within a trail in (Alicudi). Most inclusions are vapour dominated at room temperature.

MICROTHERMOMETRY AND RAMAN ANALYSES

Composition of fluid phases

The dominant fluid inside Type I and II fluid inclusions in quartz xenoliths is pure carbon dioxide, melting instantaneously within a narrow temperature interval between -56.8 and -56.4 °C, with most data at -56.6°C. Two exceptions are observed: 1) a few early Type I inclusions in quartz xenoliths from Filicudi contain substantial amounts of water (20 to 30 % in vol.) recognised as a thin film of water wetting inclusion walls; 2) some early Type I inclusions in quartz xenolith from Alicudi show a considerable Tm's depression for CO_2 (down to -59.5°C) that indicate the presence of other gaseous species besides CO_2. Raman measurements indicate the presence of 1-14 mole % N_2 ± 1-10 mole % CO.

Homogenisation temperatures and density calculations

Fluid inclusions always show trapping of both high-density and low-density CO_2-rich fluids, corresponding to Type I and Type II inclusions, respectively. Obtained

microthermometric data are reported in Fig. 5. In all cases, Type I inclusions show liquid homogenisation in a large interval of temperatures indicating that most inclusions are partly decrepitated. On the other hand, Type II inclusions always homogenise to the vapour and appear undisturbed, since the Th intervals are much narrower. Single homogenisation data sets vary within the different volcanic cycles and are discussed as follows:

Quartz xenoliths from Alicudi: early Type I inclusions in xenoliths from Scoglio Galera and Torrente Cirino basalts (1st and 2nd cycles) homogenise to liquid phase (Th_L; L+V → L) in a scattered range of temperatures between –2.5 and 19.5 °C (d= 0.93 - 0.61 g/cm^3) (Fig. 5). The lowest temperatures around –2.5 °C to belong to a CO_2 + N_2 fluid inclusion, with density value of 0.83 g/cm^3.

Low density Type II inclusions homogenise to the vapour phase (Th_V; L+V → V) in the range of temperatures between –6 and 31 °C, with most measurements between 22 and 31°C (d= 0.22 - 0.47 g/cm^3) (Fig. 5). In xenoliths from andesites of the 3thcycle, only low-density Type II fluid inclusions are present.

Quartz xenoliths from Filicudi: early Type I fluid inclusions from Filo del Banco (1st cycle) and Bue Marino lavas (3rd cycle) show a well defined distribution of values between 21.4 and 31.1°C corresponding to densities of 0.76 – 0.47 g/cm^3. Mixed CO_2 + H_2O inclusions show partial homogenisation temperatures for the CO_2 to the vapour phase comprised between 27 and 29°C (Fig. 5). Corresponding fluid compositions were calculated to be 30 mole % CO_2 and 70 mole % H_2O, with bulk densities of 0.82 – 0.70 g/cm^3.

Late Type II inclusions have Th_V between 18 and 30°C (d=0.41-0.18 g/cm^3).

Quartz xenoliths from Vulcano: Early Type I inclusions homogenise to the liquid phase (Th_L) over a wide range of temperatures, which slightly differ within different cycles (Fig. 5). Th_L vary between: 18.1 and 31 °C (d= 0.79-0.52 g/cm^3; for Sponda Lena basaltic andesites (1st cycle), 11.6 and 30.2 °C (d= 0.85-0.59 g/cm^3) for The Spiaggia Lunga shoshonitic basalts (2nd cycle), 23.3 and 30.7 °C (d= 0.74-0.55 g/cm^3) for Lentia-Mastro Minico dacites and rhyolites (3rd cycle), and 6.3 and 30.8 °C (d=0.84 – 0.54 g/cm^3) from Vulcanello KS leucite-tephrites (6th cycle).

Late Type II Late Type II vapour-rich inclusions show homogenisation temperatures (Th_V) in a more restricted range (Fig. 4): 18 and 31°C, with a maximum at 29°C (d= 0.40-0.18 g/cm^3; Fig. 5)) for Sponda Lena basaltic andesites (1st cycle), 21-31 °C (d= 0.42-0.2 g/cm^3) for The Spiaggia Lunga shoshonitic basalts (2nd cycle), 9 and 30°C (d= 0.35-0.13 g/cm^3) for Lentia-Mastro Minico dacites and rhyolites (3rd cycle), and 31 and 17°C (d=0.38 – 0.17 g/cm^3) from Vulcanello KS leucite-tephrites (6th cycle).

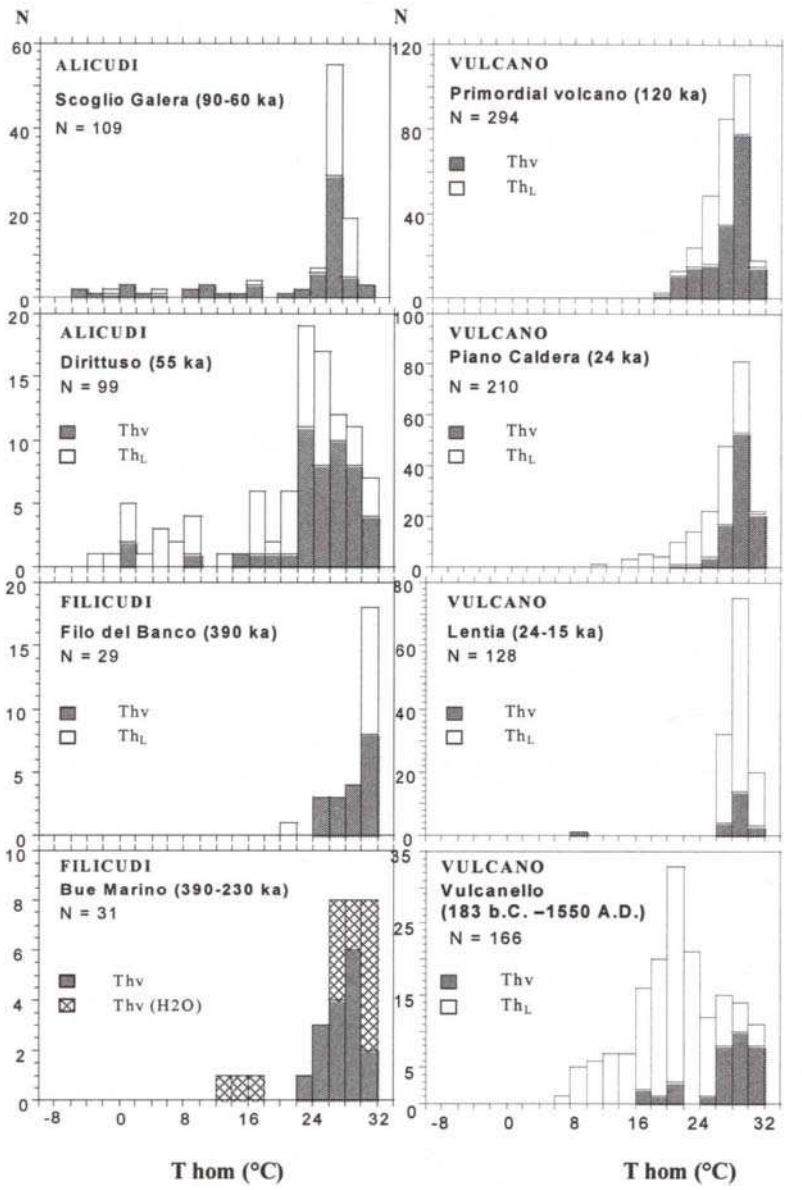

Fig.5. Histograms of homogenisation temperatures for fluid inclusions present in xenoliths of the studied volcanic islands. Histograms report homogenisation temperatures to the liquid phase (Th_L) for early Type I fluid inclusions and homogenisation temperatures to the vapour phase (Th_V) for late Type II fluid inclusions.

DISCUSSION

Fluid inclusion survival in xenoliths and timing of resetting processes

During ascent within magmas, fluid inclusions in crustal xenoliths undergo various modification processes. The ascent paths of host lavas differ, in fact, from isochoric P-T conditions of isolated fluid inclusions. At the host magma temperature, the difference in pressure between the fluid contained in the inclusions and the external lithostatic pressure conditions, may exceed the maximum pressure values for the host mineral ($P_{fluid} >> P_{rock}$; Vityk and Bodnar, 1995; Touret, 2001), causing decrepitation (i.e. fluid loss) and/or stretching (i.e. increase of inclusion volume), with consequent lowering of trapped fluid density. At 1100°C and surface pressure, a CO_2 fluid inclusion with a density of about 1 g/cm^3 has an internal pressure of more than 1 GPa (Holloway, 1981) and should decrepitate (Anderson and Neumann, 2001).

The presence of abundant fluid inclusions in mantle and crustal xenoliths indicates, however, that inclusions can survive such overpressures or that the fluid loss and the density decrease can be minimal. For this reason, it is commonly accepted that the maximum density value obtained from a fluid inclusion population represents the minimum trapping pressure conditions (Andersen and Neumann, 2001).

Modification of inclusions during ascent always decreases fluid inclusion density with respect to the actual trapping conditions, and loss of fluid from the inclusions may occur also when no decrepitation is visible (i.e. through dislocations; Viti and Frezzotti, 2000). Values of reset densities depend on many factors, including velocity of ascent (host xenoliths) and crack-healing rates (host mineral). Timing of such fluid-density re-equilibration processes are not very well constrained. Wanamaker et al. (1990) estimated from experimental studies on CO_2 inclusions in olivine that significant density changes can occur in the inclusions within several days.

Most reset fluid inclusions have variable densities, which imply that re-equilibration of inclusions may occur to different extents and at different depths; consequently, these inclusions have no petrological meaning. In some cases, however, it has been observed that reset fluid inclusions have densities which cluster around a specific value, corresponding to lower pressure conditions. Such a character indicates that inclusion densities have been reset at specific depths representative for precise magma stagnation levels, where time was long enough to re-equilibrate the fluid at the new P and T conditions and eventually to trap new inclusions (Frezzotti et al., 1991; Vaggelli et al., 1993; Clocchiatti et al., 1994; Lima, 1996; Hansteen et al., 1998).

The residence time of xenoliths within shallower accumulation levels must, however, be shorter than xenoliths "life time" to prevent complete disaggregation within the host magma. Melting rates are chiefly controlled by magmatic temperatures, initial xenolith temperature, melting temperature and viscosity. McLeod and Sparks (1998) have estimated that melting rates for crustal rocks in basaltic magmas are extremely fast and in the order from 1 to 10 mm per hour, with slower rates for higher-silica compositions (i.e. high-viscosity melts). For a quartz-rich composition such as that of xenoliths from the Aeolian lavas, this would correspond to a maximum residence time of a few days.

We assume that this was the maximum possible time of ascent for xenoliths from their depth of origin. Further evidence for this assumption comes from the recognition that decrepitation of Type I inclusions occurred without re-equilibration to the densities

of the later Type II inclusions. This implies that magma residence at shallow pressures, that led to trapping of late Type II CO_2 fluids, was very short, less than the few-days estimated for overall ascent of the xenoliths. .

Regional barometry

Before any meaningful geological interpretation can be proposed it is necessary first to describe fully the conditions under which Type I and Type II carbonic fluids are trapped, and second to verify the fluid-xenoliths evolution in the different islands.

The temperature conditions for the fluids at the time of trapping are based on homogenisation temperatures of silicate melt inclusions that are present both in phenocrysts of host lavas and in the same quartz xenoliths (Gioncada et al., 1998; Zanon, 2000). Homogenisation temperatures of silicate-melt inclusions present in quartz xenoliths vary according to host lavas compositions. Measured values are between 1065 and 1105°C (±10°C) (basaltic lavas), and 980°C (±10 °C) (rhyolitic lavas). For that reason, we assume 1090°C (± 10°C) as a mean trapping temperature for fluid inclusions present in xenoliths contained in basalts, and 980°C (± 10°C) for fluid inclusions in those xenoliths hosted in rhyolitic lavas. Note that an error of ± 10 °C does not affect the resulting pressure values, which vary consequently only by ± 20 bars.

Fig. 6 shows estimated trapping pressures for Type I and Type II CO_2 fluids inside the xenoliths beneath the different islands. Although it is clear that a number of Type I inclusions are partly decrepitated, maximum pressures obtained should still be representative, since they correspond to Moho depths, which represent the highest possible pressure values for crustal rocks (Fig. 6).

Alicudi: The first two volcanic cycles (Scoglio Galera, 90 ky and Dirittuso 55 ky) have early Type I fluid inclusions indicating pressures of trapping of about 0.6 GPa (about 24 km) at temperatures of 1090°C, corresponding to crustal depths close to the Moho (Fig. 6).

Low-density Type II fluid inclusions have densities equivalent to pressures between 0.17 and 0.02 GPa, pointing to a shallow trapping event at 6-4 km depth. Beneath Alicudi Island, the presence of low-density fluid inclusions in andesitic lavas of Filo dell'Arpa (about 28 ka) indicates very shallow trapping conditions of about 1 km depth.

Filicudi: early Type I CO_2 and mixed CO_2+H_2O inclusions, although having different densities, give isochores that cross each other at about 1100°C for a pressure interval between 0.4 and 0.3 GPa (15 – 12 km). Such a path is consistent with the interpreted temperatures of 1090°C for fluid trapping conditions. Simultaneous trapping at a given P, T conditions of fluids of different compositions favour the hypothesis that fluids have different origins. It is likely that pure CO_2 fluids are related to the host basalt, while aqueocarbonic fluids might have been generated during melting of host xenoliths.

Low densities type II CO_2 inclusions correspond to pressures of about 0.12 and 0.07 GPa (5 – 3 km; Fig. 6) at the inferred temperatures.

Vulcano: Undisturbed early Type I CO_2-inclusions from Primordial Vulcano and Sponda Lena give maximum pressure estimates of 0.56 – 0.43 GPa at 1090°C. Such pressures correspond to depths of 21-16 km and are suggestive for lower-crustal depths of origin

for most quartz xenoliths, since the Moho beneath Vulcano has been estimated at 21 – 25 km (Falsaperla et al., 1984). Early Type I inclusions in quartz xenoliths from the Lentia rhyolites have densities that correspond to shallower mid-crustal conditions (Fig. 6): 0.35 – 0.2 GPa (13–8 km) for magma temperatures of 980°C. This may indicate that quartz xenoliths in rhyolitic lavas originated at shallower depths. Concerning the recent activity at Vulcanello, Type I fluid inclusions record the deepest accumulation zone (5.8 GPa), pressure conditions.

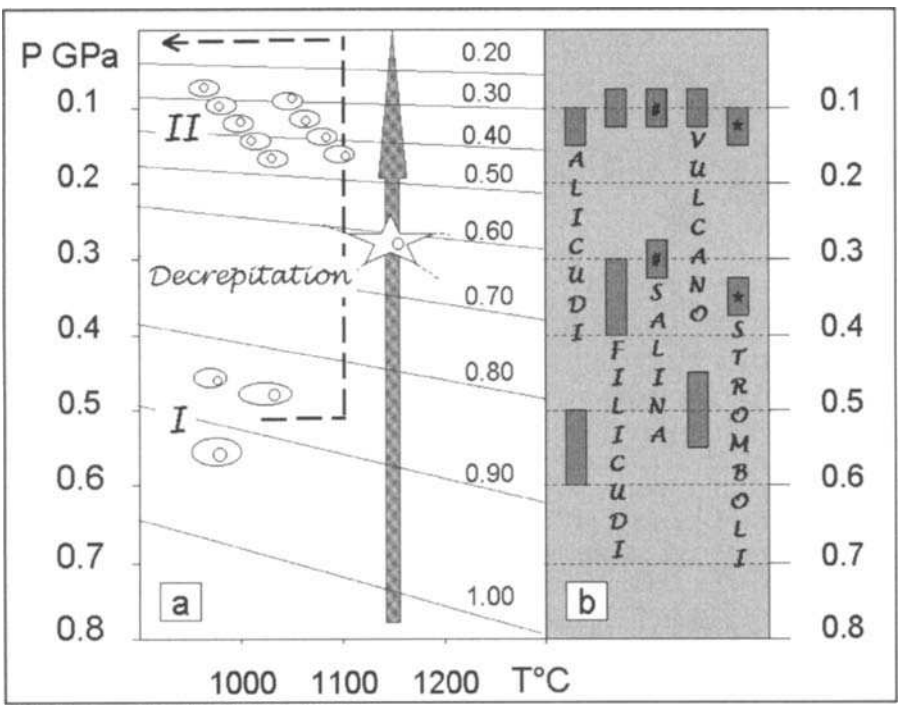

Fig. 6. Summary and interpretation of fluid inclusion data from the Aeolian archipelago a) P, T fluid isochore evolution (dotted arrow path). Single isochores are reported and densities are indicated (g/cm^3). For each volcanic cycle, two distinct fluid-trapping episodes are present: the first at high pressure corresponding to early Type I fluid inclusions and the latter shallower pressures corresponding to late Type II fluid inclusions, see text. b) Isothermal section at 1090°C. Grey boxes indicate pressures obtained from present study. Data from Stromboli (grey boxes marked *) are from Vaggelli et al., 2001; data from Salina (grey boxes marked #) are from Zanon, 2002.

Low-densities of Type II inclusions systematically fall within a restricted interval corresponding to pressures comprised between 0.14 and 0.07 GPa (5.6 – 3 km; Fig. 6) at the inferred temperatures. In addition, there is a remarkable overlap between the pressure ranges for the different xenoliths from all studied volcanic cycles (Fig. 6).

Stromboli: Texturally early and late CO_2 fluid inclusions in quartz xenoliths from the island of Stromboli define two distinct trapping pressure ranges, similarly to the other

volcanoes studied. Vaggelli et al. (2001) analysed fluid inclusions in quartz xenoliths from Strombolicchio (200 ka) and Paleostromboli (60 ka) and estimated maximum pressures of 0.35 GPa for high density CO_2 fluid inclusions. Using a mean crustal density of 2.8 g/cm^3 this corresponds to depths of about 14 km at 1090°C (Fig. 6).

Low density CO_2 fluid inclusions give maximum pressures of 0.15 – 0.1 GPa (5.7 - 4 km).

Salina: Preliminary investigations by Zanon (2002) of fluid inclusions in quartz xenolith hosted in Monte dei Porri andesitic lavas (70 ka) show similar bimodal density distribution for CO_2 inclusions. The highest densities of 0.69 g/cm^3, corresponding to pressures of about 0.32 GPa (about 13 km), are associated to high density CO_2 fluids, while a maximum pressure of 0.12 GPa (about 4 km) is obtained by the abundant late low-density CO_2 inclusions.

Implications for models of volcanic plumbing systems

The study of fluid inclusions in quartz xenoliths provides new barometric information that is useful for assessing the pathways of magmas within the crust and to work out models for the plumbing system of volcanoes in the Aeolian arc.

Figure 7 shows the reconstructed model for the magma plumbing system beneath the Aeolian arc with inferred locations of magma accumulation sites.

The deepest level is characterized by pressure conditions ranging from 0.6 to 0.35 GPa passing from western to eastern islands. These pressures correspond to depths at the limit between the crust and mantle (Moho) in the Aeolian arc, which increases from Stromboli (about 16 km) to Alicudi (about 25 km). Trapping at high pressure is accompanied by melting of crustal rocks with formation of high-silica melts, which are found as glass inclusions in crystals within most quartz xenoliths.

A second, shallower level of fluid entrapment occur at pressure of about 0.15 - 0.1 GPa corresponding to a depth of about 6 - 4 km (Fig. 7). This level is common to all of the Aeolian volcanoes investigated. At this stage, fluid entrapment is not accompanied by melting, but rather by recrystallization of quartz xenoliths.

Finally, an intermediate level of fluid entrapment (13-10 km) is encountered at Vulcano, where detailed investigation have been carried out on a large number of xenoliths coming from various stratigraphic levels (Fig. 7). Note that such an intermediate level is associated with rhyolitic magmas, which are lacking in the western and eastern volcanoes.

We suggest that these various levels represent zones of magma accumulation and differentiation within the crust and at the mantle-crust boundary. The occurrence of a deep level of magma accumulation and differentiation has been suggested for Vulcano by petrological and geochemical studies of volcanic rocks (De Astis et al., 1997, 2000). According to these authors, mafic magmas coming from the mantle accumulated at the Moho by underplating. Here, liquids underwent processes of fractional crystallisation, crustal assimilation and mixing with continuously injected magmas, which gave derivative melts that preserved mafic compositions but display increasing radiogenic Sr and other crustal signatures. The fluid and melt inclusion studies provide additional important evidence for the presence of a magma accumulation level at the Moho, with important crustal melting events.

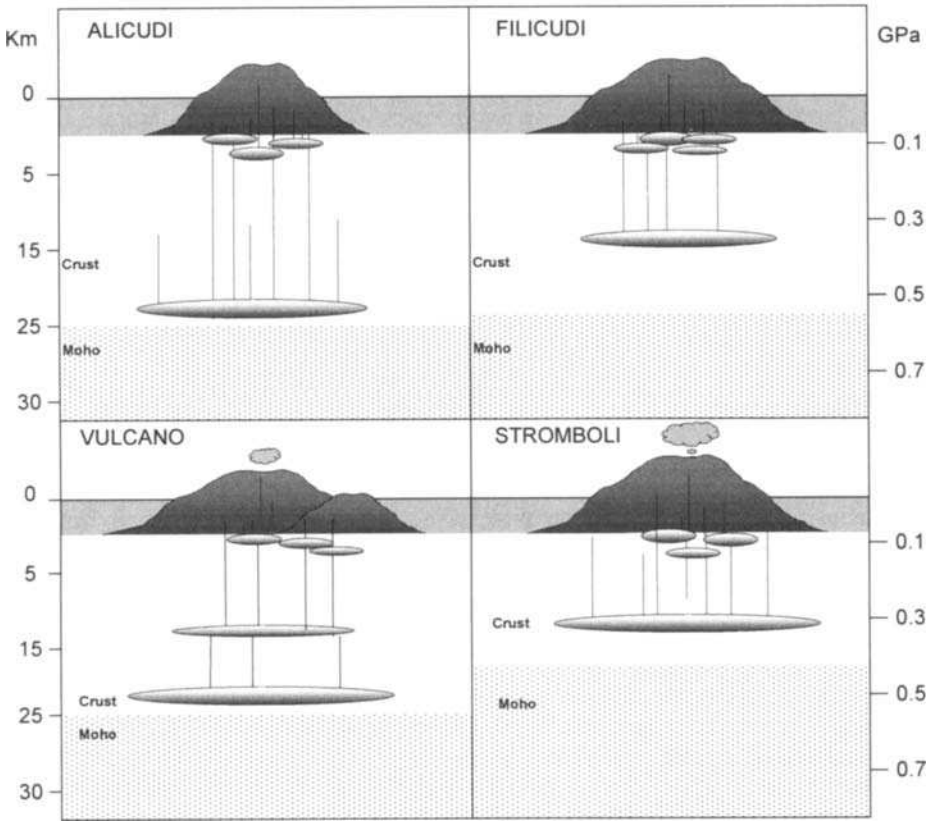

Fig. 7 – Schematic section modelling the magma plumbing system beneath the Aeolian arc from west to east, as inferred from fluid inclusion study. Lithological boundaries are from Falsaperla et al., 1984. Fluid inclusion data for Stromboli are from Vaggelli et. al. (2001). Mafic magmas evolved in a deep storage level located in the lower- crust, close to the Moho. Conditions of neutral buoyancy for ascending magmas are also met at about 6 – 4 km and indicate the presence shallow magma chambers, which appear to be located at the boundary between the intrusive complex and the underlying metamorphic basement. An additional intermediate level for magma ponding has been identified at Vulcano and corresponds to rhyolitic lava compositions, see text.

The occurrence of such a zone at a regional scale suggests that this most likely represents the depth where the mafic magmas pond beneath the lower crust. Such a magma provide heat for crustal melting, which liberate CO_2-rich ($\pm$ N_2 $\pm$ CO $\pm$ H_2O) fluids, found as part of the early trapped Type I inclusions. The much lower solubility of CO_2 in melts compared to that of H_2O can in fact explain the presence of free CO_2 in the xenoliths, as water would have been partitioned into the crustal melts.

The low-density fluid inclusions are trapped at shallower depth in a higher-level zone for magma accumulation, where quartz recrystallization and trapping of late fluid phases occur. It has been proposed by many authors at the Aeolian Islands and elsewhere, that low-density fluid inclusions in xenoliths may reflect a period of residence in shallow

magma chambers (Frezzotti et al., 1991; Vaggelli et al., 1993; Clocchiatti et al., 1994; Lima, 1996; Hansteen et al., 1998). Since low-density inclusions are present in all investigated xenoliths we suggest that shallow magma chambers is another feature of regional significance; these reservoirs represent the sites where magmas ponded and fractionated immediately before being erupted to the surface (Fig. 7). The apparent occurrence of shallow level magma chambers at a constant depth beneath the arc testify to the occurrence of a geological discontinuity of regional significance (intermediate-upper crust?).

The intermediate level of fluid inclusion trapping is detected only at Vulcano, by the present study. This is interpreted to reveal the occurrence of a magma chamber sited at a depth of about 13-10 km. As noted above, the occurrence of this intermediate level of magma accumulation is associated with the onset of rhyolitic activity at Vulcano. Therefore, this magma chamber may represent the site where mafic magmas undergo evolutionary processes dominated by fractional crystallisation, which allow magma to reach rhyolitic compositions. It is interesting to note that that the occurrence of an intermediate-depth magma chamber (about 12 km) has been envisaged for Lipari, on the basis of mineral chemistry data (Mazzuoli, personal communication); Lipari has been characterised by abundant rhyolitic volcanism during the last 10 ka.

In conclusion, the model for the plumbing system of Aeolian volcanoes which comes out of the present study is as follows (Fig. 7):

1. Magma underplating occurs at the base of the crust. Here magmas undergo fractional crystallization plus assimilation and mixing, preserving, however, mafic compositions. Most of the mafic Aeolian magma may be directly fed by such a reservoir.
2. Shallow level magma chambers occur beneath all of the investigated islands. These are fed by the deep magma chambers. The occurrence of quartz xenoliths, which contain both low-density and high-density fluids, the lack of extensive density resetting for Type I deep fluids, and the preservation of quartz xenoliths themselves, all suggest that the residence time of deep magma and related quartz xenoliths in the shallow chambers is very short, possibly a few days.
3. An intermediate-level magma chamber which occurs at Vulcano and, probably, at Lipari. In this chamber large amounts of rhyolitic liquids form from basic parents by evolutionary processes dominated by fractional crystallisation.

The above model implies that the large quantities of mafic magmas which characterize the early stages of the activity of most islands reflect tapping of deep level reservoirs, where dominant mixing processes do not allow magma differentiation toward silicic composition. On the other hand, the evolution in the shallow magma chambers is regionally less important. The intermediate-level magma chambers, which are particularly abundant only in the central island of Vulcano and Lipari are sites of extensive fractional crystallisation processes.

Implications for strategies of volcano monitoring

The models worked out for the Aeolian arc suggests that al the magmas arising from the upper mantle undergo a polybaric evolution. High-pressure magma chambers essentially experience mixing-dominated evolutionary processes, whereas fractional crystallisation is the dominant evolutionary mechanism at intermediate and low pressures.

High-density CO_2 inclusions in quartz-rich xenoliths are entrapped at high pressures, but survived during transport and residence at shallow levels. The lack of fluid density resetting at the new P-T conditions suggests that the time elapsed since upraise from deep to shallow magma reservoirs is relatively short: long ascent and residence times would either re-equilibrate the fluid to new P-T conditions, or would bring to a total loss of the fluid, with decrepitation of the inclusions. Presently available data do not allow to put precise constraints on the time necessary for decrepitation and/or re-equilibration. However, data discussed above suggest that this is of the order of a few days.

If these conclusions are accepted, the obvious implication is that the magma uprising from the depth reside for a very short time in the shallow reservoir. This supports the view of Sparks et al. (1987) that input of magma into the shallow level magma chambers actually triggers volcanic eruptions. This also allows to furnish indications on one of the most outstanding problems of modern volcanology: the forecasting of volcanic eruptions and the strategies of volcano monitoring.

Uprising of magma within the crust is likely accompanied by seismic activity. Monitoring of this activity may reveal new magma ascent episodes and, therefore, represent an important hint that something important is going to happen in the shallow system and, possibly, at the surface.

The conclusion drawn by the present study is that working out models on the internal structure of volcanoes represents and important step to understand both magma evolution processes and to establish correct and reliable strategies for monitoring active volcanoes.

SUMMARY AND CONCLUSIONS

1. Fluid inclusion data suggest that the magma feeding system beneath the Aeolian Island is characterised by multiple magma chambers that persisted throughout the overall arc evolution. Deep and shallow level reservoirs occur at a regional scale, whereas intermediate magma chambers developed an Vulcano and Lipari.
2. Deep magma chambers are the only ones active during the early stages of the exposed activity. Evolutionary processes in the deep chambers are dominated by mixing processes, which inhibit evolution of magma toward salic compositions, explaining why mafic magmas represent the bulk of the lowest exposed rocks in the Aeolian islands. Ponding of mafic magmas in the deep reservoirs release heat and fluids into the crust and may give rise to partial melting processes in the host rocks.
3. Intermediate level reservoirs become active with ongoing volcanism; evolution processes in these magma chambers are dominated by fractional crystallisation that draw magma toward rhyolitic compositions.
4. Shallow-level reservoirs are always confined at the same depth of about 5 km, suggesting the existence of a boundary between crustal layers with different mechanical characteristics..
5. The shallow magma chambers are fed by the deep reservoirs and are the sites of evolutionary processes such as fractional crystallisation and mixing. On the other hand, crustal assimilation and mixing with mantle-derived magmas appear to be the dominant processes occurring in the deep reservoirs. Partial melting of wall rocks - generating high-silica liquids which mixed with mantle derived magma - may have

generated the observed considerable isotopic variations (De Astis et al., 1997; Del Moro et al., 1998).

6. Fluid inclusion studies also suggest that the residence time of magmas in the shallow reservoir is very short and less than a few days, since there is little evidence of resetting of high-density fluid inclusions in quartz-rich xenoliths. This implies that magma ascent from deep reservoirs immediately precede and may actually trigger volcanic eruptions.

Acknowledgements

We thank J. B. Lowenstern and R..J. Bodnar for constructive reviews. M.L.F. is grateful to R..J. Bodnar and B. De Vivo for invitation to the workshop on volcanic systems: "Melt inclusions: methods, applications and problems" in Sorrento. Researches on Italian recent and active volcanism are financially supported by I.N.G.V. - G.N.V. (Istituto Nazionale di Geofisica e Vulcanologia – Gruppo Nazionale di Vulcanologia), and by local projects from the Universities of Perugia (A.P.) and Siena (P.A.R 2001 – Quota Progetti, M.L.F.). Raman microprobe facilities were provided by P.N.R.A., the Italian Organisation for Scientific Research in Antarctica.

References

Albarede, F., 1992, How deep do common basaltic magmas form and differentiate Journal of Geophysical Research, 97 (B7). 10997-11009.

Andersen, T. and E.R. Neumann, 2001, fluid inclusions in mantle xenoliths. Lithos, 55, 301-320

Andersen, T., S.Y. O'Reilly. and W.L. Griffin, 1984, The trapped fluid phase in upper mantle xenoliths from Victoria, Australia: implications for mantle metasomatism. Contrib Mineral. Petrol., 88, 72-85, 1984.

Barberi, F., P. Gasparini, F. Innocenti, and L. Villari, 1973, Volcanism of the southern Tyrrhenian Sea and its geodynamic implications., J. Geophys. Res., 78, 5221-5232.

Barberi, F., F. Innocenti, G. Ferrara, J. Keller, and L. Villari, 1974, Evolution of Aeolian arc volcanism (Southern Tyrrhenian Sea)., Earth Planet. Sci. Letters, 21, 269-276.

Beccaluva, L., G. Gabbianelli, F. Lucchini, P.L. Rossi, and C. Savelli, 1985, Petrology and K/Ar ages of volcanics dredged from the Eolian seamounts: implications for geodynamic evolution of the southern Tyrrhenian basin., Earth Planet. Sci. Lett., 74, 187-208.

Brown, P.E., 1989, FLINCOR: a fluid inclusion data reduction and exploration program., Second Biennal Pan-Am Conf. Fluid Inclusions Program Abstr. 14.

Calanchi N., Peccerillo A., Tranne C.A., Lucchini F., Rossi P.L., Kempton P., Barbieri M. and Wu T.W., 2002, Petrology and geochemistry of volcanic rocks from the island of Panarea: implications for mantle evolution beneath the Aeolian island arc (Southern Tyrrhenian sea). J. Volcanol. Geotherm. Res., 115, 367-395.

Calcagnile, G., and Panza, G. F., 1979, Crustal and upper mantle structure beneath the Apennines region as inferred from the study of Rayleigh waves. J. Geophys., *45*, 319-327.

Clocchiatti, R., A. Del Moro, A. Gioncada, J.L Joron, M. Mosbah, L. Pinarelli, and A. Sbrana, Assessment of a shallow magmatic system: the 1888-90 eruption, Vulcano Island, Italy. 1994, Bull. Volc.., 56, 466-486,.

De Astis, G., L. La Volpe, A.Peccerillo, and L. Civetta, 1997, Volcanological and petrological evolution of Vulcano island (Aeolian Arc, southern Tyrrhenian Sea). Journal of Geophysical Research 102 (b4), 8021-8050.

De Astis, G., A. Peccerillo, P. D. Kempton, L. La Volpe, and T.W. Wu, 2000, Calcalkaline to potassium-rich magmatism in the Aeolian Arc: geochemical and Sr, Nd, Pb isotopic constraints from the Island of Vulcano (Aeolian arc). Contribution to Mineralogy and Petrology 139, 684-703.

De Paolo, D.J., 1981, Trace elements and isotopic effects of combined wallrock assimilation and fractional crystallization. Earth Planet. Sci. Lett., 53, 189-202.

Ellam, R.M. and R.S. Harmon, 1990, Oxygen isotope constraints on the crustal contribution to the subduction-related magmatism of the Aeolian Islands, Southern Italy. J. of Volc. Geother. Res., 44, 105-22.

Ellam, R.M., M.A. Menzies, C.J. Hawkesworth, W.P. Leeman, M. Rosi, and G. Serri, 1988, The transition from calc-alcaline to potassic orogenic magmatism in the Aeolian Islands, Southern Italy., Bull. Volcanol., 50, 386-398.

Falsaperla, S., G. Lanzafame, V. Longo and S. Spampinato, 1999, Regional stress field in the area of Stromboli (Italy): insight into structural data and crustal tectonic earthquakes., J. Volc. Geotherm. Res., 88, 147-166.

Finetti, I., 1982, Structure, stratigraphy and evolution of Central Mediterranean., Boll. Geofis. Teor. Appl., 24, 247-312.

Frezzotti, M.L., B. De Vivo and R. Clocchiatti, 1991, Melt - mineral - fluid interactions in ultramafic nodules on alkaline lavas from M.Etna (Sicily, Italy) as recorded by melt and fluid inclusions J. Volc. Geotherm. Res 47, 209-219.

Frezzotti M.L., V. Zanon, A. Peccerillo, I. Nikogosian, Silica-rich melts in quartz xenoliths from Vulcano Island and their bearing on processes of crustal anatexis and crust-magma interaction beneath the Aeolian Arc, southern Italy, J. Petrol., in press.

Gillot, P.Y., 1987, Histoire volcaniques des iles Eoliennes: arc insulaire ou complexe orogenique anulaire? Doc.Trav. IGAL. 11; 35-42.

Gioncada, A., R. Clocchiatti, A. Sbrana, P. Bottazzi, D. Massare, and L. Ottolini, 1998, A study of melt inclusions at Vulcano (Aeolian Islands, Italy): insight on the primitive magmas and on the volcanic feeding system. *Bull. Volc.*, 60, 286-306,.

Hansteen, T.H., A. Klugel and H.U. Schminke, 1998, Multistage magma ascent beneath the Canary Islands. Evidence from fluid inclusions., Contrib. Mineral. Petrol., 107, 242-254.

Hildreth, W. and N. Moorbath, 1988, Crustal contribution to arc magmatism in the Andes of Central Chile., Contrib. Mineral. Petrol., 98, 455-489.

Holloway, J.R., 1981, Compositions and volumes of supercritical fluids in the earth's crust, in MAC Short Course in Fluid Inclusions, Eds. L.S. Hollister, and M.L. Crawford, Mineralogical Association of Canada, 13-38.

Honnorez, J., and J. Keller, 1968, Xenolithe in vulkanischen Gesteiner der Äolischen Inseln (Sizilien)., Geol. Rundschau, 57 (3), 719-736.

Lima, A. 1996, CO_2 fluid inclusion in a gabbroic xenolith from Panarea (Aeolian Islands): a contribution to the understanding of pressure evolution of the subvolcanic magmatic system. Acta Vulcanol., 8 (2), 139-146.

McLeod P. and R.S.J. Sparks, 1998, The dynamics of xenolith assimilation. Contrib. Mineral. Petrol., 132, 1, 21-34.

Patino L.C., M.J. Carr and M.D. Feigenson, 2000, Local and regional variations in Central American lavas controlled by variation in subducted sediments imput. Contrib. Mineral. Petrol. 138, 265-283.

Peccerillo, A., and T.W. Wu, 1992, Evolution of calc-alkaline magmas in continental arc volcanoes: evidence from Alicudi, Aeolian arc (southern Tyrrhenian Sea, Italy)., J. Petrol., 33 (6), 1295-1315.

Peccerillo, A., P.D. Kempton, R.S. Harmon, T.W. Wu, A.P. Santo, A.J. Boyce, and A. Tripodo, 1993, Petrological and geochemical characteristics of the Alicudi volcano, Aeolian islands, Italy: implications for magma genesis and evolution., Acta Vulcanol., 3, 235-249.

Roedder, E., 1965, Liquid CO_2 inclusions in olivine-bearing nodules and phenocrysts from basalts., Am. Mineral., 50, 1746-1782.

Rottura, A., A. Del Moro, L. Pinarelli, R. Petrini, A. Peccerillo, A. Caggianelli, G.M. Bargossi and G. Piccarreta, 1991, Relationships between intermediate and acidic rocks in orogenic granitoids suites: petrological, geochemical and isotopic (Sr, Nd, Pb) data from Capo Vaticano (southern Calabria, Italy). Chem. Geol. 92, 153-176.

Santo A. P., A.H. Chen, E. Clack, N. Farrar and A. Tsegaye, 1995, $^{40}Ar/^{39}Ar$ ages of Filicudi island volcanics: implication for the volcanological history of the Aeolian arc Italy. Acta Vucanol., 7, 13-18.

Selli, R., 1985, Tectonic evolution of the Tyrrhenian Sea. In Geological evolution of the Mediterranean basin, Eds. D.J.W. Stanley, F.C., Springer, New York Berlin Heidelberg, 131-151.

Touret, J.L.R., 2001, Fluids in metamorphic rocks. Lithos, 55, 1-18.

Turner, S. and J. Foden, 2001, U, Th and Ra disequilibria, Sr, Nd and Pb isotope and trace element variations in Sunda arc lavas: predominance of a subducted sediment component. Contrib. Mineral. Petrol. 142, 43-57.

Vaggelli, G., H.E. Belkin, and L. Francalanci, 1993, Silicate-melt inclusions in the mineral phases of the Stromboli volcanic rocks: a contribution to the understanding of magmatic processes. Acta Vulcanol., 3, 115-125.

Vaggelli G., L. Francalanci, G. Ruggieri and S. Testi, 2001, Geol. Soc. It. Abstr. Prog., 45.

Van Dijk, J.P. and P.J.J. Scheepers, , 1995, Neotectonic rotations in the Calabrian Arc: implications for a Pliocene-Recent geodynamic scenario for the central Mediterranean. Earth Sci. Rev. 39, 207-246.

Vroon, P.Z., M.J. van Bergen, W.M. White, and J.C. Varekamp, 1993, Sr, Nd and Pb isotope systematics of the Banda arc, Indonesia: combined subduction and assimilation of continental material. J. Geophys. Res., 98, 22349-22666.

Viti C. and M.L. Frezzotti, 2000, Re-equilibration of glass and CO_2 inclusions in xenolith olivine: A TEM study. Am. Mineral., 85: 1390-1396

Vityk, M.O., and R.J. Bodnar, Statistical microthermometry of synthetic fluid inclusions in quartz during decompression reequilibration., Contrib. Mineral. Petrol., 132, 149-162, 1998.

Wanamaker B.J., T.F Wong, and B. Evans, 1990, Decrepitation and crack healing of fluid inclusions in San Carlos olivine. J. Geophys. Res., 95, 15623-15641.

Werre, R.W., R.J. Bodnar, P.M. Bethke, and P.B. Barton, 1979, Geol. Soc. Am. Abstr. Progr., 11, 539, 1979.

Wezel, F.C., 1985, Structural features and basin tectonics of the Tyrrhenian Sea. In Geological evolution of the Mediterranean Basin., Ed. D.J.W. Stanley, Springer, New York Berlin Heidelberg, 153-194.

Zanon, V., 2000, Fluid and melt inclusions in xenoliths from the Aeolian Isalnds: volcanological and magmatological implications. Ph.D. Thesis. University of Perugia (in Italian).

Zanon V., 2002, Soc. It. Min. Petrol., Abstr. Prog., 156-7.

This Page Intentionally Left Blank

Volatiles, magmatic degassing and eruptions of Mt. Somma-Vesuvius: Constraints from silicate melt inclusions, Cl and H_2O solubility experiments and modeling

James D.Webster[1], Benedetto De Vivo[2], and Christine Tappen[1]

[1]Department of Earth and Planetary Sciences, American Museum of Natural History, Central Park West at 79th Street, New York, New York 10024 USA
[2]Dipartimento di Geofisica e Vulcanologia, Universita de Napoli Federico II, Via Mezzocannone 8, 80134, Napoli, Italy

ABSTRACT

The eruptive styles of Mt. Somma-Vesuvius vary dramatically and appear to correlate with pre-eruptive magma compositions. Explosive eruptions occurring in the past 3550 years involved magmas enriched in H_2O, Cl, S, F, and P and characterized by elevated (S/Cl). To interpret volatile exsolution and magmatic degassing, we have determined the solubilities of H_2O and Cl for melts of natural Mt. Somma-Vesuvius phonolite and phonotephrite in hydrothermal experiments conducted at 500 and 2000 bars and temperatures of 946 – 1166° C. The solubility of Cl in phonolite melts is a complex function of pressure and the assemblage of volatile phases. For melts with low H_2O contents and saturated in hypersaline liquid, Cl solubility decreases marginally with decreasing pressure; whereas, Cl solubility increases with decreasing pressure with vapor plus hypersaline liquid stable. Chlorine solubility in hypersaline liquid-saturated melts also varies strongly with melt composition; the Cl content of phonolite melt is approximately one-half that of phonotephrite melt at both pressures.

Differentiation of the Cl-enriched Mt. Somma-Vesuvius magmas occurred via crystallization and fractionation of clinopyroxene, olivine, plagioclase, and other phenocrysts. Crystallization increased the volatile abundances of residual fractions of melt while simultaneously reducing Cl solubility, and this increased the potential for pre-eruptive saturation of compositionally evolved magmas in one or more volatile phases. Comparison of the experimental results with the pre-eruptive abundances of volatiles in Mt. Somma-Vesuvius magmas (determined from melt inclusions) and with modeled Cl solubilities in H_2O-poor, hypersaline liquid-saturated melts indicates that many compositionally evolved magmas did exsolve or would have exsolved hypersaline liquid (with or without vapor) initially. The passively-erupted, lava- and scoria-forming magmas were more likely to exsolve hypersaline liquid (with or without vapor); whereas, the H_2O-enriched, explosively erupting, pumice-forming magmas were more likely to exsolve vapor (with or without hypersaline liquid).

Prior experimental investigations have argued that the H_2O and Cl concentrations of silicate melt, aqueous vapor, and hypersaline liquid should be invariant as crystallization occurs at constant pressure and temperature. However, the ascent, crystallization, and differentiation of magmas *in nature* involves simultaneous changes in bulk melt composition, temperature, and pressure, and the solvus for vapor plus brine (i.e., hypersaline liquid) varies as a function of each of these variables. Consequently, the solubilities of H_2O and Cl in vapor- plus hypersaline liquid-saturated magmas, undergoing ascent and compositional evolution, will not be fixed by the phase assemblage. Instead, the volatile concentrations of

vapor and hypersaline liquid will and do change during eruptive and pre-eruptive magmatic degassing.

INTRODUCTION

Mount Somma-Vesuvius is a composite stratovolcano in southern Italy that threatens the lives and property of the more than 3 million inhabitants of the Naples region. The magmas of this volcano span a range of compositions, but most are potassic and variably enriched in volatiles (H_2O, S, and Cl) and fluxing components (F and P_2O_5) (Vaggelli et al., 1993; Marianelli et al., 1995; 1999; Belkin et al., 1998; Lima et al., 1999; Webster et al, 2001;

Table 1. Composition of starting materials.

Constituents (wt.%)	Phonolite [S(9)2]	Phonotephrite [V6]
P_2O_5	0.02	0.92
SiO_2	58.37	47.5
SO_2	0.01	0.01
TiO_2	0.16	1.01
Al_2O_3	19.74	17.30
MgO	0.16	4.07
CaO	1.80	9.89
MnO	0.17	0.14
FeO	1.86	6.64
Na_2O	8.18	2.41
K_2O	6.95	7.29
F	0.72	0.21
Cl	0.62	0.48
Total	98.78	99.26

Phonolite glass prepared in sealed gold capsule and fused at 1010° C and 2000 bar (electron microprobe analysis); phonotephrite rock sample analyzed by (Belkin, 1993a). All iron as FeO.

Raia et al., 2000). During the past 35 ka, the magmas have generated at least eight violent, plinian to subplinian eruptions and dozens of comparatively passive, interplinian eruptions. Although Mt. Somma-Vesuvius is one of the most well-studied volcanoes on Earth (Santacroce et al., 1993; De Vivo et al., 1993; Spera et al., 1998; De Vivo and Rolandi, 2001 and references therein), much is not yet known about the magmatic system driving its eruptions. This lack of information is relevant to larger issues since degassing phenomena in H_2O-, S-, Cl-, P-, and F-enriched magmas and relationships between degassing and eruptive process are of considerable importance but still poorly understood.

Systematic investigation of the abundances of volatiles and fluxing components in silicate melt inclusions (MI) from Mt. Somma-Vesuvius pumices, scoria, and lavas illuminates

intriguing relationships involving pre-eruptive volatile abundances and eruptive styles. One recent finding is that MI erupted during activities prior to 14.0 ka (i.e., pre-caldera activities) are compositionally distinct from MI erupted during 3.55 ka and younger activities (post-caldera eruptions) which indicates that the compositions of younger magmas were different from those erupted before 14 ka (Webster et al., 2001). The latter eruptions generated the Mt. Somma caldera in which the younger Vesuvius crater resides. Another new observation is that post-caldera (< 3.55 ka) tephra erupted during plinian and subplinian eruptions contain MI enriched in H_2O and characterized by elevated (S/Cl) ratios; whereas, MI in more passively erupted scoria and lava generally contain less H_2O and show distinctly lower (S/Cl) (Webster et al., 2001). Thus, explosively erupted magmas younger than 3.55 ka are enriched in H_2O and S. This relationship presents the interesting prospect that monitoring the concentrations of S and Cl in crater gases may facilitate the prediction of violent eruptions in future.

Given these recent observations on Mt. Somma-Vesuvius and the more general understanding that the exsolution and expansion of volatile components in most magmas provide the driving force for violent eruptive behavior, we have conducted volatile solubility experiments in melts of Mt. Somma-Vesuvius phonolite and phonotephrite at shallow crustal conditions and we report on the state of progress of our experiments. We focus on the solubilities of Cl and H_2O as a function of melt evolution and pressure because Mt. Somma-Vesuvius magmas, MI, and matrix glasses are strongly enriched in both of these components. We also apply a newly developed Cl solubility model to better understand the exsolution and degassing of hypersaline liquid and vapor from Mt. Somma-Vesuvius magmas as they ascend from the chamber toward the vent, undergo crystallization, release volatiles, and erupt. Our new constraints on pressures of volatile saturation and volatile phase exsolution bear on prior eruptive processes, and they may provide information for interpreting and forecasting future eruptions of this historic and well-monitored volcanic system.

Geologic background

Most Mt. Somma-Vesuvius eruptions involved basic, silica-undersaturated, potassic magmas ranging in composition from tephrite and trachybasalt to phonolite, but less-alkaline, basaltic trachyandesite magmas were also involved (Sigurdsson et al., 1985; Joron et al., 1987; Belkin et al., 1993a;b; De Vivo et al., 1993). The eruptive styles have varied dramatically during the past 5.5 ka. Strombolian-style, scoria-forming eruptions and effusive lava flows (involving H" 0.01 km^3 of magma) were common and were punctuated by comparatively rare but highly explosive plinian to subplinian eruptions of pyroclastic flows and surges (involving 0.1 to several km^3 magma) (Rolandi et al., 1998). Eruptive styles vary not only with the (S/Cl) ratios of magma, they also correlate with major-element compositions of matrix glasses and whole rocks (Ayuso et al., 1998). Passively erupted trachybasaltic to phonotephritic magmas contained comparatively less SiO_2, Na_2O, and K_2O, whereas plinian and subplinian magmas involved phonolitic compositions (Civetta and Santacroce, 1992). These geochemical differences correlate with significantly longer magmatic repose periods that precede plinian and subplinian events (Macedonio et al., 1990), because these eruptions typically followed extensive chemical differentiation of melt to phonolite compositions. The longer repose times and magma evolution preceding violent eruptions are consistent with the premise that the pre-eruptive, magmatic volatile abundances of this volcano had a dominant control on eruptive styles (Webster and De Vivo, 2002), because the magmas had adequate time to evolve to greater volatile abundances. Furthermore, other work (Marianelli

et al., 1999) suggests that the intrusion, mingling, and mixing of mafic, volatile-charged magma with these more-evolved magmas may have also influenced eruptive processes.

METHODS

Experimental methods

Chlorine and H_2O solubility experiments were conducted at 500 and 2000 bar with an Avellino (erupted H" 3.55 ka) phonolitic pumice at 946-1057° C (except for one run at 1166° C) and with a sample of phonotephritic lava (erupted in 1944) at 1122°-1135°C (Table 1). Twenty to forty milligrams of powdered phonolite or phonotephrite were melted with one to eight milligrams of distilled water ± crystalline NaCl and KCl. The experiments were conducted for durations of 3 to 11 days, but most were run for at least 5 days. Excess volatiles were added such that the silicate melts coexisted with one or more volatile phases (e.g., vapor, hypersaline liquid, vapor plus hypersaline liquid, or supercritical fluid). Iron was added as Fe_3O_4 to several of the longer duration experiments to reduce the loss of Fe from the melt to the precious metal capsules.

The experiments were conducted with Au and Au-Pd capsules in an internally heated pressure vessel (IHPV) at the American Museum. Temperature was monitored with chromel-alumel thermocouples, and temperature variations of most runs were typically d" 10° C - several experiments involved variations as high as 20° C. Pressure was monitored with factory-calibrated bourdon tube gauges. The experiments were quenched isobarically. Most quenches were fairly rapid; for example, the 1135° C experiment was quenched to 600°C in approximately 25 seconds.

The f_{O2} was not intentionally buffered for most experiments. These runs were conducted at the ambient f_{H2} of the pressure IHPV. The ambient O_2 buffering capacity of the IHPV was determined with a H_2 sensor, and the IHPV imposes a f_{H2} that is roughly equivalent to that of the $Mn_{1-x}O$-Mn_3O_4 solid oxygen buffer at 820° and 2 kbar for runs with a water activity of one. So, assuming that the f_{H2} imposed on the charges was greater than or equivalent to the ambient f_{H2} of the IHPV, then the f_{O2} of these runs was lower than that of the $Mn_{1-x}O$-Mn_3O_4 buffer. Additional details on experimental methodology are available in Webster and De Vivo (2002).

Analytical methods

The run-product glasses were analyzed for Si, Al, Na, K, Ca, Fe, Mn, Ti, Mg, F, P, S, and Cl with a Cameca SX-100 electron microprobe at the American Museum using wavelength-dispersive techniques at 15 keV and 10 nanoamps beam current for major and minor elements and 40 nanoamps for S and Cl. One set of analyses (4 to 8 per glass) was conducted with a defocussed electron beam (4 μm diameter) and peak count times of 10 to 30 seconds. The samples were moved under the defocussed beam during analysis to minimize Na, F, and K migration. Using this technique on obsidian, the electron microprobe determined 4.4 wt.% Na_2O in comparison with 4.3 wt.% Na_2O determined by wet-chemical analysis. The Cl concentrations were checked in a second set of analyses (10 to 20 analyses per glass with 45 to 60 second count times) conducted on vesicle-free glass with a 2 μm-diameter beam. Replicate analyses on a single spot show Cl counts are stable at these conditions. Obsidians of known composition were also used to establish the analytical accuracy and precision for Cl. The microprobe determined 0.19 to 0.21 wt.% Cl in an obsidian containing 0.20 wt.% Cl as determined by wet chemical analysis. Sulfur K-α wavelength scans were performed on

these glasses to determine if the S peak conforms to that of barite or troilite. The S peak is consistent with that of barite, and appropriate standard materials were used.

Ratios of H/Si were analyzed by secondary ion mass spectrometry (SIMS) with a Cameca IMS-3f ion microprobe at the Woods Hole Oceanographic Institution to determine the H_2O concentrations of felsic to basaltic "standard" glasses and some of the run product glasses.

Table 2 Experimental run conditions and run product characteristics.

Run number	Run T (°C)	Run P (bar)	Run duration (hours)	Starting material	Cl in glass (wt.%)	Molar A/CNK	Molar N/NK	H_2O in glass (wt.%)
1-01-40C	946	500	190	phonolite	0.74	0.86	0.62	3.0
1-01-40B	946	500	190	phonolite	0.73	0.87	0.58	4.3
1-01-40A	946	500	190	phonolite	0.55	0.89	0.62	4.34, 4.4
1-02-12A	1001	500	284	phonolite	0.77	0.87	0.61	1.39
1-02-12B	1001	500	284	phonolite	0.55	0.88	0.63	3.50
1-02-12C	1001	500	284	phonolite	0.86	0.87	0.63	2.66
1-02-19C	1000	500	115	phonolite	0.42	0.89	0.64	3.79
1-02-19A	1000	500	115	phonolite	0.72	0.87	0.62	1.38
1-02-22B	1000	500	167	phonolite	0.41	0.89	0.64	3.41
1-02-22A	1000	500	167	phonolite	0.43	0.88	0.63	4.00
1-00-37D	1057	2000	163	phonolite	0.43	0.91	0.63	(6)
1-00-37B	1057	2000	163	phonolite	0.30	0.93	0.62	(6.5)
1-00-44A	1010	2000	216	phonolite	0.54	0.82	0.64	6.43
1-00-44C	1010	2000	216	phonolite	0.88	0.97	0.62	(4)
1-01-41C	1166	2000	140	phonolite	0.80	0.86	0.58	(1)
1-01-45	998	2000	72	phonolite	0.43	0.89	0.65	(6.5)
1-02-03B	998	2000	140	phonolite	0.72	0.87	0.61	2.7
1-02-03C	998	2000	140	phonolite	0.07	0.90	0.63	6.84, 6.0
1-02-11A	997	2000	193	phonolite	0.84	0.85	0.61	4.3
1-02-11B	997	2000	193	phonolite	0.34	0.89	0.64	7.2
1-02-11C	997	2000	193	phonolite	0.97	0.85	0.63	5.9
1-02-17B	1000	2000	186	phonolite	0.26	0.97	0.62	6.24
1-02-17A	1000	2000	186	phonolite	0.29	0.91	0.64	5.26
1-99-3A	1122	500	118	phonotephrite	1.44	0.57	0.41	(2.2)
1-00-9	1135	2000	118	phonotephrite	1.53	0.58	0.41	(2.9)

Molar A/CNK = [moles Al_2O_3/(moles Na_2O+K_2O+CaO)]. Molar N/NK = [moles Na_2O/(moles Na_2O+K_2O)]. Water in glass (normal text = FTIR; underlined text = SIMS; parentheses = computed). All run glasses are aphyric, except for runs 1-01-40C (5 % crystals) and 1-00-44C (trace crystals).

Five to ten replicate analyses were conducted, and the primary O^- ion beam was typically 10 to 15 μm in width. All constituents were analyzed as high-energy ions to minimize the effects of mass interferences and reduce matrix effects, and only positively charged, secondary ions with excess kinetic energies in the 75 ± 25 eV range were analyzed. The SIMS ion yields for Na, K, and Cl were determined for the glasses, and comparison of the ion yields with the electron microprobe results implies that the SIMS data were free of matrix effects, so the reported H_2O concentrations should be accurate within ± 0.3 wt.% H_2O.

Chips of run-product glass were doubly polished and cleaned with acetone prior to FTIR analysis. Sample thickness was adjusted from 30 to 160 microns to prevent IR detector saturation based on total H_2O. A Nicolet 20SXB FTIR spectrometer equipped with a Spectra

Tech IR Plan microscope was used to obtain spectra in the range of the mid-IR region (4000 to 1400 cm^{-1}) and near-IR region (6500 to 3700 cm^{-1}) at the American Museum. FTIR measurements were collected in transmittance mode at room temperature, and the spectrometer was purged with dry nitrogen at 15 liters/minute. Spectra were collected in % transmittance versus wavenumber then converted to absorbance versus wavenumber with Nicolet OMNIC software. For each spot analysis, 1024 scans were performed, and each glass chip was measured in 3 to 4 different spots. Molecular H_2O concentrations were determined with the 5200 cm^{-1} band intensity, and hydroxyl abundance was determined using the intensity of the 4500 cm^{-1} band. Total H_2O concentrations were determined from the intensity of the 3570 cm^{-1} and were checked from the summation of molecular and hydroxyl water. Concentrations were calculated using the Beer-Lambert Law. Extinction coefficients (Mandeville et al., 2002) for Fe-free andesite glass ($\varepsilon_{3570} = 69.21 \pm 79$ L/mol cm, $\varepsilon_{5200} = 1.46 \pm 0.06$ L/mol cm, and $\varepsilon_{4500} = 0.89 \pm 0.06$ L/mol cm) were used to determine total H_2O concentrations. Glass densities were calculated from electron microprobe oxide data and the Gladstone Dale rule (Gladstone and Dale, 1864; Silver and Stolper, 1989) with a computer program provided by J. Dixon. Thicknesses of the doubly polished chips were measured 8 to 10 times each using a Mitutoyo digimatic indicator with a precision of ± 2 μm. The H_2O contents of other glasses were computed by assuming that the difference between 100 wt.% and the electron microprobe total represents an approximate value for H_2O (Table 2).

RESULTS

All run products consist of vesicular glasses and salts. The glasses of all but two experiments are aphyric (Table 2). The compositions of the salts were not determined, but they appear as white films on the glass, are highly soluble in water, and are assumed to be chloride-dominated.

Chlorine solubility in aluminosilicate melts is a strong function of composition. For a given bulk melt composition at a fixed pressure, maximum Cl solubilities occur in melts containing low to moderate H_2O contents (Fig. 1a,b), because higher H_2O concentrations reduce the Cl activity of melt and coexisting volatile phase(s). At comparatively H_2O-poor conditions, Cl solubility varies inversely with the silica concentration of melts. At 2000 bars, the single H_2O-poor phonotephrite melt (with 48 wt.% SiO_2) contains 1.53 wt.% Cl (Fig. 2) whereas the averaged Cl content of the five most Cl-enriched and H_2O-deficient phonolite melts (with approximately 58 wt.% SiO_2) is 0.84 wt.%. In a similar manner, the melt of the phonotephrite run at 500 bars dissolved 1.44 wt.% Cl, and the five most Cl-enriched and H_2O-deficient phonolite melts dissolved an average of 0.77 wt.% Cl. Recent investigation also demonstrates that Cl solubility varies dramatically with the molar (Al_2O_3/Na_2O+K_2O+CaO), the (CaO+MgO/Na_2O+K_2O), and other melt compositional parameters (Webster and De Vivo, 2002).

Chlorine solubility in volatile phase-saturated melts is a complex function of pressure (Figure 1). The maximum Cl solubility in H_2O-poor phonolite and phonotephrite melts observed at 2000 bars appears greater than that at 500 bars, but the larger data set shows this difference to be insignificant, statistically. Hence, the maximum Cl solubility in H_2O-poor melts does not vary strongly with pressure from 500 to 2000 bars. This observation is consistent with that recorded previously for molten haplogranite (Webster, 1997), topaz rhyolite (Webster and Rebbert, 1998), and andesite and basalt (Webster et al., 1999). For each of these bulk compositions, the 2000-bar run-product glasses contain marginally greater Cl abundances than their 500-bar equivalents.

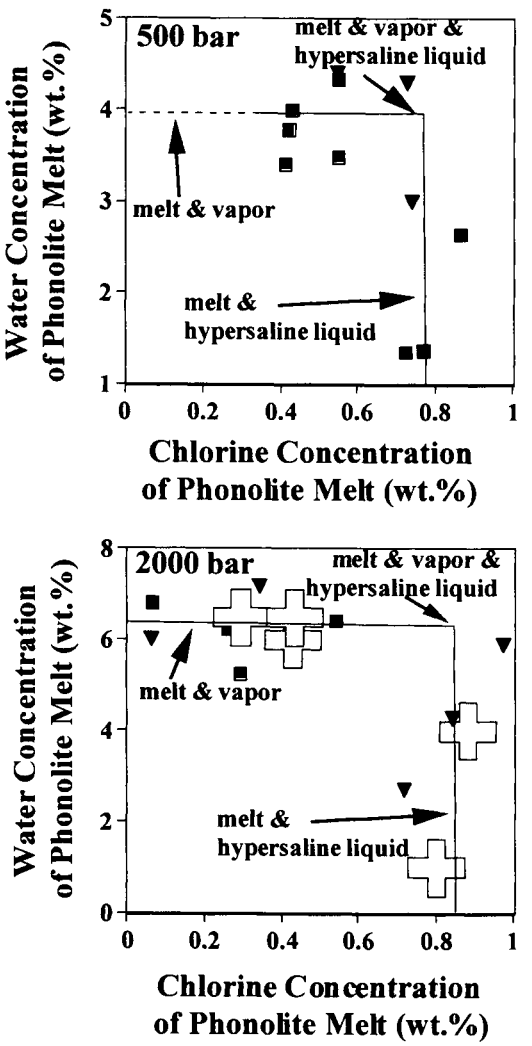

Figure 1. Curves expressing solubilities of H2O and Cl (wt.%) in volatile phase-saturated melts of Mt. Somma-Vesuvius phonolite at (A) 500 bar and 946 – 1000° C and (B) 2000 bar and 997 – 1057° C (with one 1166° C experiment). With constant and equivalent melt compositions, temperature, and pressure, the melts along vertical curves are saturated in hypersaline liquid, and melts along horizontal curves are saturated in vapor; melts are saturated in vapor plus hypersaline liquid at point of intersection of two curves. Water solubility varies much more strongly with pressure than Cl solubility. Water concentrations of run product glasses determined by FTIR (squares), SIMS (triangles), and computed by difference (large crosses). Size of symbols is approximately equivalent to precision on quoted H2O concentrations; Cl analyses are reproducible to ± 100 - 300 ppm for most glasses.

The complex nature of Cl dissolution in melt as a function of pressure, becomes apparent when it is noted that Cl solubility increases with decreasing pressure at H_2O-enriched conditions. The H_2O-poor glasses plotting along the vertical curves in Figure 1(A, B), involved the addition of Cl to the starting materials as NaCl-KCl salts and/or solutions. In contrast, the Cl in the majority of the H_2O-enriched glasses plotting along the horizontal curves in this figure was derived solely from that present in the natural rock powders, and the Cl concentrations of the melts (and run-product glasses) were varied by changing the ratios of H_2O to phonolite rock powder in the starting experimental charges. It is important to note that the range in (H_2O/rock powder) of the H_2O-enriched, 500-bar experiments is roughly equivalent to that of the H_2O-enriched, 2000-bar experiments, and yet, most of the 500-bar, H_2O-enriched, run product glasses contain > 4000 ppm Cl whereas the 2000-bar, H_2O-enriched glasses generally contain < 5000 ppm Cl. Thus, the melts of the lower pressure experiments conducted at H_2O-enriched conditions dissolved more Cl than those of the 2000-bar experiments, even though the bulk Cl contents in the system were roughly equivalent. All Cl not sequestered by the silicate melt was dissolved by the volatile phase(s). Consequently, H_2O-enriched

phonolite melt dissolves more Cl at 500 bar than at 2000 bar. This inverse relationship between pressure and the Cl solubility of H_2O-enriched melts has also been observed for phonolite melts (Signorelli and Carroll, 2000) and other melts saturated in vapor plus hypersaline liquid (Shinohara et al., 1989; Metrich and Rutherford, 1992; Shinohara, 1994).

Water solubility in phonolite melt varies with the Cl concentration of the melt and with other compositional parameters (Fig. 1). The H_2O concentrations of the 500-bar experimental glasses containing from 0.4 - 0.6 wt.% Cl, for example, range from 3 to 4.3 wt.%. This dispersion in H_2O, which applies to melts at a fixed pressure, is an apparent consequence of subtle variations in the molar (Al_2O_3/Na_2O+K_2O+CaO), molar (Na_2O/Na_2O+K_2O), and the F and Cl concentrations of the phonolite melts (Table 2). These melt parameters vary because of differences in the ratio of (H_2O+NaCl+KCl/rock powder) in the starting materials of the experimental charges.

DISCUSSION

Phase relations of hydrous, Cl-bearing experiments

The abundance of Cl in the phonolite and phonotephrite melts was controlled by equilibrating the melt with volatile phases, but correct determination of the volatile phase assemblage in each experiment is difficult because (1) the phase relations vary strongly with the electrolyte content of the system, and (2) the influence of Mg, Fe, and Ca (i.e., other cations present in these experiments) on electrolyte phase equilibria at elevated pressure and temperature is unknown even though the phase relations for NaCl and KCl solutions have been addressed previously (Sourirajan and Kennedy 1962; Bodnar et al. 1985; Chou 1987).

The solubilities of Cl and H_2O in volatile phase-saturated phonolite melts are shown in Figure 1 (A,B), and the stability of vapor versus hypersaline liquid varies with the (H_2O/Cl) ratio of the melt (Signorelli and Capaccioni, 1999). The horizontal curve depicts melt coexisting with vapor, the vertical curve represents melt with hypersaline liquid, and the point of intersection of the two curves represents melt coexisting with vapor and hypersaline liquid. At the conditions represented by the solid curves, exclusive of the point where vapor and hypersaline liquid coexist with melt, the concentrations of H_2O and Cl in silicate melt are free to vary as the H_2O and Cl contents of the system change - because the melt is in equilibrium with only one volatile phase. The Cl content of H_2O-poor melts does not vary significantly with changing H_2O in melt, however. In contrast, at the point of intersection of the two curves, the variability of the volatile contents of melt at conditions favoring subcritical volatile phase behavior is different. The system has one less degree of freedom because 3 phases are stable, and the phase rule requires that the activities of H_2O and Cl in all 3 phases are fixed (at those of the invariant point) if the H_2O and Cl contents in the system are changed. Detailed discussions of these theoretical phase relationships are available in Shinohara et al. (1989), Shinohara (1994), Candela and Piccoli (1995), and Webster et al. (1999).

It is also important to be aware of the differences between these hydrothermal experiments, with their inherent inadequacies, and the more tightly constrained nature of theory. It is highly likely that some of our experiments involved melt coexisting with vapor plus hypersaline liquid even though they do not plot at the point of intersection of the horizontal and vertical parts of the solubility curves (Fig. 1). Theoretically, if melt, hypersaline liquid, and vapor were stable at run conditions, then the melts should plot at the intersection of the two curves. This discrepancy is a result of differences in the compositions of the melts in

each of the experiments. The melt compositions of different experiments should be fixed at the point of intersection of the curves, only if the bulk melt compositions, temperature, and pressure of each experiment are identical. This is clearly not the case for our runs (Table 2), because the temperature and pressure show slight variations and the compositions show more marked differences. Thus, many of the other experiments (i.e., those plotting closest to the intersection of the vertical and horizontal curves) may have involved melt, vapor, and hypersaline liquid, and the curves represent averaged volatile solubilities for all of the experiments. Consequently, the only firm conclusions that we can draw, based on theoretical constraints, prior discussion (Shinohara et al., 1989; Webster et al., 1999), and our 500-bar and 2000-bar data sets, are that the experiments: (1) containing the lowest H_2O and highest Cl contents involved silicate melt plus hypersaline liquid; (2) containing comparatively more H_2O and the same (highest) Cl abundances involved melt, vapor, and hypersaline liquid (and hypersaline liquid was the volumetrically dominant volatile phase); (3) containing the lower Cl and higher H_2O contents involved melt, vapor, plus hypersaline liquid (and vapor was the volumetrically dominant volatile phase); and (4) experiments containing the lowest Cl and highest H_2O contents involved melt plus vapor.

Degassing of Cl-enriched, Mt. Somma-Vesuvius magmas

Given that the highly explosive, plinian and subplinian eruptions at Mt. Somma-Vesuvius involved volatile-charged phonolitic magmas it is informative to apply the experimentally determined volatile solubilities (Fig. 1, 2) to degassing phenomena in phonolitic and associated

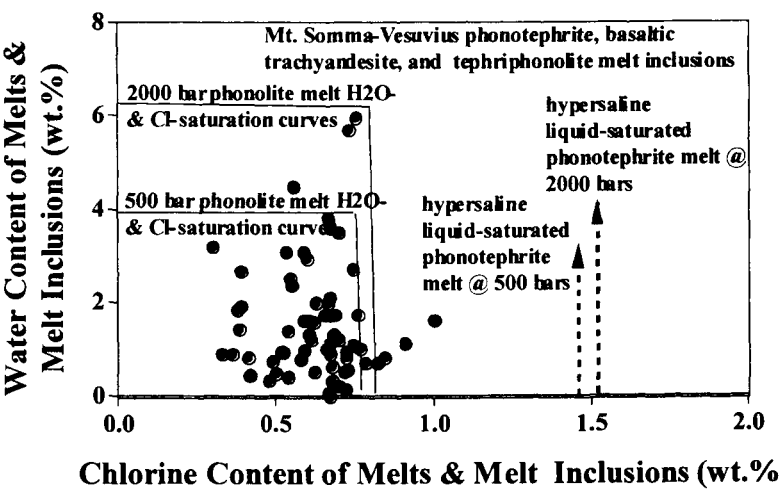

Figure 2. Curves expressing solubilities of H2O and Cl (wt.%) in volatile phase-saturated melts of Mt. Somma-Vesuvius phonolite (solid curves) and phonotephrite (dashed lines) at 500 and 2000 bars compared with H2O and Cl concentrations of silicate melt inclusions (filled circles) from Mt. Somma-Vesuvius. Compositions of melt inclusions include phonotephrite, basaltic trachyandesite, and tephriphonolite. The difference in Cl contents of hypersaline liquid-saturated phonotephrite versus hypersaline liquid-saturated phonolite melts demonstrates the strong influence of melt composition on Cl solubility. The heights of dashed curves have no significance.

melts at shallow crustal pressures. Saturation of magma in a volatile phase may occur through several "end-member" type scenarios including: (1) crystallization that increases the volatile

contents of residual fractions of melt because volatiles behave as incompatible elements (meaning that the volatile contents of residual melt increase until they equal those of the volatile solubility curve that is relevant to that melt composition, pressure, and temperature), (2) crystallization that changes the bulk composition of residual fractions of melt in such a way that one or more of the volatile components exceeds its solubility in melt (meaning that the volatile solubility curve shifts with bulk composition), and/or (3) a reduction in confining pressure that decreases volatile solubilities in melt (causing the volatile solubility curve to sweep toward lower volatile concentrations and achieve volatile contents that are equivalent to those of a given aliquot of melt). With regard to the second situation, experimental studies have determined that the solubilities of Cl (Webster and De Vivo, 2002), CO_2 (Dixon et al., 1995), and S (Carroll and Webster, 1994) vary markedly with melt composition, so in theory, magmas may saturate and exsolve Cl-, CO_2-, and/or S-rich, aqueous volatile phases if the melts evolve to compositions characterized by lower volatile solubilities. The solubility of H_2O, on the other hand, does not vary as significantly with changing melt composition (Moore et al., 1995; 1998).

Numerous studies have explored the exsolution of Cl-bearing volatile phases from magmas at Mt. Somma-Vesuvius through interpretation of MI compositions (Signorelli and Capaccioni, 1999; Signorelli et al., 1999; Signorelli and Carroll, 2000; Raia et al., 2000; Webster et al., 2001, Webster and De Vivo, 2002). The compositions of more than 250 MI in clinopyroxene and olivine phenocrysts from 28 individual rock samples of Mt. Somma-Vesuvius pumice, lava, and scoria (Marianelli et al., 1995; 1999; Belkin et al., 1998; Lima et al., 1999; Raia et al., 2000; Webster et al., 2001) show that the magmas were enriched variably in H_2O, Cl, S, P, and F and that pre-eruptive abundances of CO_2 in these magmas were low. As explained in the cited references, several of the studies involved partially crystallized MI that required reheating to glass before analysis, and some MI lost H_2O by diffusion while they were remelted. The extent of H_2O loss is considered minor.

We can compare the experimentally determined H_2O concentrations for vapor phase-saturated phonolite and phonotephrite melts with their abundances in the MI (Fig. 2). The MI vary in composition from phonotephrite and basaltic trachyandesite to tephriphonolite; few MI are phonolitic. Even though the melt and MI compositions differ from one to another, H_2O solubility does not vary dramatically through this range in composition. Computing the H_2O concentrations of H_2O-saturated phonolite and phonotephrite melts, with the model of Moore et al. (1995; 1998), determines that the difference in H_2O solubility is less than 0.5 wt.%. This difference is much smaller than the wide range in H_2O contents of the MI, so the H_2O values are useful for providing constraints on magmatic degassing. Those MI containing the highest H_2O contents and low to moderate Cl concentrations, for instance, represent melts that were or would have saturated in a H_2O-dominated vapor phase at 2000 bars or lower pressures (Figures 1 and 2). Clearly, the two MI that lie on or near the horizontal part of the 2000-bar curve represent aliquots of melt that would have exsolved vapor at this pressure. Most MI, however, lie below and to the left-hand side of the 500-bar saturation curves indicating that these MI represent melts that were or would have become saturated in vapor with or without hypersaline liquid at pressures of entrapment less than or near 500 bars.

In contrast, it is more difficult to interpret the exsolution of hypersaline liquid from melts represented by those MI containing the highest Cl and low to moderate H_2O concentrations (Fig. 2), because Cl solubility varies markedly with melt composition and because Mt. Somma-Vesuvius melts span a range of compositions. At 500 and 2000 bars, Cl

solubility in phonolite melt is slightly more than half that in the phonotephrite melt (Fig. 2). Clearly, most MI contain Cl concentrations (i.e., 3000 to 8000 ppm) that are approaching those of hypersaline liquid-saturated phonolite melts, but the compositions of most of these MI are more primitive. However, the Cl and H_2O concentrations of Mt. Somma-Vesuvius magmas will increase as they evolve toward phonolite compositions, because H_2O- and/or Cl-bearing phenocrysts are not abundant in these rocks and because H_2O and Cl respond like incompatible elements during crystallization. This follows from prior observations (Sigurdsson et al., 1985; Joron et al., 1987; Macedonio et al., 1990; Civetta and Santacroce, 1992; Belkin et al., 1993a;b; De Vivo et al., 1993; Ayuso et al., 1998; Webster and De Vivo, 2002) indicating that plinian and sub-plinian eruptive behavior is associated with dramatic changes in bulk melt composition and increasing volatile abundances in residual melt during differentiation.

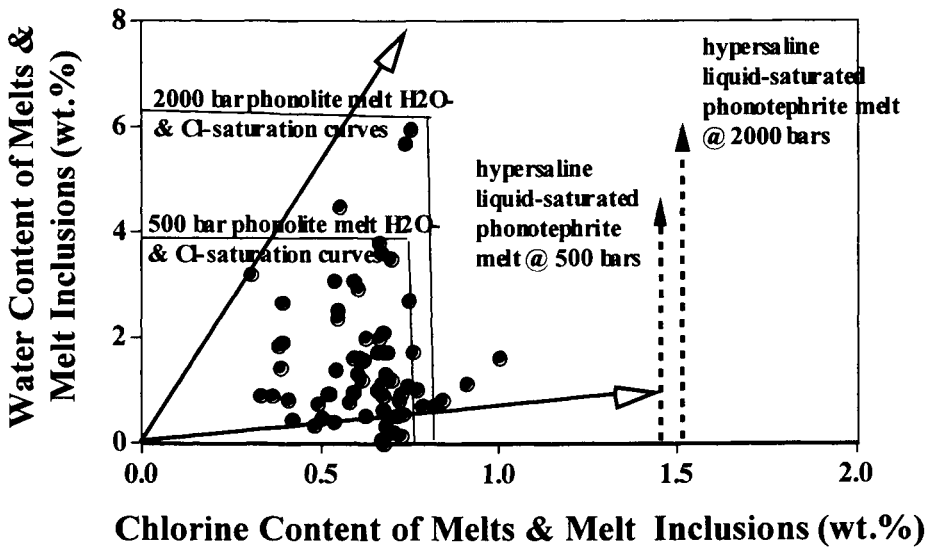

Figure 3. Curves expressing effect of magma evolution via fractional crystallization of H2O- and Cl-deficient phenocrysts on the Cl and H2O concentrations of residual melt (represented by lines with arrows) compared with curves expressing solubilities of H2O and Cl in volatile phase-saturated melts of Mt. Somma-Vesuvius phonolite (solid curves) and phonotephrite (dashed lines) and H2O and Cl in silicate melt inclusions (filled circles) from Mt. Somma-Vesuvius. Magma evolution increases H2O and Cl contents of residual melt until melt composition achieves abundances of H2O and Cl in volatile phase-saturated melt for a given temperature and pressure; subsequent crystallization causes one or more volatile phases to exsolve. Continued fractional crystallization at closed-system conditions drives melt compositions along volatile solubility curves to higher (H2O/Cl) ratios. The heights of dashed curves have no significance.

Magmatic crystallization increases the H_2O and Cl abundances of residual melts along trajectories oriented toward the volatile saturation curves and away from the origin. These compositional paths are linear because the volatiles behave, in effect, as incompatible elements in Mt. Somma-Vesuvius magmas (see open arrows in Fig. 3). The system remains volatile phase undersaturated until the melt composition intersects the volatile saturation curve for that pressure and temperature. It is important to understand that saturation in a H_2O-dominated vapor is not the only means of exsolving a volatile phase from Cl-bearing magmas. Magmas

may, alternatively, saturate in hypersaline liquid if the H_2O contents are significantly less than that required for H_2O saturation (Webster, 1997). Take, for example, the compositions of the most H_2O-deficient MI (Fig. 3). Any phonolitic MI with these Cl and H_2O contents represent melts that would saturate in and exsolve hypersaline liquid at pressures of 500 to 2000 bars.

Once a volatile phase exsolves, the H_2O and Cl concentrations of the melt are restricted to the values of the volatile saturation curves – relevant for that pressure, temperature, and composition - if the volatile phase remains in equilibrium with the melt (i.e., for closed-system conditions). Continued crystallization of a hypersaline liquid-saturated, phonolite melt at 2000 bars, for example, will force additional H_2O and Cl from the melt to the hypersaline liquid. Relatively more H_2O leaves the melt because Mt. Somma-Vesuvius magmas, like most magmas, contain far more H_2O than Cl and because Cl typically partitions in favor of volatile phases relative to phonolite and other silicate melts (Carroll and Webster, 1994; Signorelli and Carroll, 2000). Consequently, the melt composition moves to greater H2O contents along the vertical part of the 2000-bar saturation curve (Fig. 3), and with continued crystallization the phase assemblage varies from melt plus hypersaline liquid to melt plus vapor plus hypersaline liquid (at the intersection of the two curves). Under these conditions, the H2O and Cl activities of melt, vapor, and hypersaline liquid are fixed and the ratio of (vapor/hypersaline liquid) increases because vapor replaces hypersaline liquid as additional H2O and Cl exsolve from the melt (at the theoretical condition of constant bulk melt composition). With continued crystallization, the hypersaline liquid is completely replaced by vapor and the compositions of melt and vapor are again free to evolve toward lower and lower Cl contents (at high and comparatively fixed H2O concentrations along the horizontal volatile solubility curves).

In nature, magmatic crystallization is a result of decreasing temperature, so the effect of temperature should be addressed. There is, however, very little experimental evidence to suggest that Cl solubility varies significantly with temperature (Webster, 1997), and H_2O solubility varies marginally with temperature (Moore et al., 1998), so we assume that modest changes in temperature have a negligible influence on the solubilities of either volatile to a first approximation. Decreasing temperature does shift the critical point for the (NaCl-H_2O) system toward higher H_2O contents, and it reduces the width of the solvus (Fig. 4). Consequently, the stability field for vapor plus brine, in the more complex pseudo-system (phonolite melt -tephriphonolite melt - phonotephrite melt - H_2O) may change with temperature.

The bulk compositions of residual fractions of melt in Mt. Somma-Vesuvius magmas evolve with differentiation and Cl solubility in hypersaline liquid-saturated melts varies strongly with composition, so the vertical part of the Cl and H_2O solubility curves shifts with changing melt composition. Chlorine solubility in H_2O-poor melts can be computed for changing melt composition at constant pressure and closed-system conditions (Webster and De Vivo, 2002). Previous investigation (Signorelli and Capaccioni, 1999) modeled the evolution of Vesuvius magmas and resultant volatile phase exsolution, but the influence of melt composition on Cl solubility was not addressed. Our computations determine the shift in the vertical solubility curve for hypersaline liquid-saturated melts (Fig. 4). The dominant phenocrysts in Mt. Somma-Vesuvius rocks include clinopyroxene, olivine, leucite, sanidine, and plagioclase; iron-titanium oxides and apatite are common accessory phases. We have computed the influence of up to 30 wt.% crystallization of each phenocryst and d" 5 wt.% crystallization of apatite and these oxides to constrain the relative effects of each phase on

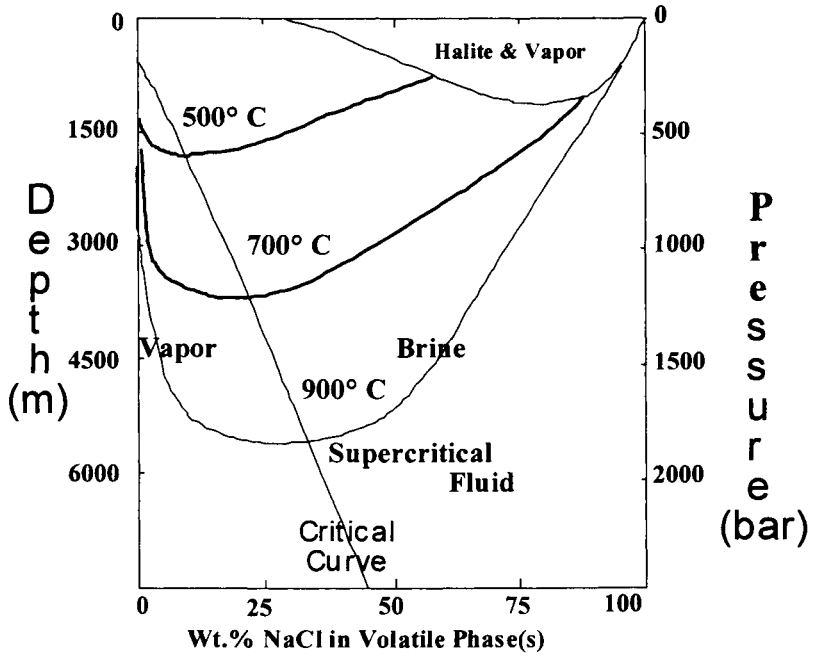

Figure 4. Phase equilibria for the system: NaCl-H2O at shallow crustal pressures modified after Sourirajan and Kennedy (1962), Bodnar et al. (1985), and Chou (1987). The brine phase of this binary system is considered analogous to the hypersaline liquid exsolved from natural Cl-enriched magmas.

changes in melt composition, Cl solubility, and hypersaline liquid exsolution. The solubility of H_2O in silicate melts varies much less than that of Cl with these changes in melt composition, so we assume that the relationship between H_2O solubility and melt composition is negligible. In effect, the shift in the horizontal part of the solubility curves is negligible with modest changes in temperature. It is clear that, among the predominant phenocrysts, the crystallization of olivine and clinopyroxene has the greatest effect on reducing Cl solubility, whereas plagioclase has a lesser influence.

Fractionation of leucite or sanidine, on the other hand, actually serves to enhance Cl solubility in melt and inhibit hypersaline liquid exsolution, because it decreases the SiO_2 content and increases the CaO and MgO concentrations as well as the (Na_2O/Na_2O+K_2O) ratio of the melt. The crystallization of iron-titanium oxides and apatite has a relatively minor effect on Cl solubility, but interestingly, the crystallization of Cl-bearing apatites reduces Cl solubility while simultaneously sequestering Cl from residual melt. As a consequence of clinopyroxene, plagioclase, and apatite crystallization, Cl solubility decreases which shifts the vertical part of the solubility curve toward the origin. The petrographic and geochemical observations of Joron et al. (1987) indicate that the evolution of Mt. Somma-Vesuvius phonotephrite to phonolite melt compositions is a function of olivine, clinopyroxene, and plagioclase (with or without leucite) crystallization, and Belkin et al. (1998) concluded that melt evolution was dominated by fractionation of clinopyroxene. This causes the (CaO+MgO) contents of melts to decrease from 16 to < 2 wt.%, respectively, and the change in melt composition engenders a strong reduction in Cl solubility. This also means that the chemical evolution of a volatile phase-saturated melt to phonolitic compositions at closed-

system conditions will result in the sequestering of much more Cl into the volatile phase(s) than will occur with less evolved phonotephrite and tephriphonolite melts. In summary, crystallization forces all excess H_2O and Cl into the volatile phase(s) and drives residual melt compositions along H_2O-Cl solubility curves toward lower Cl and higher H_2O contents. Moreover, if crystallization is dominated by clinopyroxene and plagioclase, the solubility curves will shift, simultaneously, to lower Cl concentrations due to changing melt composition, and this further enhances the Cl concentrations of volatile phases.

The influence of melt composition on Cl solubility and degassing processes can be equally significant within the compositional field for evolving phonolite melts. For example, after extensive magmatic differentiation has occurred (i.e., once the Ca and Mg contents of the residual melt have dropped to appropriately lower levels), the compositional evolution of phonolite melts will be dominated by leucite or sanidine crystallization, and the solubility of Cl in the melt will begin to increase again because of decreasing SiO_2 and increasing CaO, MgO and (Na_2O/Na_2O+K_2O) (Fig. 5). This is consistent with the observation of increasing Cl with increasing (Na_2O/K_2O) in Mt. Somma-Vesuvius whole-pumice samples and glassy

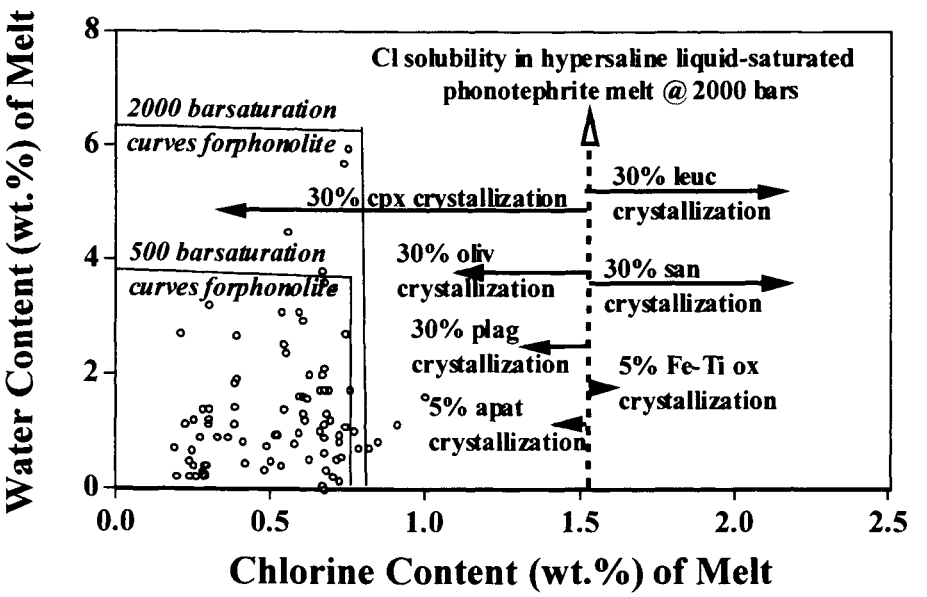

Figure 5. Curves expressing the solubilities of H2O and Cl (wt.%) in volatile phase-saturated melt of Mt. Somma-Vesuvius phonolite at 500 and 2000 bars compared with H2O and Cl concentrations of silicate melt inclusions (circles) from Mt. Somma-Vesuvius and the computed change in the solubility of Cl in brine-saturated melt (at 2000 bars with initial composition of phonotephrite) as a function of fractional crystallization of clinopyroxene (cpx), olivine (oliv), plagioclase (plag), leucite (leuc), sanidine (san), apatite (apat), and iron-titanium oxides (Fe-Ti ox). Ends of solid arrowheads represent the Cl content of hypersaline liquid-saturated melt after fractional crystallization of 30 wt. % or 5 wt.% crystallization of the mineral listed. Crystallization of clinopyroxene and olivine have the greatest effect in reducing Cl solubility; whereas, leucite and sanidine fractionation increase Cl solubility. Crystallization of clinopyroxene and olivine will reduce Cl solubility into the range of Cl contents of Mt.Somma-Vesuvius melt inclusions and lead to hypersaline liquid exsolution. The height of dashed curve has no significance.

mesostases (i.e., the *leucite effect* described by Signorelli and Capaccioni [1999]). Crystallization that is dominated by leucite and sanidine will enhance Cl solubility in melt and reduce the tendency of hypersaline liquid exsolution.

These modifications in the bulk composition of the melt should also affect the phase relations of coexisting vapor and hypersaline liquid. Crystallization modifies the abundances of Ca, Mg, Fe, Na, K, and H in the melt and coexisting aqueous volatile phases, and the position of the critical curve and the width of the vapor plus brine solvus are presumably strong functions of the Ca, Mg, Fe, Na, K, and H contents of the volatile phases. Thus, even though two volatile phases may coexist with melt (which should serve to fix the Cl and H_2O concentrations of the melt), any change in the solvus resulting from changing cation abundances in the volatile phases will preclude compositional buffering in the system. Unfortunately, however, there are no published experimental data that bear on the phase equilibria of complex electrolyte solutions at magmatic conditions, so we cannot model, quantitatively, changes in the critical point and solvus of such compositionally complex systems.

The final type scenario for volatile phase exsolution involves the influence of changing pressure on volatile solubilities. If pressure is reduced from 2000 to 500 bars under closed-system conditions, the Cl and H_2O contents of phonolite melt will be constrained to shift from the 2000-bar to the 500-bar solubility curves. The solubility of H_2O in melt will diminish by one third if the melt is vapor dominated, whereas Cl solubility decreases only marginally if hypersaline liquid is the dominant volatile phase. Thus, for H_2O-enriched melts saturated in vapor, magma ascent will exsolve a significant quantity of H_2O from melt to vapor, which will involve a significant increase in the mass of vapor in the magma. In contrast, for hypersaline liquid-saturated magma, the ascent of magma will exsolve comparatively less Cl from melt to hypersaline liquid and the quantity of magmatic hypersaline liquid will not increase as significantly with Cl-enriched melts and only one stable volatile phase. The response of vapor- and hypersaline liquid-bearing magmas to decreasing pressure is more difficult to address simply because the effect of pressure on the equilibria of aqueous Ca-, Mg-, Fe-, Na-, K-, and H-bearing chloride volatile phases at magmatic conditions is unknown, so we do not discuss this situation further.

Volatile phase exsolution and eruptive processes

Eruptive styles of Mt. Somma-Vesuvius magmas correlate with volatile abundances and the type of volatile phases that exsolves. Melt inclusions suggest that magmatic CO_2 abundances were low at some stages of magma evolution (Marianelli et al., 1995), so H_2O, Cl, and S appear to have played a more dominant role in magmatic and eruptive processes. The MI also show (Fig. 6) that scoria and lava samples erupt from H_2O-poor, Cl-enriched magmas that are more likely to exsolve hypersaline liquid (with or without vapor), whereas magmas associated with comparatively explosive eruptions that form pumice are more likely to release an aqueous vapor (with or without hypersaline liquid). Crystallization and magma evolution increase the abundances of H_2O and Cl in residual melt along linear paths while concurrently reducing the solubility of Cl in the melt. And, as noted previously, the order of appearance of vapor versus hypersaline liquid varies with the (H_2O/Cl) ratio of the melt. The projection of the most Cl-enriched MI compositions (which are associated with scoria- and lava-forming eruptions) to higher total volatile abundances clearly indicates that melt compositions like these will intersect the vertical portion of the solubility curves meaning that the solubility limit for Cl is achieved before the solubility limit for H_2O. Consequently,

hypersaline liquid (with or without vapor) exsolves first. Conversely, projecting the increase in the abundances of H_2O and Cl in the more H_2O-enriched MI (which are associated with pumice-forming eruptions) suggests that, initially, these magmas are more likely to exsolve vapor than hypersaline liquid. This is consistent with an earlier observation that cumulate and subeffusive nodules erupted during plinian events tend to contain abundant, H_2O-rich fluid inclusions; whereas these inclusions are much more rare in nodules brought to the surface during non-plinian events (Belkin and De Vivo, 1993).

It is important to understand that with continued ascent and depressurization of hypersaline liquid-saturated magma at closed-system conditions, aqueous vapor will exsolve from the hypersaline liquid and the magma will thereafter evolve in the presence of two stable volatile phases (Fig. 4). However, the initial (hypersaline liquid/vapor) ratio of this situation will be significantly greater than that associated with explosively erupting Mt. Somma-Vesuvius magmas.

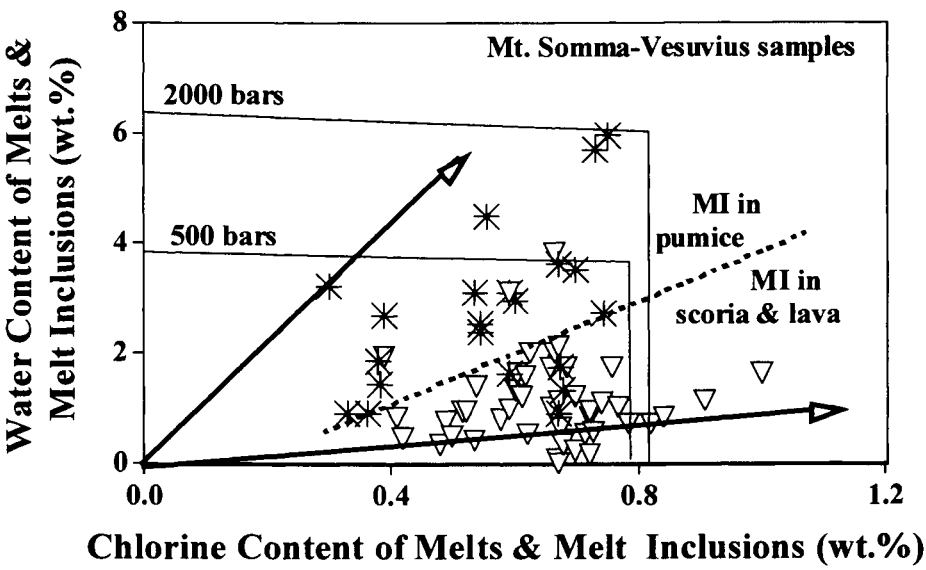

Figure 6. Curves expressing the concentrations of H2O and Cl (wt.%) in volatile phase-saturated melt of Mt. Somma-Vesuvius phonolite at 500 and 2000 bars compared with H2O and Cl concentrations of Mt. Somma-Vesuvius melt inclusions (of phonotephrite to tephriphonolite composition). Melt inclusions in explosively erupted, pumice-forming magma shown as asterisks, and inclusions erupted during comparatively passive scoria- and lava-forming behavior shown as triangles. Increasing abundances of volatiles in residual melt (resulting from fractional crystallization) and/or reduction in the Cl solubility of the melt, (due to crystallization dominated by clinopyroxene and olivine - see Fig. 5) results in hypersaline liquid saturation (with or without vapor) of residual melt for MI erupted in lava and scoria. In contrast, these same processes are more likely to result in exsolution of vapor (with or without hypersaline liquid) for explosively erupting, pumice-forming Mt. Somma-Vesuvius magmas.

In summary, explosive, pumice-forming eruptions at Mt. Somma-Vesuvius occur after extensive compositional evolution of magma to phonolitic compositions that are enriched in H_2O, Cl, and S. These evolved magmas are more likely to exsolve an aqueous vapor with or without hypersaline liquid. Comparatively passive eruptive behavior that generates lava flows and scoria occurs from less-evolved magmas that contain less H_2O and exhibit lower

(S/Cl) ratios. The latter magmas are more likely to exsolve hypersaline liquid with or without vapor, initially. The solubility of associated magmatic gaseous compounds, such as CO_2, HCl, and others, is significantly greater in vapor versus hypersaline liquid (Hedenquist and Lowenstern, 1994), so explosive eruptions may involve more of these species than passive eruptions. For example, plinian eruptions involve magmas that are enriched in S and the solubility of S is greater in vapor versus hypersaline liquid, so it follows that pre-eruptive magmatic degassing may emit vapors that are distinctly enriched in S. These conclusions are based on the observation that CO_2 is not particularly abundant in these magmas and the assumption that the vapor pressure of CO_2 does not exert a strong control on degassing.

The timing of volatile exsolution bears strongly on eruptive process. Prior investigations have concluded that volatile phases exsolved from Mt. Somma-Vesuvius magmas at shallow crustal depths prior to eruption. Pre-eruptive volatile phase exsolution has been called upon, based on MI studies (Marianelli et al., 1999; Signorelli and Capaccioni, 1999; Raia et al., 2000; Webster et al., 2001). Isotopic evidence (Cortini and Hermes, 1981) and fluid inclusion geobarometry (Belkin et al., 1985; Cortini et al., 1985; Belkin and De Vivo, 1993) also indicate that eruptions were fed from shallow (4 to 5 km depth) and deeper (roughly 8 to 13 km depth) magma chambers. Furthermore, recent tomographic data (Zollo et al., 1998) indicate a sharp transition into a low-velocity zone (representing a magma chamber) at about 10 km depth. Thus, the findings of Cortini and Hermes (1981), Belkin et al. (1985), Cortini et al. (1985), Belkin and De Vivo (1993), and Marianelli et al. (1995; 1999) are consistent with a model that suggests shallow and deep magma chambers underlie this volcano (Lima et al., this volume). Comparison of our experimental results with the MI compositions implies that vapor, with or without hypersaline liquid, may have exsolved from compositionally evolved phonolite magmas at depths of at least 6 km (i.e., at pressures of at least 2000 bar), so our results are also consistent with prior findings and with the results of Lima et al. (this volume).

Acknowledgements. We gratefully acknowledge review of the manuscript by H. Belkin. Support for this study was provided by the INGV-GNV to B. De Vivo for years 2000-2001 and by NSF award EAR-9526622 to J. D. Webster.

REFERENCES

Ayuso R.A., B. De Vivo, G. Rolandi, R.R. Seal II and A. Paone, 1998, Geochemical and isotopic (Nb-Pb-Sr-O) variations bearing on the genesis of volcanic rocks from Vesuvius, Italy. J. Volcanol. Geotherm. Res., **82**, 53-78.

Belkin H.E. and B. De Vivo, 1993, Fluid inclusion studies of ejected nodules from plinian eruptions of Mt. Somma-Vesuvius. In. Vesuvius, Eds. B. De Vivo, R. Scandone and R. Trigila, J. Volcanol. Geotherm. Res., **58**, 89-100.

Belkin H.E., C.R.J. Kilburn and B. De Vivo, 1993a, Sampling and major element chemistry of the recent (A.D. 1631-1944) Vesuvius activity. J. Volcanol. Geotherm. Res., **58**, 273-290.

Belkin H.E., C.R.J. Kilburn and B. De Vivo, 1993b, Chemistry of the lavas and tephra from recent (A.D. 1631-1944) Vesuvius (Italy) volcanic activity. U.S. Geol. Surv. Open-File Rep. 93-399, 44 p.

Belkin H.E., B. De Vivo, E. Roedder and M. Cortini, 1985, Fluid inclusion geobarometry from ejected Mt. Somma-Vesuvius nodules. Am. Mineral., **70**, 288-303.

Belkin H.E., B. De Vivo, K. Török and J.D. Webster, 1998, Pre-eruptive volatile content, melt inclusion chemistry, and microthermometry of interplinian Vesuvius lavas (pre-1631 A.D). J. Volcanol. Geotherm. Res., **82**, 79-95.

Bodnar R.J., C.W. Burnham and S.M. Sterner, 1985, Synthetic fluid inclusions in natural quartz. III. Determination of phase equilibrium properties in the system H_2O-NaCl to 1000° C and 1500 bars. Geochim. Cosmochim. Acta, **49**, 1861-1873.

Burnham C.W., 1981, Nature of multicomponent aluminosilicate melts. In. Chemistry and Geochemistry of Solutions at High Temperatures and Pressures, Eds. D.T.Rickard and F.E. Wickman, Pergamon Press, vols. 13 & 14, pp. 197-229.

Candela P.A. and P.M. Piccoli, 1995, Model ore-metal partitioning from melts into vapor and vapor/brine mixtures. In. Magmas, Fluids, and Ore Deposits, Ed. J.F.H. Thompson, Min. Ass. Can., 23, 101-127.

Carroll M.R. and J.D. Webster, 1994, Solubilities of sulfur, noble gases, nitrogen, chlorine, and fluorine in magmas. In. Volatiles in Magmas, Eds. M.R. Carroll and J.R. Holloway, Rev. Min., 30, 231-279.

Chou I-M., 1987, Phase relations in the system NaCl-KCl-H_2O. III: Solubilities of halite in vapor-saturated liquids above 445°C and redetermination of phase equilibrium properties in the system NaCl-H_2O to 1000° C and 1500 bars. Geochim. Cosmochim. Acta, **51**, 1965-1975.

Civetta L. and R. Santacroce, 1992, Steady state magma supply in the last 3400 years of Vesuvius activity. Acta. Vulcan., **2**, 147-159.

Cortini M. and D.H. Hermes, 1981, Sr isotopic evidence fro a multi-source origin of the potassic magmas in the Neapolitan area (S. Italy). Con. Min. Petrol., **77**, 47-55.

Cortini M., A. Lima and B. De Vivo, 1985, Trapping temperatures of melt inclusions from ejected Vesuvian mafic xenoliths. J. Volcanol. Geotherm. Res., **26**, 167-172.

De Vivo B., R. Scandone, and R.Trigila, 1993, Special Issue: Mount Vesuvius. J. Volcanol. Geotherm. Res., **58**, 1-381.

De Vivo B. and G. Rolandi, Eds., 2001, Mt. Somma-Vesuvius and volcanism of the Campanian Plain. Min. Petrol., **73**, 233 p.

Dixon J.E., E.M. Stolper and J.R. Holloway, 1995, An experimental study of water and carbon dioxide solubilities in mid-ocean ridge basaltic liquids. Part I: Calibration and solubility models. J. Petrol., **36**, 1607-1631.

Gladstone J.H. and T.P. Dale, 1864, Researches on the refraction, dispersion, and sensitiveness of liquids. Phil. Trans. Royal Soc. Lond., **153**, 317-343.

Hedenquist J.W. and J.B. Lowenstern, 1994, The role of magmas in the formation of hydrothermal ore deposits. Nature, **370**, 519-527.

Joron J.L., N. Métrich, M. Rosi, R. Santacroce and A. Sbrana, 1987, Somma-Vesuvius. III. Chemistry and petrography. in "Quaderni de la ricerca scientifica", In "Quaderni de la ricerca scientifica", Ed. R. Santacroce, CNR Publ., **8**, 105-174.

Lima A., H.E. Belkin and K. Török, 1999, Primitive silicate-melt inclusions in compositionally diverse clinopyroxene phenocrysts from the medieval scorias from the Terzigno Formation: Clue to understanding of Vesuvius magmatic processes. Min. Petrol., **65**, 185-206.

Lima A., L.V. Danyushevsky, B. De Vivo and L. Fedele, 2003.A model for the evolution of the Mt. Somma-Vesuvius magmatic system based on fluid and melt inclusion investigations. This volume.

Macedonio G., M.T. Pareschi and R. Santacroce, 1990, Renewal of explosive activity at Vesuvius: models for the expected tephra fallout. J. Volcanol. Geotherm. Res., **40**, 327-342.

Mandeville C.M., J.D. Webster, M.J. Rutherford, B.E.Taylor, A. Timbal and K. Faure, 2002, Determination of molar absorptivities for infrared absorption bands of H_2O in andesitic glasses. Am. Min., **87**, 813-821.

Marianelli P., N. Métrich, R. Santacroce, and A. Sbrana, 1995, Mafic magma batches at Vesuvius: a glass inclusion approach to the modalities of feeding stratovolcanoes. Con. Min. Petrol., **120**, 159-169.

Marianelli P., N. Métrich, A. Sbrana, 1999, Shallow and deep reservoirs involved in magma supply of the 1944 eruption of Vesuvius. Bull. Volcanol., **61**, 48-63.

Metrich N. and M. J. Rutherford, 1992, Experimental study of chlorine behavior in hydrous silicic melts. Geochim. Cosmochim. Acta, **56**, 607-616.

Moore G., R. Vennemann and I.S.E. Carmichael, 1995, The solubility of water in magmas to 2 kbar. Geol., **23**, 1099-1102.

Moore G., R. Vennemann and I.S.E. Carmichael, 1998, An empirical model for the solubility of H_2O in magmas to 3 kilobars. Amer. Min., **83**,136-142.

Raia, F., J.D. Webster and B De Vivo, 2000, Pre-eruptive volatile contents of Vesuvius magmas: constraints on eruptive history and behavior. I - The medieval and modern interplinian activities, Eur. J. Min., **12**, 179-193.

Rolandi G., P. Petrosino and J. Mc Geehin, 1998, The interplinian activity at Somma-Vesuvius in the last 3500 years. J. Volcanol. Geotherm. Res., **82**, 19-52.

Santacroce R., A. Bertagnini, L. Civetta, P. Landi, and A. Sbrana, 1993, Eruptive dynamics and petrogenetic processes in a very shallow magma chamber reservoir, the 1906 eruption of Vesuvius. J. Petrol., **34**, 383-425.

Shinohara H., 1994, Exsolution of immiscible vapor and liquid phases from a crystallizing silicate melt: Implications for chlorine and metal transport. Geochim. Cosmochim. Acta, **58**, 5215-5222.

Shinohara H., J.T. Iiyama and S. Matsuo, 1989, Partition of chlorine compounds between silicate melt and hydrothermal solutions. Geochim. Cosmochim. Acta, **53**, 2617-2630

Signorelli S. and B. Capaccioni, 1999, Behavior of chlorine prior and during the 79 AD Plinian eruption of Vesuvius (southern Italy) as inferred from the present distribution in glassy mesostases and whole-pumices. Lithos, **46**, 715-730.

Signorelli S. and M. R. Carroll, 2000, Solubility and fluid-melt partitioning of Cl in hydrous phonolitic melts. Geochim. Cosmochim. Acta, **64**, 2851-2862.

Signorelli S., G. Vaggelli and C. Romano, 1999, Pre-eruptive volatile (H_2O, F, Cl, and S) contents of phonolitic magmas feeding the 3550-year old Avellino eruption from Vesuvius, southern Italy. J. Volcanol. Geotherm. Res., **93**, 237-256.

Sigurdsson H., S. Carey, W. Cornell and T. Pescatore, 1985, The eruption of Vesuvius in A.D. 79. Nat. Geog. Res., **1**, 332-387.

Silver L.A. and E.M. Stolper, 1989, Water in albitic glasses. J. Petrol., **30**, 667-709.

Sourirajan S. and G. C. Kennedy, 1962, The system H_2O-NaCl at elevated temperatures and pressures. Amer. J. Sci., **260**, 115-141.

Spera F.J., B. De Vivo, R.A. Ayuso and H.E. Belkin, Eds., 1998, Vesuvius. J. Volcanol. Geotherm. Res., **82**, 247 p.

Vaggelli G., B. De Vivo and R. Trigila (1993) Silicate melt inclusions in recent Vesuvius lavas (1631-1944). II. Analytical chemistry. J. Volcanol. Geotherm. Res., **58**, 367 – 376.

Webster J.D., 1997, Exsolution of magmatic volatile phases from Cl-enriched mineralizing granitic magmas and implications for ore metal transport. Geochim. Cosmochim. Acta, **61**, 1017-1029.

Webster J.D. and B. DeVivo, 2002, Experimental and modeled solubilities of chlorine in aluminosilicate melts, consequences of magma evolution, and implications for exsolution of hydrous chloride melt at Mt. Somma-Vesuvius. Amer. Min., **87**, 1046-1061.

Webster J.D. and C.R. Rebbert, 1998, Experimental investigation of H_2O and Cl solubilities in F-enriched silicate liquids: implications for volatile saturation of topaz rhyolite magmas. Con. Min. Petrol., **132**, 198-207.

Webster J.D., R.J. Kinzler and E.A. Mathez, 1999, Chloride and water solubility in basalt and andesite liquids and implications for magmatic degassing. Geochim. Cosmochim. Acta, **63**, 729-738.

Webster J.D., F. Raia, B. DeVivo and G. Rolandi, 2001, The behavior of chlorine and sulfur during differentiation of the Mt. Somma-Vesuvius magmatic system. Min. Petrol., **73**, 177-200.

Zollo A, P. Gasparini, J. Virieux, G. Biella, E. Boschi, P. Capuano, R. de Franco, P. Dell'aversana , R. de Matteis, G. de Natale, G. Jannaccone, I. Guerra, H. Le Meur and L. Mirabile, 1998, An image of Mt. Vesuvius obtained by 2D seismic tomography. J. Volcanol. Geotherm. Res., **82**, 161-173.

A model for the evolution of the Mt. Somma-Vesuvius magmatic system based on fluid and melt inclusion investigations

Annamaria Lima[1], Leonid V. Danyushevsky.[2], Benedetto De Vivo[1], and Luca Fedele[1]

[1] Dipartimento di Geofisica e Vulcanologia. University of Napoli "Federico II", Napoli, Italy.
[2] School of Earth Sciences and CODES SRC, Univ. of Tasmania, Hobart, Tasmania, Australia.

ABSTRACT

In this paper, we present compositional data of reheated silicate melt inclusions (MI) from cumulate nodules and from one skarn xenolith trapped by olivine and clinopyroxene crystals. All MIs were analyzed by electron microprobe, while some were selected to be analyzed by secondary ion mass spectrometry (SIMS). Based on petrography and mineral compositions, clinopyroxene in the studied nodules can be divided into three types: cumulus pyroxene; post-cumulus pyroxene and fassaitic pyroxene present in the skarn nodule. The coherent trends displayed by the compositions of cumulus and post-cumulus clinopyroxene suggest that they formed at variable stages of fractionation of a single magmatic system. MIs in nodules display large compositional variations. Their compositions are not consistent with an olivine-clinopyroxene co-crystallization, which is a well-established feature of Vesuvius volcanism. Olivine and clinopyroxene from the nodules may have crystallized from the pre-79 AD Vesuvius magmas. Alternatively, variations in MI compositions may result from post-entrapment re-equilibration with their hosts during residence within the magmatic system prior to eruption. The compositions of MIs in clinopyroxene from the skarn nodule are characterized by anomalously low TiO_2 and P_2O_5 contents and high Na_2O/K_2O values. FI and MI, in conjunction with data available from previous research, suggest that Mt. Somma-Vesuvius plumbing system is made up of small magma chambers at depths greater than 3.5 km and that possibly a larger chamber exists at or below 12 km. The entire system likely resembles a complex feeding column which is dominated by multiple mush zone environments (small magma chambers), and thus includes a variety of local crystallization environments characterized by contrasting cooling rates and P-T conditions.

INTRODUCTION

Mt. Somma-Vesuvius is one of the best studied active volcanoes on the Earth due to both interest of the scientific community in the origin of silica-undersaturated alkaline rocks, and the necessity of assessing the risk that this volcano presents for the population inhabiting its slopes (about one milion inhabitants).

Melt inclusion studies is a powerful tool for understanding crystallization and mixing histories of magmas and also the conditions of primary melt generation and extraction. Melt inclusion compositions retain valuable information on pre eruptive magma chemistry, including

volatile contents. For these reasons we have analyzed by electron microprobe (EMP) and secondary ion mass spectrometry (SIMS) reheated melt inclusions (RMI) hosted in olivine and clinopyroxene from four cumulates and one skarn ejecta collected in Mt Somma Vesuvius volcanic products. To delineate the magma evolution and crystallization history of the Mt.

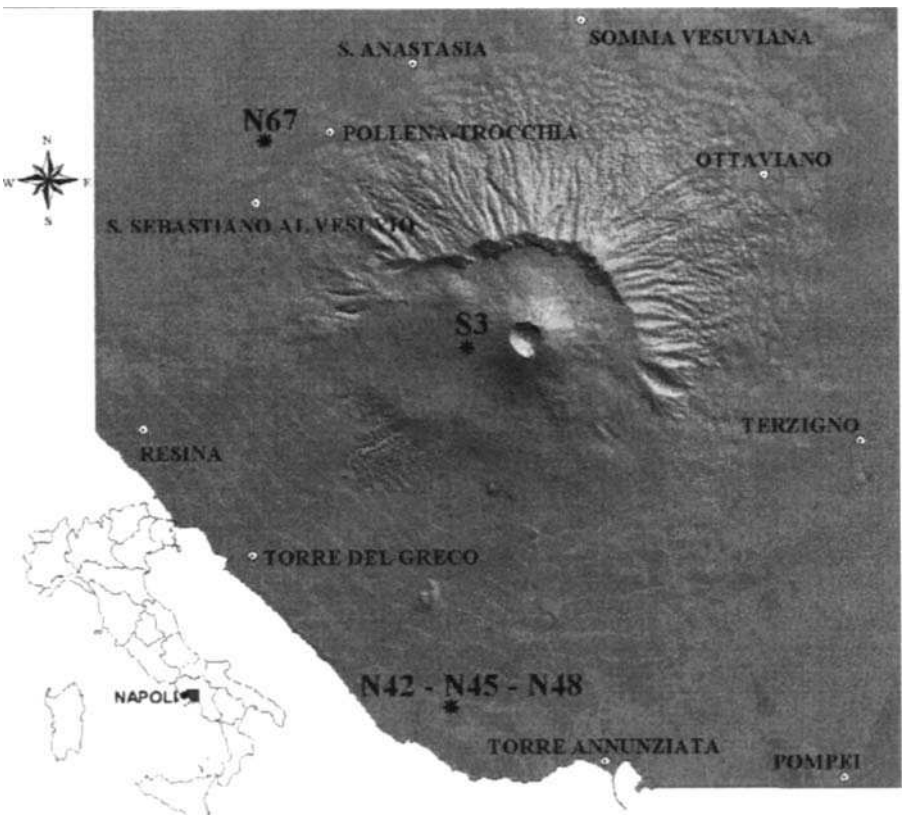

Fig. 1 - Studied Xenoliths location map.

Somma-Vesuvius system these new data have been compared with MI data on olivine and clinopyroxene from lava, scoria and pumice of post-79 AD activity and also with the post-79 volcanic bulk rock compositions. In addition we propose a model of the Mt. Somma-Vesuvius plinian and inter-plinian activity which implies a long repose time after the 1944 eruption.

GEOLOGICAL SETTING

During the Quaternary period, potassium-rich volcanism developed in central and southern Italy forming the Roman Comagmatic Province (Washington, 1906) located along the Tyrrhenian margin and extending from Vulsini to the Vulture Volcanic Complex. This volcanism is related to intense block-faulting and rifting which took place from the Upper Miocene on the western side of the Appennine chain (Beccaluva et al., 1991; Turco and Zuppetta, 1998).

The Mt. Somma Vesuvius complex is a composite volcano situated on a NW SE fault in the southernmost end of the Roman Province, south of the Campanian Plain (Figure 1).

Numerous detailed field studies (e.g. Arnò et al., 1987; Santacroce, 1987; Rolandi et al., 1993a,b,c; Rolandi, 1997; Rolandi et al., 1998) and careful documentation of trace-element (Joron et al, 1987; Civetta and Santacroce, 1992; Belkin et al., 1993; Villemant et al., 1993; Belkin et al., 1998; Raia et al., 2000; Webster et al., 2001) and isotopic compositions (e.g. Civetta et al., 1991; Caprarelli et al., 1993; D'Antonio et al., 1995; Ayuso et al., 1998; Somma et al. 2001) of Mt. Somma-Vesuvius volcanics resulted in significant advances in our understanding of the magmatic history of this volcano.

Mt. Somma began its eruptive activity at least 35 ka BP (Scandone et al., 1993), however the first episode of volcanic activity within the Mt. Somma-Vesuvius area has been dated at 400 ka BP and occurred in a marine environment (Brocchini et al., 2001). According to Rolandi et al. (1998) Vesuvius cone is significantly younger, being built by post-472 AD interplinian activity that followed the 472 AD plinian eruption. A longer period of Mt. Somma activity (up to 3.5 ka at least) has been also suggested by Webster et al (2001) on the basis of geochemical evidence.

The eruptive styles and cyclicity of the Mt. Somma-Vesuvius system have varied widely. The effusive lava flow and scoria eruptions were the most common type of volcanism during the past 3.5 ka, but they were periodically superseded by highly explosive plinian eruptions of pumice and ash that also involved pyroclastic flows and surges.

Mt. Somma-Vesuvius products include basic, silica-undersaturated, potassic rocks, ranging from tephrite to phonolite, and less alkaline basaltic trachyandesites. Ayuso et al. (1998) have separated Mt. Somma-Vesuvius volcanics into three age groups characterised by a gradual change in their compositions. The three groups display distinct positive trends of alkalis versus silica, which become increasingly steeper with age. In the first group, there is an increase in silica and alkalis with time, whereas an opposite tendency is observed in two younger groups.

Despite a significant effort put into understanding Mt. Somma-Vesuvius magmatism, the depth and physical parameters of its magma chamber(s) remain uncertain. Using petrological and isotopic data, Santacroce et al. (1993) suggested that a single magma reservoir is located at a shallow depth within the limestone basement, whereas others used isotopic and CO_2-rich fluid inclusion data to infer the existence of at least two reservoirs (Cortini and Hermes, 1981; Belkin et al., 1985; Cortini et al., 1985; Belkin and De Vivo, 1993; Marianelli et al., 1999). Geodetic data showed the absence of ground deformations in recent years, which would be expected if a shallow magma chamber existed, and high resolution seismic tomography investigations also did not resolve a shallow magma chamber. Instead, the latter study identified a sharp transition to a low-velocity zone at >8 km, which may represent the top of a magma chamber (Zollo et al., 1998; Auger et al., 2001). This confirmed earlier findings of Belkin et al. (1985), Belkin and De Vivo (1993), and Marianelli et al. (1999).

PREVIOUS STUDIES OF MT. SOMMA-VESUVIUS NODULES

A variety of metamorphic and metasomatized sedimentary nodules, ranging from carbonates to silicic skarn rocks, and also cumulate ejecta are commonly present in later Mt. Somma-Vesuvius pyroclastic products. Originally described by Zambonini (1910), these nodules have been extensively studied by Hermes and Cornell (1978, 1981, 1983), Barberi and Leoni (1980)and Fulignati et al. (1998). Hermes and Cornell (1978) have distinguished four varieties

of nodule ejecta: 1) biotite-bearing pyroxenite, wehrlite, and dunite "accumulative" rocks; 2) "skarns", which are metasomatized carbonates; 3) recrystallized carbonate hornfels and 4) shallow plutonic rocks. The skarn and cumulate rocks were studied in more detail. Hermes and Cornell (1981) have analysed interstitial glasses in the cumulate nodules. The glasses have diverse compositions that change from sample to sample within a single eruptive episode and encompass the entire compositional range of lavas and tephra.

Numerous studies on fluid and melt inclusions (De Vivo et al., 1982; Belkin et al., 1985; Cortini et al., 1985; Belkin and De Vivo, 1993; Fulignati et al., 2000a, 2000b; Fulignati et al., 2001; Gilg et al., 2001) have attempted to constrain physical parameters of nodule genesis. Cortini et al. (1985) reported crystallisation temperatures of phenocrysts (850 - 1050 °C for skarns and 1170 - 1240 °C for cumulate rocks) derived from MI studies. Belkin et al. (1985) and Belkin and De Vivo (1993) estimated the depths of nodule formation (1 - 3.5 kbar) from the densities of CO_2-rich fluid inclusions. These inclusions display a wide range of densities in a single rock, and sometimes in a single mineral. However, an important feature of the depth distribution is that it shows discrete groups, rather than a continuum, suggesting that these rocks underwent a multistage crystallization history. The multistage history is also indicated by Sr isotopes (Cortini and Hermes, 1981). Minerals of the cumulate rocks generally are in disequilibrium with each other with respect to Sr isotopes. This shows that these rocks recorded different environments with distinct Sr isotopic compositions.

Belkin and De Vivo (1993) examined fluid inclusions in clinopyroxenes from cumulate and subeffusive nodules from plinian eruptions. They report trapping depths between ~4 and ~10 km; they also report abundant H_2O-rich fluid inclusions in plinian ejected nodules, whereas in non-plinian eruptions such inclusions were rare. According to Belkin and De Vivo (1993), fluid inclusions in plinian nodules record a higher pre-eruptive H_2O content of the magma.

Gilg et al. (2001) have described in detail mineralogy, fluid inclusions and C, O, Pb, Sr, and Nd isotopic compositions of skarn ejecta and associated xenolithic nodules. The fluid inclusion study emphasizes the presence of several immiscible fluids (silicate melt - aqueous chloride-rich liquid - carbonate/sulfate melt) and suggests that skarns of Vesuvius were formed by magmatic fluids. Similar conclusions are reported by Fulignati et al. (2001). Nd and Pb isotopic compositions of skarns are more variable than those of lavas and pyroclastic rocks. The oxygen isotopic composition of the skarn-forming fluid ($\delta^{18}O=12\pm1‰$) is much higher than that of magmatic fluid in equilibrium with igneous rocks of Vesuvius. According to Gilg et al. (2001), involvement of ^{18}O-enriched carbonate wall rocks played a prominent role in the generation of the isotopic characteristics of the skarns.

METHODS AND STUDIED SAMPLES

Rock samples were crushed by hand, and olivine and clinopyroxene phenocrysts were hand-picked from the 0.5-2 mm grain fraction. Multiple doubly polished thick sections (150-300 μm) were prepared for MI observation and microthermometry. Microthermometry experiments were carried out using a Linkam 1500 stage for MI, and a Linkam 600 stage for CO_2–rich inclusions, at the University of Napoli (Dipartimento di Geofisica e Vulcanologia). MI in the skarn sample were heated rapidly to 800°C, and those in cumulate xenoliths to 1000°C; then temperature was increased slowly to the homogenization temperature. As the Linkam stage cannot quench effectively, compositions of these homogenised inclusions have not been studied.

In order to obtain homogenised melt inclusion compositions, another batch of clinopyroxene and olivine phenocrysts from cumulate nodules were heated up to 1160 °C (+/- 5°C) in a DELTECH furnace (DT31 VT-OS) in nitrogen for approximately 2 hours, and quenched to glass for analysis. Skarn clinopyroxenes were heated up to 1050 °C (+/- 5°C). After quenching, single crystals were mounted on glass slides with epoxy and polished to expose reheated MI. MI were analyzed with an automated Jeol JXA-8600 electron microprobe at the University of Bristol (Department of Earth Sciences). Operating conditions used for Na, K, Al, Mg, Fe, Mn, Ca, Ti, P and F were 15 KeV and 20 nA, for S and Cl 15 KeV and 30 nA, using a defocused electron beam of 5 μm diameter. The peak counting times for Cl and F were 60s and 40s, respectively. Analysis of syntetic and natural glass standards have demonstrated no significant migration of volatiles and alkalies under the above analytical conditions. Relative one-sigma precision is estimated to be 1 to 2 % for major elements and 5 to 10 % for minor elements. Two points were usually analysed within each MI, however only one point was analysed in smaller inclusions (<10 μm).

Selected RMI in olivines and clinopyroxenes from sample S3 were analyzed for H (reported as H_2O), Li, Be, B, Rb, Sr, Y, Zr, Nb, Cs, Ce, Sm, Dy and Yb by secondary ion mass spectrometry (SIMS) at the Woods Hole Oceanographic Institution, using techniques detailed by Webster et al. (1996) and Shimizu and Hart (1982). The samples were analysed at 10 KeV accelerating potential and 1-2 nA beam current. The inclusions were analyzed in one spot, five times each in a depth profile mode. Based on SIMS analyses of synthetic and natural glasses, H_2O are reproducible to $\pm$ 0.3 to 0.4 wt% and the trace elements to 5 to 15% (for more details see Webster et al., 2001).

Melt and fluid inclusions have been studied in four cumulate nodules (samples N42, N45, N48 and S3) and one skarn nodule (sample N67). The skarn nodulewas collected at Lagno di Pollena in pre-79 AD activity products (Fig. 1). Sample S3 has been collected in the typical products of the 1944 activity, in which ejection of scoriae, lava fragments and nodules marked a significant increase in explosivity late in the eruptive event (Dolfi and Trigila, 1978). Samples N42, N45, N48 were collected at Villa Inglese from a mudflow that underlies the 1631 AD lava and overlies the 1440 AD lava. Only small chips were available from these three nodules for the current study, as they have been used previously by Hermes and Cornell (1978, 1981) for petrochemical studies and by Belkin et al. (1985) and by Cortini et al. (1985) for fluid and melt inclusion studies respectively. These samples were also characterized for Sr, Th and Pb isotopes (Cortini and Hermes, 1981; Capaldi et al., 1982; Cortini and van Calsteren, 1985).

RESULTS

Petrography and mineralogy

Samples N42, N45 and N48 are cumulate nodules (clinopyroxenites) with abundant clinopyroxene and biotite, and minor apatite, glass and olivine. Sample N67 is a skarn nodule composed mostly of phlogopite and fassaitic pyroxene with minor melilite, spinel and olivine. A detailed petrochemical description of these rocks is given by Hermes and Cornell (1978).

Sample S3 is a 5 cm long nodule of wehrlite with biotite. It has poikilitic texture with large (up to 10 mm) zoned subhedral oikocrystals of pyroxene enclosing smaller (0.2-2.5 mm) crystals of olivine and a different type of clinopyroxene. Original cumulus grains of olivine and clinopyroxene are usually resorbed and overgrown by poikilitic pyroxene, which represents a second crystallization stage. Mica sometimes is interstitial but mostly forms glomerocrystals.

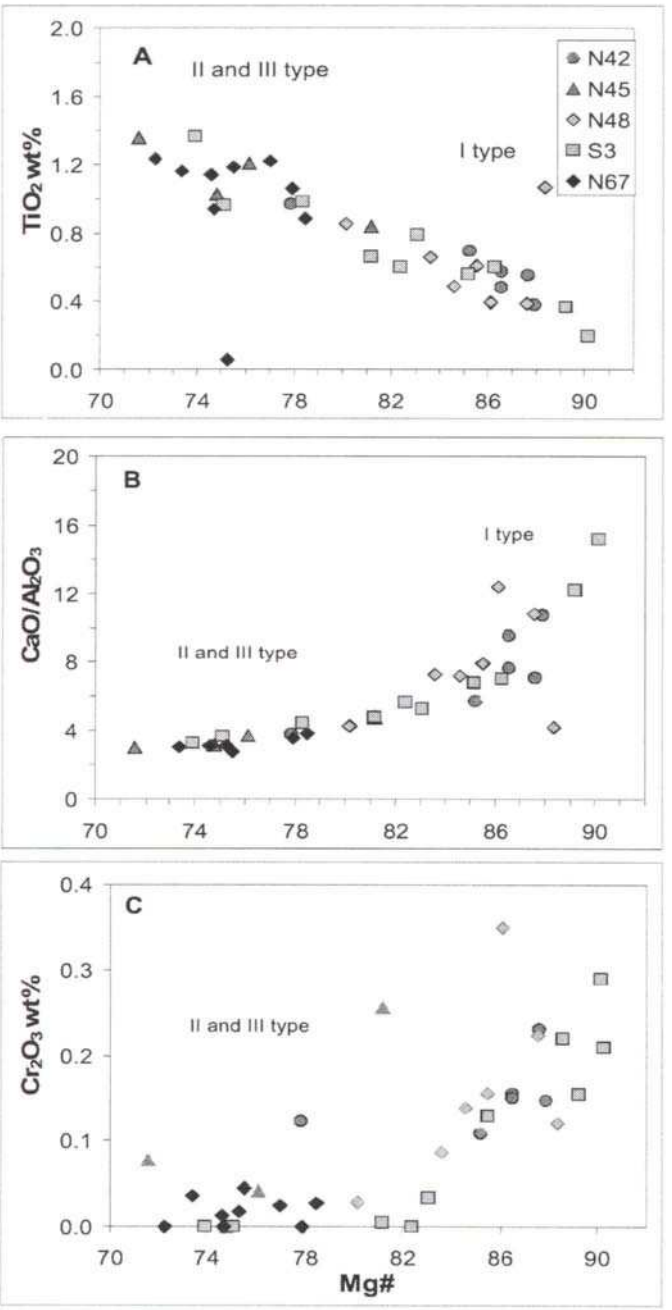

Fig. 2 - Compositions of clinopyroxene from xenoliths N42, N45, N48, N67 and S3. Types I, II and III refer to cumulus, postcumulus and skarn clinopyroxenes, respectively.

The rock has vugs filled with glass, which is also present between individual grains. Clinopyroxene and leucite microphenocrysts are present in the host lava embedding the S3 xenolith.

Table 1 shows representative compositions of clinopyroxene and olivine. Olivine compositions range from Fo_{81} to Fo_{87}. Cumulus clinopyroxene compositions vary widely, and can be broadly divided into two types (Fig. 2). The first type, original cumulus crystals, is diopsidic with Cr_2O_3 up to 0.29 wt% and Mg # (calculated on total Fe) up to 90. The second type, postcumulus overgrowth on cumulus olivine and clinopyroxene, is augitic with low Cr, lower Mg# and SiO_2, and higher TiO_2 and Na_2O compared with the first type. CaO/Al_2O_3 values correlate positively with Mg# in both types (Fig. 2B).

Clinopyroxene from skarn nodule (N67) is fassaitic. The range of Mg#, TiO_2, Na_2O, SiO_2 contents and CaO/Al_2O_3 values in these clinopyroxenes are similar to the postcumulus clinopyroxene (type II) in other nodules.

Melt inclusion trapping temperatures

The homogenisation temperatures (T_h) of MI in olivine and clinopyroxene obtained during experiments in the heating stage are within the range of those published by Cortini et al. (1985). T_h values cluster between 1150 - 1240 °C and between 1130 - 1230 °C for olivines and clinopyroxenes from cumulate rocks, respectively. The skarn clinopyroxenes have T_h values between 950 and 1080 °C. The results of the heating-stage experiments have been used to constrain the heating rates and quenching temperatures for experiments performed in the vertical furnace. The MI in skarn clinopyroxene were quenched at 1050°C (+/- 5°C), whereas the MI in cumulate olivine and clinopyroxene at 1160°C (+/- 5°C). Higher experimental temperatures have not been used to avoid overheating and melting of the host crystals.

Since the quenching temperature of reheating experiments does not reflect the true trapping temperature of the MIs, their compositions can be either depleted in the host mineral components (if the quenching temperature is below the trapping temperature), or enriched in them (if the quenching temperature is higher). Thus, the concentrations of most elements in the quenched MIs may not reflect their true values in the trapped melt. However, ratios of elements that are incompatible in the host, and also concentrations of elements that are present at similar levels in the melt and the host (such as FeO* in inclusions in magnesian Table 1 clinopyroxene and olivine, and TiO_2 and SiO_2 in inclusions in clinopyroxene), should not be affected significantly by over- or underheating.

Melt inclusion post trapping re-equilibrations

FeO* (total iron) contents in MIs in olivine from the cumulate nodule S3 correlate negatively with the Fo content of the host olivine (Fig. 3a). This correlation is unlikely to result from experimental reheating, as a similar correlation is observed in naturally quenched glassy MIs from lava and scoria of the 1906 and 1944 eruptions, and in reheated MIs from scoria of the 1906 eruption (Fig. 3a). There is a clear difference in FeO* contents between MIs from the 1906 and 1944 eruptions, with the latter having lower FeO* at a given Fo. Note that MIs from nodule S3 and from 1944 scoria display a similar trend. As discussed by Danyushevsky et al. (2000), a negative correlation between FeO* contents in MIs and the Fo content of the host olivine, when observed in a magmatic series, results from post-trapping re-equilibration of MIs with their hosts at similar temperatures. The FeO* content of the residual melt inside MIs

Sample	S3	S3	S3	S3	N42	N45	N48	N67	Oliv.[1] (22,4)*		C. cpx[2] (33, 2)		Sk-cpx[3] (10)	
Incl. no.:	231	421	211	213	10.1.2	2.1	7.1	67.5	mean	1 sigma	mean	1 sigma	mean	1 sigma
SiO_2 (wt%)	48.73	45.21	49.32	46.36	49.36	42.98	51.86	41.01	46.15	2.06	49.07	3.34	42.59	1.45
TiO_2	1.15	0.95	1.00	0.95	0.70	0.60	0.61	0.37	1.09	0.17	0.78	0.25	0.41	0.12
Al_2O_3	14.57	15.69	17.44	15.48	14.74	15.43	13.85	19.39	15.47	0.73	16.81	1.40	19.61	1.56
Cr_2O_3	nd	nd	nd	nd	0.10	0.03	0.09	0.02	0.03	0.04	0.04	0.04	0.02	0.02
FeO	6.83	8.62	5.58	8.67	4.20	4.95	3.88	3.30	8.90	0.86	5.12	0.04	3.68	0.43
MgO	5.98	6.12	3.38	4.48	6.11	5.04	8.43	1.37	5.79	0.50	4.44	1.36	2.00	1.09
MnO	0.12	0.20	0.15	0.21	0.09	0.08	0.10	0.12	0.15	0.08	0.12	1.67	0.13	0.05
CaO	8.15	8.81	8.83	9.91	10.50	12.97	7.91	14.45	8.64	0.50	8.80	0.05	12.47	1.56
K_2O	6.36	5.86	6.12	5.62	6.87	8.71	3.90	8.31	5.74	0.53	7.28	2.12	8.04	1.19
Na_2O	1.99	2.03	3.74	3.20	2.12	2.55	4.21	5.23	1.97	0.69	3.20	1.45	5.17	0.61
P_2O5	1.17	0.97	1.53	1.62	0.83	1.01	0.06	0.13	0.97	0.16	0.67	1.04	0.12	0.08
SO_3	0.60	0.49	0.36	0.11	0.37	0.44	0.28	0.24	0.46	0.13	0.28	0.46	0.27	0.17
F	0.22	0.30	0.17	0.34	0.59	0.58	0.47	0.83	0.40	0.18	0.39	0.01	0.74	0.29
Cl	0.60	0.56	0.53	0.67	0.30	0.33	0.60	0.76	0.41	0.16	0.55	0.17	0.66	0.16
H_2O	3.68	3.00	2.33	0.05	nd	nd	nd	nd	3	1	1	2	nd	nd
-Cl, F=O	0.23	0.25	0.19	0.29	0.26	0.27	0.36	0.51						
Sum	99.92	98.54	100.29	97.39	96.51	95.40	95.79	94.99	96.28	1.42	97.52	1.34	95.81	1.52
Li (ppm)	13	13	18	18					12	2	18	0		
Be	7	4	7	13					6	1	10	4		
B	23	27	31	68					24	2	100	97		
Rb	144	86	71	60					110	28	65	8		
Sr	661	415	817	941					521	118	879	88		
Y	12	14	15	17					13	4	16	1		
Zr	91	68	106	104					79	16	105	1		
Nb	35	30	45	241					32	3	143	138		
Sn	10	14	5	13					13	2	9	6		
Cs	25	22	4	6					25	2	5	2		
Ce	120	105	149	187					118	9	168	27		
Nd	83	76	100	110					84	7	105	7		
Sm	23	27	20	33					28	4	27	9		
Dy	4	6	6	7					5	1	7	1		
Yb	4	6	4	4					5	1	4	0		
Host xl	**Oliv.**	**Oliv.**	**cpx**	**cpx**	**cpx**	**cpx**	**cpx**	**cpx**						
SiO_2 (wt%)	40.42	39.43	51.77	50.82	51.74	47.17	52.15	42.44	38.96	0.82	50.67	2.14	45.37	1.91
TiO_2			0.60	0.75	0.56	1.21	0.39	0.06	0.01	0.01	0.68	0.30	0.84	0.49
Al_2O_3			3.42	3.96	3.47	6.67	2.22	10.62	0.03	0.06	4.09	1.89	8.49	1.55
Cr_2O_3	nd	nd	0.23	0.11	0.23	0.04	0.22	0.02	nd	nd	0.12	0.09	0.02	0.02
FeO	12.70	15.32	4.39	5.56	3.97	7.08	3.84	3.39	15.85	1.45	5.28	1.34	5.91	1.63
MgO	45.81	43.67	15.48	14.86	15.79	12.67	16.34	5.79	43.29	1.14	14.79	1.48	10.45	2.91
MnO	0.21	0.28	0.11	0.06	0.11	0.09	0.06	0.11	0.26	0.06	0.11	0.03	0.10	0.03
CaO	0.29	0.30	23.95	23.47	24.59	24.92	24.16	33.20	0.32	0.03	24.22	0.65	26.75	3.98
Na_2O	nd	nd	nd	nd	0.18	0.31	0.23	4.62	nd	nd	0.23	0.07	1.38	2.00
Sum	99.43	99.00	99.71	99.48	100.44	99.84	99.38	95.63	98.84	0.96	99.96	0.94	99.45	0.71
Mg# xls	86.55	83.56	86.28	82.67	87.64	76.14	88.36	75.30	82.95	1.65	83.12	5.04	75.74	1.67

[1] MI in olivine (ol), * (n,m)- number of MI analyzed by EMPA (n); number of MI analyzed by SIMS (m).

[2] MI in cumulate xenolith clinopyroxenes (cpx); [3] MI in skarn clinopyroxene, nd=not determined.

Table 1 - Representative EMPA and SIMS of reheated silicate melt inclusions and EMPA of host olivine and clinopyroxene. FeO* represents total iron, Mg# = [100* atomic (Mg/ Mg+ΣFe)]. Also shown are mean and 1 sigma for olivines and clinopyroxenes cumulate xenoliths and for skarn clinopyroxenes.

in olivine does not usually reflect its content in the trapped melt, but is a function of temporal variations in temperature after trapping (Danyushevsky et al., 2002), and it can be either lower or higher than the trapped value. Different FeO* contents of MIs from the 1906 and 1944 eruptions (Fig. 3a) thus imply different cooling histories of the two magmas, whereas similar

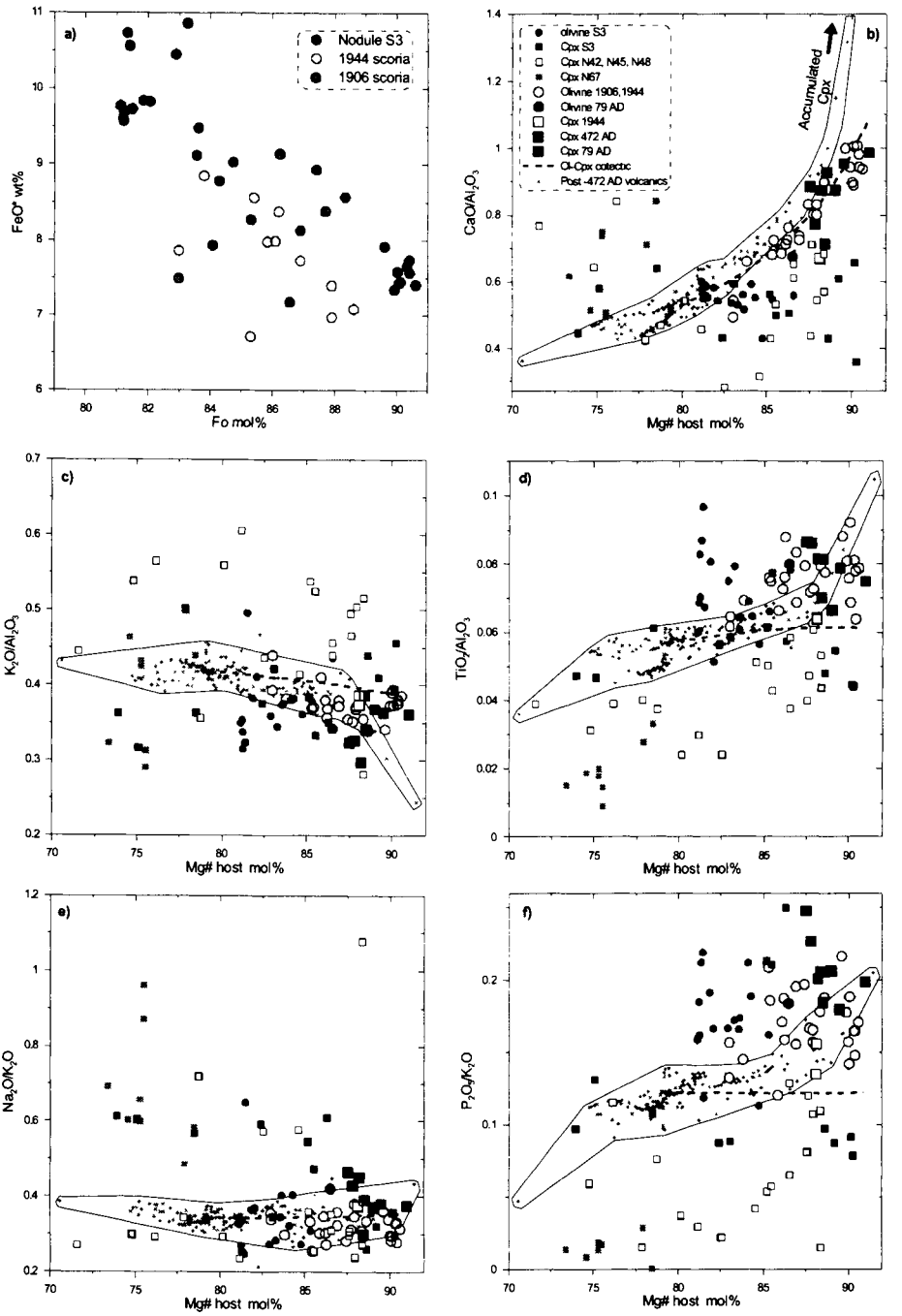
a)
Nodule S3
1944 scoria
1906 scoria
FeO* wt%
Fo mol%
b)
olivine S3
Cpx S3
Cpx N42, N45, N48
Cpx N67
Olivine 1906,1944
Olivine 79 AD
Cpx 1944
Cpx 472 AD
Cpx 79 AD
Ol-Cpx cotectic
Post -472 AD volcanics
Accumulated Cpx
CaO/Al2O3
Mg# host mol%
c)
K2O/Al2O3
Mg# host mol%
d)
TiO2/Al2O3
Mg# host mol%
e)
Na2O/K2O
Mg# host mol%
f)
P2O5/K2O
Mg# host mol%

values in MIs from the nodule S3 and the host 1944 lava indicate their common thermal evolution for some time prior to eruption. Residence time of the nodule S3 in the 1944 magma is a subject of a separate study.

Reheated melt inclusion compositions

Representative compositions of reheated melt inclusions are shown in Table 1 together with average compositions of 22 MI in olivine and 33 RMI in clinopyroxene from cumulate nodules, and 10 RMI in clinopyroxene from the skarn nodule.

Major-element compositions

The CaO/Al_2O_3 values of MIs in olivine from nodule S3 and 1944, 1906 and 79 AD volcanics are shown on Fig. 3b. Both Ca and Al are incompatible in olivine and thus these values should reflect the trapped melt compositions.

MIs in olivine from volcanic rocks show decreasing CaO/Al_2O_3 values with decreasing Fo. This trend is consistent with olivine-clinopyroxene cotectic crystallisation, modelled from the composition of an evolved melt (Fig. 3b). Note that compositions of post-472 AD Vesuvius volcanic bulk rock compositions at MgO $\gtrsim$ 4wt % do not reflect true melt compositions (Marianelli et al., 1999; Danyushevsky and Lima, 2001). These rocks represent magmas formed by evolved melts (MgO < 4 wt%) and variable amounts of accumulated clinopyroxene phenocrysts. The very tight major element compositional trends formed by 'basaltic' post-472 AD Vesuvius volcanic rocks indicate that the composition of the erupting evolved melts has changed little since 472 AD, and that the magma chamber supplying post-472 AD inter-plinian eruptions is essentially in a steady-state condition.

Also shown on Fig 3b are the compositions of reheated MIs in clinopyroxene from 1944, 472 and 79 AD Vesuvius volcanics (Marianelli et al.,1995; 1999). During cotectic crystallisaton, clinopyroxene is slightly more magnesian (1-2 mol%) than olivine (eg, Ariskin, 1999), but this difference is insignificant for the scale of Fig. 3. Although CaO/Al_2O_3 values in reheated MIs in clinopyroxene are a function of quenching temperature, a general agreement of MI compositions in olivine and clynopyroxene indicates that experimental temperatures correspond closely to trapping temperatures (1140-1160°C). We thus conclude that, since 79 AD, primitive Vesuvius magmas evolved along an olivine-clinopyroxene cotectic. The parental melts have

Figure 3. Major-element compositions of MIs in olivine and clinopyroxene from Vesuvius volcanics and nodules, plotted against Mg# of their host minerals. MIs from samples S3, N42, N45, N48 and N67 are from this study. MIs from the 1944 and 1906 AD volcanics are from Marianelli et al. (1995, 1999) and Danyushevsky and Lima (2002, unpublished). MIs from the 79 and 472 AD volcanics are from Marianelli et al. (1995) The compositions of post-472 AD inter-plinian volcanics (Belkin et al., 1993) are shown for comparison. The compositions of the equilibrium olivine for each rock sample have been calculated using an olivine-melt equilibrium model of Ford et al. (1983), assuming an Fe^{2+}/Fe^{3+} value of 6. For Vesuvius compositions, this value corresponds to oxygen fugacity just below the NNO buffer. An olivine-clinopyroxene cotectic has been modeled using olivine-melt model of Ford et al. (1983) and clinopyroxene-melt model of Ariskin (1999). All calculations have been performed using the software PETROLOG (Danyushevsky, 2001).

CaO/Al_2O_3 values of ~1. Note that in the text below we will refer to 79 AD and more recent Vesuvius rocks as post-79 AD.

The compositions of MIs in nodule S3 are not consistent with the trend of the MIs in volcanic rocks described above. The CaO/Al_2O_3 values in MIs in both olivine and clinopyroxene are relatively constant, averaging at ~ 0.5 (Fig. 3b). Note that differences between MIs in clinopyroxene from nodule S3 and from the volcanics are significant, as both were quenched from similar temperatures. The compositions of MIs in clinopyroxene from medieval cumulate nodules N42, N45 and N48 are generally consistent with those from nodule S3, however they show more scatter, and the MIs in more evolved grains (Mg# < 77) have high CaO/Al_2O_3 values, similar to MIs in clinopyroxene from the skarn nodule N67. Compared to MIs from Vesuvius volcanics, MIs in clinopyroxene from the skarn nodule N67 also have anomalously low TiO_2 and P_2O_5 and higher Na_2O contents (Figs. 3c-f). MIs in clinopyroxene from nodules N42, N45, N48 are also quite different from the MIs in Vesuvius volcanics; they have higher K_2O, and lower TiO_2 and P_2O_5 contents and occasionally higher Na_2O/K_2O values. High Na_2O/K_2O values are also common in MIs in clinopyroxene from nodule S3, which distinguish them from MIs in olivine from this nodule. Some inclusions in clinopyroxene from this nodule also have low P_2O_5/K_2O and TiO_2/Al_2O_3, which are not observed in MIs in olivine from this sample (Figs. 3c-f).

Reheated melt inclusion volatile contents

MIs in clinopyroxene and olivine phenocrysts from the post-79 AD Vesuvius volcanic rocks have relatively constant Cl/K_2O values averaging at ~ 0.1 (Fig. 4a). This implies that Cl behaves as an incompatible element during fractionation of Vesuvius magmas and its concentrations are not affected by degassing. Note that comparing H_2O and Cl contents of MI from modern lavas and scoria, Raia et al. (2000) concluded that some of them indicate partial degassing of the magma. The Cl/K_2O values in MIs from nodules S3 and N67 are consistent with the trend of the volcanics, whereas some MIs in clinopyroxene from three medieval nodules N42, N45 and N48 are clearly different, having lower Cl/K_2O values. The behaviour of F is generally similar to Cl, although it appears that F/Cl values are increasing slightly during magma evolution.

The behavior of S and H_2O is more difficult to interpret. The highest S/Cl values are observed in the most magnesian olivine and clinopyroxene phenocrysts from post-79 AD volcanics (Fig. 4b). Within the limited range of host mineral compositions for which the data are available (Mg# 85-91, Fig. 4b), it appears that S/Cl values in melt inclusions from the volcanics decrease with fractionation. A large number of MIs in clinopyroxene from the post-79 AD plinian and inter-plinian eruptions has been analysed by Belkin et al. (1998), Raia et al. (2000) and Webster et al. (2001) (Fig. 4b), however the compositions of host minerals for these MIs are unknown. Melt inclusions from inter-plinian volcanics, analysed by these authors, have low S/Cl values, and it is possible that their data set is dominated by evolved, low-Mg# clinopyroxene, whereas the data set of plinian eruptions, characterised by higher S/Cl values, is dominated by more primitive phenocrysts. The predominance of primitive, high Mg# clinopyroxene in the plinian Vesuvius volcanics has been suggested by Lima et al. (1999).

Alternatively, Webster et al. (2001) suggested that magmas causing plinian eruptions are characterised by higher S/Cl values than the inter-plinian magmas. This seems problematic as MI in primitive inter-plinian olivine and clinopyroxene also have high S/Cl values (Fig. 4b). The combined data set, containing data from 1906 and 1944 AD eruption (from Marianelli et al., 1995 and 1999, and from Danyushevsky and Lima, unpublished data 2002), on Fig. 4b is

more consistent with progressive loss of S by evolving Vesuvius magmas. The S/Cl value of the parental melts appears to remain nearly constant for the post-79 AD eruptions, averaging at ~ 0.5-0.6.

The S/Cl values in MIs from the cumulate nodule S3 differ significantly from those in MIs from the volcanics (Fig. 4b). MIs in olivine from this nodule have generally higher S/Cl values, whereas some MIs in clinopyroxene have significantly lower values, than MIs in

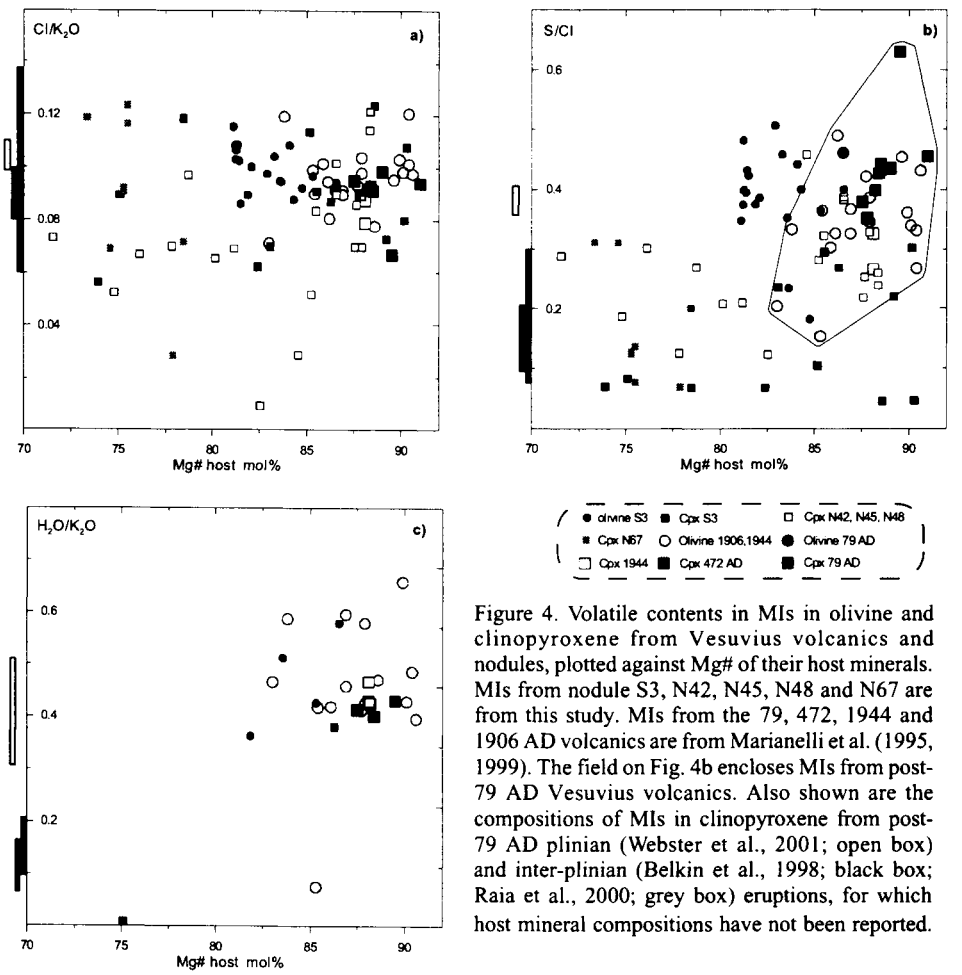

Figure 4. Volatile contents in MIs in olivine and clinopyroxene from Vesuvius volcanics and nodules, plotted against Mg# of their host minerals. MIs from nodule S3, N42, N45, N48 and N67 are from this study. MIs from the 79, 472, 1944 and 1906 AD volcanics are from Marianelli et al. (1995, 1999). The field on Fig. 4b encloses MIs from post-79 AD Vesuvius volcanics. Also shown are the compositions of MIs in clinopyroxene from post-79 AD plinian (Webster et al., 2001; open box) and inter-plinian (Belkin et al., 1998; black box; Raia et al., 2000; grey box) eruptions, for which host mineral compositions have not been reported.

compositionally similar hosts from volcanics. The S/Cl values in MIs from nodules N42, N45, N48 and N67 have S/Cl values similar to those in evolved phenocrysts from the volcanics.

The geochemistry of H_2O in the post-79 AD Vesuvius MIs appears to be similar to that of S (Fig. 4c). The highest H_2O/K_2O values (~ 0.6) are found in MI in the most primitive phenocrysts, whereas more evolved MI have lower H_2O/K_2O values. A limited number of H_2O analyses in MI from nodules precludes their detailed comparison with volcanics, however

it appears that H_2O/K_2O values in MIs in olivine from nodule S3 are consistent with those hosted by phenocrysts of similar compositions in volcanics.

Trace-element contents

The concentrations of B in MIs from nodule S3 show a positive correlation with F, which is generally consistent with compositions of MIs in clinopyroxene from the post-79 AD plinian eruptions (Fig. 5a). Sr in these MIs also correlate positively with F (Fig. 5B), but this correlation is shifted towards higher F contents compared to the compositions of whole-rock samples

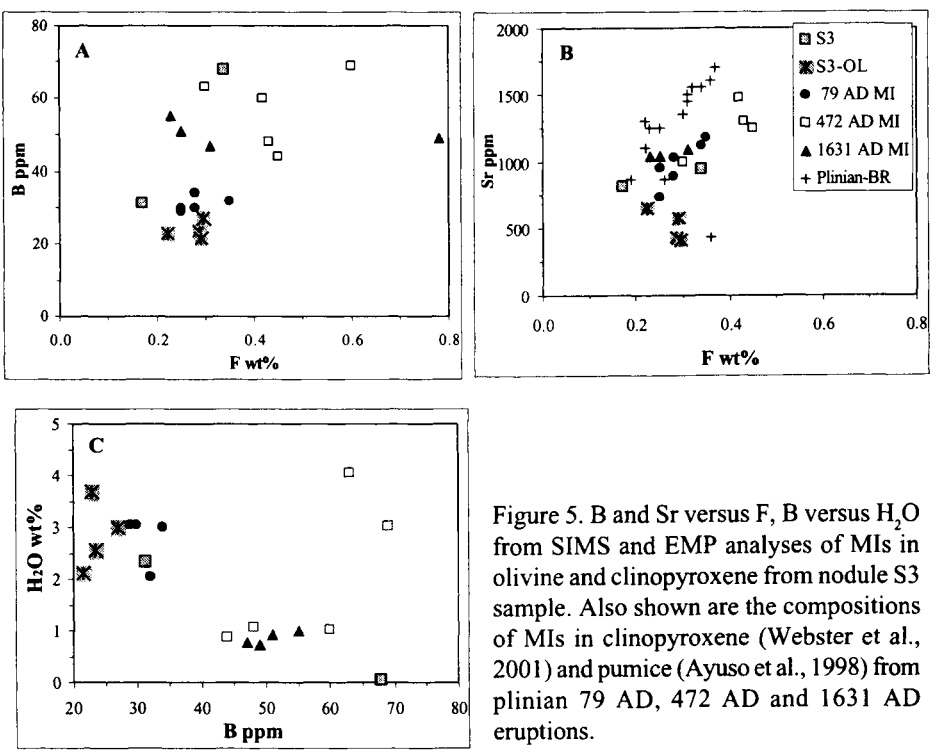

Figure 5. B and Sr versus F, B versus H_2O from SIMS and EMP analyses of MIs in olivine and clinopyroxene from nodule S3 sample. Also shown are the compositions of MIs in clinopyroxene (Webster et al., 2001) and pumice (Ayuso et al., 1998) from plinian 79 AD, 472 AD and 1631 AD eruptions.

from the post-79 AD plinian eruptions. The H_2O/B values in MIs from nodule S3 are similar to those in MIs in clinopyroxene from the 79 AD plinian eruption, and are significantly higher than in MIs from the 472 AD and 1631 AD plinian eruptions (Fig. 5C).

DISCUSSION

Eruption dynamics as suggested by clinopyroxene populations in the cumulate nodules

Based on petrography and mineral compositions, clinopyroxene in the studied nodules can be divided into three types: I) early formed, more primitive cumulus pyroxene; II) more evolved, post-cumulus pyroxene, which may reflect a secondary crystallization stage; and III) fassaitic pyroxene present in the skarn nodule (Fig. 2).

As clinopyroxene compositions are well-known to reflect chemical features of their host magmas (e.g. Nisbet & Pearce, 1977; Leterrier et al., 1982), the coherent trends displayed by the compositions of cumulus and post-cumulus clinopyroxene (Fig. 2) suggest that they were formed at variable stages of fractionation of a single magmatic system.

Higher concentrations of volatile elements in MI in more primitive phenocrysts (Fig. 4) suggest that they crystallised at greater depths. Indeed, Belkin et al. (1985) and Belkin and De Vivo (1993) have demonstrated a polybaric origin of clinopyroxene from Vesuvius nodules, based on a study of fluid inclusions. However, the host compositions have not been recorded.

The more primitive, cumulus pyroxenes may have crystallized at a higher pressure in a deeper magma chamber. The cumulate phases in the nodules may represent fragments of the crystal mush of a deep reservoir. These fragments remained in the shallow reservoirs, where post-cumulus clinopyroxenes were formed, and were later erupted during an inter-plinian event.

Compositions of melt inclusions in the studied nodules

As demonstrated in Figs 3 and 4, MIs in the nodules display large compositional variations, they differ significantly from those in phenocrysts from the post-79 AD Vesuvius volcanic rocks, and their compositions are not consistent with an olivine-clinopyroxene co-crystallisation, which is a well-established feature of Vesuvius volcanism. Moreover, significant differences exist between MIs from different nodules, between MIs in olivine and clinopyroxene from nodule S3, and between MIs in clinopyroxene of similar compositions within individual nodules. At the same time, MIs from the volcanic rocks display trends which are generally consistent with an olivine-clinopyroxene cotectic, and no systematic differences are observed between MIs in olivine and clinopyroxene.

Olivine and clinopyroxene from the nodules may have crystallised from the pre-79 AD Vesuvius magmas. As discussed by Ayuso et al. (1998), older Vesuvius volcanics have variable compositions (see also a summary in Danyushevsky and Lima, 2001), and primitive samples of some of them are characterised by lower CaO/Al_2O_3 values, which are a prominent feature of the MIs from the studied nodules (Fig. 3b). However, this cannot explain differences between MIs in olivine and clinopyroxene from nodule S3, and variations of MI compositions in similar clinopyroxene within each nodule, unless we assume that individual crystals of similar composition in the nodules originate from different eruption events.

Alternatively, variations in MI compositions may result from post-entrapment re-equilibration with their hosts during residence within the magmatic system prior to eruption. During these re-equilibration processes, the compositions of MIs are controlled by the compositions of their hosts, and thus inclusions in compositionally different minerals (i.e., olivine versus clinopyroxene host and/or clinopyroxenes of different compositions) may evolve towards different compositions. It is reasonable to assume that crystals from the nodules resided in the magmatic system for a longer time than phenocrysts from the volcanics, which may explain a large compositional diversity of the MIs from the nodules. A detailed consideration of this issue is beyond the scope of this paper.

Skarn xenoliths in Vesuvius volcanics (sample N67) provide information on the interaction of magmas with the carbonate wall-rock (see Gilg et al., 2001 for a detailed discussion). The compositions of MIs in clinopyroxene from the skarn nodule are characterized by anomalously low TiO_2 and P_2O_5 contents and high Na_2O/K_2O values (Fig. 3). Interestingly, Cl/K_2O values in these inclusions are similar to those of all Vesuvius magmas (Fig. 4), suggesting that Cl contents are not affected by carbonate assimilation.

Compositions of plinian and inter-plinian Vesuvius volcanics

The compositions of plinian volcanic rocks are usually more evolved (MgO < 4 wt%) than the inter-plinian ones (Fig. 6). The Cl, F and Sr contents increase with decreasing MgO, whereas Sm, Y and Yb decrease. Increasing Sr contents may indicate no plagioclase or K-

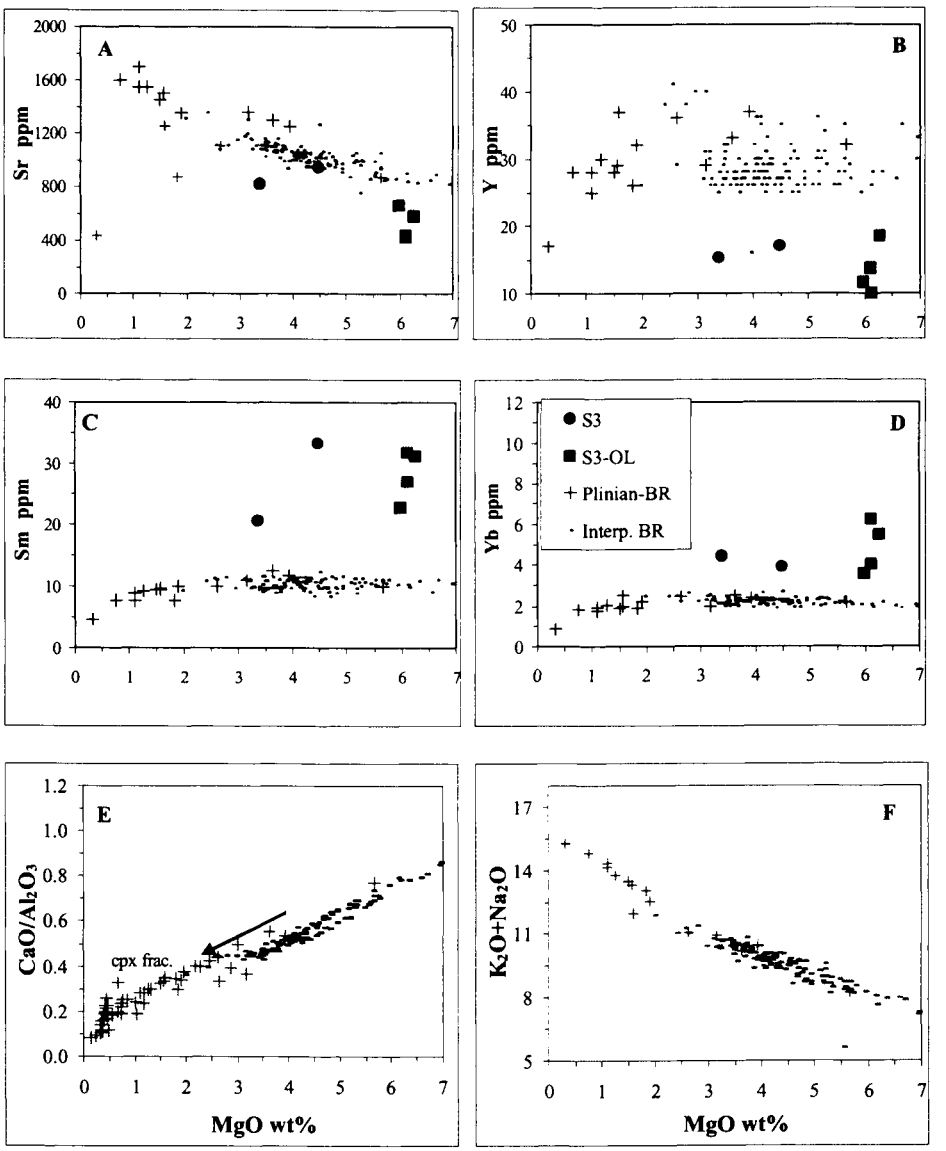

Figure 6. Sr, Y, Sm, Yb, CaO/Al2O3 and Na2O+K2O versus MgO (A-F) for post-79 AD plinian and inter-plinian Vesuvius volcanics. Data from Ayuso et al., 1998.

feldspar fractionation. Decreasing Y and P suggest apatite crystallisation, whereas decreasing Ti, Fe, Sm and Yb most likely reflect magnetite fractionation. Very low S contents (< 500 ppm, Ayuso et al., 1998), which are up to an order of magnitude lower than in MIs, indicate efficient degassing during eruption (Belkin et al., 1993a, 1998).

As discussed above, inter-plinian volcanic rocks usually have higher MgO contents because their compositions reflect accumulation of clinopyroxene by a melt with ~ 4 wt% MgO, whose composition remained unchanged since the 79 AD eruption. The similarity in composition of the plinian and inter-plinian bulk rocks with ~ 4 wt% MgO (Fig. 6) suggests that during all Vesuvius post-79 AD eruptions the composition of the melt is essentially the same. Longer non-active periods prior to the plinian eruptions (see discussion below) likely lead to the separation of early crystallised phenocrysts from the melt, and their incorporation into the well-cemented cumulate layers within the colder magma chamber. This results in eruptions of low-MgO magmas during the plinian events. In contrast, the short time intervals between inter-plinian eruptions are not sufficient for efficient solidification of the cumulate layers as the magma chamber remains at a higher temperature, and thus early-formed phenocrysts are easily incorporated into the erupting magma. This also explains the dominance of clinopyroxene phenocrysts in the inter-plinian volcanics. Indeed, olivine, being significantly denser than clinopyroxene, may be separated more efficiently from the crystallising melt, and thus olivine crystals may be buried deeper within the cumulate layers formed during each eruptive cycle.

Implications for magma origin

The B concentrations in Vesuvius MIs are significantly lower than in MIs from Vulsini (Fig. 7A), which were trapped in primitive olivine phenocrysts ($Fo_{91.7-90.5}$) (Metrich et al., 1998), however large variations in B/Ti values in Vesuvius magmas may indicate the importance of subduction zone processes and specifically slab devolatilisation in their origin (Ryan and Langmuir, 1993; Ryan et al., 1996). This is also supported by the high (> 4) B/Be values of Vesuvius MIs, which are higher than those of intraplaite magmas and more similar to subduction-related magmas (Fig. 7B).

A feeding model for the post-79 AD Mt. Somma-Vesuvius volcanism

As discussed by Rolandi et al. (1998), Mt. Somma-Vesuvius activity is characterized by cyclic events. Each cycle starts always with a plinian eruption followed by interplinian activities and by repose times of variable lengths, depending on the duration of the interplinian phase. Based on bulk rock compositional data, Ayuso et al (1998) have recognized the existence of three gradational magmatic mega-cycles: I) from 25 ka to ~14 ka BP; II) from ~ 8 to 2.7 ka BP and III) from 79 to 1944 AD. The end of each magmatic mega-cycle is characterized by a very long repose time, and a new magmatic mega-cycle (composed by different smaller cycles) always starts with a plinian eruption.

Figure 8A presents trapping depth of CO_2 primary fluid inclusions (FI) in different crystal phases of Vesuvian nodules (Belkin et al., 1985; Belkin and De Vivo, 1993). Based on FI and MI data, and on other information on the Mt. Somma-Vesuvius volcanic system, we suggest that separate small magma chambers exist at depths of >3.5 km and possibly a larger chamber at a depth of > 12 km (Fig. 8B). The entire system likely resembles a complex feeding column which is dominated by multiple mush zone environments (small magma chambers), and thus

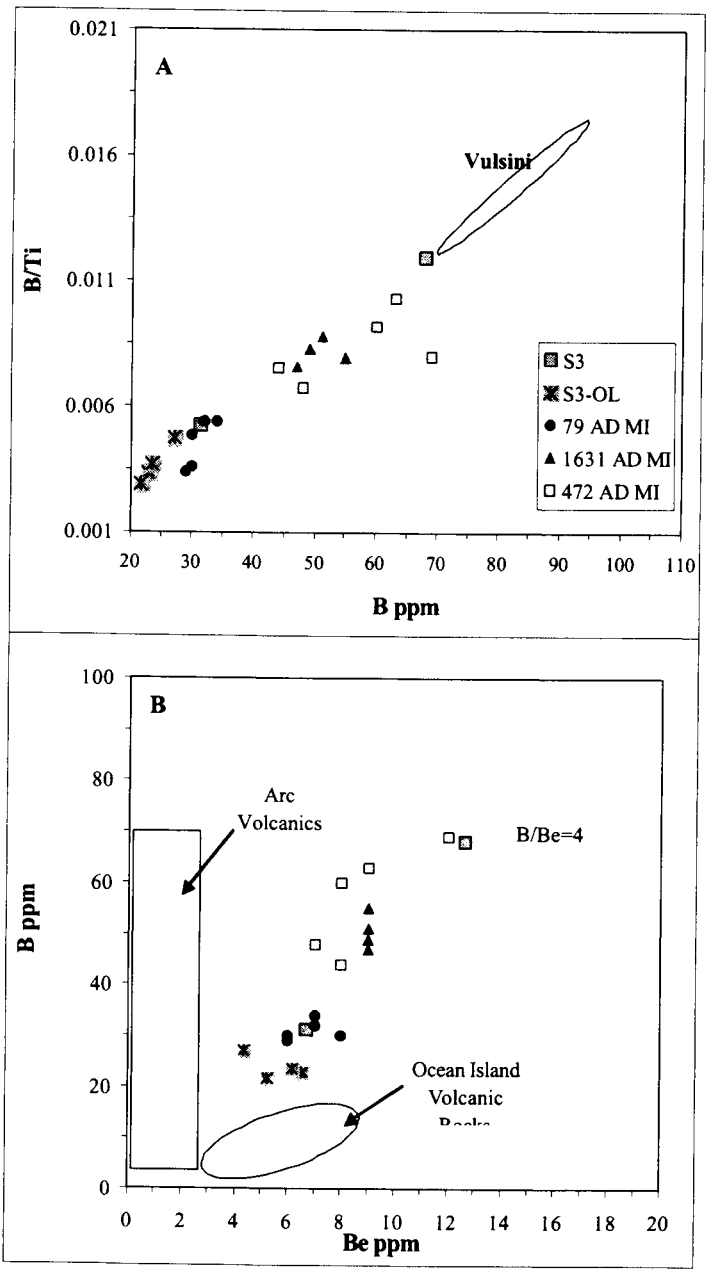

Figure 7. B/Ti versus B and B versus Be from SIMS data for MI from S3 sample olivine (OL) and clinopyroxene. Plinian (79 AD, 472 AD and 1631 AD) MI data (Webster et al., 2001) and Vulsini MI data (Metrich et al., 1998) also are shown. The ratio of B/Be=4 shown for reference. Data for reference fields are from Ryan et al., 199. See text for discussion.

includes a variety of local crystallization environments characterized by contrasting cooling rates and P-T conditions (Marsh, 1995; 1998).

Within a magmatic cycle, magmas continuously ascend through the system, experiencing simultaneous degassing and fractionation. This explains the negative correlation between volatile element contents in MI (H_2O, S) and their host phenocryst compositions (Fig. 4). The loosely cemented conduit within the volcano does not allow significant build up of volatile pressure, leading to frequent, non-violent inter-plinian eruptions. This combination of ongoing magma supply and frequent eruptions results in a nearly steady-state conditions under the volcano, which explains little variations in the composition of the erupting melt throughout

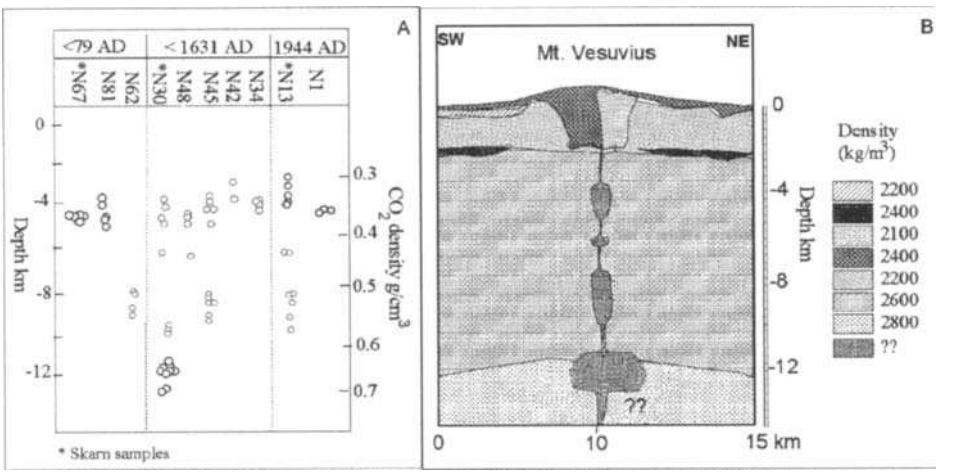

Figure 8. (A) Trapping depth in Mt. Somma-Vesuvius ejecta, from Belkin et al., 1985 calculated as a function of CO_2 primary FI densities and within the assumptions of these authors. (B) Suggested magma chamber model for post 79-AD eruptions. Density data and patterns are from a sea gravity survey by Berrino et al. (1998).

the cycle. Uneven distribution of earlier formed phenocrysts in the ascending magmas (mainly clinopyroxene with subordinate olivine) explains compositional variations of the inter-plinian volcanic rocks.

A cycle continues until the deep source of the magma is exhausted, and a repose time begins. During the repose time the conduit within the volcano is fast sealed, and when magma supply resumes, an eruption does not happen until a significant build up of volatile pressure occurs, capable of destroying the sealed top of the conduit. A violent plinian eruption reopens the conduit manifesting the beginning of a new magmatic cycle (e.g., the 472 and 1631 AD eruptions started two new cycles within the same mega-cycle). Within a mega-cycle, the composition of the deep magma source remains the same, whereas different mega-cycles correspond to the change of the primary magma composition.

Webster et al. (2001 and in this volume) suggested a different model, where the eruptive behavior correlates with the pre-eruptive volatile contents of the melt. They argue that magmas associated with explosive and subplinian events contained higher H_2O and S contents than the inter-plinian eruptions.

Although we believe that the model we propose can explain all available chemical and geophysical data, it is clear that further investigations are needed. In particular, more data are required on the volatile contents of melt inclusion in the range of phenocryst compositions from various eruption styles and dates.

The shallow magma chambers are located within the Mesozoic limestones and dolomites. As indicated by the skarn nodule N30, the carbonate sequences have a thickness of at least 12 km due to thrusting of the 6 km thick, normal carbonate platform series (Patacca et al., 1990; Berrino et al., 1998). In addition, the existence of a deep magma chamber is confirmed by recent 3D tomographic data (Auger et al., 2001), which locate a major large magma reservoir at a depth of > 10 km, though we consider the horizontal extension of the indicated magma chamber unrealistic. The seismic tomography (Zollo et al., 1998; Auger et al., 2001) does not indicate the existence of the shallower magma reservoirs likely because the resolution of the method cannot recognize shallow reservoirs < 1 km in diameter.

As discussed by Rolandi et al., 1998, in the third mega-cycle, Mt. Somma activity resumed after ~ 800 years of repose with the 79 AD plinian eruption. Other plinian and sub-plinian eruptions occurred within this mega cycle at 472 and 1631 AD. Each of these three events was followed by either weak to moderately explosive or explosive-effusive interplinian activity, and then by a repose time that for the 79 and 472 AD eruption are of 169, 492 years respectively. At present, the Mt. Somma-Vesuvius system seems to be in a repose time (Carta et al., 1981) even if it is unknown whether the last Vesuvius eruption (1944 AD) represents the closing event of the third magmatic mega-cycle, or it represents a "short" repose time within the cycle started in 1631 AD. In the first case we can forecast a very long repose time in the Vesuvius activity (probably many centuries), at the end of which a plinian eruption will occur, giving rise to the onset of the 4th magmatic mega-cycle of Mt. Somma-Vesuvius. In the second case, the lack of activity since 1944 AD may represent a repose time before a small plinian or sub-plinian event within the third mega-cycle; in this latter case the repose time will be shorter. The current repose time (58 years) is in any case anomalous for the 1631-1944 AD inter-plinian cycle, in which cyclicity of eruption has been between 7 and 30 years.

Acknowledgments. The authors are very grateful to V. Scribano for some useful petrographic observations and descriptions; to J. Webster who performed SIMS at the Woods Hole Oceanographic Institution and R. Trigila for the use of the DELTECH furnace at the Dipartimento di Scienze della Terra in Rome. A. Lima acknowledges EU-TMR Programme-Geochemical Facility that supported her stay at Bristol University for EMPA. Work carried out with funds from GNV-INGV grant for financial year 2001 to B. De Vivo.

REFERENCES

Ariskin A.A. 1999 Phase equilibria modeling in igneous petrology: use of COMAGMAT model for simulating fractionation of ferro-basaltic magmas and the genesis of high-alumina basalt. J Volcanol. Geotherm. Res., 90, 115-162

Ayuso R.A., De Vivo B., Rolandi G., Seal II R.R. and A. Paone. 1998 Geochemical and isotopic (Nd-Pb-Sr-O) variations bearing on the genesis of volcanic rocks from Vesuvius, Italy. In: Spera F.J., De Vivo B., Ayuso R.A., Belkin H.E. (eds) Vesuvius special issue. J. Volcanol. Geotherm. Res., 82:53-78

Arnò V., Principe C., Rosi M., Santacroce R., Sbrana A. and Sheridan M.F. 1987 Eruptive history. In: Santacroce R (ed) Somma Vesuvius. CNR Quad Ric Sci 114:53-103

Auger E., Gasparini P., Virieux J. and Zollo A. 2001. Seismic evidence of an extended magmatic sill under Mt. Vesuvius. Science 294: 1510-1512

Barberi M. and Leoni L. 1980 Metamorphic carbonate ejecta from Vesuvius plinian eruptions: evidence of occurrence of shallow magma chambers. Bull Volcanol 43: 107-120

Beccaluva L., Di Girolamo P. and Serri G. 1999 Petrogenesis and tectonic of Roman Volcanic Province, Italy. Lithos, 26: 191-221

Belkin H.E., De Vivo B., Roedder E. and Cortini M. 1985 Fluid inclusion geobarometry from ejected Mt. Somma-Vesuvius nodules. Am Min 70: 288-303

Belkin H.E. and De Vivo B. 1993 Fluid inclusion studies of ejected nodules from plinian eruptions of Mt. Somma-Vesuvius. In: De Vivo B., Scandone R., Trigila R. (eds) Vesuvius special issue. J Volcanol Geoth Res 58:89-100

Belkin H.E., Kilburn C.R.J. and De Vivo B. 1993 Sampling and major element chemistry of the recent (A.D. 1631-1944) Vesuvius activity. In: De Vivo B, Scandone R, Trigila R (eds) Vesuvius special issue. J Volcanol Geoth Res 58: 273-290

Belkin H.E., De Vivo B., Torok K. and Webster J.D. 1998 Pre-eruptive volatile content, melt-inclusion chemistry, and microthermometry of interplinian Vesuvius lavas (pre-A.D. 1631). In: Spera F.J., De Vivo B., Ayuso R.A. and Belkin H.E. (eds) Vesuvius special issue. J Volcanol Geotherm Res., 82:79-95.

Berrino G., Corrado G. and Riccardi U. 1998 Sea gravity data in the Gulf of Naples: a contribution to delineating the structural pattern of the Vesuvian area. In: Spera F.J., De Vivo B., Ayuso R.A. and Belkin H.E. (eds) Vesuvius special issue. J Volcanol Geotherm Res., 82: 139-151

Brocchini F., Principe C., Castradori D., Laurenzi M.A. and Goria L. 2001 Quaternary evolution of the southern sector of the Campanian Plain and early Somma-Vesuvius activity: insights from the Trecase well. Mineral. Petrol., 73: 67-91.

Capaldi G., Cortini M. and Pece R. 1982 Th isotopes at Vesuvius: evidence for open-system behavior of magma-forming processes. J. Volcanol. Geotherm. Res., 14: 247-260

Caprarelli G., Togashi S. and De Vivo B. 1993 Preliminary Sr and Nd isotopic data for recent lavas from Vesuvius volcano. In: De Vivo B., Scandone R. and Trigila R. (eds) Vesuvius special issue. J Volcanol Geoth Res 58: 377-381

Carta S., Figari R., Sartoris G., Sassi E. and Scandone R. 1988. A statistical model for Vesuvius and its volcanological implications. Bull. Volcanol. 44 (2), 129-151.

Civetta L., Galati R. and Santacroce R. 1991 Magma mixing and convective compositional layering within the Vesuvius magma chamber. Bull Volcanol 53: 287-300

Civetta L. and Santacroce R. 1992 Steady state magma supply in the last 3400 years of Vesuvius activity. Acta Volcanol., V 2: 147-152

Cortini M. and Hermes O.D. 1981 Sr isotopic evidence for a multi-source origin of the potassic magmas in the Neapolitan area (S. Italy). Contrib. Mineral. Petrol., 77: 47-55.

Cortini M. and Van Calsteren P. 1985 Lead isotopic differences between whole-rock and phenocrysts in zero age lavas. Nature, 314: 343-345.

Cortini M., Lima A. and De Vivo B. 1985 Trapping temperatures of melt inclusions from ejecta Vesuvian mafic xenoliths. J Volcanol Geotherm Res 26: 167-172

D'Antonio M., Tilton G.R. and Civetta L. 1995 Petrogenesis of Italian alkaline lavas deduced from Pb-Sr-Nd isotope relationships. In: Basu A, Hart SR (eds) Isotopic studies of crust-

mantle evolution. Am Geophys Union Monogr Dedicated to Tatsumoto M, Tilton GR, 253-267

Danyushevsky L.V. 2001 The effect of small amounts of H_2O on crystallization of mid-ocean ridge and backarc basin magmas. J Volcan Geoth Res 110: 265-280

Danyushevsky L.V., Della-Pasqua F.N. and Sokolov S. 2000 Re-equilibration of melt inclusions trapped by magnesian olivine phenocrysts from subduction-related magmas: petrological implications. Contrib Mineral Petrol, 138: 68-83

Danyushevsky L.V. and Lima A. 2001 Relationships between Campi Flegrei and Mt. Somma volcanism: evidence from melt inclusions in pyroxene phenocrysts from volcanic breccia xenoliths. Mineral Petrol 73: 107-119

Danyushevsky L.V., Sokolov S. and Falloon T.J. 2002 Melt inclusions in olivine phenocrysts: using diffusive re-equilibration to determine the cooling history of a crystal, with implications for the origin of picrites and other olivine-phyric rocks. J. Petrology, 43, No. 9 (in press)

De Vivo B., Cortini M., Belkin H.E. and Roedder E., 1982. Inclusion geobarometry from ejected mafic Vesuvian xenoliths. Geol. Soc. Am., Abstr. Programs, 14: 474.

Dolfi D. and Trigila, R. 1978 The role of water in the 1944 Vesuvius eruption. Contrib. Mineral. Petrol. 67. 297-304

Ford C.E., Russell D.G., Craven J.A. and Fisk M.R. 1983 Distribution coefficients of Mg^{2+}, Fe^{2+}, Ca^{2+} and Mn^{2+} between olivine and melt,. J Petrol 24: 256-265.

Fulignati P., Marianelli P. and Sbrana A. 1998 New insights on the thermometamorphic-metasomatic magma chamber shell of the 1944 eruption of Vesuvius. Acta Volcanol. 10: 47-54.

Fulignati P., Marianelli P., Santacroce R. and Sbrana A. 2000a The skarn shell of the 1944 Vesuvius magma chamber. Genesis and P-T-X conditions from melt and fluid inclusion data. European Journal of Mineralogy, 12: 1025-1039.

Fulignati P., Marianelli P. and Sbrana A. 2000b Glass bearing felsic nodules from crystallizing side walls of 1944 Vesuvius magma chamber. Mineralogical Magazine, 64: 481-496.

Fulignati P., Kamenetsky V.S., Marianelli P., Sbrana A. and Mernagh T.P., 2001 Melt inclusion record of immiscibility between silicate, hydrosaline, and carbonate melts: applications to skarn genesis at Mount Vesuvius. Geology, 29:1043-1046

Gilg H.A., Lima A., Somma R., Belkin H.E., De Vivo B. and Ayuso R.A. 2001 Isotope geochemistry and fluid inclusion study of skarns from Vesuvius. Mineral. Petrol., 73: 145-176

Hermes O.D. and Cornell W.C. 1978 Petrochemical significance of xenolithic nodules associated with potash-rich lavas of Somma-Vesuvius volcano. NSF Final Technical Report, Univ. of Rhode Island.

Hermes O.D. and Cornell W.C. 1981 Quenched crystal mush and associated magma compositions as indicated by intercumulus glasses. J. Volcanol. Geotherm. Res., 9: 133-149.

Hermes O.D. and Cornell W.C. 1983 The significance of mafic nodules in the ultrapotassic rocks from Central Italy – reply. J. Volcanol. Geotherm. Res., 16: 166-172.

Joron J.L., Metrich N., Rosi M., Santacroce R. and Sbrana A. 1987 Chemistry and petrography. In: Santacroce R (ed) Somma Vesuvius CNR Quad Ric Sci 114: 105-174

Leterrier J., Maury R.C., Thonon P., Girard D. and Marchal M. 1982 Clinopyroxene composition as a method of identification of the magmatic affinities of paleo-volcanic series. Earth Planet. Sci Lett., 59: 139-154.

Lima A., Belkin H.E. and Torok K. 1999 Primitive silicate-melt inclusions in compositionally diverse clinopyroxene phenocrysts from the medieval scoria from Terzigno Formation: clue to understanding of Vesuvius magmatic processes. Mineral Petrol, 65: 185-206.

Marianelli P., Métrich N., Santacroce R. and Sbrana A. 1995 Mafic magma batches at Vesuvius: a glass inclusion approach to the modalities of feeding stratovolcanoes. Contr Mineral Petrol 120: 159-169

Marianelli P., Metrich N. and Sbrana A. 1999 Shallow and deep reservoirs involved in magma supply of the 1944 eruption of Vesuvius. Bull Volcanol 61: 48-63.

Metrich N., Joron J.L. and Berthier B. 1998 Occurrence of boron-rich potassic melts in the Vulsini Volcanic District, Italy: Evidence from melt inclusions. Geochim. Cosmoch. Acta, 62: 507, 514.

Marsh B.D. 1996 Solidification fronts and magmatic evolution. Mineral. Magazine, 60, 5-40

Marsh B.D. 1998 On the interpretation of crystal size distributions in magmatic system, 39, 553-600.

Nisbet E.G and Pearce J.A. 1977 Clinopyroxene composition in mafic lavas from different tectonic settings. Contrib. Mineral. Petrol., 63: 149-160.

Patacca E., Sartori R. and Scandone P. 1990 Tyrrhenian basin and Appenninic arcs: kinematic relations since late Tortonian times. Mem. Soc. Geol. Ital. 45: 425-451.

Raia F., Webster J.D. and De Vivo B. 2000 Pre-eruptive volatile contents of Vesuvius magmas : constraints on eruptive history and behavior. I. The medieval and modern interplinian activities. Eur. J. Mineral:, 12: 179-193.

Rolandi G., Maraffi S., Petrosino P. and Lirer L. 1993a The Ottaviano eruption of Somma-Vesuvius (3760y B.P.): a magmatic alternating fall and flow-forming eruption. In: De Vivo B., Scandone R. and Trigila R. (eds) Vesuvius special issue. J Volcanol Geotherm Res 58: 43-65

Rolandi G., Mastrolorenzo G., Barrella A.M. and Borrelli A. 1993b The Avellino plinian eruption of Somma-Vesuvius (3760y B.P.): the progressive evolution from magmatic to hydromagmatic style. In: De Vivo B, Scandone R, Trigila R (eds) Vesuvius special issue. J Volcanol Geotherm Res 58: 67-68

Rolandi G., Barrella A.M. and Borrelli A. 1993c The 1631 eruption of Vesuvius. In: De Vivo B., Scandone R. and Trigila R. (eds) Vesuvius special issue. J Volcanol Geoth Res 58: 183-201

Rolandi G. 1997 The eruptive history of Somma-Vesuvius. In Volcanism and Archaeology in Mediterranean area. M. Cortini and B. De Vivo Eds, Research Signpost (Trivandrum), pp 77-88.

Rolandi G., Petrosino P. and McGeehin J. 1998 The interplinian activity of Somma-Vesuvius in the last 3500 years. In: Spera F.J., De Vivo B., Ayuso R.A. and Belkin H.E. (eds) Vesuvius special issue. J Volcanol Geotherm Res.,82:19-52

Roedder E. 1979 Origin and significance of magmatic inclusions. Bull Mineral 102: 487-510

Ryan J.G. and Langmuir C.H., 1993. The systematics of boron abundance in young volcanic rocks. Geochim. Cosmochim Acta 57, 1489-1498.

Ryan J.G., Morris J.D., Bebout G.E. and Leeman W.P. 1996 Describing chemical fluxes in subduction zones: Insights from depth-profiling studies of arc and fore-arc rocks. In: Subduction Top to bottom (ed. G.E. Bebout et al.), pp 263-268. AGU Geophys. Monogr.

Santacroce R. (ed) 1987 Somma Vesuvius. CNR Quad Ric Sci 114

Santacroce R., Bertagnini A., Civetta L., Landi P. and Sbrana A. 1993 Eruptive dynamics and petrogenetic processes in a very shallow magma reservoir: the 1906 eruption of Vesuvius. J Petrol 34: 383-425

Scandone R., Giacomelli L. and Gasparini P. 1993 Mount Vesuvius: 2000 years of volcanological observations. J. Volcanol Geotherm Res 58: 5-25.

Shimizu N. and Hart S.R. 1982 Applications of the ion microprobe to geochemistry and cosmochemistry. Ann. Rev. Earth Planet Sci, 10: 483-526.

Somma R., Ayuso R.A., De Vivo B. and Rolandi G. 2001 Major, trace element and isotope geochemistry (Sr-Nd-Pb) of interplinian magmas from Mt. Somma-Vesuvius (Southern Italy). Mineral. Petrol. 73: 121-143.

Turco E. and Zuppetta A. 1998 The Campanian volcanism in the Tyrrhenian-Apennine system. In: Spera FJ, De Vivo B, Ayuso RA, Belkin HE (eds) Vesuvius special issue. J Volcanol Geotherm Res, 82:1 - 18

Villemant B., Trigila R. and De Vivo B. 1993 Geochemistry of Vesuvius volcanics during 1631-1944 period. In: De Vivo B., Scandone R., Trigila R. (eds) Vesuvius special issue. J Volcanol. Geother. Res., 58: 291-313

Washington H.S. 1906 The roman comagmatic Region. Carnegie Inst Washington publ 57: 1-199

Webster J.D., Burt D.M. and Aguillon R.A., 1996 Volatile and lithophile trace-element geochemistry of heterogeneous Mexican tin rhyolite magmas deduced from compositions of melt inclusions. Geochim. Cosmochim. Acta 60: 3267-3283.

Webster J.D., Raia F., De Vivo B. and Rolandi G. 2001 The behavior of chlorine and sulfur during differentiation of the Mt. Somma-Vesuvius magmatic system. Mineral. Petrol., 73: 177-200.

Webster J.D., De Vivo B. and Tappen C. 2002 Volatiles, magmatic degassing and eruptions of Mt. Somma-Vesuvius: constraints from silicate melt inclusions, solubility experiments and modeling. (This volume).

Zambonini F. 1910 Mineralogia Vesuviana. Atti R. Acc. Sc. Fis., Mat. Ser 2°, 14/7: 1-463.

Zollo, A., Gasparini P., Virieux J., Biella G., Boschi E., Captano P., de Franco R., Dell'aversana P., de Matteis R., De Natale G., Jannaccone G. Guerra I., Le Meur H. and Mirabile L. 1998 An image of Mt. Vesuvius obtained by 2D seismic tomography. J. Volcanol. Geotherm. Res., 82: 161-173.

This Page Intentionally Left Blank

Author Index

This Page Intentionally Left Blank

Subject Index